Testing and Applying Thermodynamic Models for the Melting of Mantle Peridotites

by

Daoheng Wang

A thesis submitted in partial fulfillment of the requirements for the degree of

Master of Science

Department of Earth and Atmospheric Sciences
University of Alberta

Abstract

The covariance of increasing spinel Cr# and olivine Mg# ("the olivine-spinel mantle array" or "OSMA") has been used as a sensitive indicator for the melting history of mantle peridotites. The basis for this model has been largely empirical thus far. In this study, the most recent THERMOCALC-based models are used to study the melting of mantle peridotites in batch melting, isobaric fractional melting, and decompression melting, with a view to placing the OSMA array on a firmer theoretical foundation. The effects of water, bulk composition, Fe^{3+}/Fe^{2+}, temperature, and pressure on the mineralogy and phase chemistry in anhydrous and hydrous peridotites have also been modelled.

The calculated results for anhydrous batch melting of fertile source peridotites KLB-1, KR4003, and MM3 using TH21* model agree well with experiments. In contrast, modelling hydrous melting was less successful, moving the focus of the results of this study to the residual products of volatile-free melting of Earth's mantle in the context of the OSMA. Using anhydrous peridotite melting models, varying bulk Fe^{3+} had minimal effect on spinel stability. The solidus and the temperature of spinel stability for fertile peridotites are lower than for depleted peridotites. Adding alkalis can reduce the melting temperature of a lherzolite or a depleted peridotite source. With the TH21 model, spinel survives to a much higher degree of melting in batch melting (>40%) than fractional melting (<14%). The slope of the OSMA generated by fractional melting is steeper than that generated by batch melting. The maximum spinel Cr# achieved in depleted peridotites is higher than in fertile peridotites. Adding alkalis to depleted peridotites could generate extremely Cr-rich spinel (maximum spinel Cr# >85) in all melting models. The behavior of Al and Cr during batch melting, and the distribution coefficient of Al

and Cr in spinel and melt have been studied to understand the varying spinel Cr# in residual peridotites.

By studying decompression melting, with different bulk compositions following adiabats with distinct mantle potential temperatures, the evolution of mantle melting from Archean to present-day can be modelled more rigorously.

*TH21: after Tomlinson and Holland (2021)

Preface

This thesis is an original work by Daoheng Wang. No part of this thesis has been previously published.

Acknowledgments

Over three years of study in the Department of Earth and Atmospheric Sciences (EAS) have constituted one of my most important memories. I want to express my deepest appreciation to my supervisors, Dr. Robert Luth and Dr. Graham Pearson, for providing this great opportunity to do such exciting research with them. It is a beautiful experience to be their graduate student.

The completion of this thesis would not have been possible without the support and nurturing of my main supervisor, Robert Luth, who met me weekly to discuss questions with me, provided me with encouragement, patience, and many invaluable suggestions throughout this project, and shaped my scientific taste and aesthetics. I am incredibly grateful to my co-supervisor, Graham Pearson, who provided many invaluable insights into this research.

I would like to extend my deepest gratitude to my thesis defense committee members, Robert Luth, Graham Pearson, and Thomas Stachel (both examiner & chair), for their ingenious suggestions and inspiration that improved this thesis.

I want to thank Graham Pearson and Anetta Banas for their tremendous efforts in running the Diamond Exploration and Research Training School (DERTS) program. Workshops, courses, and talks provided by DERTS improved my knowledge background in mantle petrology. Friends and colleagues in DERTS program, Brody Myers, Connor Elzinga, Mei Yan Lai, Ji Zhang, and Sarah Milne extended a great amount of assistance. I also want to thank the friendship in Long Li's research group: Kan, Yuhan, Yifan, Ling, and Xueqi, and my board game friends Yanze, Lin, Chao, Shiyu, and Yiyun.

I would like to extend my sincere thanks to Roy Eccles, my supervisor during my internships between research studies, whose help cannot be overestimated. Roy provided constructive advice for creating better figures and reports, which benefited me in more expansive fields beyond the consulting work.

I want to acknowledge the DERTS program and NSERC Discovery grants to Robert Luth and Graham Pearson for funding.

I am deeply indebted to my family. Thank you for always supporting my dreams!

Table of Contents

List of Tables

List of Figures

List of Abbreviations

Cp	Heat capacity
cpx	Clinopyroxene
DP	Depleted Peridotites
DPA	Depleted Peridotites with Addition of Alkalis
g	Garnet
GPa	Gigapascal
H	Enthalpy
HGP18	Holland, Green, and Powell (2018)
KLB-1A	KLB-1 with addition of Alkalis
liq	Liquid
ol	Olivine
opx	Orthopyroxene
P	Pressure
S	Entropy
sp	Spinel
T	Temperature
TH21	Tomlinson and Holland (2021)
V	Molar volume

Chapter 1 Introduction

1.1 Significance of Melting of Mantle Peridotites

Partial or complete melting is one of the critical geological processes on the Earth making the study of partial melting an essential part of understanding the evolution of the Earth.

The proto-Earth melted during accretion and differentiation into a metallic core and a rocky mantle due to the release of gravitational energy (e.g. Ricard et al., 2009), forming a magma ocean due to the rising temperature (e.g. Abe, 1997). The blanketing effect of a proto atmosphere or a planetesimal impact could have caused another magma ocean stage of the Earth. The high degree of mantle melting in the Archean eon resulting from heat production and heat flow created the original crust and the lithospheric mantle (e.g. Benn et al., 2006; Fyfe, 1978; Taylor and McLennan, 1985). The modern Earth's mantle is mostly solid (e.g. Fiquet, 2018). Partial melting of the modern Earth could take place in the asthenosphere (e.g. Chantel et al., 2016), on the top of the transition zone, the top of the lower mantle, or core-mantle boundary where hotspots arise from (e.g. Fiquet, 2018 and references therein). However, partial melting of the present Earth is confined chiefly to the uppermost 140 km of the Earth (Foley and Pintér, 2018). Melting mainly happens in the mantle wedge at subduction zones (e.g. Carlson et al., 2005; Parman et al., 2004; Pearson and Wittig, 2008; Simon et al., 2007), divergent plate boundaries (e.g. Brey and Shu, 2018; Herzberg and Rudnick, 2012; Lee et al., 2011; Servali and Korenaga, 2018; Team, 1998), and in large and hot plumes (e.g. Arndt et al., 2009; Aulbach, 2012; Boyd, 1989; Griffin et al., 2009; Pearson et al., 1995). Overall, partial melting requires circumstances at specific locations where temperature increases, pressure drops, or volatiles are introduced.

Olivine-rich peridotite is the dominant ultramafic rock of the upper mantle. Other lithologies that result from the recycling of crustal materials (e.g. Hermann and Spandler, 2008; Kogiso et al., 2004; Nichols et al., 1994; Thomsen and Schmidt, 2008) or from the migration and solidification of incipient melts within the mantle due to the effects of volatiles (e.g. Dalton and Presnall, 1998b; Dasgupta and Hirschmann, 2007; Foley et al., 2009) make the mantle more heterogeneous. Mantle peridotites are considered 'fertile' if there has been no substantial melt extraction. Such peridotites are mineralogically lherzolites, composed of olivine, orthopyroxene, clinopyroxene, and an aluminous mineral. The aluminous mineral varies with pressure:

plagioclase, spinel, garnet as pressure increases. Upon partial melting, lherzolites evolve into harzburgite, then dunite, becoming 'depleted' after consuming clinopyroxene and then orthopyroxene (e.g. Pearson et al., 2021).

Geologists can study processes of mantle melting using natural mantle samples, which is considered an inverse approach. Natural mantle peridotites and other materials are transported to the Earth's surface mainly through the following ways: 1) Tectonically emplaced mantle rocks (e.g. Bodinier and Godard, 2003), including alpine or orogenic peridotite massifs from mountain belts and suture zones (e.g. De Roever, 1957; Den Tex, 1969), ophiolite or island arc complexes from the edge of continents (e.g. Boudier and Coleman, 1981; Mehl et al., 2003), mantle rocks above the sea level in ocean basins (e.g. Bonatti et al., 1981; Dijkstra and Cawood, 2004); 2) Abyssal peridotites from the oceanic mantle, dredged on the ocean floor (e.g. Bonatti et al., 1974; Hamlyn and Bonatti, 1980); 3) Xenoliths or nodules within host rocks of volcanic origin (e.g. Boyd and Meyer, 1979; Pearson et al., 2003); 4) Mineral inclusions in diamonds (e.g. Harte, 1999; Meyer, 1987; Pearson et al., 2003).

Experiments can be used in studying mantle melting as well. Initial melting experiments at mantle pressure was performed by Yoder Jr (1952) to determine the melting temperature of diopside at 1 GPa using an internally heated gas-media apparatus. A series of experiments were then conducted to determine the melting temperature of major components of minerals in synthetic mantle peridotites up to 5 GPa using a piston-cylinder apparatus (e.g. Boyd and England, 1960; 1962; 1963; Boyd et al., 1964; Davis and England, 1964). Experiments determining phase equilibrium relationships in synthetic mantle peridotites soon followed (e.g. Davis, 1964; Kushiro, 1965; 1968; 1969; O'Hara, 1963a; O'Hara and Yoder, 1967; Presnall et al., 1978). At the same time, melting experiments determining the phase relationships of natural mantle peridotites were conducted under anhydrous (e.g. Ito and Kennedy, 1967; O'Hara, 1963b) and hydrous conditions (e.g. Kushiro, 1968; Millhollen et al., 1974), and with the participation of CO_2 (e.g. Mysen and Boettcher, 1975). These experiments were soon followed by experiments revealing the effects of H_2O and CO_2 on the melting of peridotitic systems (e.g. Eggler, 1974; 1978; Kushiro, 1968; 1969; 1972; Presnall, 1987; Presnall et al., 1979; Wyllie and Huang, 1976). All these experiments were designed to understand the genesis of basalt magmas. By their nature, these experiments were closed systems, and thus represent 'batch melting'. However, in

nature, melting processes are more likely to be closer to fractional melting. In batch melting, a finite amount of melt is produced and equilibrates completely with the solid residue. In fractional melting, the melt is extracted as soon as it is created, and only an infinitesimal increment of melt will be in equilibrium with the solid residue at any given time. Escape of the melt by buoyant ascent limits the applicability of batch melting. The genesis of mid-ocean ridge basalt (MORB), for example, is considered near-fractional decompression melting in adiabatically ascending mantle at the mid-ocean ridge (e.g. Kushiro, 2001; McKenzie, 1984; Mckenzie and Bickle, 1988; Niu and Batiza, 1991; Sobolev and Shimizu, 1993). Mineral phase relationships and equilibrium in peridotitic systems at very high pressure up to 25 GPa have been studied since multi-anvil apparatus became commonly available in the 1980s (e.g. Canil and Scarfe, 1990; Dalton and Presnall, 1998a; Gasparik, 1996; Herzberg and O'Hara, 1998; Herzberg and Zhang, 1998; Ito et al., 1984; Kato and Kumazawa, 1985; Kudo and Ito, 1996; Ohtani and Kumazawa, 1981; Presnall and Gasparik, 1990; Presnall and Walter, 1993; Presnall et al., 1998; Takahashi, 1986).

We can also apply thermodynamic models to study the melting of mantle peridotite. Based on equilibrium thermodynamics, various thermodynamic tools have been developed to determine various geological conditions recorded within a large variety of geological settings (e.g. review by Yakymchuk, 2017). These thermodynamic tools include: 1) empirical geothermometers and geobarometers using mineral-mineral, mineral-fluid, and mineral-melt equilibria (e.g. Brey and Köhler, 1990; Grütter et al., 2006; Harley, 1984; Köhler and Brey, 1990; Krogh, 1988; Mutlu, 1998; Nickel and Green, 1985; Nimis and Grütter, 2010; Nimis and Taylor, 2000; O'Neill and Wall, 1987; O'Neill and Wood, 1979; Pelullo et al., 2022; Ravna, 2000; Taylor, 1998; Tole et al., 1993); 2) internally consistent thermodynamic databases with standard state parameters (e.g. H, S, V, Cp) for endmembers and solution models (activity-composition relations) for solids, melts, and fluids (e.g. Berman, 1988; Chatterjee et al., 1998; Gottschalk, 1997; Holland and Powell, 1985; 1990; 1998; 2011; Miron et al., 2016; 2017); 3) computer programs that use these databases to modelling thermodynamic equilibrium problems (e.g. Berman, 1991; Berman et al., 1987; Connolly, 1990; Connolly and Petrini, 2002; de Capitani and Brown, 1987; de Capitani and Petrakakis, 2010; Ghiorso et al., 2002; Powell and Holland, 1988; Spear, 1988; Xiang, 2020; Xiang and Connolly, 2022).

Compared to studies using natural mantle peridotite to deduce their origin and source, partial melting experiments and thermodynamic melting models use starting materials to study the compositions of melting products and their formation conditions. Most thermodynamic models are built based on experimental constraints. Both methods could be considered a forward research strategy to study melting processes.

1.2 Goals of This Study

The co-variation of spinel Cr# (100*Cr/(Cr+Al)) and olivine Mg# (100*Mg/(Mg+Fe)) in mantle peridotites has been used as a sensitive indicator for the degree of partial melting, magma types, and metasomatism. Whereas the origin of spinel-olivine trends in relatively fertile peridotites can be well simulated by experiments, spinel-olivine trends in peridotites that have experienced high degrees of melt depletion are more controversial and experimental constraints are few. The original bulk composition, participation of water, oxygen fugacity, pressure, and temperature are some factors we need to consider for the formation of highly depleted residual peridotites.

Thermodynamic modelling has advanced to the point where it complements experimental studies, especially given the difficulties in experiments at low degrees of partial melting. Fractional melting processes in particular are difficult to simulate experimentally, but tractable in thermodynamic modelling. Here, I use the most recent versions of THERMOCALC-based thermodynamic models, the TH21* and HGP18* model, to model the effects of water, bulk composition, Fe^{3+}/Fe^{2+}, temperature, and pressure on the residual mineralogy and phase chemistry in anhydrous and hydrous peridotites, and differences between batch and fractional melting models.

In particular, the aim is to attempt to model melting processes that can lead to extremely Cr-rich spinels and magnesian olivines in the residue: can such residues be formed by extensive single-stage melting, or are more complicated scenarios required?

*TH21: after Tomlinson and Holland (2021) and HGP18 after Holland, Green, and Powell (2018)

Chapter 2 Methodology

For this study, I mainly used the most recent versions of THERMOCALC-based models that were available to model the phase relationships of mantle peridotites. These are the models published by Holland et al. (2018) (the "HGP18" model) and by Tomlinson and Holland (2021) (the "TH21" model). There are two aspects here of the differences between TH21 and HGP18: 1) The dataset containing the thermodynamic data for the endmembers; 2) the solution models used. Therefore, the databases, models of solid solutions, silicate liquids, and aqueous fluids will be introduced in this chapter.

2.1 Principles and Backgrounds of Thermodynamic Models

Thermodynamic equilibrium is the fundamental assumption required for quantitative thermodynamic calculations. A system that reaches equilibrium means its compositions would not change with time if left indefinitely at those conditions. Geological systems in nature are not always in an equilibrium state, however, because time may not be available to attain equilibrium at a particular condition. The rate of equilibration depends on the rates of matter and energy flow when driving forces are sufficient to overcome the kinetic barriers within the system (e.g. Lanari and Duesterhoeft, 2019). Typically, the attainment of equilibrium is faster at higher temperature, so the mineralogy of rocks records some equilibrium at high temperatures before substantial cooling and then "freezing" of the equilibrium (e.g. Powell, 1978). Another feature of the achievement of equilibrium in a natural system is the scale of the equilibrium. A system may reach local or mosaic equilibrium (e.g. Carmichael, 1969; Thompson Jr, 1970), although the overall, larger-scale system is out of equilibrium, or in a metastable equilibrium state because of some constraints preventing the reaction from proceeding. Zoned minerals are an excellent example for the scale of equilibrium of a system. Equilibrium is reached within each zone, but the time is not enough for the different zones to have reached equilibrium.

For a closed system, the Gibbs energy is minimized at equilibrium at a given temperature and pressure (e.g. Anderson, 2005; Powell, 1978). The Gibbs energy of the system G_{system} is the sum of the Gibbs energies of the individual phases scaled to the amounts of those phases present in the system. For a given bulk composition, a complete thermodynamic model allows calculation of the phases present their compositions and their modal amounts.

To do so, we require thermodynamic models for each mineral of interest. These models require thermodynamic data for each endmember as functions of P and T, and a solution model to account for the variable composition of the mineral. This allows us, in principle, to find the equilibrium assemblage: the compositions and abundances of the constituent minerals that make up a specific mantle bulk composition. To extend this model to melting relationships, a thermodynamic model for the melt is required. Likewise, considering fluid-present melting requires a model for the fluid, as well as modifications to the melt model to accommodate dissolved volatiles.

2.1.1 Endmember Data (internally consistent databases)

Thermodynamic properties in an internally consistent database need to meet some requirements: 1) are compatible with thermodynamic principles; 2) have a uniform set of reference values; 3) consider all the experimental data simultaneously; 4) reproduce all the primary data within their uncertainties (e.g. Berman et al., 1986; Engi, 1992; Lanari and Duesterhoeft, 2019). The least-squares regression (REG; e.g. Holland and Powell, 1985) and the mathematical programming technique (MAP; an extension of the linear programming technique (LIP); e.g. Berman et al., 1986) are two primary techniques that have been used to determine internally consistent thermodynamic datasets. The Bayesian approach (BAYES; e.g. Chatterjee et al., 1998) is a better yet more complex technique and can be used to optimize the thermodynamic datasets. These standard state properties in the internally consistent database are derived from either direct measurement (e.g. Charlu et al., 1975; Dachs et al., 2012; Newton, 2018) or indirectly, based on experiments constraining phase equilibrium data (e.g. Ferry and Spear, 1978; Holland, 1980; Koziol and Newton, 1989). The main internally consistent thermodynamic datasets and approaches are summarized by Lanari and Duesterhoeft (2019) (see Table 1).

2.1.2 Solution Models

Most phases of interest have variable composition, which requires a solution model. Mixing usually causes enthalpy changes, whereas configurational entropy will ensure a reduction in free energy on mixing even when there are no enthalpy changes. The simplest model is an ideal solution, where there is a random distribution of atoms and no enthalpy of mixing. Real solutions are non-ideal, though some of them are close to an ideal solution. The simplest non-ideal

solution is a regular solution, which add enthalpies of mixing to an ideal solution model. Regular solutions are non-ideal but have equal entropy of mixing with ideal solutions.

2.1.2.1 Solids

Mantle minerals such as olivine, pyroxene, spinel, and garnet, require consideration of the substitution of ions with similar chemical properties. Each mineral can be considered a mixture of different endmembers. The Gibbs free energy for a solid solution at a specific PT can be calculated through:

$$G = \sum x_i \mu_i^{\circ} + RT \sum x_i \ln a_i \quad 2.1$$

Where μ_i° is chemical potential for pure endmember i; x_i is the mole fraction; $\sum x_i \mu_i^{\circ}$ is the physical mixture Gibbs energy; R is the universal gas constant; $a_i = \gamma_i x_i$ is the activity of endmember i. γ_i is the activity coefficient, for ideal solutions, $\gamma_i = 1$.

For example, for a simple solid solution model like a regular solid solution, we can write:

$$\Delta_a G^{P,T} = \sum x_i \, \Delta_f G_i^{P,T} + RT \sum x_i \, ln x_i + \sum W_{ij} x_i x_j \quad 2.2$$

$\Delta_a G^{P,T}$ is the apparent Gibbs free energy; $\Delta_f G_i^{P,T}$ is the standard Gibbs free energy for each endmember and can be calculated using thermodynamic data.

$$\Delta_f G^{P,T} = \Delta_f H^{P_0,T_0} - TS^{P_0,T_0} + \int_{T_0}^{T} Cp\,dT - T\int_{T_0}^{T} \frac{Cp}{T} dT + \int_{P_0}^{P} V\,dP \quad 2.3$$

$\Delta_f H^{P_0,T_0}$ is the enthalpy of formation from the elements or oxides at P_0 (1 bar) and T_0 (298.15 K); S^{P_0,T_0} is the entropy at P_0 and T_0; Cp is the heat capacity; V is the molar volume of the phase.

W_{ij} is the interaction energy for mixing of endmember i and j. For a symmetric solution: $W_{ij} = W_{ji}$, but many actual solutions are asymmetric. The interaction energies can be functions of P and T and can be written as W = a + bT + cP, where a, b, and c are constant.

2.1.2.2 Silicate Liquids

The silicate liquid, or melt, is a disordered silicate-rich phase. The activity-composition (a-x) relations of endmembers of the silicate liquids are more uncertain than for crystalline silicates because of the lack of long-range structure in the liquids. Each silicate liquid has various Si-O

polymeric units, and the size and shape distribution of these polymeric units could decide the number and nature of each cation 'site'. Site and polymeric units distributions are crucial in the thermodynamics of silicate liquids (Powell, 1978).

To simplify the problem, a set of linearly independent compositional endmembers are considered in different studies. To model basaltic melts, JH15 (Jennings and Holland, 2015) defined the endmembers of silicate melts as $NaAlSi_2O_6$-$CAMgSi_2O_6$-$CaAl_2SiO_6$-Mg_2SiO_4-Fe_2SiO_4-Si_2O_4-$CrO_{1.5}$-$FeO_{1.5}$. They also introduced a Temkin-type of entropy model: different numbers of species are assigned in octahedral-like sites (M), aluminosilicate framework (F), and additional larger sites (A). The a-x relations of silicate melts are therefore defined using the ideal activities on the various sites with non-ideal terms from a regular solution of these eight endmembers (Jennings and Holland, 2015). The melt model of HGP18 (Holland et al., 2018) incorporated 12 endmembers, including $NaAlSi_2O_6$-$KAlSi_2O_6$-$CaSiO_3$-Al_2SiO_5-$CaAl_2SiO_6$-$Mg_4Si_2O_8$-$Fe_4Si_2O_8$-Si_4O_8-$CrO_{1.5}$-TiO_2-$FeO_{1.5}$-H_2O. Importantly for our purposes, this model explicitly considered H_2O. The TH21 model (Tomlinson and Holland, 2021) further updated anhydrous melt endmembers to Al_2SiO_5-$CaSiO_3$-$Mg_4Si_2O_8$-$Fe_4Si_2O_8$-Si_3O_6-$CrO_{1.5}$-TiO_2-$FeO_{1.5}$-$NaAlSiO_4$-$KAlSi_2O_6$-$CaAl_2Si_2O_8$-$NaAlSi_3O_8$-$KAlSi_3O_8$-$Mg_2Si_2O_6$, with only M and F sites were considered. However, the TH21 model did not include H_2O, meaning that this model cannot be used for modelling of hydrous melting. Mg_2SiO_4-$KAlO_4$-Fe_2SiO_4-Na_2SiO_3-Al_2O_3-$CaSiO_3$-SiO_2 were defined as liquid thermodynamic components in MELTS (Ghiorso and Sack, 1995); Mg_2SiO_4-$KAlO_4$-Fe_2SiO_4-Na_2SiO_3-Al_4O_6-$Ca_2Si_2O_6$-Si_4O_8 were defined in PMELTS, and the calculation of molar Gibbs free energy of formation of silicate liquids used these endmembers (Ghiorso et al., 2002).

2.1.2.3 Aqueous Fluids

Aqueous fluids can be modelled in two different ways: 1) as "associated" or "molecular" solutions, with primary constituents of interest are H_2O and CO_2, with H_2, O_2, CO, etc.; 2) as "ionic" or "electrolytic" solutions. "Associated" solutions are usually used at mantle conditions because of the high temperatures involved. Ionic or electrolytic solutions are primarily used at crustal conditions (< 800°C), although there are recent efforts to extend these models to higher temperatures (Huang and Sverjensky, 2019; Sverjensky, 2019). The thermodynamic formulation used in HGP18 is a molecular model.

For each endmember in the fluids:

$$a_i = f_i / f_i^{\circ} \quad (2.4)$$

$f_i = \gamma_i P_i$ is the fugacity of i, where P_i is the partial pressure of i in a solution; γ_i is the fugacity coefficient; f_i° is the fugacity for i at the standard state. Therefore, I can calculate the apparent Gibbs free energy of fluids by combining the above equations.

2.1.3 Available Programs

Gibbs free energy minimizers like THERIAK-DOMINO (de Capitani and Petrakakis, 2010) and PERPLE_X (Connolly, 1990; Connolly and Petrini, 2002) can be used with various databases. MELTS (Ghiorso and Sack, 1995) and PMELTS (Ghiorso et al., 2002) use the database of BE88 (Berman, 1988) as their standard state properties datasets and their own solution models. THERMOCALC (Powell and Holland, 1988; Powell et al., 1998) and GIBBS (Spear, 1988) are phase equilibrium calculators. The newest version of the THERMOCALC series, THERMOCALC 350-β, is linked to ds63 updated from HP98 (Holland and Powell, 1998) and HP11 (Holland and Powell, 2011). GIBBS incorporates several datasets, including HP98 and HP11. Other limited-use computer programs like GeoPS (Xiang, 2020; Xiang and Connolly, 2022) and HeFESTo (Stixrude and Lithgow-Bertelloni, 2011) provide more options for thermodynamic equilibrium calculations in specific situations.

2.2 Thermodynamic Models used in This Study

2.2.1 Thermodynamic Databases

Internally consistent thermodynamic datasets, ds633 (https://hpxeosandTHERMOCALC.org/) and ds634 (https://filedn.com/lU1GlyFhv3UuXg5E9dbnWFF/TJBHpages/2021model.html) (these datasets are included in Appendix C), extended from the database of Holland and Powell (2011), are used in this study. Dataset ds633 has 289 phases; ds634 has 291 phases (ferric biotite and ordered biotite were added). Both versions have 22 silicate liquid endmembers and 26 aqueous fluid species. Enthalpies in the datasets are determined through least-squares regression (REG) on calorimetric, phase equilibria, and natural mineral partitioning data. Entropies, volumes, heat capacities, thermal expansions and compressibilities are taken as known. The principles behind deriving the data in the building of these datasets are shown in Holland and Powell (1985; 1990; 1998; 2011) and Powell and Holland (1985).

2.2.2 Models of Solid Solutions

All minerals in mantle peridotites are solid solutions, requiring both thermodynamic data for their compositional endmembers and a solution model to describe the solid solution. The details of solid solution models for olivine, orthopyroxene, clinopyroxene, garnet, spinel, and plagioclase are from Holland et al. (2018) and Tomlinson and Holland (2021).

Olivine: Both models incorporate $CaMgSiO_4$ (monticellite), Fe_2SiO_4 (fayalite), Mg_2SiO_4 (forsterite), and $MgFeSiO_4$ (cfm) as olivine endmembers, and the solution model is described in Holland et al. (2018) and Tomlinson and Holland (2021).

Orthopyroxene: Nine endmembers of orthopyroxene are considered in both models, including $Mg_2Si_2O_6$ (enstatite), $Fe_2Si_2O_6$ (ferrosilite), $MgFeSi_2O_6$ (fm), $CaMgSi_2O_6$ (ortho-diopside), $MgAl_2SiO_6$ (Mg-Tschermak), $MgCrAlSiO_6$ (cren), $Mg_{1.5}AlTi_{0.5}SiO_6$ (obuf), $MgFeAlSiO_6$ (mess), and $NaAlSi_2O_6$ (ortho-jadeite).

Clinopyroxene: Ten endmembers of clinopyroxene are considered in both models, including $CaMgSi_2O_6$ (diopside), $Fe_2Si_2O_6$ (clino-ferrosilite), $CaAl_2SiO_6$ (Ca-Tschermak), $CaCrAlSiO_6$ (crdi), $CaFeAlSiO_6$ (cess), $Ca(Mg_{0.5}Ti_{0.5})AlSiO_6$ (cbuf), $NaAlSi_2O_6$ (jadeite), $Mg_2Si_2O_6$ (clinoenstatite), $MgFeSi_2O_6$ (cfm), and $KAlSi_2O_6$ (kjd).

Spinel: In the HGP18 model, spinel is composed of 8 endmembers: $MgAl_2O_4$ (ordered and inverse spinel), $FeAl_2O_4$ (ordered and inverse hercynite), Fe_3O_4 (ordered and inverse magnetite), $MgCr_2O_4$ (ordered picrochromite), and Mg_2TiO_4 (qandilite). The spinel model in TH21 replaces qandilite with Fe_2TiO_4 (ulvospinel).

Garnet: Both models use endmembers $Mg_3Al_2Si_3O_{12}$ (pyrope), $Fe_3Al_2Si_3O_{12}$ (almandine), $Ca_3Al_2Si_3O_{12}$ (grossular), $Ca_3Fe_2Si_3O_{12}$ (andradite), $Mg_3Cr_2Si_3O_{12}$ (knorringite), and $Mg_{3.5}AlTi_{0.5}Si3O_{12}$ (tig).

Plagioclase: $KAlSi_3O_8$ (sanidine), $NaAlSi_3O_8$ (albite), and $CaAl_2Si_2O_8$ (anorthite) are the endmembers of plagioclase in HGP18. TH21 adds $ab_{50}an_{50}$ (made from ordered albite and anorthite) as an additional endmember of plagioclase.

2.2.3 Models for Silicate Liquids

At the time of this work, the most up-to-date model for silicate melt is that described by TH21, but this model does not incorporate H_2O, limiting its usage to the anhydrous system. Because we are interested as well in hydrous melting, I also evaluated the silicate melt model of HGP18, which does include H_2O.

Fourteen endmembers are considered in TH21 silicate melt model, compared to 12 endmembers in HGP18 melt model (Table 2.1). Compared to HGP18, TH21 adds $CaAl_2Si_2O_8$ (anL), $NaAlSi_3O_8$ (abL), $KAlSi_3O_8$ (kfL), and $Mg_2Si_2O_6$ (enL) as additional order parameters. Si_4O_8 (q4L), $NaAlSi_2O_6$ (jdL), and $CaAl_2SiO_6$ (ctL) in HGP18 are replaced by Si_3O_6(q3L) and $NaAlSiO_4$ (neL). In addition, as mentioned in 2.1.2.2, M, F, and A sites in the HGP18 silicate melt model are reduced to M and F sites in TH21, so the calculation of ideal activities on these sites would be simpler.

Table 2.1 Endmembers in models for silicate liquids from HGP18 and TH21

HGP18		TH21	
Same	Different	Same	Different
$KAlSi_2O_6$	Si_4O_8	$KAlSi_2O_6$	Si_3O_6
$CaSiO_3$	$NaAlSi_2O_6$	$CaSiO_3$	$NaAlSiO_4$
Al_2SiO_5	$CaAl_2SiO_6$	Al_2SiO_5	$CaAl_2Si_2O_8$
$Mg_4Si_2O_8$	H_2O	$Mg_4Si_2O_8$	$NaAlSi_3O_8$
$Fe_4Si_2O_8$		$Fe_4Si_2O_8$	$KAlSi_3O_8$
$CrO_{1.5}$		$CrO_{1.5}$	$Mg_2Si_2O_6$
TiO_2		TiO_2	
$FeO_{1.5}$		$FeO_{1.5}$	

These updates in TH21 were designed to better predict the concentration of silica in the liquid. The introduction of an enstatite component provides additional flexibility in modelling the Gibbs free energy relations between forsterite and silica components. Using wollastonite and anorthite to replace the CATS endmember has the same effect as providing greater flexibility in modelling the free energy of the melt. The change in the size of silica endmember and sodic melt species aims to represent the silica melts better.

2.2.4 Models for Aqueous Fluids

As described above, the TH21 melt model is anhydrous, while the HGP18 one contains water, so I can consider melting in the presence of a hydrous fluid with HGP18. This requires a model for aqueous fluids, which in HGP18 contains endmembers corresponding to the silicate melt endmembers, except that it has one less order variable, $CaAl_2SiO_6$ (ct). This fluid is strictly H_2O-silicate, and does not have CO_2, CO, CH_4, or H_2. In the aqueous fluid model, the interaction energy between water and other endmembers is considered, but the interaction energy between endmembers other than water is set as zero because of their low concentrations.

Chapter 3 Testing of Models

In this chapter, I address the fundamental question: How well do the currently available thermodynamic models reproduce phase relationships in peridotite systems? To do this I applied the most recent THERMOCALC-based models and compared the results with experimental results in anhydrous and hydrous peridotite systems. Of particular interest is evaluating how well these models reproduce the mineralogy and mineral chemistry of the residues of partial melting, because we are interested in exploring the influence of water, bulk composition, temperature, and pressure on the melting process. In particular, this would provide insight into, for example, the evolution of spinel chemistry during partial melting to understand how high-Cr spinel forms. These models can also be used to study the general behaviour of some elements such as Cr and Al during melting to understand better the melting process of mantle peridotites.

The use of the two silicate melt models, TH21 and HGP18, adds complexity to the analysis below. Additional complexity is introduced because the thermodynamic models for the crystalline solid solution phases plagioclase, orthopyroxene, clinopyroxene, spinel, and garnet have continued to evolve, and differ in detail between the two models.

To test the situation as best we could, with an eye on our goal of modelling the residues of (ideally) hydrous partial melting, we looked at how well both melt models did in modelling anhydrous melting and further explored if the use of the newer TH21 solid solution models had any effect on the results of modelling hydrous melting with the HGP18 melt model. Table 3.1 summarizes the models used in this study (input files are in Appendix C).

Table 3.1. Thermodynamic models used in this study

Model (this study)	Silicate melt model	Solid solution models
TH21	TH21	TH21
HGP18	HGP18	HGP18
WL22-3	HGP18	TH21

The bulk and mineral compositions for mantle peridotites used in this study are listed in Table 3.2. The mineral proportions and compositions at the pressure and temperature conditions of the experimental studies are considered to evaluate the model. Experimental data on the partial melting of peridotites are essential for testing these models, so our choice of bulk compositions

was guided by the available experimental data on anhydrous and hydrous melting of natural peridotites. Previous workers have used the KLB-1 composition as representative of "fertile" peridotites in both experimental studies (e.g. Falloon et al., 1999; Herzberg and Zhang, 1996; Hirose, 1997; Hirose and Kawamoto, 1995; Hirose and Kushiro, 1993; Takahashi et al., 1993) and thermodynamic modelling (e.g. Holland et al., 2018; Jennings and Holland, 2015; Xiang, 2020; Xiang and Connolly, 2022). In addition, the KR4003 composition was extensively studied between 2.5 to 7 GPa (Walter, 1998) and provides a second "fertile" bulk composition to explore. MM3, synthesized using minerals separated from a disaggregated Kilbourne Hole spinel lherzolite nodule, was first used in the melting experiments at 1 GPa by Baker and Stolper (1994) to represent primitive mantle composition and then used by Falloon et al. (1999) at experiments at 1 to 1.5 GPa. DPA was first used in the melting experiments by Mitchell and Grove (2015) to represent a bulk composition of depleted peridotite that had been metasomatized by a slab melt, approximated by adding alkalis. DP is the bulk composition we created by reducing the alkalis from Mitchell and Grove (2015) to the level of depleted peridotite from Workman and Hart (2005) to better approximate a depleted mantle composition, while still allowing comparison to the results of the DPA composition.

3.1 Pseudosection Results of KR4003

The P-T pseudosections for the KR4003 bulk composition with 0.3 wt% Fe_2O_3 with the HGP18 and TH21 models are shown in Figure 3.1 and 3.2. These results were compared with the WL22-3 "mixed model" system (Figure 3.3) to evaluate the effect of using the TH21 solid solution models and the HGP18 melt model to see which model would be better for hydrous modelling.

Table 3.2 Bulk and mineral compositions in this study

		Mode	SiO_2	TiO_2	Al_2O_3	Cr_2O_3	FeO	MnO	MgO	CaO	Na_2O	K_2O	NiO	Total	Reference
KLB-1	bulk		44.84	0.11	3.51	0.32	8.20	0.12	39.52	3.07	0.30	0.02	n.d.	100.01	Davis et al., 2009
KLB-1A	bulk		44.70	0.11	3.50	0.32	8.20		39.39	3.06	0.59	0.13		100.00	
KLB-1	ol	0.60	40.58	0.00	0.03	0.01	10.05	0.15	48.39	0.09	0.02	0.01	n.d.	99.32	Davis et al., 2009
KLB-1	opx	0.23	54.18	0.10	5.35	0.35	6.35	0.13	32.08	0.82	0.11	0.03	n.d.	99.50	Davis et al., 2009
KLB-1	cpx	0.14	51.33	0.55	7.83	0.69	3.18	0.07	14.83	19.50	1.68	0.02	n.d.	99.68	Davis et al., 2009
KLB-1	sp	0.02	0.13	0.11	59.30	8.53	11.12	0.10	20.01	0.01	0.01	0.02	n.d.	99.34	Davis et al., 2009
KR4003	bulk		44.90	0.16	4.26	0.41	8.02	0.13	37.30	3.45	0.22	0.09	0.24	99.18	Walter, 1998; Xue et al., 1990
KR4003	ol	0.49	39.80	0.02	0.02	0.00	9.85	0.12	49.61	0.11	0.00	n.d.	0.35	99.88	Luth, unpublished
KR4003	opx	0.32	54.62	0.12	4.82	0.28	6.61	0.13	32.81	0.72	0.10	n.d.	0.11	100.32	Luth, unpublished
KR4003	cpx	0.17	50.64	0.97	7.76	0.66	3.55	0.09	16.22	18.69	1.21	n.d.	0.05	99.84	Luth, unpublished
KR4003	sp	0.02	0.06	0.37	58.17	8.27	11.41	0.10	21.18	0.00	0.02	n.d.	0.39	99.97	Luth, unpublished
MM3	bulk		45.50	0.11	3.98	0.68	7.18	0.13	38.30	3.57	0.31	0.00	n.d.	99.76	Baker and Stolper, 1994
MM3	ol	0.50	40.40	-	-	0.03	9.20	0.14	49.80	0.08	-	-	0.37	100.02	Baker and Stolper, 1994
MM3	opx	0.30	54.70	0.11	4.73	0.49	5.88	0.14	32.90	0.86	0.12	-	0.10	100.03	Baker and Stolper, 1994
MM3	cpx	0.17	51.80	0.43	6.80	1.09	2.85	0.08	15.70	19.60	1.62	-	0.05	100.02	Baker and Stolper, 1994
MM3	sp	0.03	0.04	0.12	54.99	13.00	10.39	0.10	21.01	-	-	-	0.35	100.00	Baker and Stolper, 1994
DPA	bulk		44.06	0.08	2.17	0.45	8.04	0.12	42.10	1.99	0.59	0.13	0.28	100.01	Mitchell and Grove, 2015
DP0.5A	bulk		44.36	0.08	2.18	0.45	8.10		42.39	2.00	0.36	0.07		100.00	
DP	bulk		44.06	0.08	2.17	0.45	8.04	0.12	42.10	1.99	0.13	0.01	0.28	99.43	Na_2O and K_2O from Workman and Hart (2005)

n.d.=not determined; KLB-1A=KLB-1+alkalis; DP=depleted peridotite; DPA=depleted peridotite + alkalis; DP0.5A=depleted peridotite+0.5*alkalis (added for DPA);

3.1.1 HGP18

As shown in Figure 3.1, as pressure increases, the stable mineral assemblages in the subsolidus change from plagioclase lherzolite to plagioclase spinel lherzolite, spinel lherzolite, spinel-garnet lherzolite, and finally garnet lherzolite. Above 3 GPa, garnet wehrlite (g+ol+cpx) becomes stable near the solidus, reflecting the increasing solubility of orthopyroxene into clinopyroxene with increasing temperature. At pressures where spinel is stable, once melting begins, spinel disappears at lower T than clinopyroxene. I will focus on the P-T region over which spinel is stable because of the goal of determining how high-Cr spinels form. Spinel is stable in the subsolidus in peridotites up to 2 GPa and disappears ~ 80 to 120°C above the solidus in this model. Clinopyroxene disappears at temperatures ~50°C higher than spinel, leaving a harzburgite residue until orthopyroxene, then olivine dissolve into the melt at progressively higher temperatures.

3.1.2 TH21

The P-T pseudosection calculated with TH21 is shown in Figure 3.2. At 1 GPa, the solidus in is ~ 1200°C. With the increasing temperature, spinel disappears first above the solidus at around 1315°C and then reappears at 1376°C after clinopyroxene goes out at 1318°C. Orthopyroxene goes out at 1473°C before spinel goes out again at 1576°C. At 2 GPa, the solidus increases to 1375°C. Clinopyroxene goes out first above the solidus at 1431°C, followed by orthopyroxene at 1575°C. Spinel disappears after orthopyroxene at 1648°C.

Compared with the results of HGP18, the P-T pseudosection calculated for TH21 (Figure 3.2) has an expanded pressure range of spinel stability below the solidus (compare sp+ol+opx+cpx fields in Figure 3.1 and 3.2). Above the solidus, TH21 extended the upper boundary of the spinel stability area to higher pressure and temperature, from ~2.1 GPa, 1417°C to ~4.5 GPa, 1741°C. In addition, the field of spinel-garnet lherzolite expands in this model. The results above the solidus are also quite different; spinel persists ~120 to 380°C above the solidus and is stable to much higher pressure in the presence of liquid.

Other differences include the appearance of new spinel-bearing phase assemblages, such as spinel like liq+ol+opx+sp+g, a slender and narrow area in Figure 3.2, liq+ol+opx+sp, and liq+ol+sp appeared in the liq+ol+opx area from the HGP18 model. The large liq+ol+opx field in

Figure 3.1 collapses to a much smaller one, replaced with a liq+ol+opx+sp field. The intersection of the orthopyroxene-out line and the solidus increases from 3 GPa, 1508°C to 3.3 GPa, 1529°C.

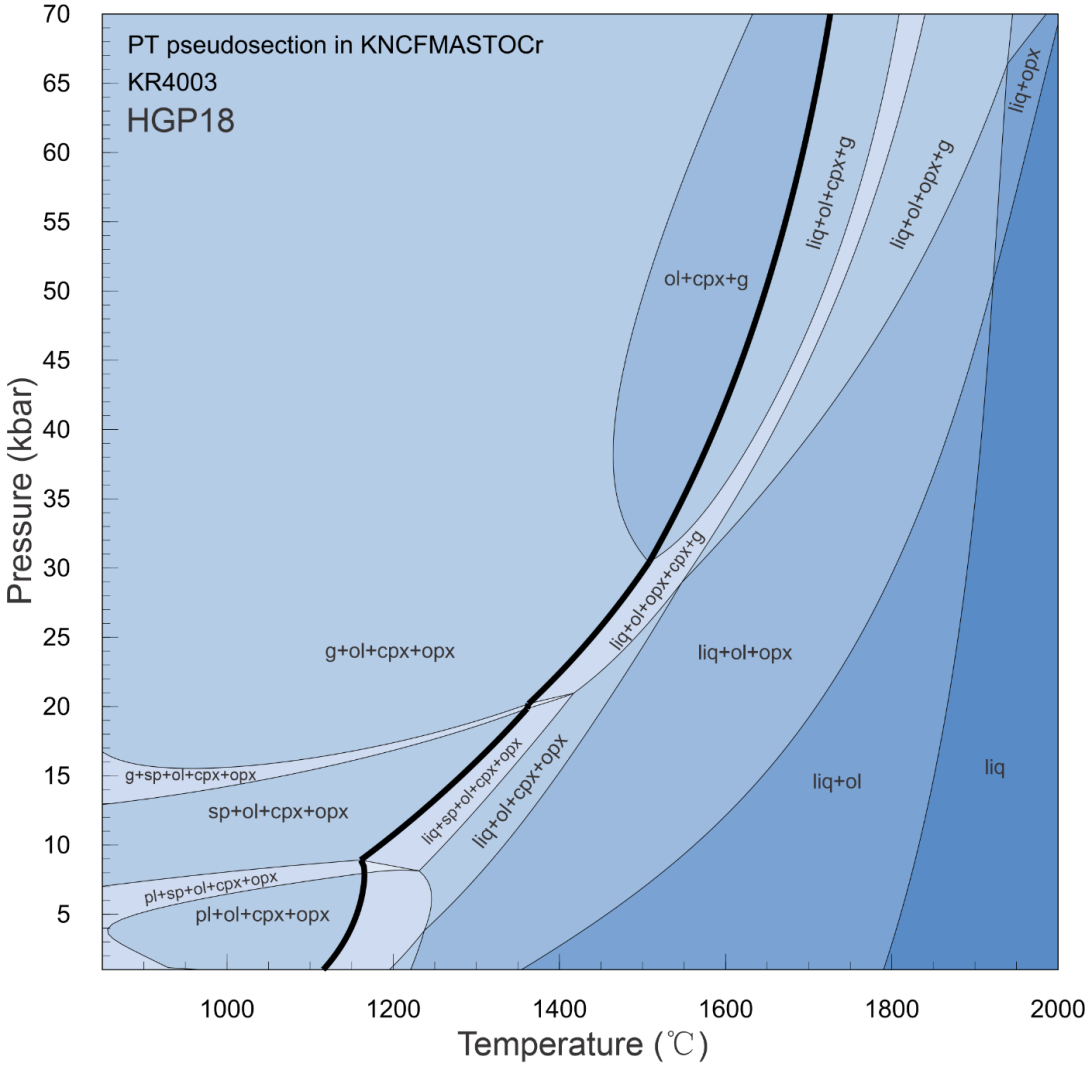

Figure 3.1 P-T pseudosection of KR4003 in KNCFMASTOCr under HGP18. The solidus is highlighted as a bold curve.

The liquidus in the TH21 model is ~50°C lower than HGP18, but the liq+ol field is much larger, especially at high pressure due to the steeper slope of the orthopyroxene-out line in the TH21 model. In the TH21 model, at <1.4 GPa, above the solidus, spinel and clinopyroxene disappear together, then spinel reappears with increasing temperature. Spinel disappears first from liq+ol+opx+cpx+sp with increasing temperature, then re-precipitates when the temperature continues to rise, and finally vanishes after the disappearance of orthopyroxene. In contrast, spinel disappears first from the same assemblage with increasing temperature without

reappearing in the HGP18 model system. These differences reflect the improvements to the TH21 model primarily because of consideration of higher-pressure data from Walter (1998) and Ionov et al. (2010). Therefore, the TH21 model should reproduce the experimental results better. Though, more experimental constraints would be welcome.

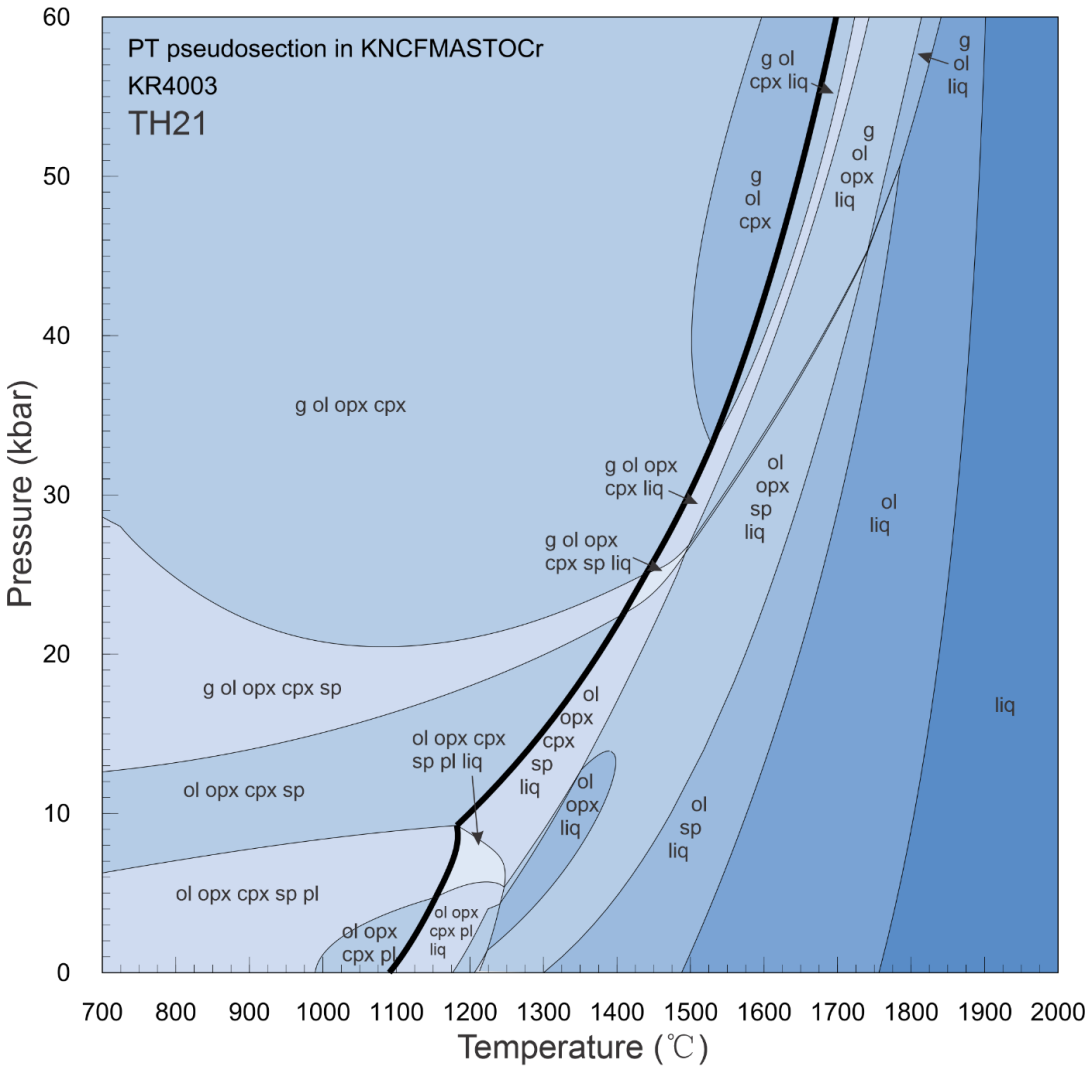

Figure 3.2 P-T pseudosection of KR4003 in KNCFMASTOCr under TH21. The solidus is highlighted as a bold curve.

3.1.3 WL22-3

As shown in Figure 3.3, the solidus of the WL22-3 model shifts to lower temperatures, but univariant lines below the solidus shows no difference with the TH21 model, which is as expected as the only difference between the two models is the melt model used. All univariant lines and invariant points above the solidus from the WL22-3 model differ from the TH21

model, illustrating the sensitivity of the results to the melt model. The temperature of clinopyroxene-out, orthopyroxene-out, and the liquidus in the WL22-3 model are higher than TH21. The spinel stability area splits into two parts in the WL22-3 model. The invariant point where both spinel and orthopyroxene disappear shifts from around 4.5 GPa, 1741°C in the TH21 model to 2.3 GPa, 1746°C in the WL22-3 model. However, the WL22-3 model is closer to the better anhydrous model, TH21, compared with HGP18, especially when considering the stability field for spinel. More experimental data at <4 GPa for KR4003 need to be obtained to compare these two models more rigorously. At the present time, however, it appears that the HGP18 melt model cannot reproduce the results of the TH21 melt model in the anhydrous system at low pressure, and we conclude that the WL22-3 combined model cannot replace TH21.

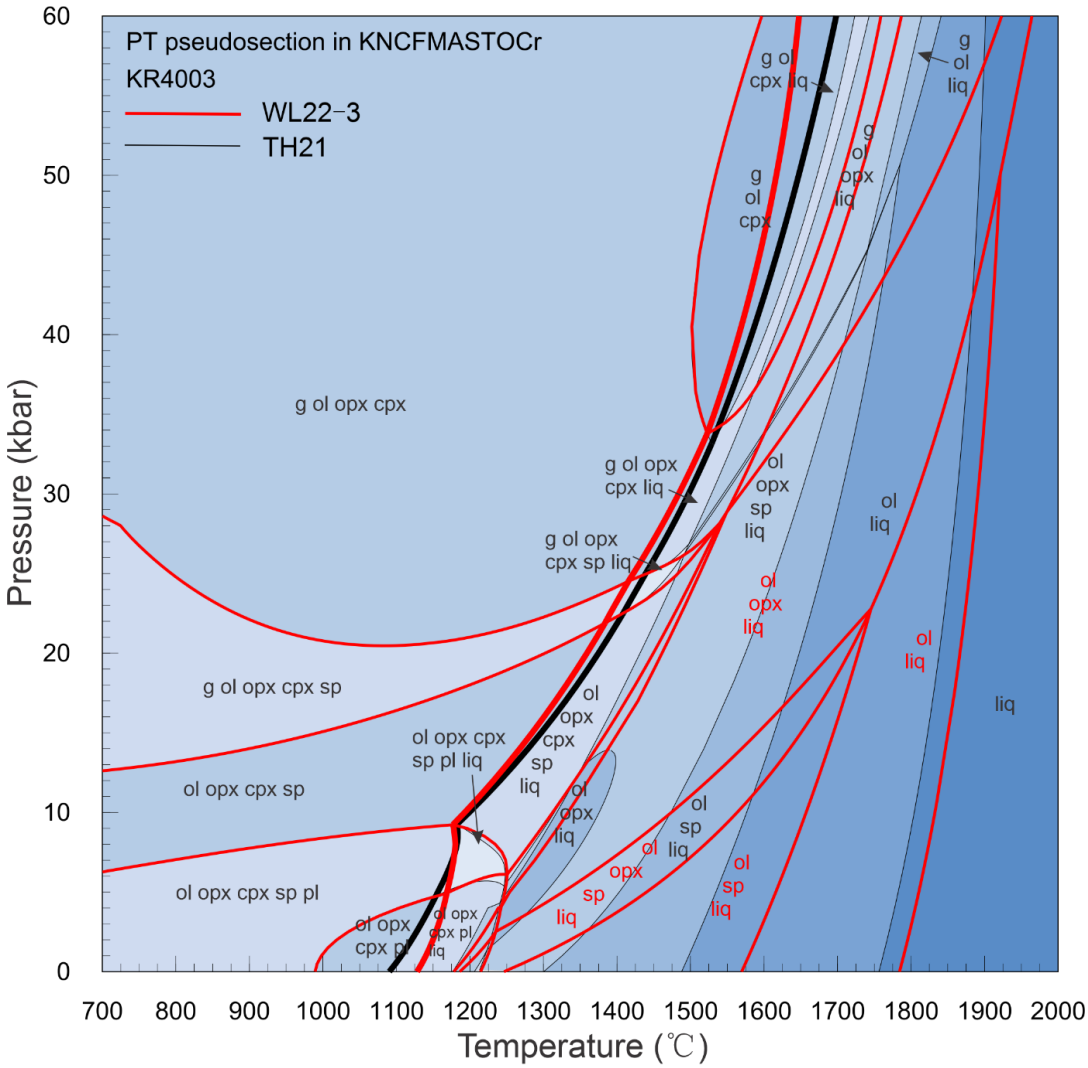

Figure 3.3 P-T pseudosection of KR4003 in KNCFMASTOCr under TH21 (black curve) and WL22-3 (red curve). The solidus is highlighted as a bold curve.

3.2 Effect of Changing Bulk Ferric Iron Content

The bulk ferric iron content of mantle peridotite is within the range of 0.1-0.4 wt% (e.g. Canil et al., 1994), and contents of 0.18 wt% and 0.3 wt% are used in Tomlinson and Holland (2021) and Holland et al. (2018), respectively. As such, I tested the TH21 model with both 0.18 wt% and 0.3 wt% bulk ferric iron content (Figure 3.4). The decrease of ferric iron content decreases the pressure and temperature of the invariant point where the orthopyroxene-out line intersects the solidus. The reduction of ferric iron also slightly reduces the range of fields of spinel stability. Overall, the change in the bulk ferric iron content seems not to have a large influence on the P-T pseudosection, or on the behavior of spinel.

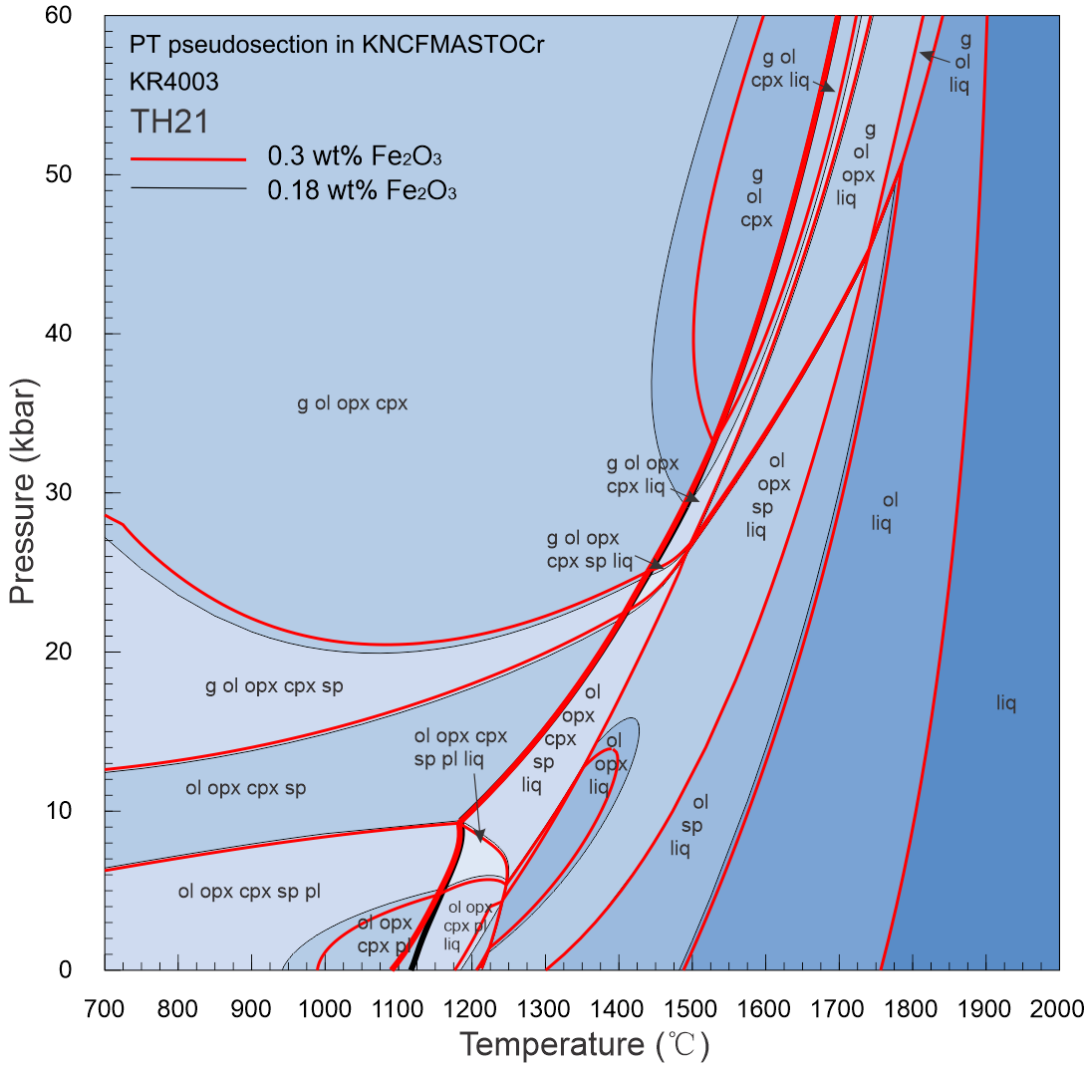

Figure 3.4 P-T pseudosection of KR4003 in KNCFMASTOCr under TH21 with 0.18 wt% (black curve) and 0.3 wt% (red curve) Fe_2O_3. The solidus is highlighted as a bold curve.

3.3 Comparison with Experimental Results: Anhydrous Melting

3.3.1 KLB-1

The differences among these versions of models are shown in section 3.1 and 3.2. To evaluate which version would be the best current option to model the peridotite system, I compared the modelling results with experimental results at the same PT conditions using the same bulk compositions.

KLB-1 has been extensively used as a spinel lherzolite xenolith from the Kilbourne Hole crater in New Mexico. I modelled the mineralogy and mineral chemistry under the same conditions as the experiments from Falloon et al. (1999) at 1 GPa. I then calculated the bulk chemical compositions of residues to compare the model and experimental results (Table 3.3). The results in Table 3.3 show that the experimental model reproduces the phase assemblages in most experiments but systematically overestimates olivine Mg# compared to experimental results. From this table, TH21 and WL22-3 are better than HGP18 in reproducing the mineralogy, especially in terms of spinel stability. However, olivine Mg# from WL22-3 is closer to the experiments (also shown in Figure 3.7). The liquids from three experiments (T-4061, T-4082B, T-4129B) from Falloon et al. (1999) were analyzed for their chemical composition. With that information, we can calculate the modal abundances of minerals through mass balance (Figure 3.5). Compared to the experimental results, the modelling results are slightly more enriched in olivine while less enriched in orthopyroxene at the same degree of melting. The results from TH21 are closer to the experimental results.

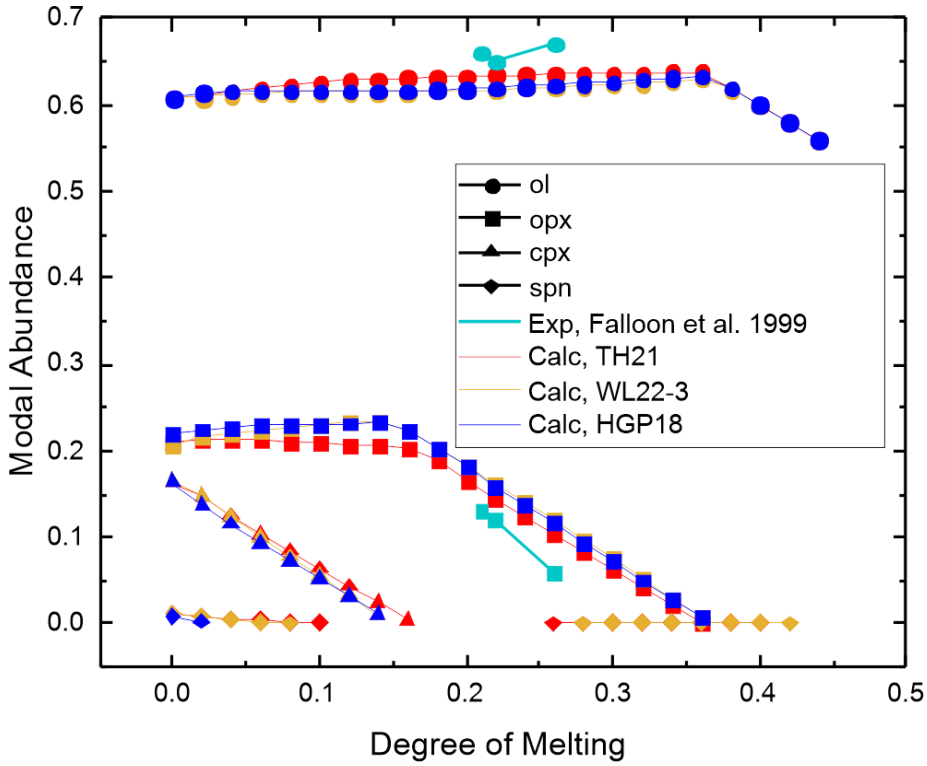

Figure 3.5 Modal abundances from melting experiments and modelling results for KLB-1 at 1 GPa. Different colours show different models and experimental results; different minerals are shown in different shapes as specified in the legend.

The chemical compositions of the residues based on the abundances and compositions of minerals from melting experiments and modelling results are shown in Figure 3.6 and 3.7. The residue compositions from modelling results show excellent agreement with experiments as a function of temperature (Figure 3.6). MgO increases with increasing temperature, while other components decrease. The residue chemistry results from the TH21 model are closer to the experimental results except for the FeO content. The results from WL22-3 and HGP18 models mostly overlap. The same trends are shown in Figure 3.7 as well, where modelling results are generally collinear with experimental results as a function of residue MgO content.

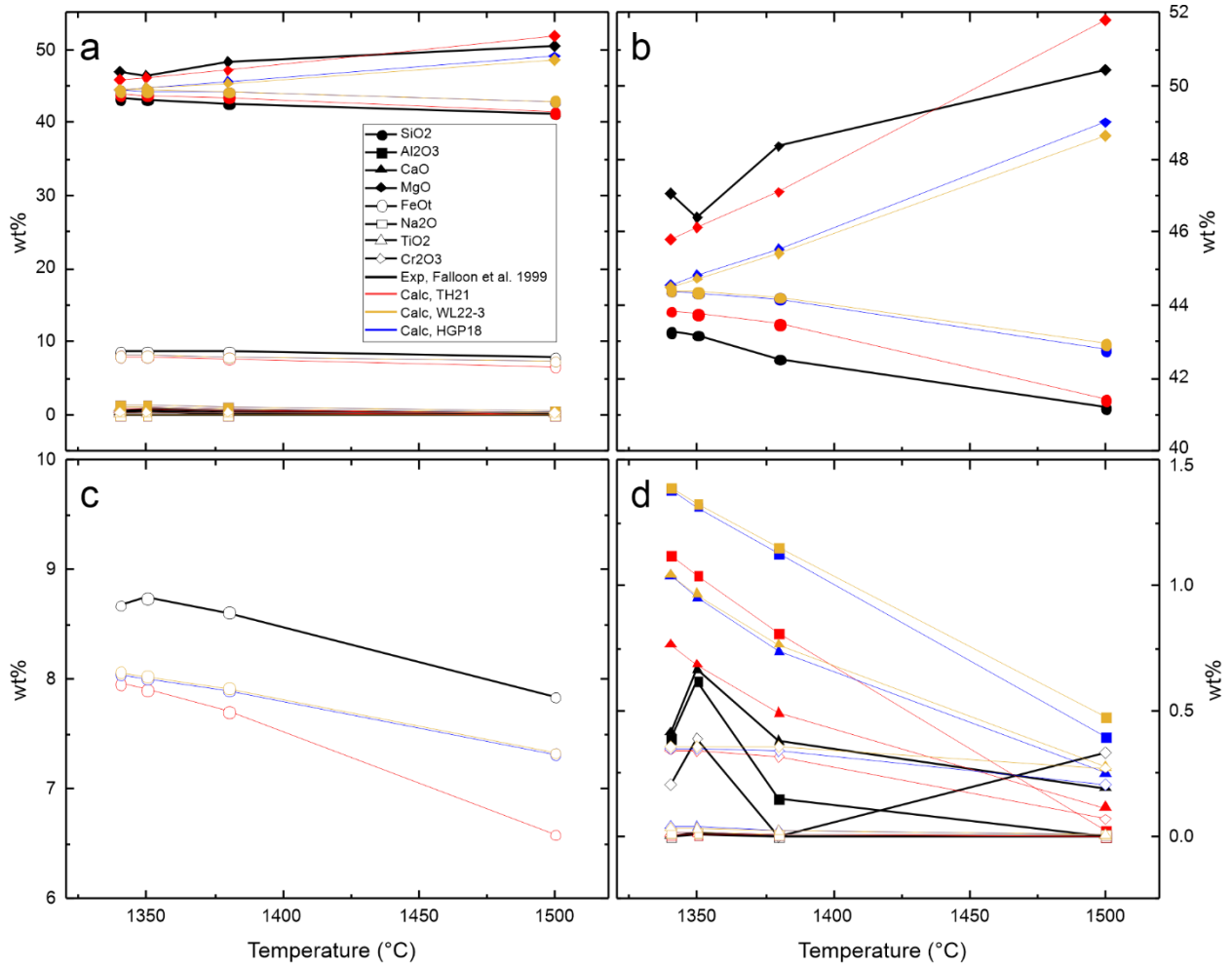

Figure 3.6 Residue compositions from melting experiments and modelling results with TH21, WL22-3, and HGP18 of KLB-1 at 1 GPa as a function of temperature. a: wt% of all components analyzed; b: SiO_2 and MgO; c: FeOt, d: Al_2O_3, CaO, Na_2O, TiO_2, Cr_2O_3. Different models and experimental results are shown in different colours; different components are shown in different shapes as specified in the legend.

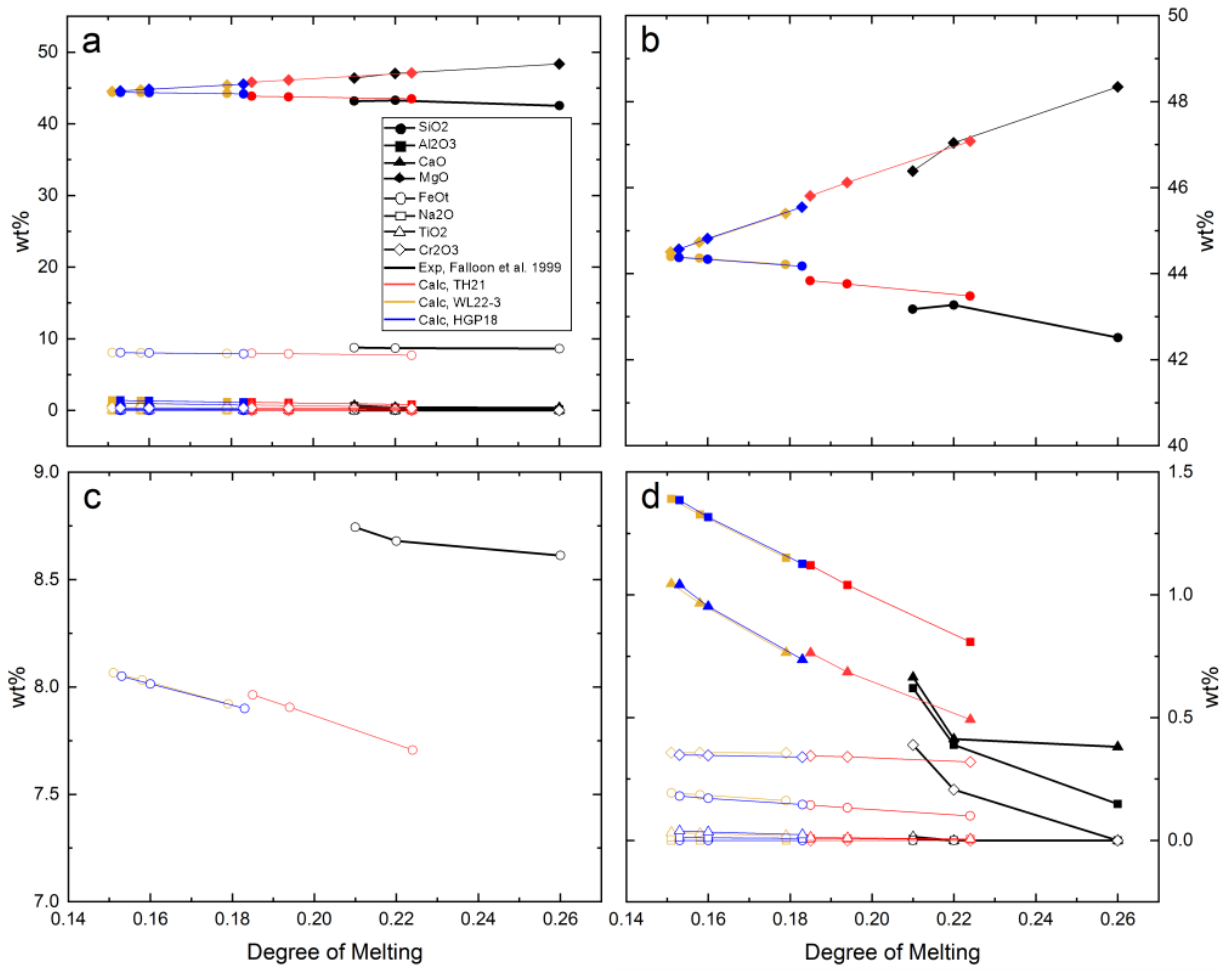

Figure 3.7 Residue compositions from melting experiments and modelling results with TH21, WL22-3, and HGP18 of KLB-1 at 1 GPa as a function of melt fraction. a: wt% of all components analyzed; b: SiO_2 and MgO; c: FeOt, d: Al_2O_3, CaO, Na_2O, TiO_2, Cr_2O_3. Different models and experimental results are shown in different colours; different components are shown in different shapes as specified in the legend.

Olivine Mg# from experimental and modelling results show the same trend (Figure 3.8), increasing with the increasing temperature. However, as stated previously, the olivine Mg# from the modelling is higher than those in the experiments.

The relationship between spinel and olivine is shown in Figure 3.9. Three experiments contain both olivine and spinel in the residue, and all concentrate at low olivine Mg#. The spinel Cr# and Mg# from TH21 and WL22-3 are closer to the experimental results.

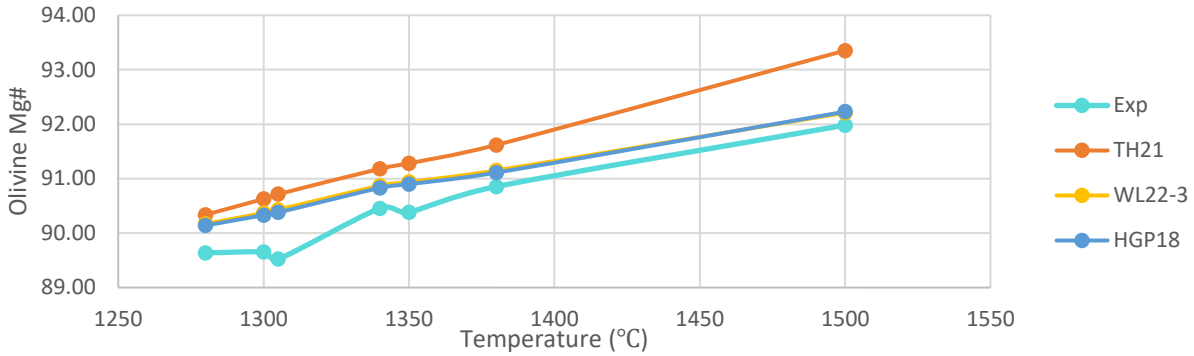

Figure 3.8 Olivine Mg# from melting experiments and modelling results. Olivine Mg# increases with temperature at 1 GPa.

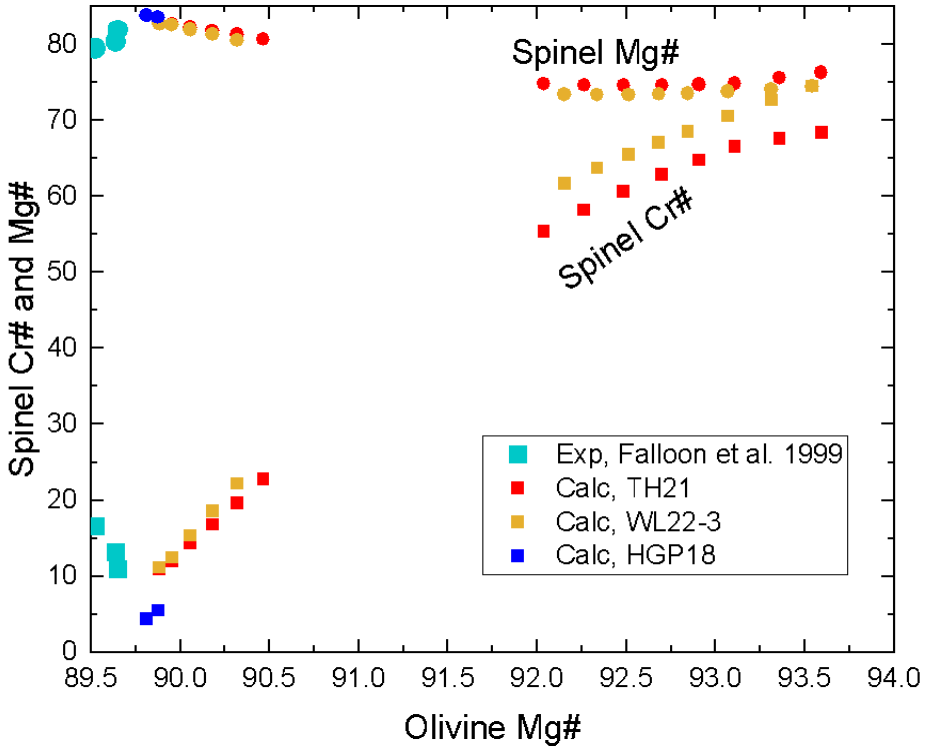

Figure 3.9 Modal abundances from melting experiments and modelling results for KLB-1 at 1 GPa. Different colours show different models as specified in the legend; spinel Cr# (square) increases with olivine Mg#; spinel Mg# (circle) decreases with olivine Mg#.

In summary, 1) TH21 performs better in modelling the phases assemblages; 2) TH21 and WL22-3 perform better in modelling spinel chemistry; 3) HGP18 has better performance in modelling the olivine Mg#; 4) TH21 has better performance in modelling the residue compositions.

Table 3.3 KLB-1 experimental and modelling results at 1 GPa

Run no.	T (°C)	Phases (Exp)	Ol Mg# (Exp)	Sp Cr# (Exp)	Phases (TH21)	Ol Mg# (TH21)	Sp Cr# (TH21)	Phases (HGP18)	Ol Mg# (HGP18)	Phases (WL22-3)	Ol Mg# (WL22-3)	Sp Cr# (WL22-3)
KLB1-10-2	1280	liq sp ol opx cpx	89.64	13.14	liq sp ol opx cpx	90.34	20.08	liq ol opx cpx	90.14	liq sp ol opx cpx	90.17	18.42
T4130	1300	liq sp ol opx cpx	89.65	10.95	liq ol opx cpx	90.63		liq ol opx cpx	90.33	liq ol opx cpx	90.37	
KLB1-10-3	1305	liq sp ol opx cpx	89.52	16.58	liq ol opx cpx	90.71		liq ol opx cpx	90.38	liq ol opx cpx	90.43	
T-4082	1340	liq ol opx	90.45		liq ol opx	91.18		liq ol opx	90.83	liq ol opx	90.87	
T-4129	1350	liq ol opx	90.38		liq ol opx	91.28		liq ol opx	90.90	liq ol opx	90.94	
T-4061	1380	liq ol opx	90.85		liq ol opx	91.62		liq ol opx	91.11	liq ol opx	91.15	
T-4173	1500	liq ol	91.98		liq spn ol	93.35	67.63	liq ol opx	92.23	liq sp ol opx	92.21	62.40

Highlighted: green = reproduced experimental phase assemblages, yellow= did not reproduce experimental results

3.3.2 MM3

MM3 is a synthetic primitive mantle composition constructed by mixing olivine, orthopyroxene, clinopyroxene, and spinel in the proportion of 0.50:0.30:0.17:0.03 (Baker and Stolper 1994). I calculated the mineralogy and mineral chemistry within the spinel stability field at 1GPa under the TH21, HGP18, and the WL22-3 model using MM3 as the bulk composition (Table A1.2) and compared them with the experimental results from Baker and Stolper (1994) and Falloon et al. (1999).

The phase assemblages, olivine Mg#, and spinel Cr# from modelling and experimental results are summarized in Table 3.4. By counting the number of experiments that matches the modelling results, we can conclude that models TH21 and WL22-3 are 30% better at modelling the phase assemblages and 3 times better at modelling the appearance of spinel than HGP18.

The modal abundances of spinel and clinopyroxene decrease with the degree of melting at first, after which orthopyroxene is consumed (Figure 3.10). The modal abundance of spinel increases slightly between clinopyroxene-out and orthopyroxene-out and then decreases in the TH21 and WL22-3 model. Modal olivine increases before orthopyroxene disappears, suggesting a peritectic melting reaction. Once orthopyroxene is consumed, olivine mode decreases as liquid abundance increases.

The compositions of the residues of partial melting using MM3 as the bulk composition and the TH21 and WL22-3 models at the PT conditions from experiments is shown in Figure 3.11, 3.12 and 3.13. Experiments from Baker and Stolper (1994) were conducted at 1 GPa, while experiments from Falloon et al. (1999) were conducted at both 1 and 1.5 GPa.

Residue compositions in the experiments and calculations generally show the same trends. Bulk rock MgO increases with increasing temperature, whereas most other oxides decrease. In detail, FeO from the TH21 and WL22-3 model are lower than in the experimental results. To assess the influence of ferric iron I used for modelling on the FeO content, I used 0.003 wt% ferric iron to compare with the results from using 0.3 wt% ferric iron under the WL22-3 model. FeO from modelling with 0.003 wt% ferric is closer to experimental results, but the change does not affect other oxides.

Table 3.4 Phase assemblages, olivine Mg#, and spinel Cr# from MM3 experimental and modelling results

Run no.	Ref	P (GPa)	T (°C)	Phases (Exp)	Ol Mg# (Exp)	Sp Cr# (Exp)	Phases (TH21)	Ol Mg# (TH21)	Sp Cr# (TH21)	Phases (HGP18)	Ol Mg# (HGP18)	Sp Cr# (HGP18)	Phases (WL22-3)	Ol Mg# (WL22-3)	Sp Cr# (WL22-3)
55T	Baker and Stolper 1994	1	1270	liq sp ol opx cpx	90.78	29.45	liq sp ol opx cpx	91.42	23.07	liq sp ol opx cpx	91.25	19.73	liq sp ol opx cpx	91.30	21.35
20	Baker and Stolper 1994	1	1270	liq sp ol opx cpx	90.71	27.98	liq sp ol opx cpx	91.42	23.07	liq sp ol opx cpx	91.25	19.73	liq sp ol opx cpx	91.30	21.35
15	Baker and Stolper 1994	1	1280	liq sp ol opx cpx	90.81	27.51	liq sp ol opx cpx	91.51	24.60	liq sp ol opx cpx	91.31	22.61	liq sp ol opx cpx	91.35	22.61
16	Baker and Stolper 1994	1	1300	liq sp ol opx cpx	90.90	36.99	liq sp ol opx cpx	91.75	28.87	liq ol opx cpx	91.47		liq sp ol opx cpx	91.50	25.95
24	Baker and Stolper 1994	1	1330	liq sp ol opx cpx	91.28	49.77	liq sp ol opx	92.33	39.88	liq ol opx cpx	91.82		liq sp ol opx cpx	91.86	33.94
21	Baker and Stolper 1994	1	1350	liq sp ol opx	91.42	56.17	liq sp ol opx	92.54	44.58	liq ol opx	92.11		liq sp ol opx	92.17	40.91
22	Baker and Stolper 1994	1	1360	liq sp ol opx	91.52	57.09	liq sp ol opx	92.66	46.71	liq ol opx	92.18		liq sp ol opx	92.25	42.86
26	Baker and Stolper 1994	1	1390	liq sp ol opx	92.09	58.57	liq sp ol opx	92.90	50.69	liq ol opx	92.41		liq sp ol opx	92.47	48.06
T-4243	Falloon et al. 1999	1	1400	liq ol opx	92.35		liq sp ol opx	93.16	54.43	liq ol opx	92.49		liq sp ol opx	92.55	49.61
T-4330	Falloon et al. 1999	1	1440	liq ol opx	92.23		liq sp ol opx	93.80	61.70	liq ol opx	92.82		liq sp ol opx	92.87	55.22
T-4264	Falloon et al. 1999	1	1450	liq ol	93.14		liq sp ol opx	93.98	63.53	liq ol opx	92.91		liq sp ol opx	92.96	56.52
T-4335	Falloon et al. 1999	1.5	1425	liq sp ol opx	91.56	47.38	liq sp ol opx	92.82	46.30	liq ol opx	92.23		liq sp ol opx	92.29	42.03
T-4309	Falloon et al. 1999	1.5	1500	liq ol opx	92.31		liq sp ol opx	94.02	60.75	liq ol opx	92.88		liq sp ol opx	92.93	53.86
T-4333	Falloon et al. 1999	1.5	1525	liq ol	92.98		liq sp ol opx	94.57	65.76	liq ol opx	93.13		liq sp ol opx	93.17	57.26
T-4326	Falloon et al. 1999	1.5	1550	liq ol	93.17		liq sp ol	94.89	67.92	liq ol opx	93.39		liq sp ol opx	93.42	60.52

Highlighted: green = reproduced experimental phase assemblages, yellow= did not reproduce experimental result

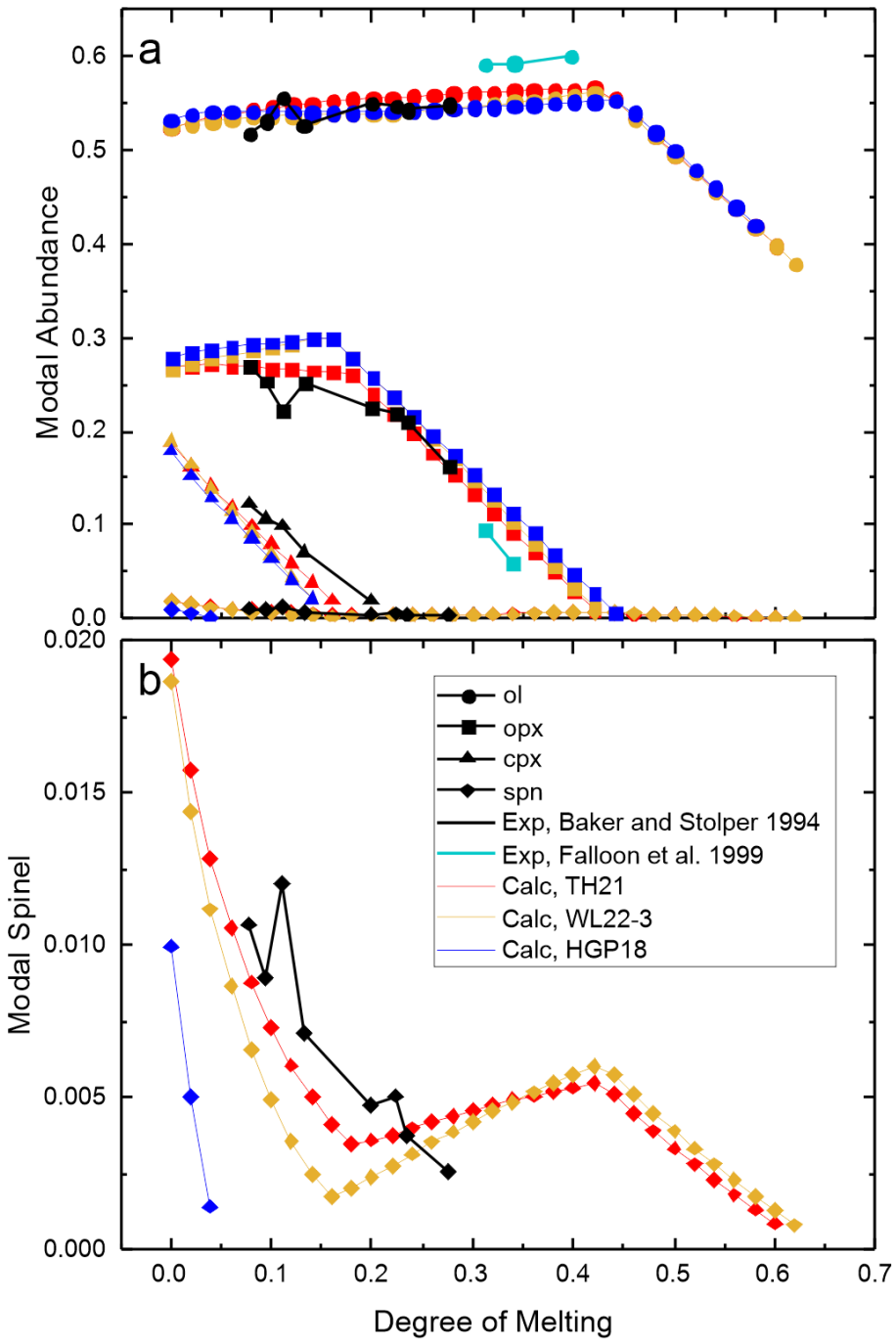

Figure 3.10 Modal abundances as a function of degree of melting, derived from melting experiments and modelling results of MM3 at 1 GPa. a: modal abundance of all minerals in residue; b: Modal spinel. Different colours show different models; different minerals are shown in different shapes as specified in the legend.

To compare with trends observed in experimental samples, I plotted both experimental and theoretical residue compositions against MgO (Figure 3.12). The trends in the chemical

compositions of the residues from the TH21 and WL22-3 models are consistent with the experimental results.

I calculated spinel Cr#, Mg# and olivine Mg# as a function of the degree of melting (Figure 3.14). Spinel Cr# increases with the degree of melting, while spinel Mg# decreases slightly and then increases. The calculated results for the TH21 and WL22-3 models are more consistent with spinel behaviour in the experiments, with spinel remaining a residual phase to high degrees of melting (>60%). In contrast, model HGP18 results predict that spinel is exhausted rapidly, before 5% melting, an outcome that would predict that spinel would be a rarity in natural peridotites, which it is not. The trends of olivine Mg# from modelling lead to higher Mg# at a given melting degree than experimental results, with similar values from the different models.

I also looked at the relationship between spinel Cr# and olivine Mg# from the TH21 and WL22-3 model and experiments (Figure 3.15). Spinel Cr# consistently increases with Olivine Mg# in both the experiments and the calculations, but the olivine Mg# is higher in the modelled results than in the experiments. Models with 0.003 wt% ferric iron have the lowest olivine Mg#, closest to the experimental results than the WL22-3 model with 0.3 wt% ferric iron.

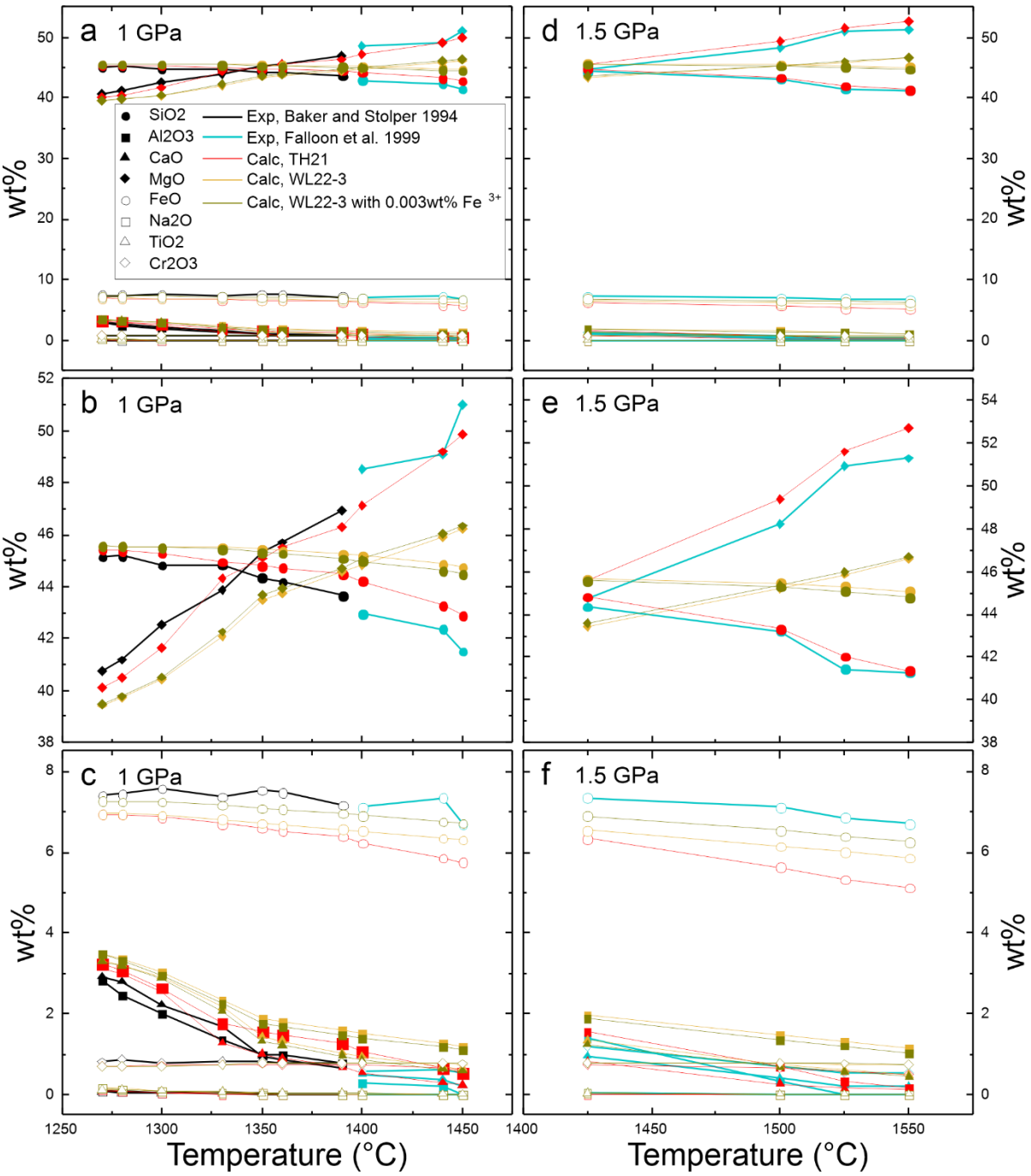

Figure 3.11 Residue compositions from melting experiments and modelling results of MM3 at 1 (a, b, c) and 1.5 (d, e, f) GPa as a function of temperature.
a, d: wt% of all oxide components; b, c, e, f: expanded view. Different models and experimental results are shown in different colours; different components are shown in different shapes as specified in the legend.

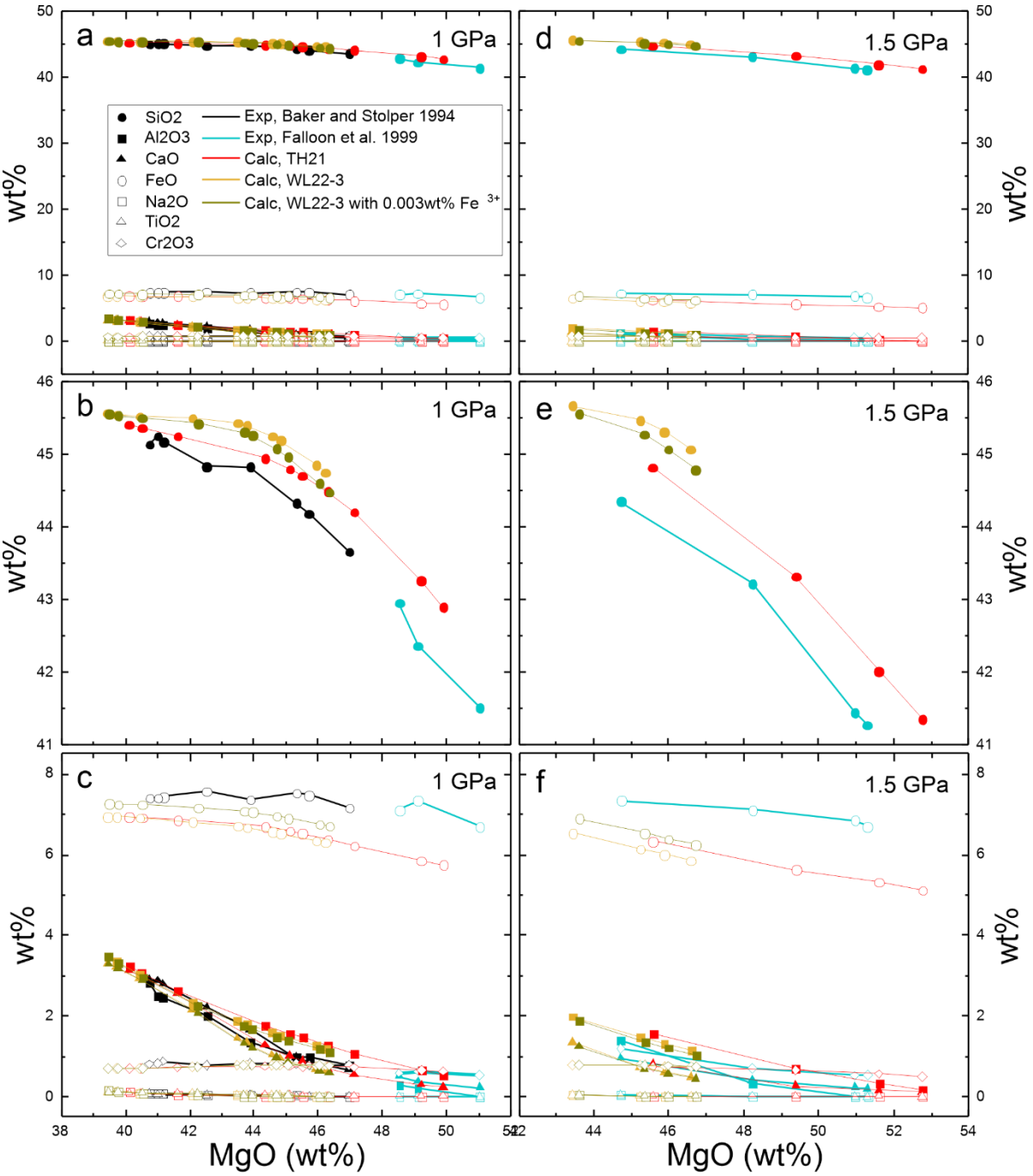

Figure 3.12 Residue compositions from melting experiments and modelling results of MM3 at 1 (a, b, c) and 1.5 (d, e, f) GPa as a function of MgO content in the residue. a, d: wt% of all oxide components; b, c, e, f: expanded view. Different colours show different models and experimental results; different components are shown in different shapes as specified in the legend.

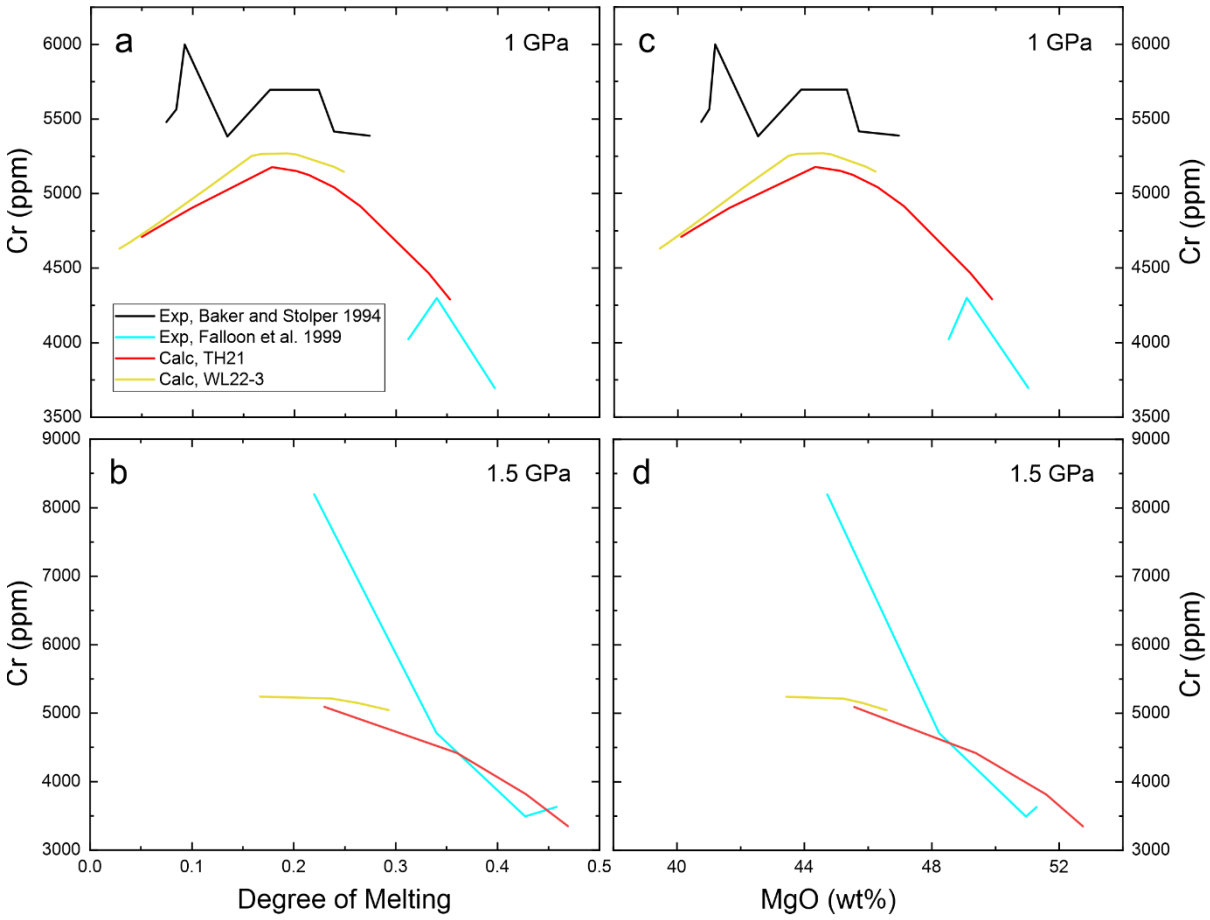

Figure 3.13 Residue Cr from melting experiments and modelling results of MM3 at 1 and 1.5 GPa as a function of melt fraction (a, b) and MgO (c, d). Different line colours show different models and experimental results.

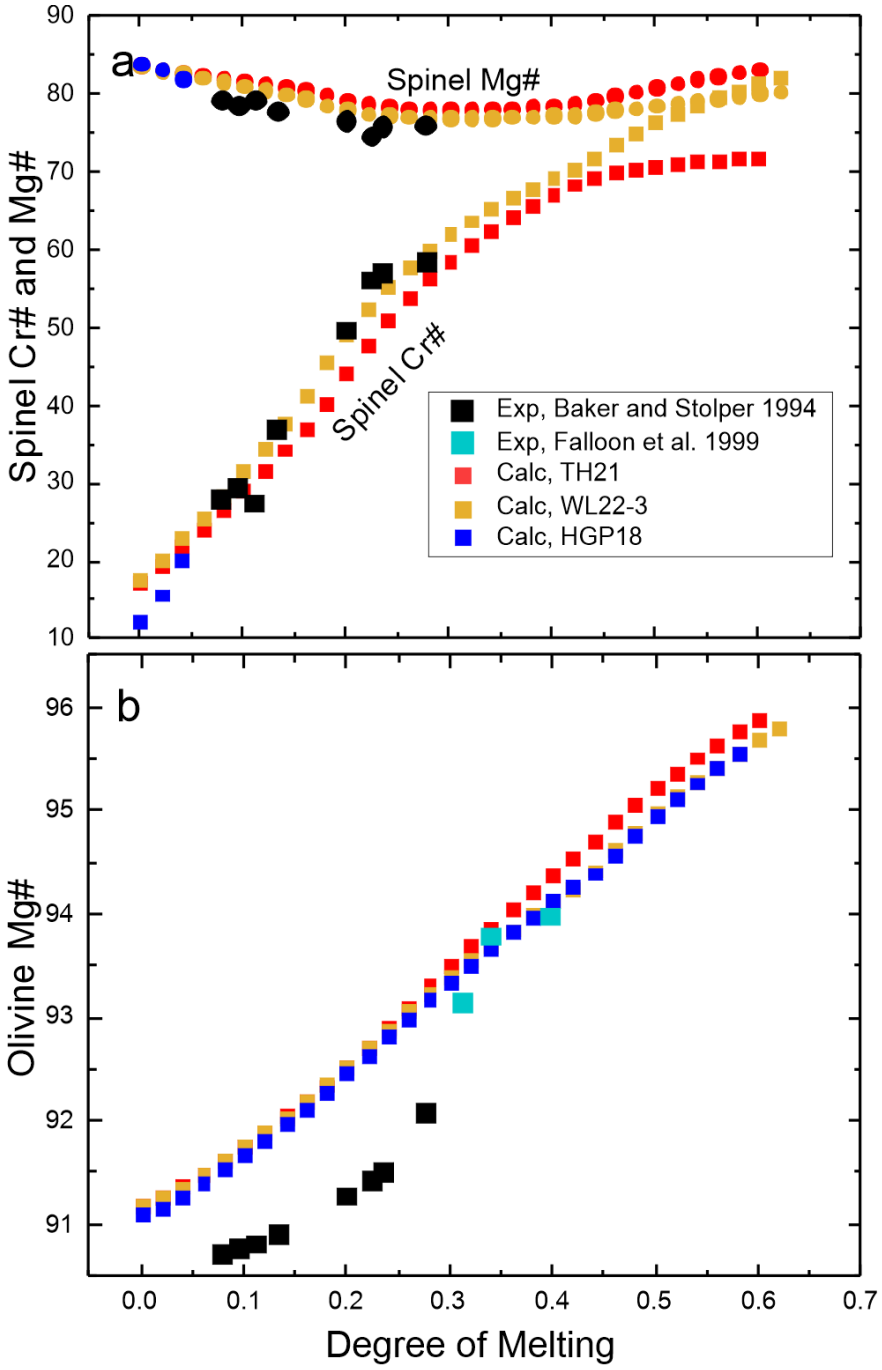

Figure 3.14 Spinel Cr# and Mg# (a), and olivine Mg# (b) from melting experiments and modelling results of MM3 at 1 GPa. Different models and experimental results are shown in different colours as specified in the legend; olivine Mg# and spinel Cr# (square) increases with melting; spinel Mg# first decreases slightly then increases with melting in the general form of parabola.

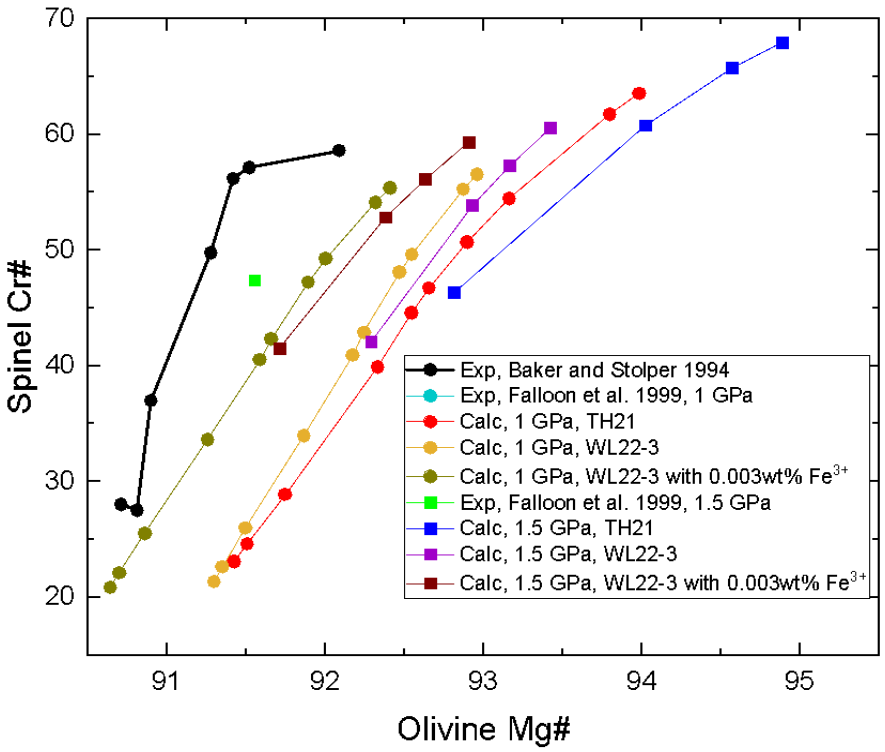

Figure 3.15 Spinel Cr# variation with olivine Mg# from melting experiments and modelling results of MM3 at 1 (curves with circles) and 1.5 (curves with squares) GPa. Spinel Cr# increases with olivine Mg#. Different models and experimental results are shown in different colours as specified in the legend.

3.3.3 KR4003

Another test of the thermodynamic models comes from the mineral chemistry of the natural KR4003 xenolith (Walter, 1998; Xue et al., 1990) – the starting composition for key melting experiments that are used to constrain the thermodynamic models. Can the models reproduce the mineral chemistry of this xenolith?

At an assumed pressure of 1.5 GPa, the 2-pyroxene thermometer of Taylor (1998) gives a result of 1092°C for the natural peridotite KR4003. At 1092°C, the mineral Cr# and modal abundances calculated through mass balance are very close to our modelling results as discussed in detail in Chapter 4 (Figure 4.5, 4.6). The clinopyroxene and orthopyroxene Cr# and the olivine Mg# (Figure 4.6) for the natural sample are slightly higher than the modelling results, while the spinel Cr# is lower by ~10%. The calculated modal orthopyroxene for the natural sample is slightly higher than the modelling result, while modal olivine is lower by ~5%. The contribution of each

mineral to the bulk Al_2O_3 concentrations in the natural KR4003 sample generally agrees with the modelling results (Figure 4.7). The contribution of clinopyroxene to the bulk Cr_2O_3 concentrations in the natural KR4003 sample, however, is about double that of the calculated result. The contribution of orthopyroxene and spinel to the bulk Cr_2O_3 generally agrees with the calculation results.

3.4 Comparison with Experimental Results: Hydrous Melting

3.4.1 KLB-1

The WL22-3 model was used for most of these calculations because it used the most up-to-date solid solution models, especially for spinel. I compared modelling results to experimental data to test how well the model reproduces experimental results.

Unfortunately, there are limited experimental studies of hydrous melting of peridotite with sufficient analytical data to test our models against. Hirose (1997) and Hirose and Kawamoto (1995) studied hydrous melting of KLB-1, and I compared our modelling results to their experimental data (experimental and modelling conditions see Figure 3.16 and Table 3.5). The degree of melting in the models and these experiments generally agree within 6%, except for two experiments with a much larger deviation. Mineral assemblages in the experiments had spinel, but the model failed to predict spinel for nearly half of the experimental data points. Only one modelling result, with the addition of 0.2 wt% water, has very close spinel Cr# and Mg# (deviations less than 2 in absolute value). In general, we consider that the current thermodynamic model for wet melting of peridotite does not simulate the observed changes in modal mineralogy during partial melting of a hydrous lherzolite, which prevents its use in exploring how spinel chemistry, in particular, evolves during melting.

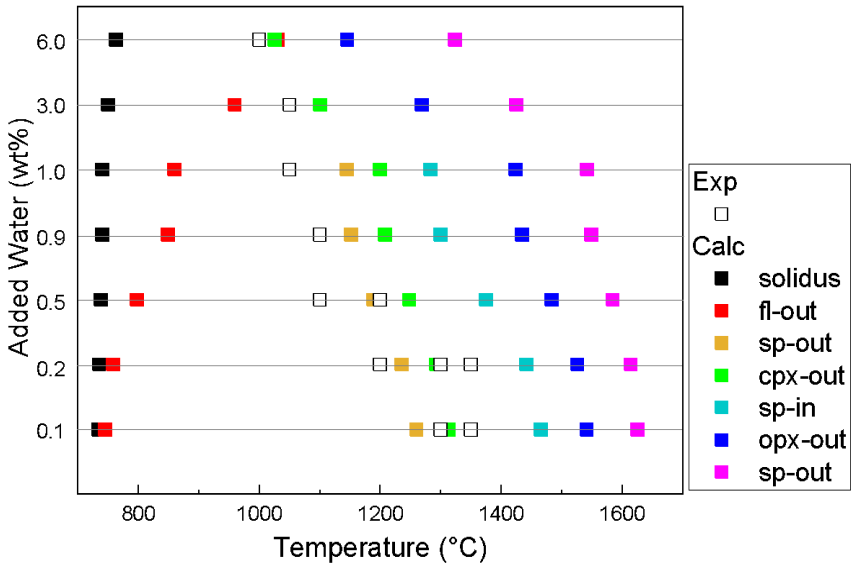

Figure 3.16 The experimental conditions and mineral-out conditions from modelling. The experimental conditions are shown as black hollow squares. The disappearance/appearance of phases from the residue is shown by the different colours of solid squares as specified in the legend.

Table 3.5 The phase assemblage and spinel Mg#, Cr#, and olivine Mg# for hydrous melting experiments and modelling of KLB-1 at 1 GPa

Added H_2O wt%	T (°C)	Methods	Phases	Liquid mode	Sp Mg#	Sp Cr#	Ol Mg#
0.1	1300	Exp	liq sp ol opx cpx	0.178	75.98	42.58	91.71
		Calc	liq ol opx cpx	0.138			91.01
	1350	Exp	liq sp ol opx	0.296	76.55	55.67	91.89
		Calc	liq ol opx	0.180			91.38
0.2	1200	Exp	liq sp ol opx cpx	0.124	80	17.54	90.48
		Calc	liq sp ol opx cpx	0.079	81.24	19.59	90.52
	1300	Exp	liq sp ol opx cpx	0.218	76.37	56.84	91.72
		Calc	liq ol opx	0.169			91.21
	1350	Exp	liq sp ol opx	0.380	75.94	69.47	92.86
		Calc	liq ol opx	0.200			91.51
0.5	1100	Exp	liq sp ol opx cpx	0.070	77.17	11.46	89.56
		Calc	liq sp ol opx cpx	0.082	81.29	17.18	90.43
	1200	Exp	liq sp ol opx	0.201	74.15	58.85	92.13
		Calc	liq ol opx cpx	0.141			90.86
0.9	1100	Exp	liq sp ol opx cpx	0.134	72.55	34.46	90.15
		Calc	liq sp ol opx cpx	0.129	79.37	23.63	90.64
1	1050	Exp	liq sp ol opx cpx	0.158	69.39	31.45	
		Calc	liq sp ol opx cpx	0.114	80.23	19.59	90.50
3	1050	Exp	liq sp ol opx cpx	0.221	60.26	64.12	
		Calc	liq sp ol opx cpx	0.262	72.32	41.91	91.10
6	1000	Exp	liq sp ol cpx	0.230	60.20	66.65	
		Calc	liq fl sp ol opx cpx	0.290	70.66	44.52	91.11

3.4.2 Mitchell and Grove 2015 & 2016

Mitchell and Grove conducted a series of hydrous melting experiments in two articles (Mitchell and Grove, 2015; Mitchell and Grove, 2016). We tested the WL22-3 model by attempting to replicate their results. I also compared the WL22-3 model with PMELTS.

3.4.2.1 Compare WL22-3 with PMELTS

I calculated the mineralogy and mineral abundances for the experimental conditions of Michell and Grove (2015) using THERMOCALC and PMELTS and compared the modelling results with the experiments (Table 3.6, Table A2.2).

In general, the mineralogy predicted by THERMOCALC with WL22-3 is much closer to the experimental results than that from PMELTS (Table 3.6), but reproduces the experimental mineral assemblage in only 7 out of 17 experiments. Comparing the chemical compositions of the melts predicted by the two models with the experimental results demonstrates that neither model reproduces the chemical compositions of the melts (Table A2.2).

Table 3.6 The mineral assemblages from experiments, WL22-3, and PMELTS under the conditions from Mitchell and Grove (2015)

No.	P (GPa)	T (°C)	Mix*	Mineral assemblage-Experiment	Mineral assemblage-WL22-3	Mineral assemblage-PMELTS
C507	1	1215	E	liq ol opx cpx	liq spn ol	liq ol
C508	1	1235	E	liq ol opx	liq spn ol	liq ol
C494	1	1235	D	liq ol opx cpx	liq spn ol opx	liq ol
C490	1	1235	D	liq spn ol opx	liq spn ol opx	liq ol
C498	1	1250	B	liq spn ol opx	liq spn ol opx	liq spn ol
C561	1.2	1135	E	liq spn ol opx	liq spn ol opx	liq spn ol
C555	1.2	1170	E	liq spn ol opx	liq spn ol opx	liq ol
C554	1.2	1185	E	liq spn ol opx	liq spn ol opx	liq ol
C553	1.2	1215	E	liq ol spn	liq spn ol opx	liq ol
C559	1.2	1250	E	liq ol spn	liq spn ol opx	liq ol
C470	1.2	1295	C	liq ol opx	liq spn ol opx	liq spn ol
C481	1.2	1335	A	liq ol opx cpx	liq ol opx cpx	liq spn ol opx cpx
C471	1.2	1363	A	liq ol opx	liq ol opx cpx	liq spn ol opx cpx
C473	1.6	1340	C	liq ol opx	liq spn ol opx	liq spn ol
C463	1.6	1380	B	liq ol opx	liq ol opx	liq spn ol opx
C474	1.6	1420	A	liq ol opx	liq spn ol opx	liq spn ol opx cpx
C465	2	1470	A	liq ol opx	liq spn ol opx	liq spn ol opx cpx

*Starting materials, see Mitchell and Grove (2015)

Highlighted: green = reproduced experimental phase assemblages, yellow= did not reproduce experimental results

3.4.2.2 Residue Composition

To explore if there were other areas of agreement between the models and the experiments, I analyzed the relationship between spinel Cr# and olivine Mg# for modelling and experimental results of Mitchell and Grove (2015, 2016) (Figure 3.17). The model predicts slightly higher olivine Mg# relative to the experimental results. The spinel Cr# predicted by the model fails to reproduce the experimental results. Only four modelling results for the conditions of Mitchell and Grove (2016) generate spinel compared with ten in experiments, and the modelling results have lower spinel Cr# and higher olivine Mg# than the experiments.

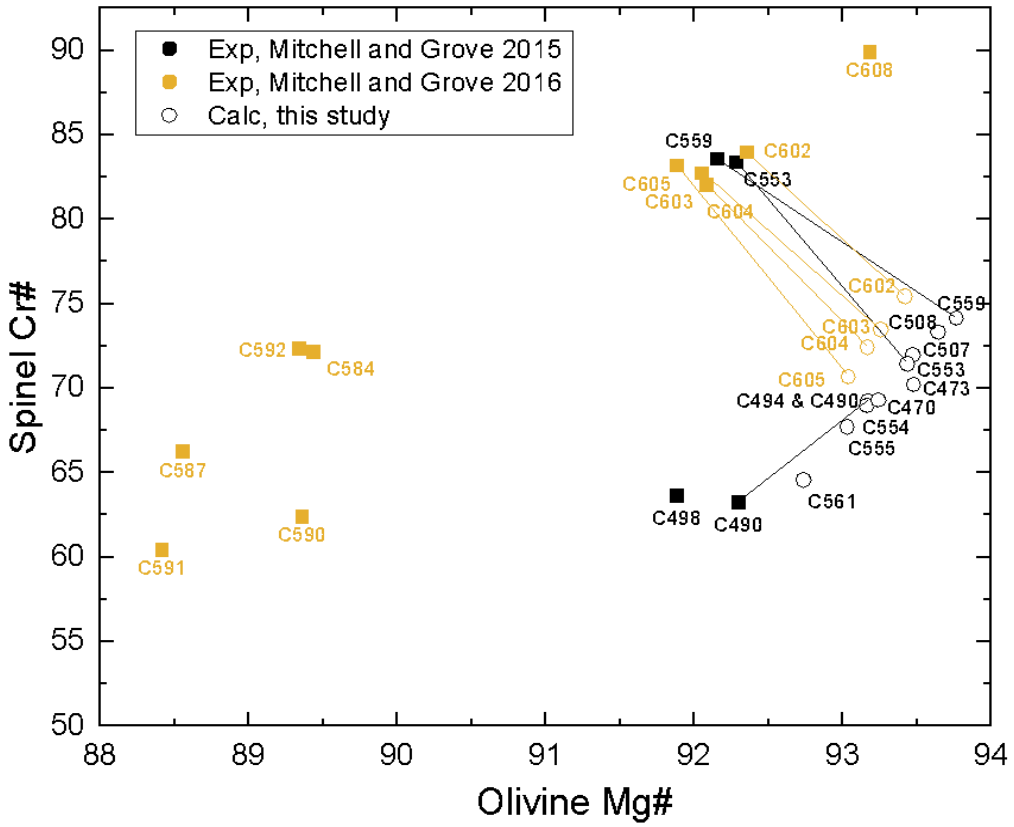

Figure 3.17 The relationship of spinel Cr# and olivine Mg# from modelling and experimental results under the conditions from Mitchell and Grove (2015, 2016). Results from different experimental studies and modelling results are shown by different symbols as specified in the legend. Corresponding experimental and modelling conditions are connected by lines.

The residue compositions from modelling and experimental results under the WL22-3 model are shown in Figure 3.18. The modelling results for conditions from Mitchell and Grove (2016) have a wider range of MgO content, higher SiO_2 and Al_2O_3 content, and lower CaO and FeO content

than the experimental results. As discussed in 3.2, the lower contents of FeO in the modelling results are because the ferric iron content is considered in our models. The modelling results for the conditions from Mitchell and Grove (2015) are much closer to the experimental results than from Mitchell and Grove (2016).

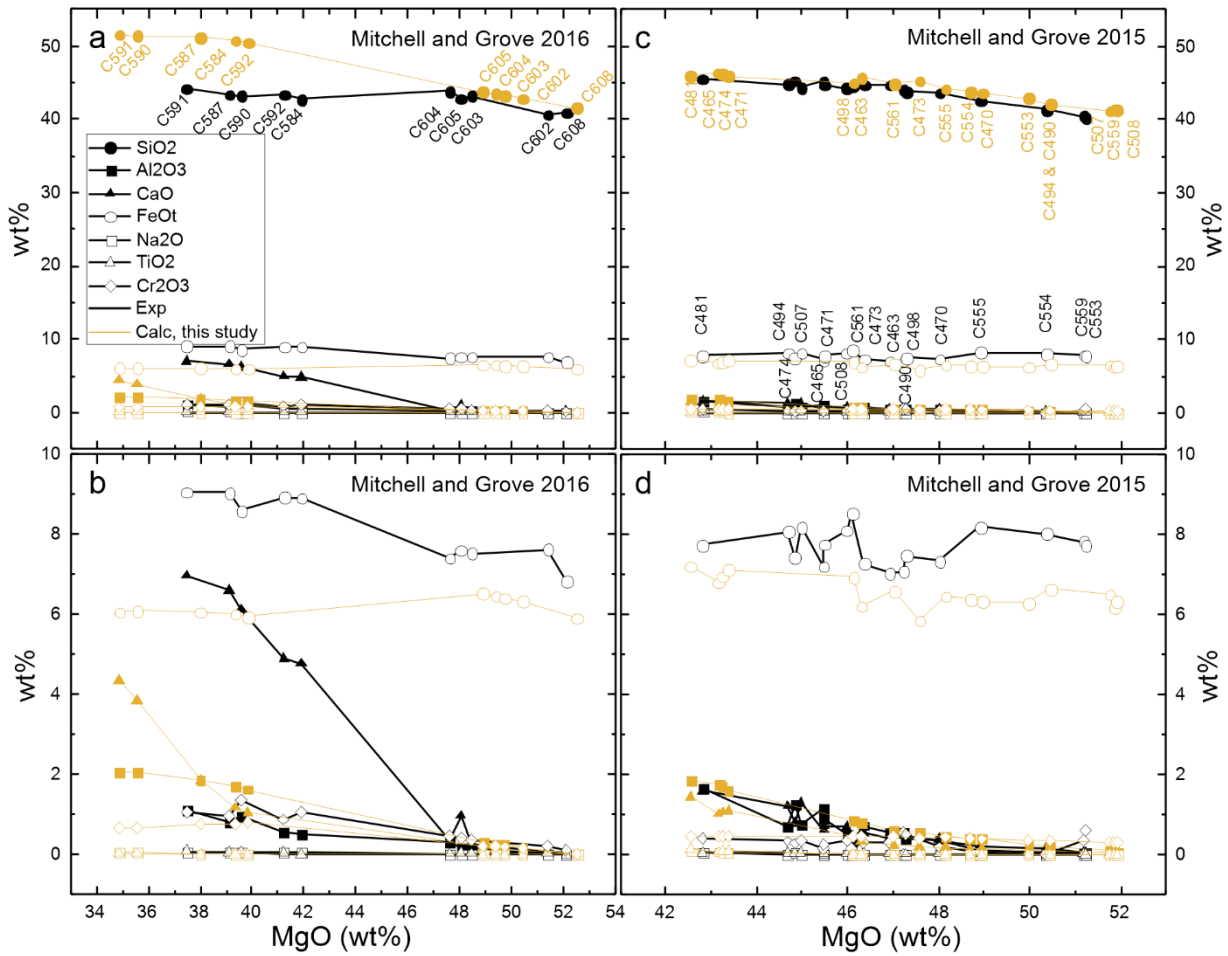

Figure 3.18 Residue compositions from modelling and experimental results under the conditions from Mitchell and Grove 2015 (c, d) and 2016 (a, b). a,c: wt% of all oxide components; b, d: expanded view. Modelling and experimental results are shown in different colours with the text of the experiment number on the line; different components are shown in different shapes as specified in the legend.

3.4.2.3 Influence of Water

As shown in Section 3.4.2.2, the WL22-3 hydrous model cannot reproduce experimental results from the Mitchell and Grove studies (2015, 2016). To determine whether varying the water content of the bulk composition can explain these discrepancies, I modelled the experiments from Mitchell and Grove (2016), but with only half the water contents compared with those

reported for the experiments. The phase assemblages from modelling and experimental results are shown in Table 3.7. Neither the calculations with the original or half water contents can reproduce the mineralogy from the melting experiments.

The results for the residue compositions are similar to those of the original modelling results except for the lower MgO contents (Figure 3.19). The higher water contents of liquids for the modelling results compared to the experimental results may reflect water loss from the experiments. The calculated water contents in the liquids for the models with half water contents are much closer to the experiments (Figure 3.20). As expected, reducing the water content decreases the melt amount and, therefore, sympathetically increases the modal abundances of the residual minerals (Figure 3.21a). If we only focus on the residual mineralogy, the relative modal abundances of the olivine for the models with half the water contents are smaller by ~10% than those with original water contents. The modal abundances of orthopyroxene and clinopyroxene are higher (Figure 3.21b). The main reason for the lower residual MgO contents is the higher modal abundances of the orthopyroxene and clinopyroxene for the models with half water contents. In conclusion, modelling with half amount of water cannot reduce the difference between hydrous experiments and modelling results.

Table 3.7 The mineral assemblages from experiments and WL22-3 under the conditions from Mitchell and Grove (2016) and with half bulk water content

Exp	P	T	Mix*	Added H_2O (wt%)	Phases (Exp)	Phases (Calc)	Phases (Calc with half water)
C608	1.2	1240	A	5.00	liq ol sp	liq ol	liq ol opx
C602	1.2	1180	B	5.00	liq ol sp	liq ol opx sp	liq ol opx
C603	1.2	1160	B	4.86	liq ol opx sp	liq ol opx sp	liq ol opx
C604	1.2	1140	B	5.01	liq ol opx sp	liq ol opx sp	liq ol opx
C605	1.2	1120	B	4.98	liq ol opx cpx sp	liq ol opx sp	liq ol opx
C584	1.2	1120	C	8.60	liq ol opx cpx sp	liq ol opx	liq ol opx cpx
C592	1.2	1120	C	9.26	liq ol opx cpx sp	liq ol opx	liq ol opx cpx
C587	1.2	1100	C	8.71	liq ol opx cpx sp	liq ol opx cpx	liq ol opx cpx
C590	1.2	1080	C	8.31	liq ol opx cpx sp	liq ol opx cpx	liq ol opx cpx
C591	1.2	1060	C	9.17	liq ol opx cpx sp	liq ol opx cpx	liq ol opx cpx

*Starting materials, see Mitchell and Grove (2015)

Highlighted: green = reproduced experimental phase assemblages, yellow= did not reproduce experimental results

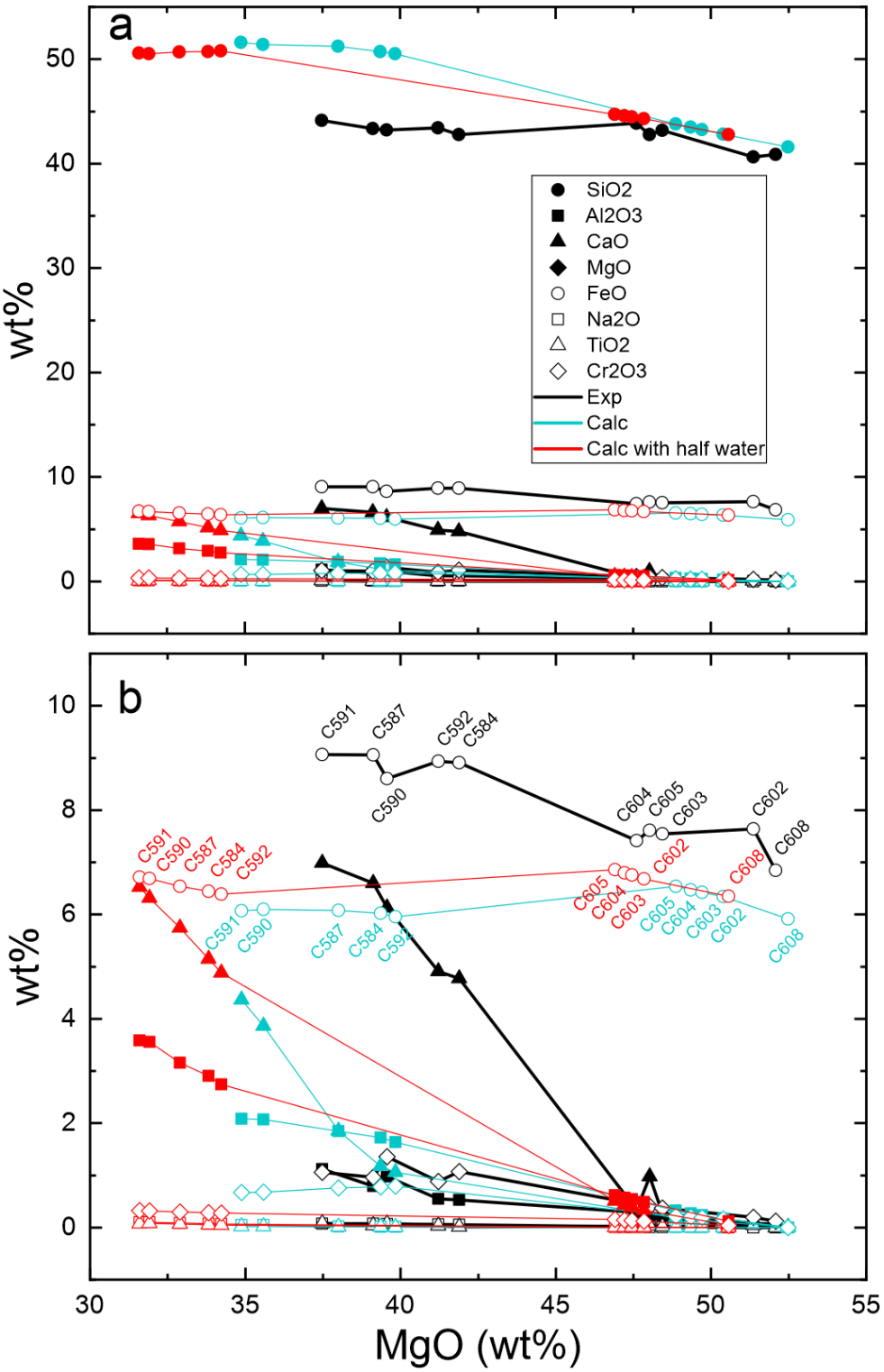

Figure 3.19 Residue compositions from modelling results with different water contents and the experimental results from Mitchell and Grove (2016). a: wt% of all oxide components; b: expanded view. Models with different water contents and experimental results are shown in different colours with the text of the experiment number on the line; different components are shown in different shapes as specified in the legend.

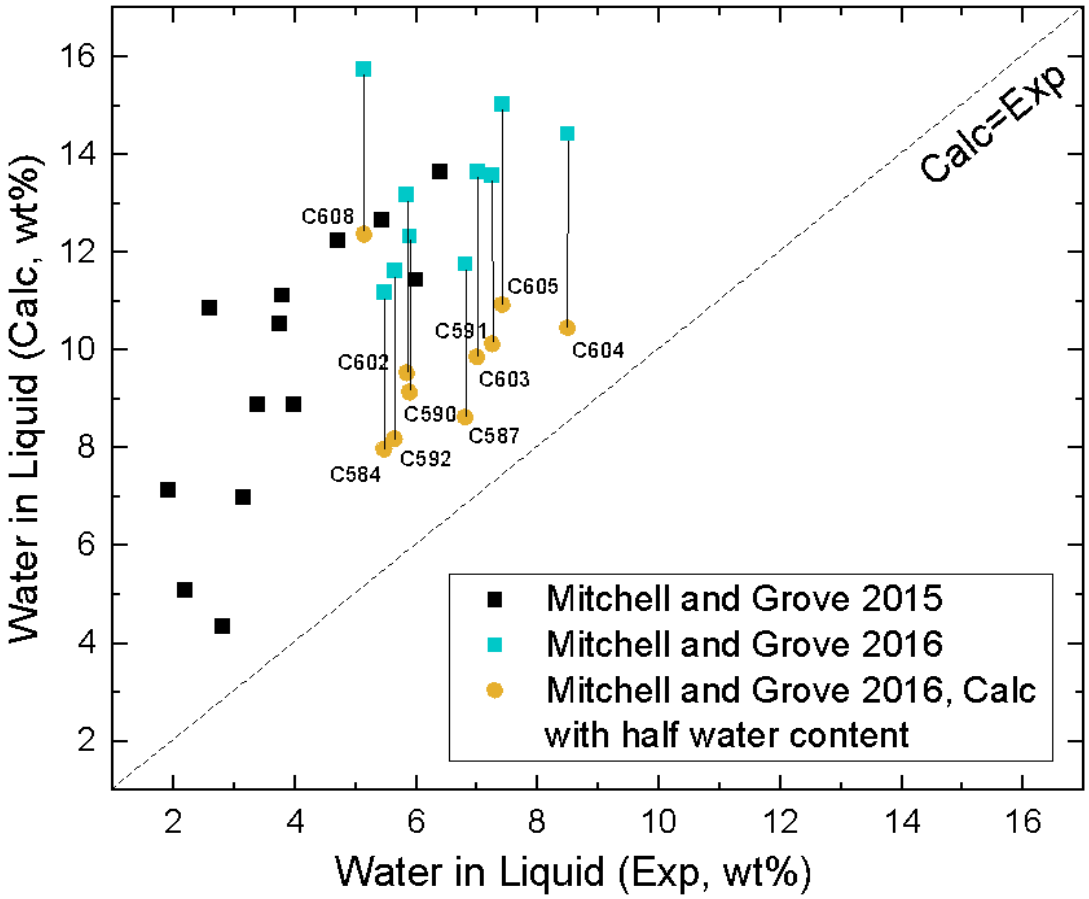

Figure 3.20 Water in liquids (melts) from experimental (Exp) and modelling (Calc) results. Models with different water contents and experimental results are shown in different colours as specified in the legend; models with different water contents reproducing Mitchell and Grove 2016 are connected using black lines. Water contents in liquid from modelling results are higher than experimental results.

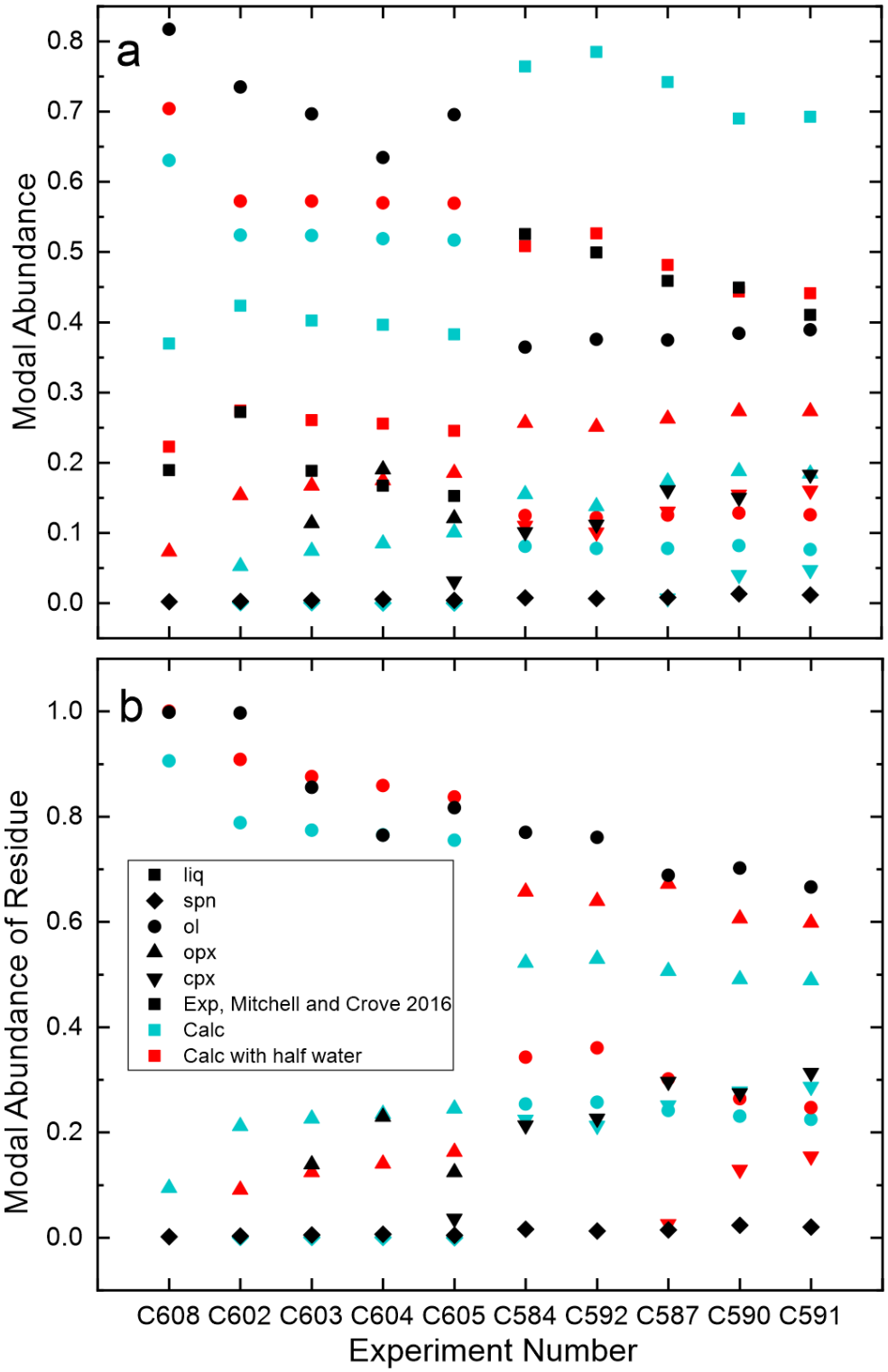

Figure 3.21 Modal Abundances from modelling results with different water contents under the conditions of Mitchell and Grove (2016). a: modal abundances of all phases; b: modal abundances of phases in residue. Models with different water contents and experimental results are shown in different colours; different phases are shown in different shapes as specified in the legend.

3.4.2.4 Influence of Bulk Cr/Al

As shown in Section 3.4.2.2, spinel Cr# predicted by thermodynamic modelling is lower than the experimental results of Mitchell and Grove (2016). To study the influence of bulk Cr/Al values on the modelling results, I calculated models with different bulk Cr/Al values. The spinel Cr# and olivine Mg# become slightly higher with higher bulk Cr/Al (Figure 3.22). However, the modal abundances of the spinel from models with multiple bulk Cr/Al increased (Figure 3.23b). The modal abundances of the orthopyroxene from models with multiple Cr/Al become slightly higher than models with original bulk Cr/Al. In contrast, the modal abundances of the liquid and olivine become slightly lower (Figure 3.23a). In conclusion, the bulk Cr/Al value has positive correlation with modal spinel, olivine Mg#, and spinel Cr#, but the influence on spinel Cr# and olivine Mg# is very limited (increase spinel Cr# and olivine Mg# by ~0.5% if double the bulk Cr/Al).

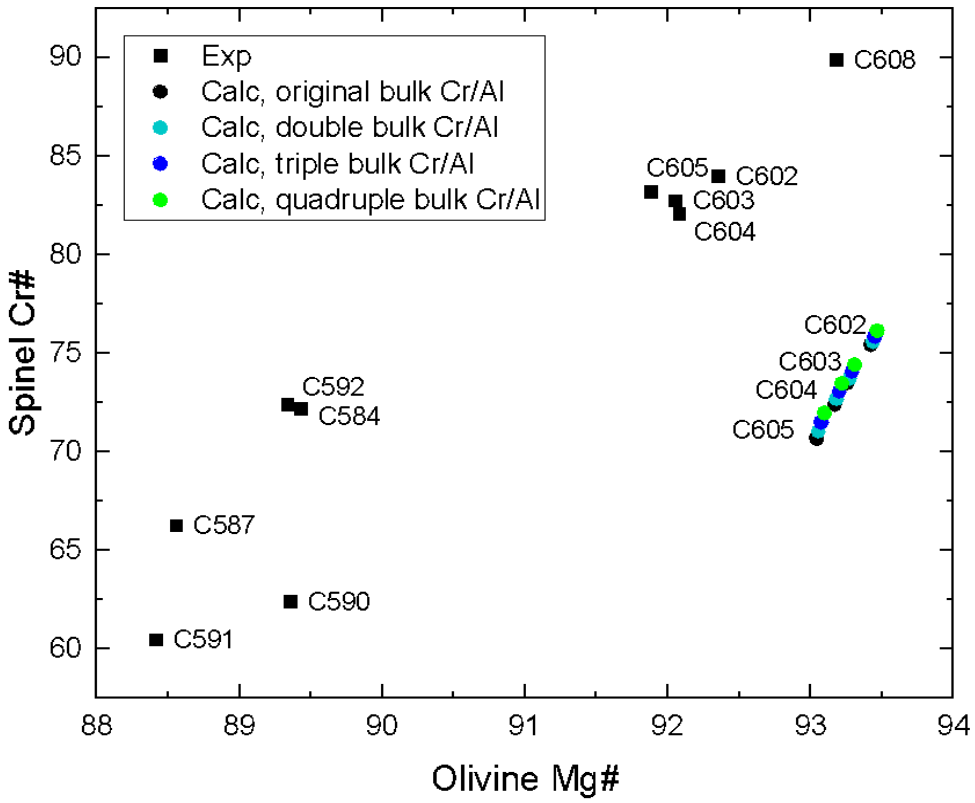

Figure 3.22 The relationship of spinel Cr# and olivine Mg# for modelling results with different bulk Cr/Al contents under the conditions from Mitchell and Grove (2016). Experimental results are shown as black squares; modelling results with different bulk Cr/Al are shown as circles in different colours.

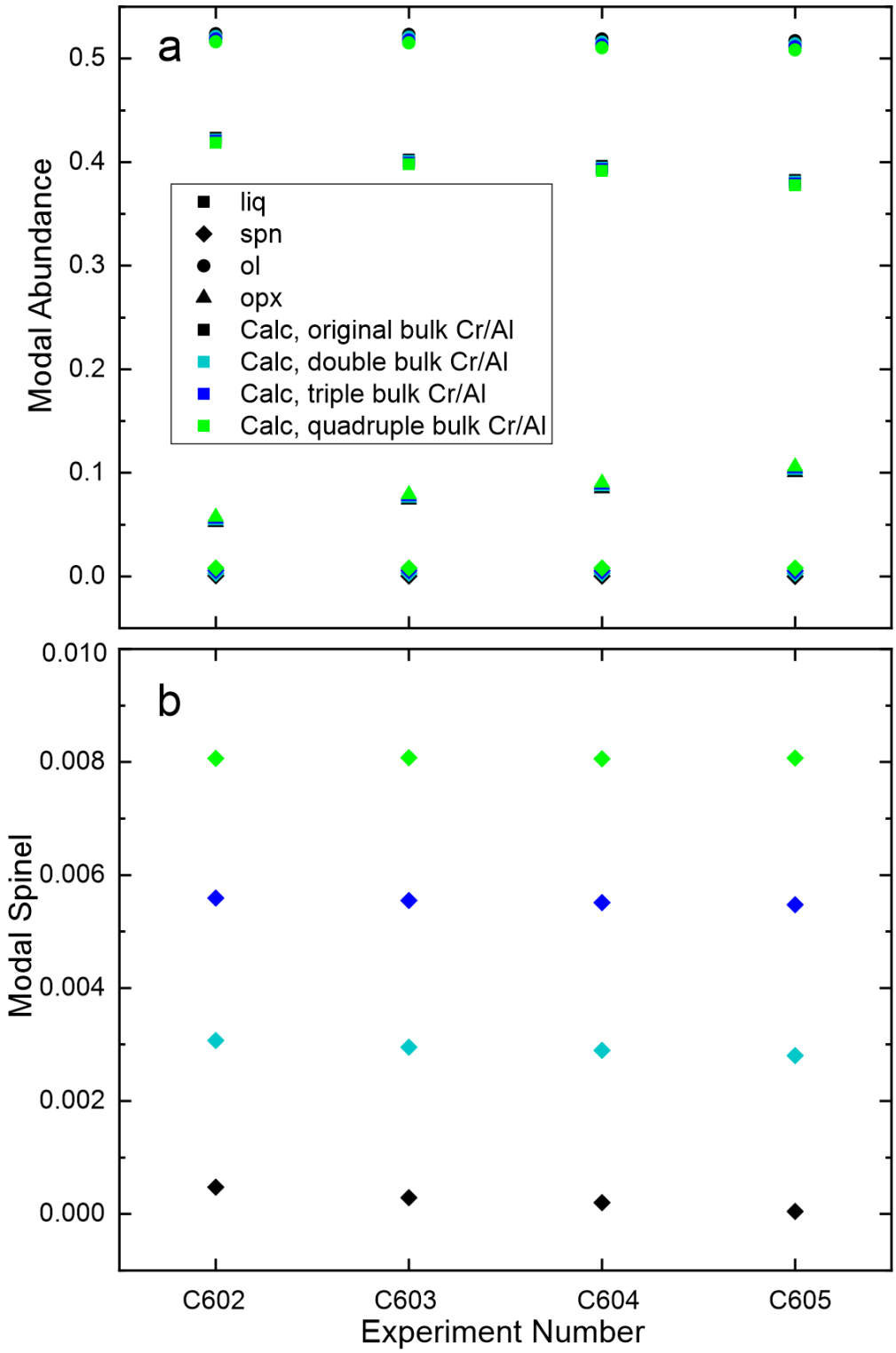

Figure 3.23 Modal abundances for modelling results with different bulk Cr/Al contents under the conditions from Mitchell and Grove (2016). a: modal abundances of all phases; b: modal spinel. Different phases are shown in different shapes; different bulk Cr/Al are shown in different colours as specified in the legend.

3.5 Discussion and Conclusions: The Model to Use

3.5.1 Discussion

The most recent THERMOCALC-based models have been tested in this chapter. HGP18, TH21, and WL22-3 can be used in anhydrous modelling, whereas WL22-3 and HGP18 can model hydrous melting. WL22-3 is the model that combines solid solution models from TH21 and fluid and melt models from HGP18. These models have large differences in P-T pseudosection using the same bulk composition as shown in 3.1. TH21 is the best anhydrous model, especially in modelling spinel chemistry, to reproduce experimental results, as shown in Section 3.3. Therefore, TH21 has better solid solution models than HGP18. With the same fluid and melt models but a better solid solution model, WL22-3 is a better hydrous model than HGP18. However, Table 3.5 and Figure 3.15 show that WL22-3 is still inadequate to reproduce spinel chemistry for hydrous peridotite melting conditions.

3.5.2 Conclusions

Bulk rock ferric iron content has a minimal influence on the boundaries of phase assemblages and residual compositions in thermodynamic models of peridotite melting. Different versions of THERMOCALC-based models were tested using available experimental data. In P-T pseudosection, the boundaries of phase assemblages for the WL22-3, TH21, and HGP18 models are very different from each other. However, they have similar trends in the covariance of spinel Cr# and olivine Mg#.

After comparing models with experiments of hydrous peridotite melting, unfortunately, we are forced to conclude that even the best hydrous model (WL22-3) cannot reproduce hydrous experiments. The mineral assemblages, spinel Cr#, and olivine Mg# calculated under the WL22-3 hydrous model are very different from the hydrous experiments. However, similar tests investigating the anhydrous melting of peridotites at mantle conditions show that the TH21 is the best anhydrous model.

3.5.3 Possible Future Hydrous Experiments

At present, we cannot model hydrous melting scenarios with any confidence. If more hydrous melting experiments are conducted, thermodynamic models of hydrous peridotite melting at mantle P-T conditions can be improved to provide better predictions.

Chapter 4 Results of Modelling Different Melting Processes of Peridotite

4.1 P-T Pseudosections in the KNCFMASTOCr System

4.1.1 KLB-1 and KR4003 – "Fertile" peridotite compositions

P-T pseudosections at 0-6 GPa and 700-2000 °C for the KLB-1 and KR4003 bulk compositions are shown in Figure 4.1. Similar to the results for KR4003 discussed in Chapter 3, the TH21 model for KLB-1 extends the upper boundary of the spinel stability field to much higher pressure and temperature (~4.53 GPa, 1729°C) compared with the HGP18 model (~2.15 GPa, 1415°C). Above the solidus, the phase relationships also differ between the two models with new fields such as liq+ol+opx+sp+g (slender and narrow area), liq+ol+opx+sp, and liq+ol+sp appearing in the TH21 model, whereas the HGP18 model just predicts stability for liq+ol+opx in the same P-T region. The intersection of the orthopyroxene-out curve and the solidus increases from 2.96 GPa and 1520°C to 3.26 GPa and 1533°C.

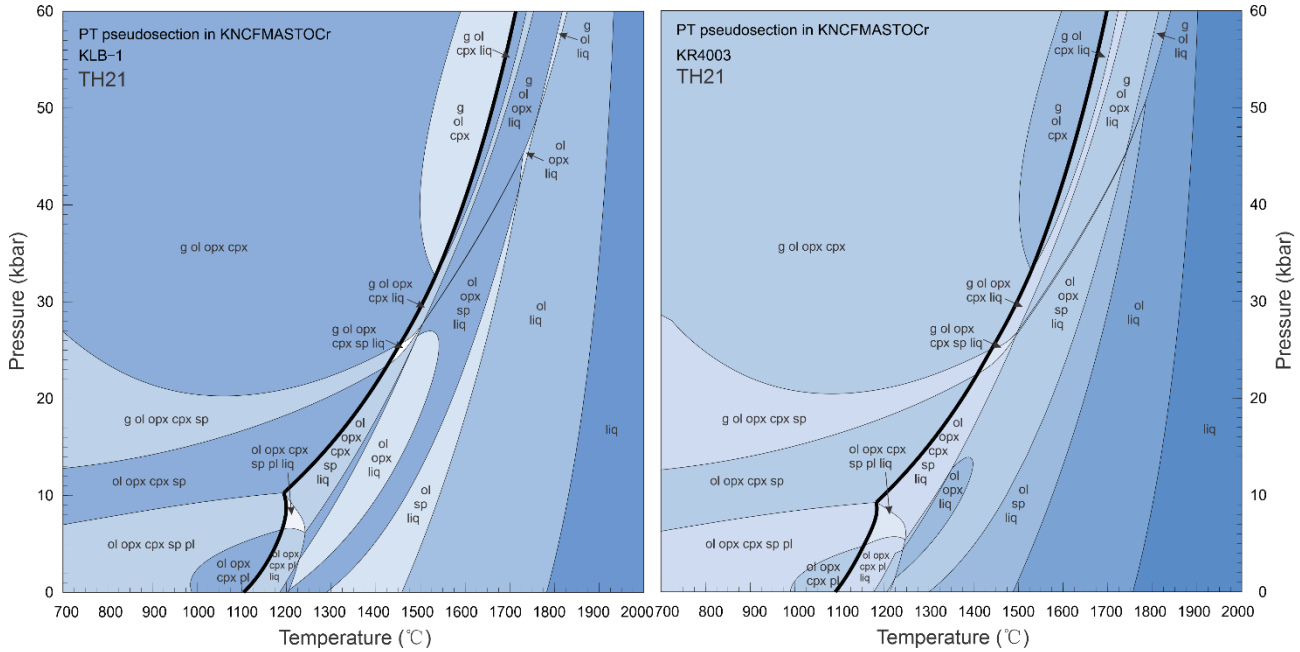

Figure 4.1 P-T pseudosections for KLB-1 and KR4003 compositions calculated with 0.3 wt% Fe_2O_3 and TH21 model. The solidus for both bulk compositions is shown as a bold curve.

4.1.2 Depleted Peridotite (DP) Composition

The P-T pseudosection for the depleted peridotite composition (DP, Table 3.2) at 0-6 GPa and 1000-2000°C is shown in Figure 4.2. The solidus temperature, the spinel-out curve and

orthopyroxene-out curve temperature, and the spinel stability pressure for the DP composition are all higher than the fertile peridotites, KLB-1 and KR4003, although the clinopyroxene-out temperature is similar to the fertile peridotites. The orthopyroxene-out line does not intersect the solidus for this composition, so there is no wehrlite (g+ol+cpx(+liq)) field at >3 GPa for this system.

4.1.3 Depleted Peridotite with Added Alkalis (DPA) Composition

The P-T pesudosection for the depleted peridotite composition with added alkalis (DPA, Table 3.2) is shown in Figure 4.2. The solidus temperature for DPA is lower than for DP as well as even that of the fertile peridotite compositions. The maximum pressure of stability of spinel and the clinopyroxene-out temperature are higher. The spinel-out temperature for the DPA composition, like the DP, is higher than for the fertile peridotites. The orthopyroxene-out temperature for the DPA is lower than the DP and lower than the fertile peridotites at P<3 GPa but higher than the fertile peridotites at P>3 GPa. The intersection of the orthopyroxene-out curve and the solidus in the DPA system is at ~2.2 GPa and 1350°C, lower than the fertile peridotites.

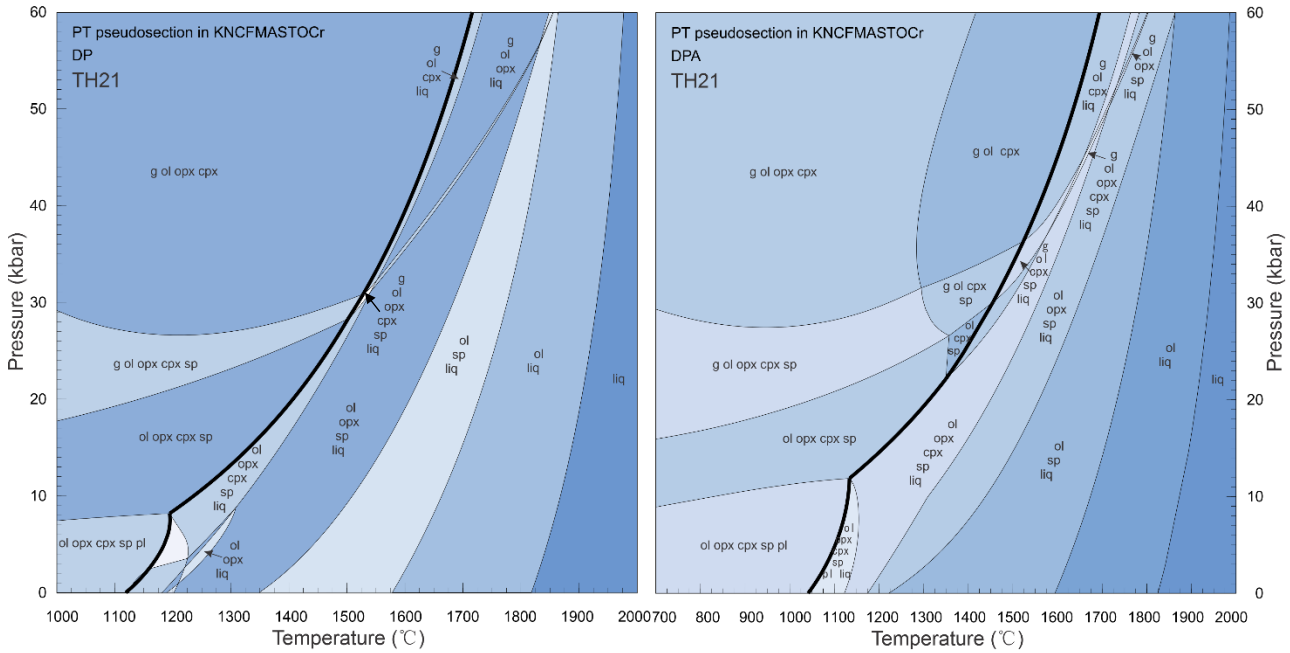

Figure 4.2 P-T pseudosection for DP and DPA compositions calculated with 0.3 wt% Fe_2O_3 and TH21 model. The solidus for both bulk compositions is shown as a bold curve.

Below the solidus, the pressure range of spinel stability (sp+ol+opx+cpx(+g)), especially the spinel+ garnet region for the DPA is the largest among these calculated bulk compositions. In contrast, spinel is stable over the smallest pressure range in the fertile peridotite. The predicted expansion of spinel stability field in melt-depleted compositions is in agreement with results from experiments (e.g. O'Neill, 1981; Klemme, 2004).

4.2 Isobaric Melting of KR4003 at 1.5 GPa

4.2.1 Residue composition

To examine how the residue of partial melting evolves at the upper-most mantle pressure, I calculated the compositions and modal abundances of the residue when KR4003 melts at 1.5 GPa, (Figure 4.3). As shown in Figure 4.3, the bulk MgO content of the residue increases with increasing temperature, whereas the other oxides in the residue decrease, except for Cr_2O_3. The Cr_2O_3 in the residue increases slightly with increasing temperature until clinopyroxene disappears, whereupon the Cr_2O_3 decreases.

Examining specifically the evolution of spinel Cr# and olivine Mg# with increasing temperature (Figure 4.4), we see that above the solidus, the spinel Cr# and olivine Mg# both increase with temperature until spinel disappears.

4.2.2 Evolution of Modal Mineralogy with Increasing Temperature

The modal abundances of the phases change systematically as T increases (Figure 4.5). Olivine remains the most abundant phase above the solidus and only decreases once all other minerals are exhausted. Below the solidus, the modal abundance of clinopyroxene increases with increasing temperature. The modal abundances of spinel and orthopyroxene first increase as modal garnet decreases until garnet disappears; thereafter, spinel and orthopyroxene decrease with increasing temperature. Above the solidus, modal orthopyroxene and olivine increase as modal spinel and clinopyroxene decrease until clinopyroxene disappears, leaving a spinel harzburgite residue until orthopyroxene, then spinel, disappears.

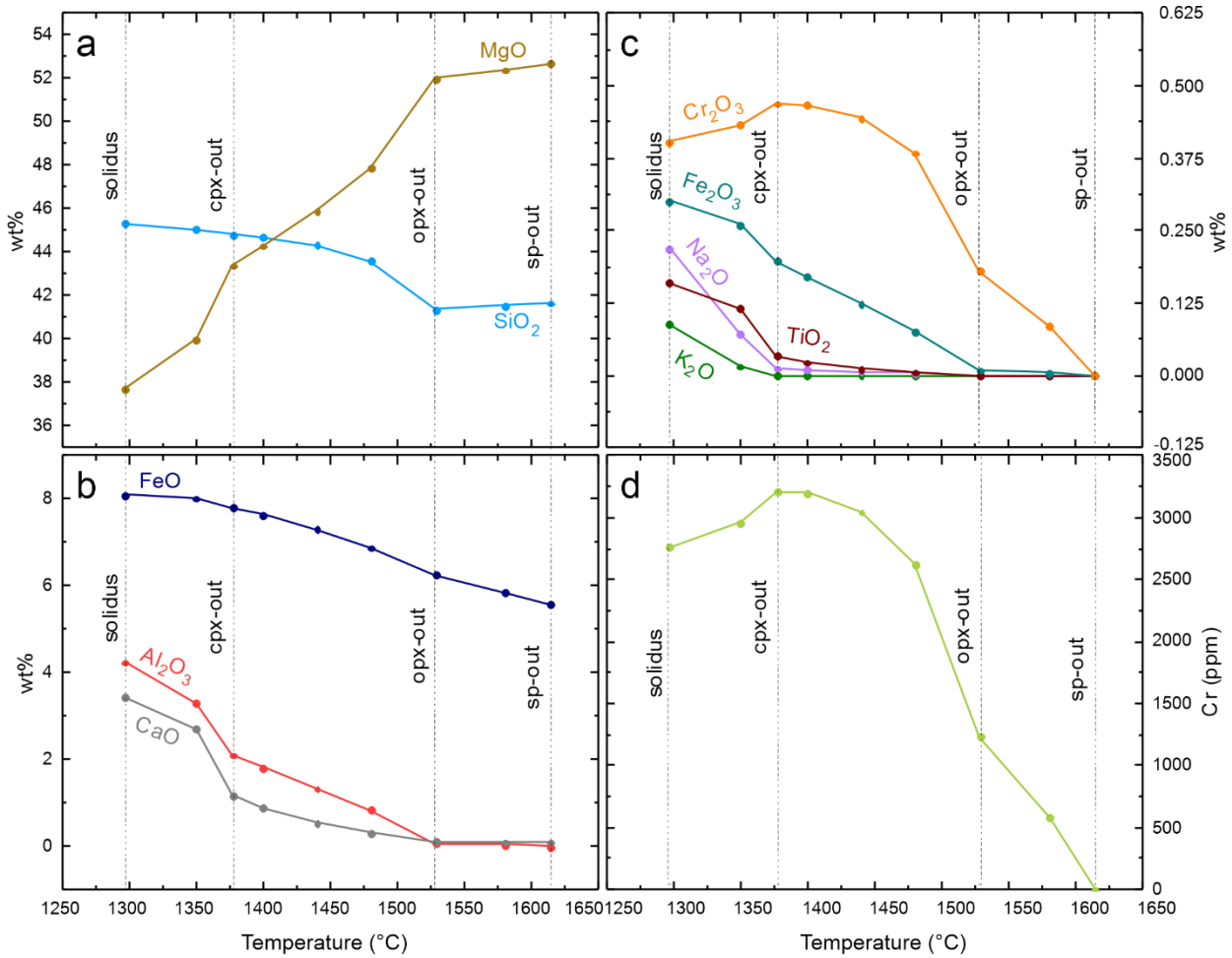

Figure 4.3 Relationship of the residual chemical compositions and temperature for the melting of KR4003 at 1.5 GPa. a MgO and SiO_2; b FeO, Al_2O_3, and CaO; c Cr_2O_3, Fe_2O_3, Na_2O, TiO_2, and K_2O; d Cr in ppm. The temperature of the disappearance of phases is shown as a vertical dotted line.

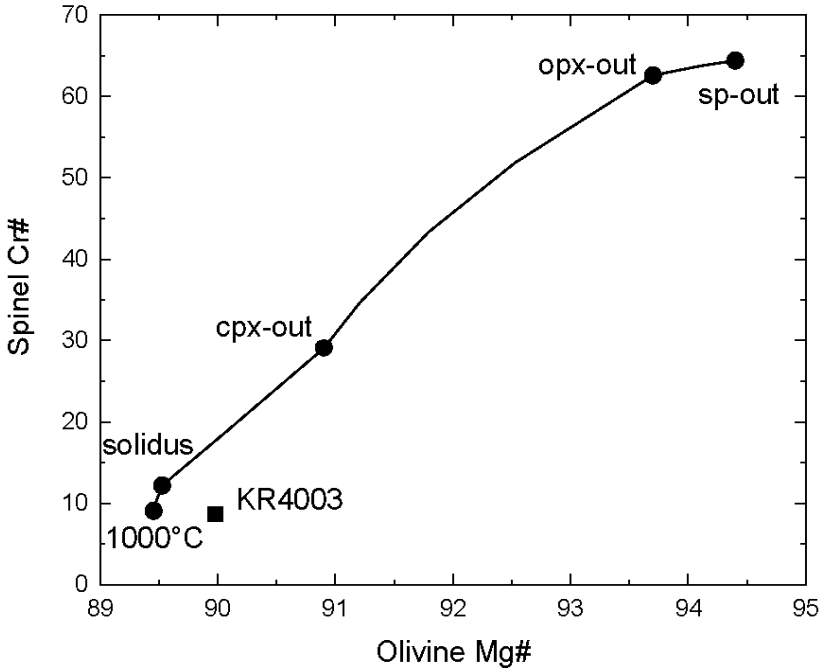

Figure 4.4 The relationship between spinel Cr# and olivine Mg# for KR4003 at 1.5 GPa.

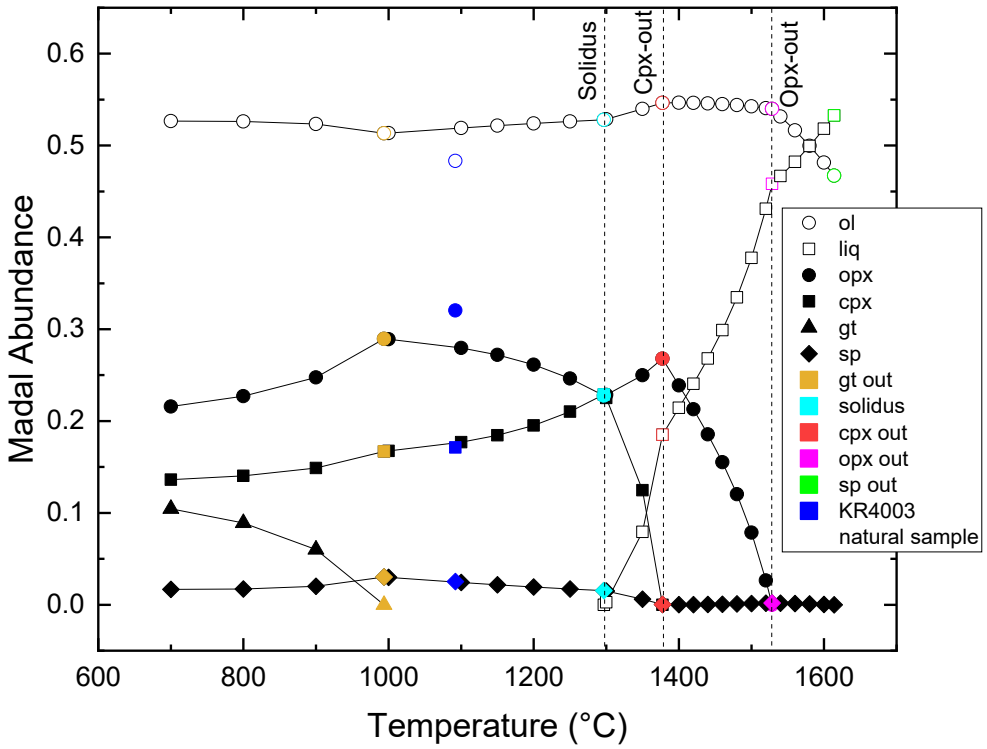

Figure 4.5 The modal abundances for KR4003 as temperature increases at 1.5 GPa. Opx, cpx, gt, and sp are shown by different black solid shapes; ol and liq are shown by different black hollow shapes. The disappearance of phases and the natural sample of KR4003 are shown in different colours as specified in the legend.

4.2.3 Evolution of Cr_2O_3, Al_2O_3, and Cr# in Minerals with Increasing Temperature

Spinel has the highest Cr# (Figure 4.6), then orthopyroxene, clinopyroxene, and garnet. Garnet Cr# increases with increasing temperature until garnet disappears, while the Cr# of the other minerals decrease. After the disappearance of garnet, the Cr# of all minerals increases with increasing temperature. Above the solidus, the Cr# of spinel, orthopyroxene and clinopyroxene all increase more rapidly with increasing temperature, reflecting preferential partitioning of Al into the liquid. Spinel Cr# increased the most, reaching ~65 when spinel disappears.

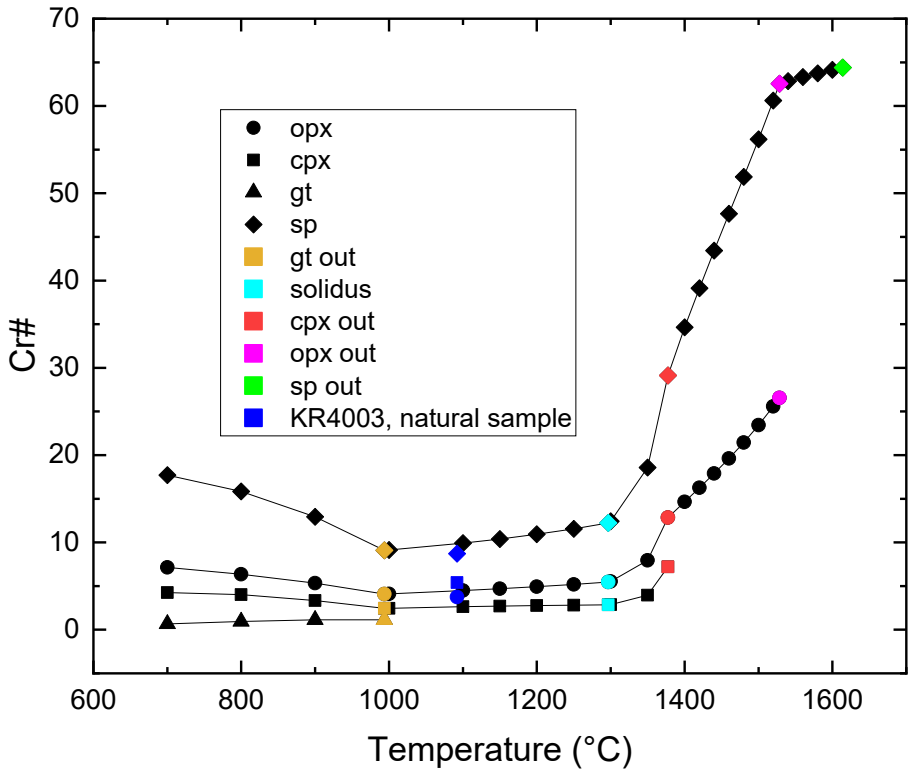

Figure 4.6 The mineral Cr# for KR4003 changes with the temperature at 1.5 GPa. Opx, cpx, gt, and sp are shown by different black solid shapes. The disappearance of phases and the natural sample of KR4003 are shown in different colours as specified in the legend.

The contribution of each mineral to the bulk Cr_2O_3 and Al_2O_3 concentrations in the residue above the solidus at 1.5 GPa illustrates the behaviour of Al and Cr during melting (Figure 4.7). From 1000°C to the solidus, Cr and Al partition from spinel into the pyroxenes. From the solidus to clinopyroxene-out at 1377°C, Al mainly goes from the clinopyroxene and spinel into the liquid. At the same time, Cr partitions from the clinopyroxene and spinel into orthopyroxene and liquid. Al goes from the orthopyroxene to the liquid, and Cr goes from the orthopyroxene to the

liquid and spinel from 1377 -1528°C (orthopyroxene-out). Finally, Al and Cr go from the spinel to the liquid until spinel vanishes at 1614°C.

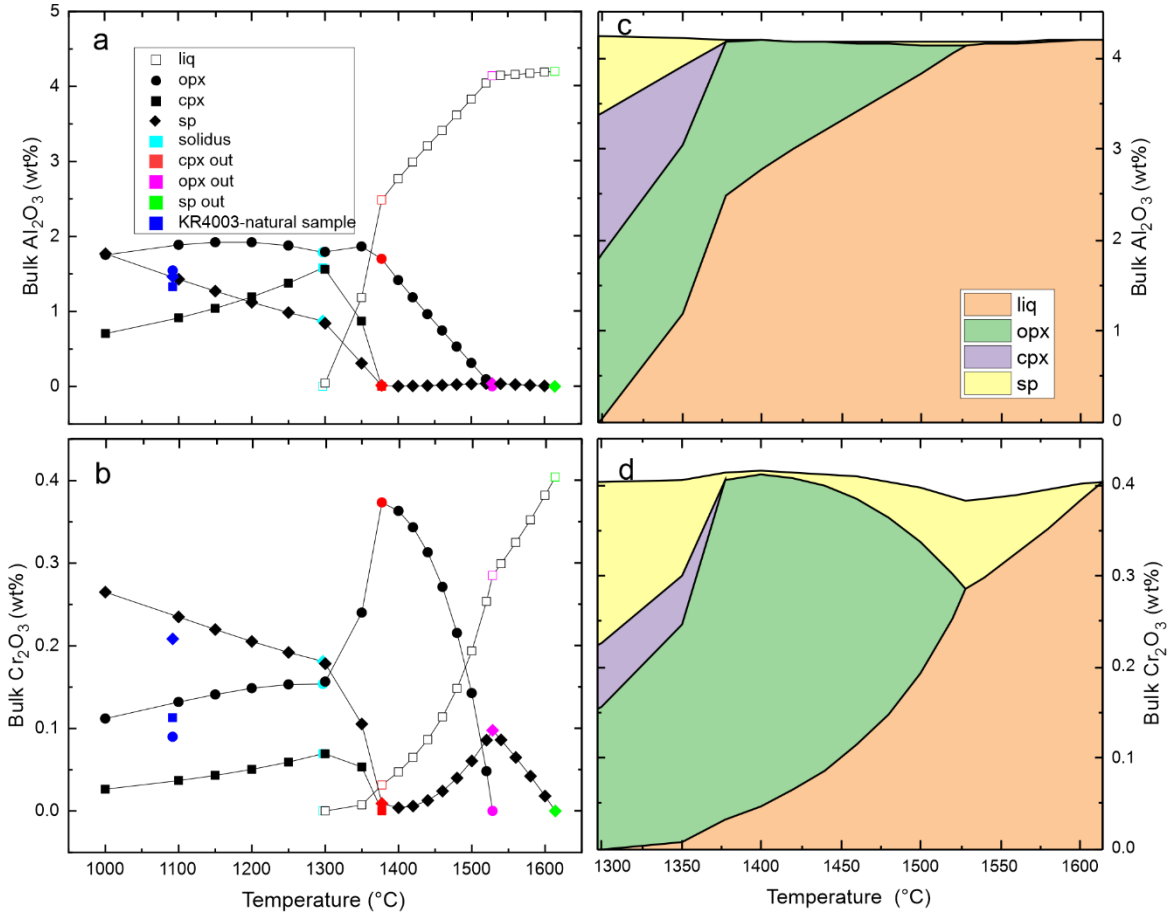

Figure 4.7 Bulk Al_2O_3 (a, c) and Cr_2O_3 (b, d) for phases of KR4003 change with the temperature during melting at 1.5 GPa. This shows the contribution of each mineral to whole-rock Cr_2O_3 and Al_2O_3 concentrations given by (mass fraction of mineral) × (mineral wt% Al_2O_3 or Cr_2O_3); a and b are the absolute values; c and d are the stacked area plots.

4.3 Isobaric Batch Melting: The Effects of Bulk composition

4.3.1 Residue Mineralogy and Spinel Chemistry

Alkalis can have a significant effect on the melting relations of peridotite (Hirschmann et al 1998; Hirschmann, 2000). In order to further compare the mineralogy and mineral chemistry of fertile and depleted peridotites and the influence of the addition of alkalis during batch melting, I calculated the modal abundances for the minerals in KLB-1, DP, and DPA at 2 GPa from solidus to the temperature where spinel disappears (Figure 4.8). Both KLB-1 and KR4003 are widely

used primitive mantle peridotites, and as shown in 4.1.1, their P-T pseudosections are similar. KLB-1 was used here to represent primitive mantle peridotites.

Olivine is the most abundant mineral in all compositions, as expected. DPA has the highest modal olivine among these bulk compositions, and DP has the highest modal orthopyroxene; KLB-1 has the lowest modal olivine, and DPA has the lowest modal orthopyroxene. The modal orthopyroxene for DP is higher than its modal clinopyroxene, but for DPA this relationship is reversed. The relative solidus temperatures for these starting compositions are DP>KLB-1>DPA. Above the solidus, clinopyroxene disappears first in these systems, then orthopyroxene, then spinel.

I also calculated mineral Mg# and Cr# for the KLB-1, DP, and DPA compositions with increasing temperature at 2 GPa (Figure 4.9). The olivine, orthopyroxene, and clinopyroxene have similar Mg# (>88.5), and their Mg# increases with temperature above the solidus as FeO partitions preferentially into the melt. The spinel Mg# is the lowest among these minerals but also increases with the temperature above the solidus. All three bulk compositions show similar trends of Mg# evolution with increasing temperature.

The Cr# is the highest in spinel and is progressively lower in orthopyroxene, clinopyroxene, and garnet in that order. The DPA has the highest spinel Cr# among these three bulk compositions at the same temperature above ~1400°C. The highest spinel Cr# for the DPA is over 85. The highest spinel Cr# for the DP is ~80, compared with the value for the KLB-1 at ~65.

The Al_2O_3 and Cr_2O_3 contents, Mg#, Cr#, $Fe^{3+}/\sum Fe$, and modal abundances for spinel in the model systems of the KLB-1, DP, DPA at 2 GPa are shown in Figure 4.10 and 4.11. Spinel Cr_2O_3 increases with temperature, while spinel Al_2O_3 shows the opposite trend. Spinel Mg# fluctuates at ~80; spinel Cr# increases with temperature from ~20 near the solidus until the spinel vanishes. Modal spinel decreases with temperature. The $Fe^{3+}/\sum Fe$ of spinel increases with temperature.

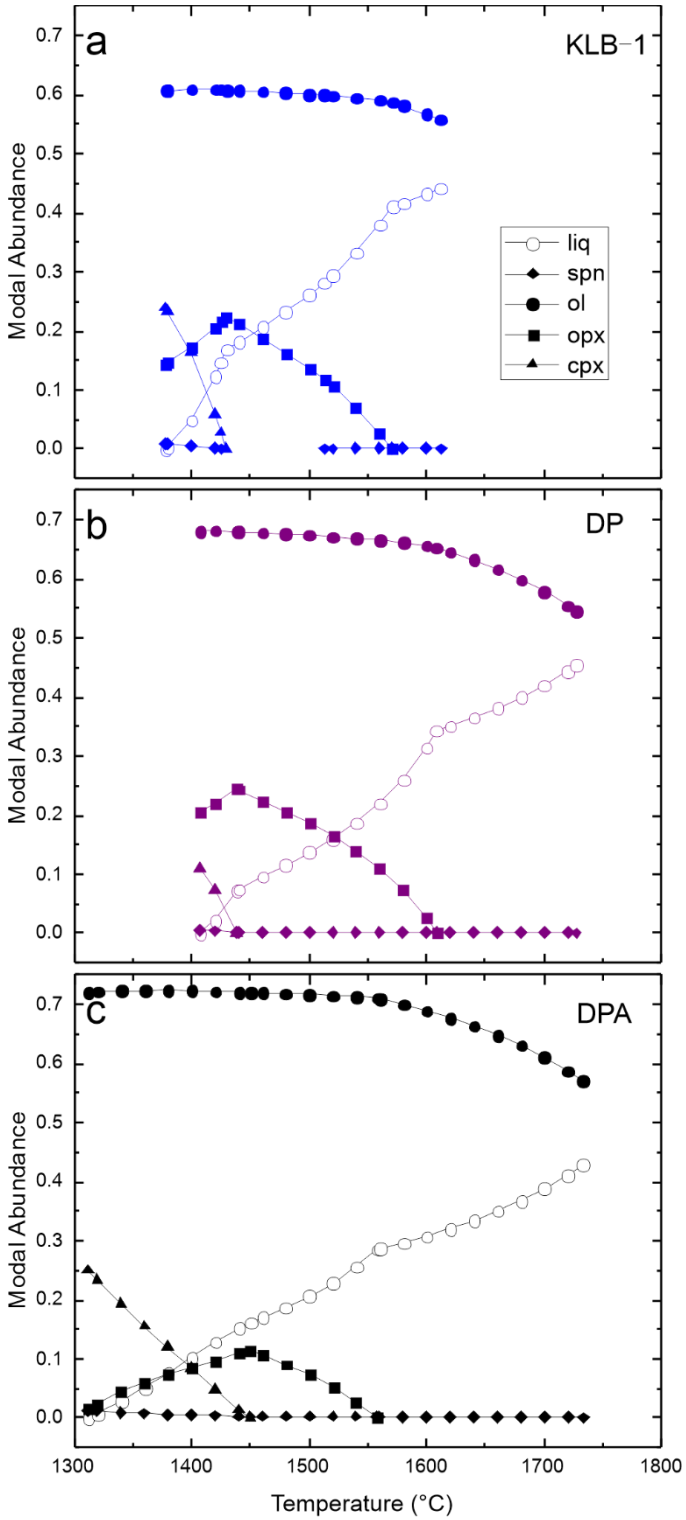

Figure 4.8 Modal abundances for phases in the KLB-1 (a), DP (b), and DPA (c) compositions at 2 GPa. Different phases in residue are shown by different solid shapes, and the liquid fraction is shown by hollow circles as specified in the legend.

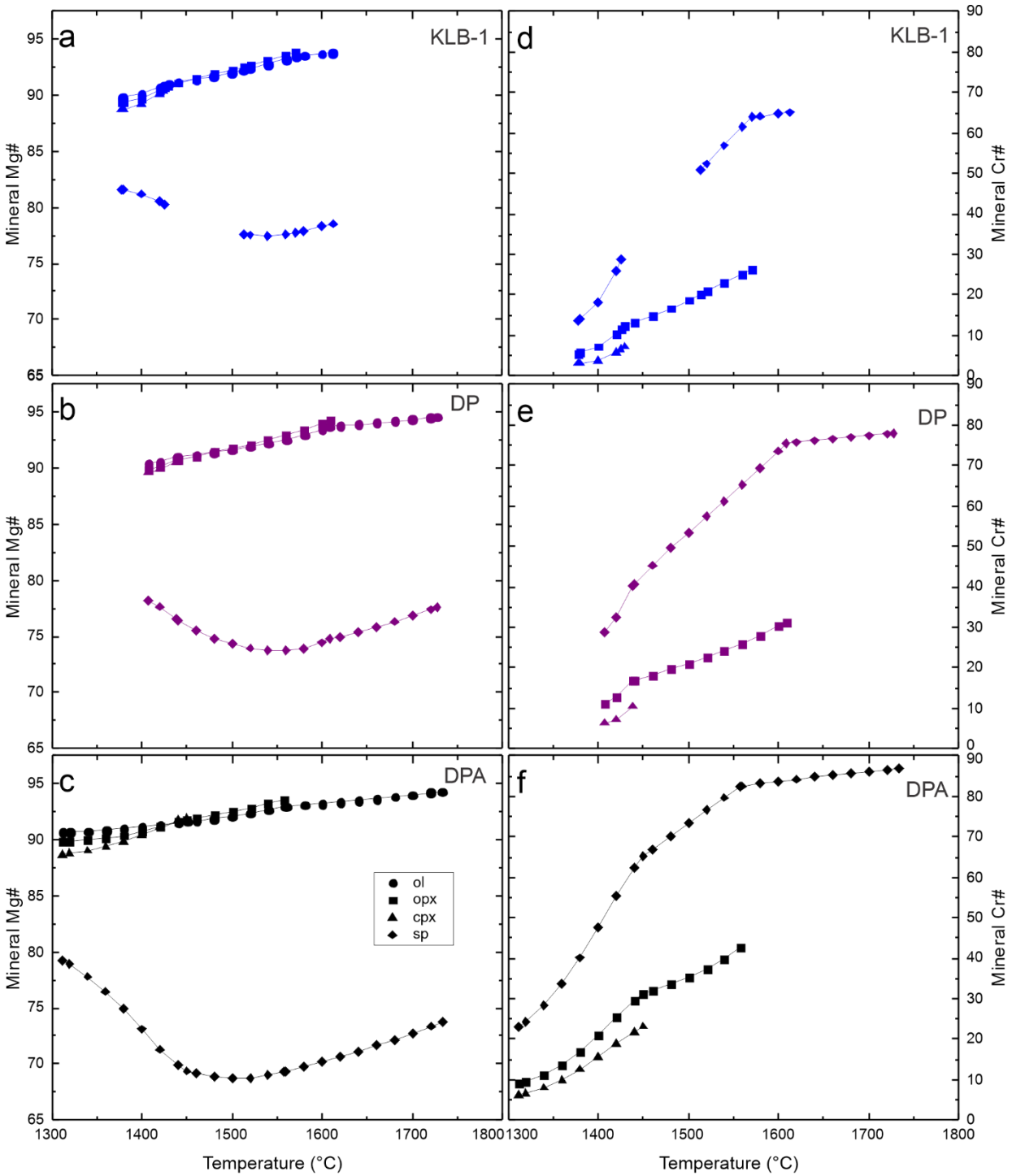

Figure 4.9 Mineral Mg# (a, b, c) and Cr# (d, e, f) for the KLB-1, DP, and DPA peridotite starting compositions as temperature increases at 2 GPa. Different minerals are shown by different solid shapes as specified in the legend.

Figure 4.10 Spinel Al_2O_3, Cr_2O_3, Mg#, and Cr# change with the temperature for the KLB-1, DP, and DPA peridotite starting compositions at 2 GPa

	Al_2O_3 and Cr_2O_3 VS Temperature	Mg# and Cr# VS Temperature
KLB-1	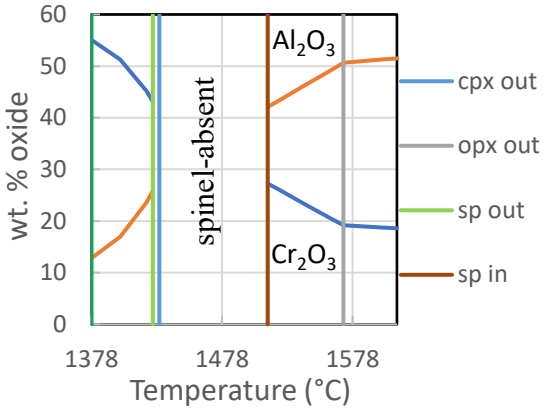	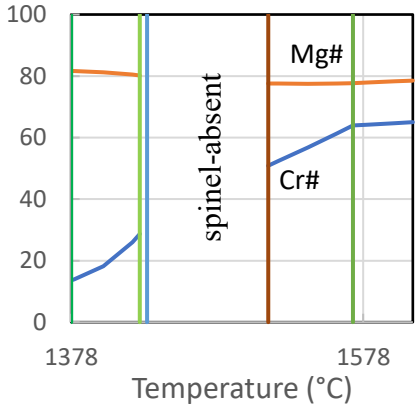
DP	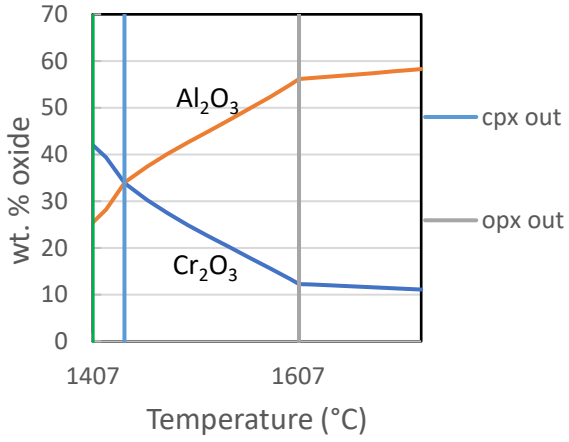	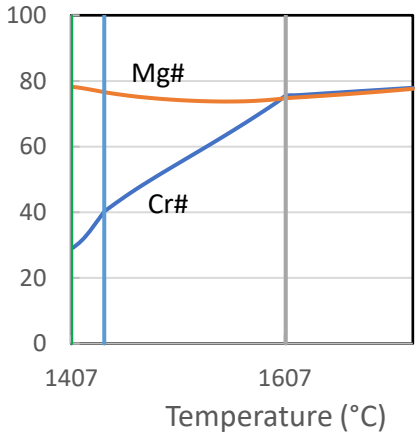
DPA	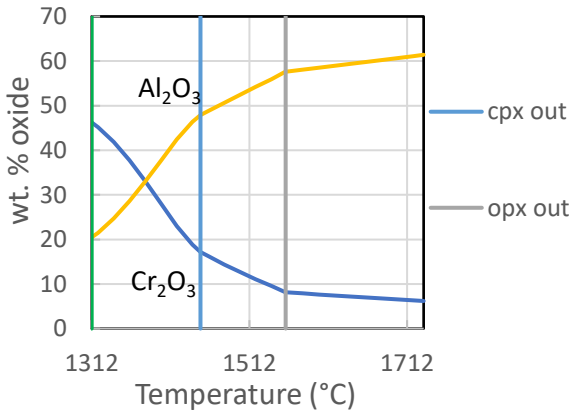	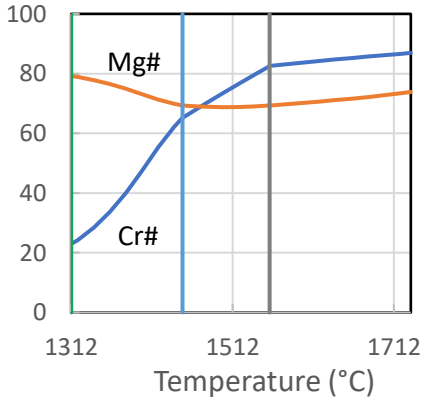

Figure 4.11 Variations in $Fe^{3+}/\sum Fe$ in spinel and modal spinel change with the temperature during melting of the KLB-1, DP, and DPA peridotite starting compositions at 2 GPa

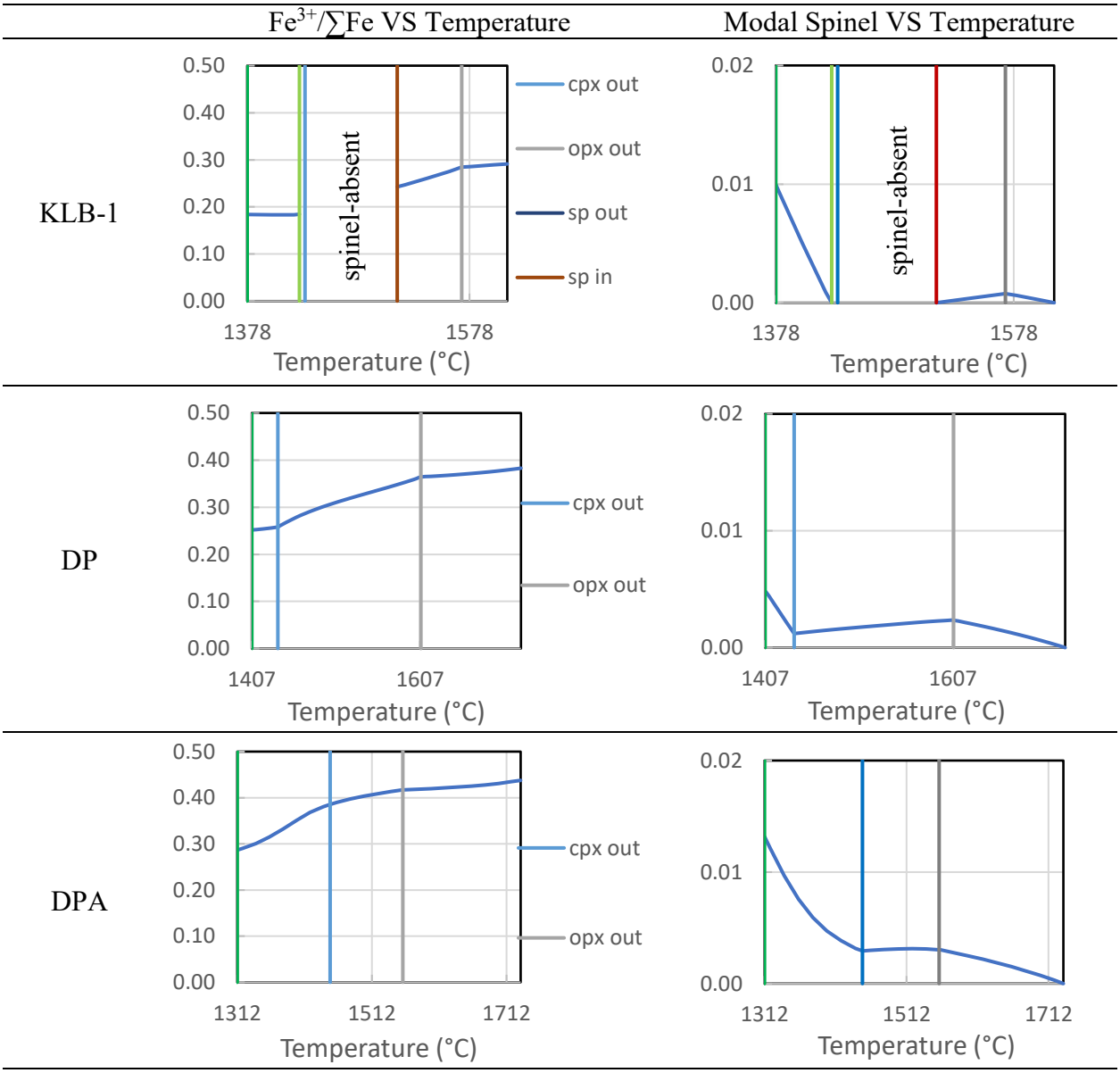

4.3.2 Evolution of Residue Chemistry during Batch Melting

The relationship between residue Al_2O_3 and CaO changing with the degree of melting is shown in Figure 4.12, which is used to illustrate the evolution of Al and Ca via batch melting and the influence of bulk composition and pressure. Both residue Al_2O_3 and CaO decrease with the degree of batch melting of KR4003, MM3, and KLB-1 at 1 GPa, KR4003, KLB-1, DP, and DPA at 2 GPa. Residue concentrations of Al_2O_3 of KR4003, KLB-1, and MM3 decrease from 4 wt%

to near 0 at 1 GPa, and residue CaO contents decrease from around 4.5 wt% to almost 0. The two values for KR4003 and KLB-1 at 2 GPa have the same trend as 1 GPa. For the depleted peridotites, DPA and DP, the residue contents of both Al_2O_3 and CaO decrease from around 2.5 wt% to near 0 during batch melting at 2 GPa. For a given fertile bulk composition, residue Al_2O_3 contents are higher than CaO contents, at increasing pressures. For depleted starting compositions, Ca and Al are either fairly similar, or (for DPA) Ca exceeds Al. Adding alkalis decreases residue Al_2O_3 contents for batch melting.

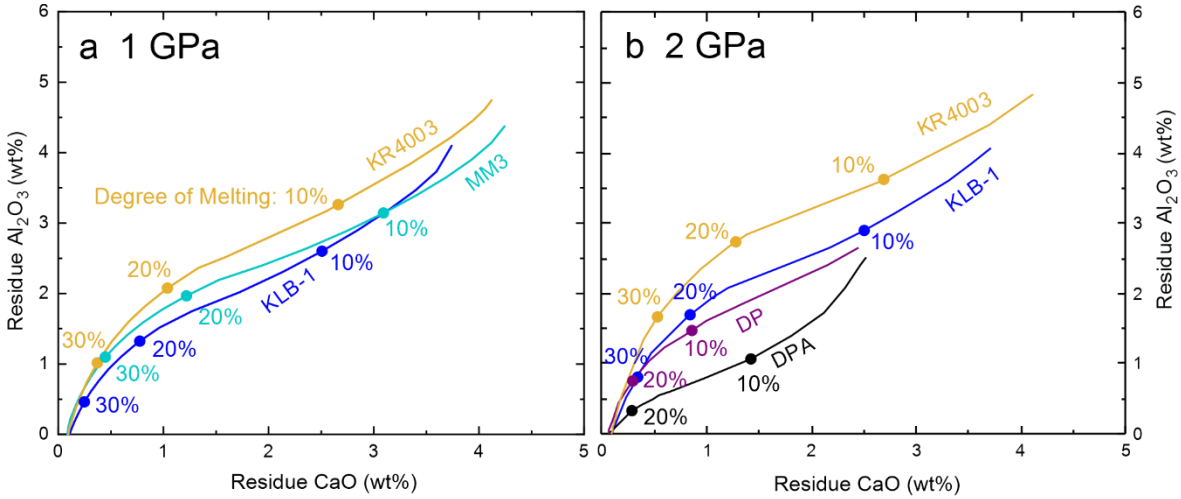

Figure 4.12 The relationship between residue Al_2O_3 and CaO during batch melting of fertile and depleted peridotite starting compositions. Degree of melting increases from right to left, with the numbers on each curve specifying the amount of melting in percent. Compositions of KLB-1, KR4003, MM3, DP, and DPA are given in Table 3.2

The combination of bulk rock Cr# and CaO/Al_2O_3 values can be used for determining the melting conditions of mantle peridotites (Su and Chen, 2018). These parameters for the residues from the batch melting of MM3, KLB-1, and KR4003 at 1 GPa, KLB-1, KR4003, DP, and DPA at 2 GPa are shown in Figure 4.13 to illustrate the influence of bulk composition, pressure, and degree of melting on residue Cr# and CaO/Al_2O_3. The residue bulk Cr# increases with the degree of melting in all cases. Residue CaO/Al_2O_3 values for MM3, KLB-1, and KR4003 at 1 GPa first increase slightly, then decreases from 1 to 0.5, then increases again to over 2 with the degree of melting. At 2 GPa, the residue CaO/Al_2O_3 for the DPA composition first increases to near 1.5 with the degree of melting, then decreases, then increases from 1 to over 4. Compared to the value for the DP, KR4003 and KLB-1, which decreases first to less than 0.5, then increases to over 4. Residue CaO/Al_2O_3 increases until clinopyroxene is out, then decreases, reflecting the

pyroxenes' behaviour during melting. At a higher degree of melting (>25%), residue Cr# in depleted peridotites is higher than in fertile peridotites at the same pressure, and for melting of the same bulk composition, at any given melt-fraction, residue Cr# is slightly lower at higher pressure with the same residue CaO/Al_2O_3. Adding alkalis increases residue CaO/Al_2O_3 in batch melting.

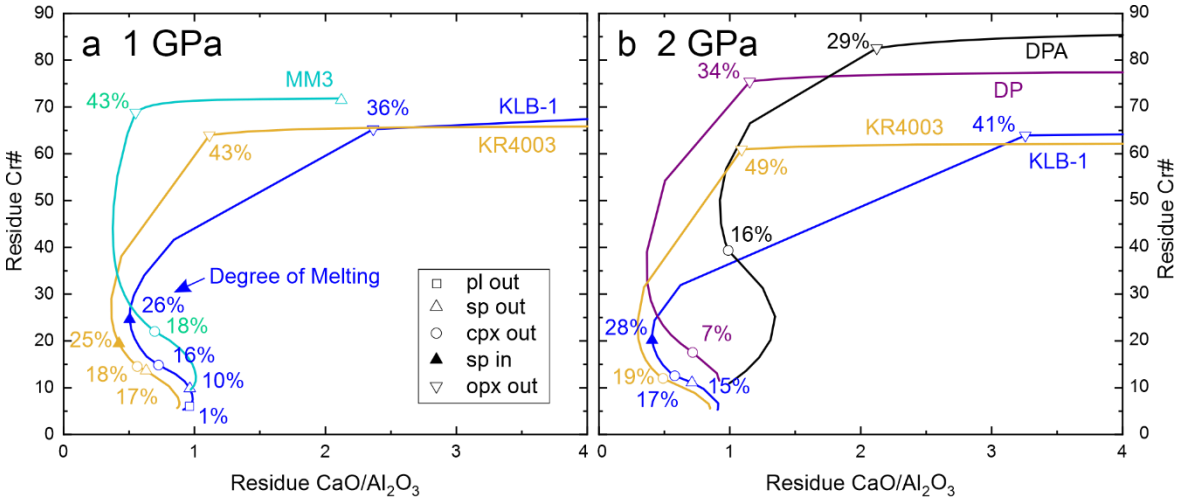

Figure 4.13 The relationship between the residue Cr# and CaO/Al_2O_3 during batch melting of various peridotite starting compositions. Degree of melting increases from bottom to top, with the numbers on each curve specifying the amount of melting in percent. The disappearance/appearance of phases from the residue is shown by the different symbols as specified in the legend. Compositions of KLB-1, KR4003, MM3, DP, and DPA are given in Table 3.2

The relationship between residue Cr/Al and residue FeO (total) is another approach for determining the melting conditions of lithospheric mantle. The evolution of this relationship during batch melting of KLB-1, KR4003, and MM3 at 1 GPa, KLB-1, KR4003, DP, and DPA at 2 GPa is shown in Figure 4.14 to illustrate the influence from bulk composition and degree of melting on residue Cr# and FeO. Residue FeO decreases with the degree of melting, while residue Cr/Al increases. FeO decreases faster after clinopyroxene goes out and faster after orthopyroxene goes out. Fertile peridotites have similar residue Cr/Al, but FeO contents are different at the same value of Cr/Al (KLB-1> KR4003> MM3). Residue Cr/Al in depleted peridotites is higher than in fertile peridotites at the same pressure, and for the melting of the same bulk composition, residue Cr/Al is lower at higher pressure with the same FeO content. Adding alkalis increases residue FeO in batch melting.

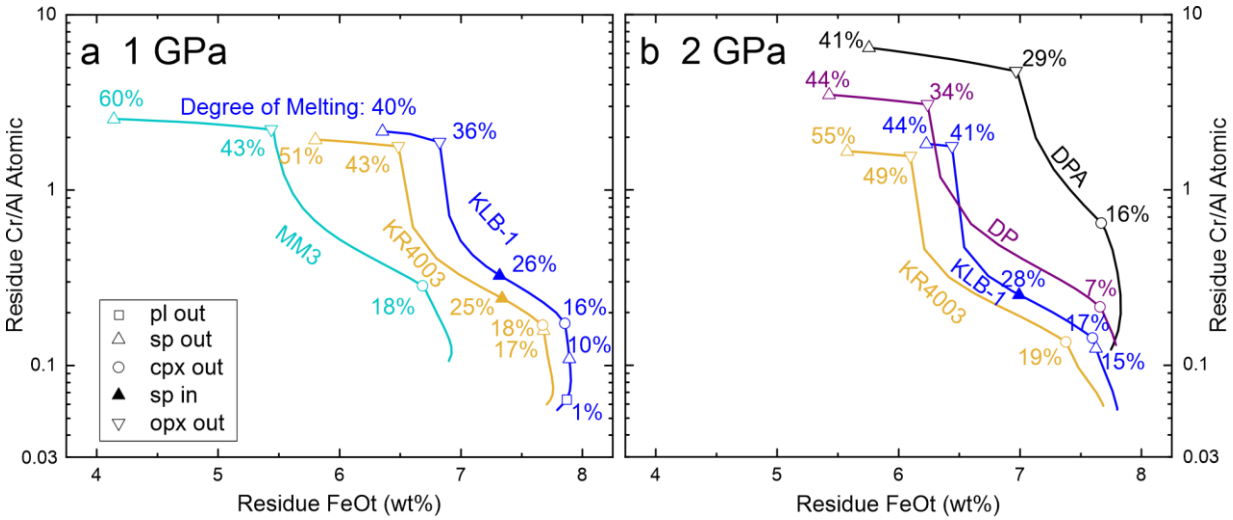

Figure 4.14 The relationship between residue Cr/Al and FeOt during batch melting of various peridotite starting compositions. Degree of melting increases from bottom to top, with the numbers on each curve specifying the amount of melting in percent. The disappearance/appearance of phases from the residue is shown by the different symbols as specified in the legend. Compositions of KLB-1, KR4003, MM3, DP, and DPA are given in Table 3.2.

The co-evolution of spinel Cr# and olivine Mg# during batch melting of different bulk compositions at 1 and 2 GPa is illustrated in Figure 4.15. At 1 GPa, KR4003, KLB-1, and MM3 reach spinel Cr# of ~70 with over 40% degree of melting. MM3 has the highest olivine Mg# of over 95 as it reaches the highest spinel Cr#, whereas KLB-1 has the lowest Mg# (~93.5). Spinel initially disappears during melting of KR4003 at ~10% and KLB-1 at ~17% degree of melting, then reappears at ~25% melting.

The spinel Cr# for the DPA starting composition increases faster than DP and KLB-1 with increasing olivine Mg# at 2 GPa, surpassing the value for DP and KLB-1 when olivine Mg# is ~ 91. DPA has the highest spinel Cr# among these bulk compositions, reaching a value of over 85 with >94 olivine Mg#. DP has higher spinel Cr# than KLB-1 at the same olivine Mg#, reflecting the less fertile bulk compositions of DP related to KLB-1. Clinopyroxene disappears first in the melting of DPA, DP, and KR4003 at less than 20% melting. In contrast, spinel disappears first in melting of KLB-1 at 15% melting. Orthopyroxene disappears at over 40% for fertile peridotites and around 30% for depleted peridotites. The maximum Cr# achieved before spinel is exhausted varies from ~65 in KR4003 to >85 in DPA. DPA, DP, and KR4003 have similar olivine Mg# of

around 94.5 when they reach the highest spinel Cr#, while the value of olivine Mg# for KLB-1 is less than 94.

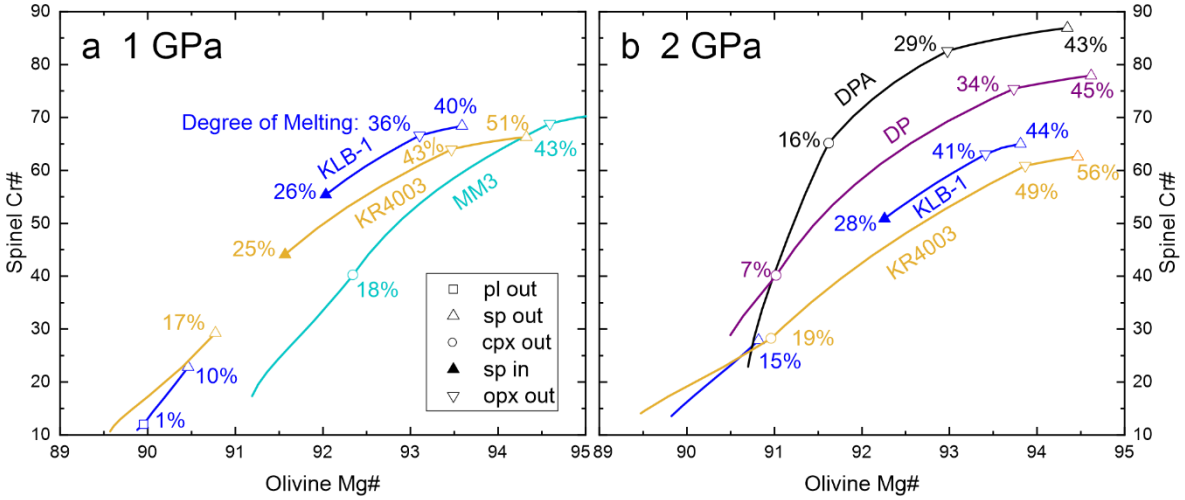

Figure 4.15 The relationship between spinel Cr# and olivine Mg# during batch melting of peridotites of varying composition. Degree of melting increases from left to right, with the numbers on each curve specifying the amount of melting in percent. The disappearance/appearance of phases from the residue are shown by the different symbols as specified in the legend. Compositions of KLB-1, KR4003, MM3, DP, and DPA are given in Table 3.2.

4.4 Isobaric Fractional Melting at 1 and 2 GPa

4.4.1 Residue Mineralogy

To further explore how melting residues evolve in different melting scenarios, I calculated the isobaric fractional melting of KLB-1, KR4003, and DPA at 1 GPa and the melting of KLB-1, DP, and DPA at 2 GPa. To approximate fractional melting, I extracted the melts when they reached 0.5%, then reset the bulk composition and repeated the exercise. I analyzed how the modal abundances changed with temperature during the melting process. As shown in Figure 4.16, the solidus temperature for the DPA starting composition at 1 GPa is the lowest among these conditions, and the two fertile peridotites have similar solidus temperatures.

Olivine has the highest modal abundance among these phases, and the modal olivine increases with increasing degree of melting. The modal orthopyroxene increases before the clinopyroxene dissolves, then decreases. During the melting of fertile peridotites, the spinel dissolves before the clinopyroxene, while the spinel dissolves after the clinopyroxene during the isobaric fractional melting of the DP and DPA. Plagioclase appears as a residual phase at low degrees of melting (~

1125 to 1160°C) of the DPA at 1 GPa but does not appear during the melting of fertile peridotites at the same pressure.

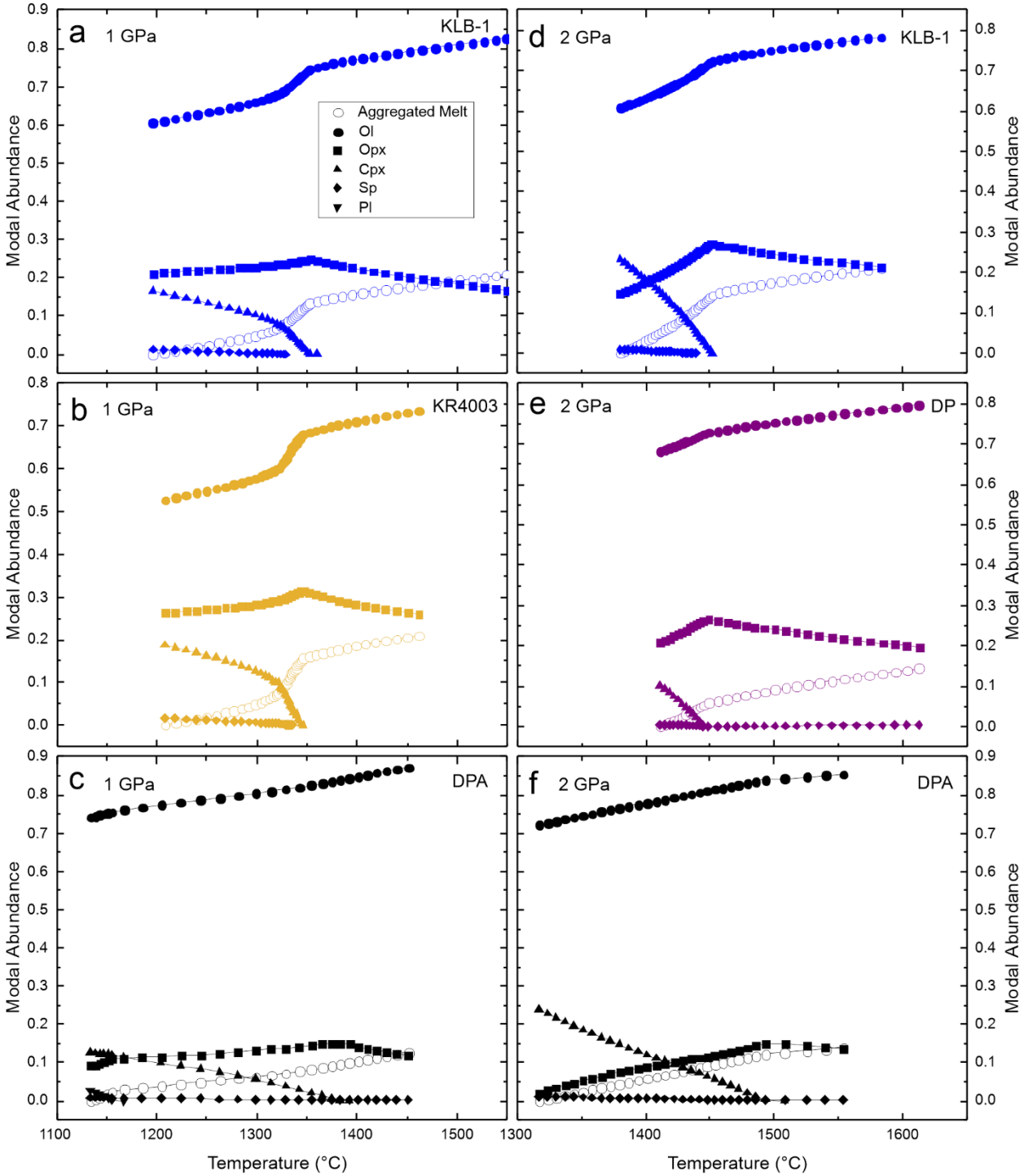

Figure 4.16 The modal abundances of phases during isobaric fractional melting of KLB-1 (a, d), KR4003 (b), DP (e), and DPA (c, f) at 1 (a, b, c) and 2 (d, e, f) GPa. Different phases in residue are shown by different solid shapes, and the aggregated melt is shown by hollow circles as specified in the legend.

4.4.2 Evolution of Residue Chemistry during Isobaric Fractional Melting

The evolution of Ca and Al during isobaric fractional melting at 1 and 2 GPa is illustrated in Figure 4.17, which shows the relationship between residue Al_2O_3 and CaO changing with the degree of isobaric fractional melting of KLB-1, KR4003, and DPA at 1 GPa and KLB-1, DP, and DPA at 2 GPa. Both residue Al_2O_3 and CaO decrease with the degree of melting. The residue Al_2O_3 of DPA decreases from 2 to near 0 at 1 and 2 GPa, and residue CaO decreases from 2 to 0.5. The residue Al_2O_3 of KLB-1 decreases from 3.5 to around 0.5 with over 20% degree of melting, and the residue CaO decreases from 3 to near 0. Residue Al_2O_3 of KR4003 decreases from around 4 to 1 at 1 GPa, and residue CaO decreases from near 3.5 to around 0.3 with over 20% degree of melting. Same with the batch melting shown in 4.3.2, residue Al_2O_3 in fertile peridotites is higher than in depleted peridotites at the same pressure with the same residue CaO. For the melting of the same bulk composition, residue Al_2O_3 is higher at higher pressure with the same residue CaO. Adding alkalis decreases residue Al_2O_3 in depleted peridotites in isobaric fractional melting.

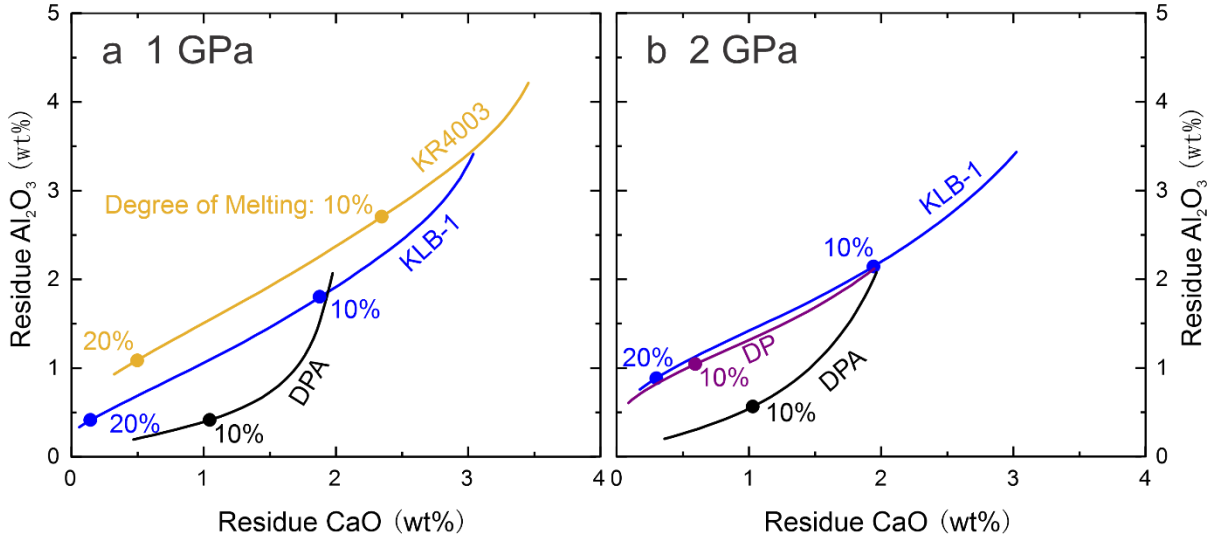

Figure 4.17 The relationship between residue Al_2O_3 and CaO during isobaric fractional melting of various peridotite starting compositions. Degree of melting increases from right to left, with the numbers on each curve specifying the amount of melting in percent. Compositions of KLB-1, KR4003, DP, and DPA are given in Table 3.2.

The Cr# and CaO/Al_2O_3 systematics for the residues of melting KLB-1, KR4003, and DPA at 1 GPa and KLB-1, DP, and DPA at 2 GPa are shown in Figure 4.18. As expected, the residue Cr# increases with the degree of melting. The residue CaO/Al_2O_3 for the DPA first increases rapidly

with the degree of melting, then decreases at 1 and 2 GPa, compared to the value for KLB-1, and KR4003, which only increase slightly before 10% of the degree of melting, and then decrease. The residue CaO/Al_2O_3 for DP decreases with the degree of melting. Residue Cr# in depleted peridotites is higher than in fertile peridotites at the same pressure, and for the melting of the same bulk composition, residue Cr# is slightly lower at higher pressure with the same residue CaO/Al_2O_3. The relationship between residue Cr# and CaO/Al_2O_3 in isobaric fractional melting is very different from batch melting as the trends are clearer than batch melting. Adding alkalis increases residue CaO/Al_2O_3 in isobaric fractional melting.

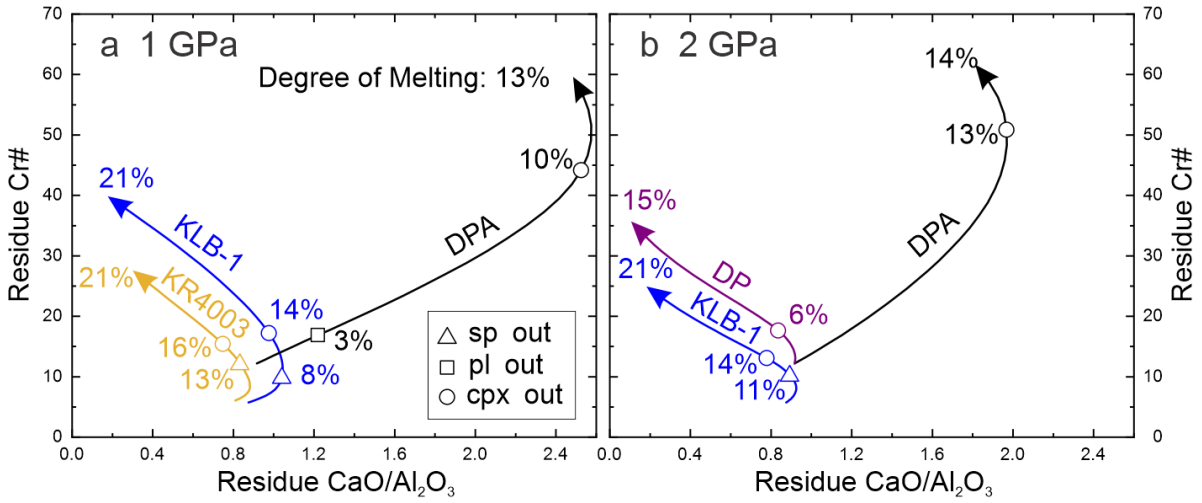

Figure 4.18 The relationship between the residue Cr# and CaO/Al_2O_3 during isobaric fractional melting of various peridotite starting compositions. Degree of melting increases from bottom to top, with the numbers on each curve specifying the amount of melting in percent. The disappearance of phases from the residue are shown by the different symbols as specified in the legend. Compositions of KLB-1, KR4003, DP, and DPA are given in Table 3.2.

The relationship between residue Cr/Al and FeO changing with the degree of isobaric fractional melting of KLB-1, KR4003, and DPA at 1 GPa and KLB-1, DP, and DPA at 2 GPa is shown in Figure 4.19. Residue Cr/Al increases with the degree of melting. Residue FeO for KLB-1 and KR4003 at 1 GPa and DPA at 1 and 2 GPa first increases then decreases with the degree of melting. Residue FeO for DP and KLB-1 at 2 GPa decreases with the degree of melting. Similar to the batch melting models, residue Cr/Al in depleted peridotites is higher than in fertile peridotites at the same pressure, and for melting of the same bulk composition, residue Cr/Al is lower at higher pressure with the same FeO content during isobaric fractional melting. Adding alkalis increases residue FeO in isobaric fractional melting.

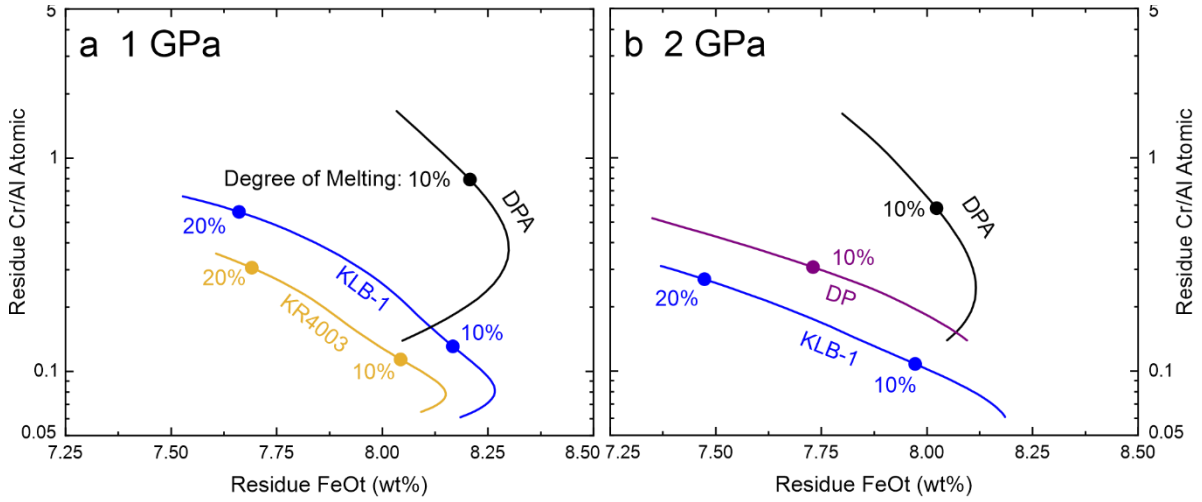

Figure 4.19 The relationship between residue Cr/Al and FeOt during isobaric fractional melting of various peridotite starting compositions. Degree of melting increases from bottom to top, with the numbers on each curve specifying the amount of melting in percent. Compositions of KLB-1, KR4003, DP, and DPA are given in Table 3.2.

The evolution of spinel Cr# and olivine Mg# with the degree of melting in isobaric fractional melting of KLB-1, KR4003, and MM3 at 1 GPa and DPA, DP, and KLB-1 at 2 GPa is shown in Figure 4.20. Spinel Cr# and olivine Mg# increase with increasing melting. The spinel Cr# and olivine Mg# for fertile peridotites are lower than the values for the DP and DPA. At 1 GPa, spinel goes out first during the isobaric fractional melting of KR4003 and KLB-1 and reaches the highest spinel Cr# of less than 30 before disappearing at ~13% degree of melting. For the isobaric fractional melting of DPA at 1 GPa, plagioclase goes out first at 3% melting, the spinel Cr# of near 30 of DPA, and the olivine Mg# of near 90.8, and then clinopyroxene goes out at 10% melting, the spinel Cr# of ~75, the olivine Mg# of 91.2. DPA has the highest spinel Cr# and olivine Mg# at 13% melting at 1 GPa. At 2 GPa, spinel goes out at 11% melting of KLB-1, with spinel Cr# of ~30 and olivine Mg# of ~90.7. Clinopyroxene goes out first in isobaric fractional melting of DPA at 13% melting and of DP at 6% melting. DPA has higher spinel Cr# of over 85 and lower olivine Mg# of around 91.6 than DP which has spinel Cr# of 70 and olivine Mg# of 92 at 14% melting.

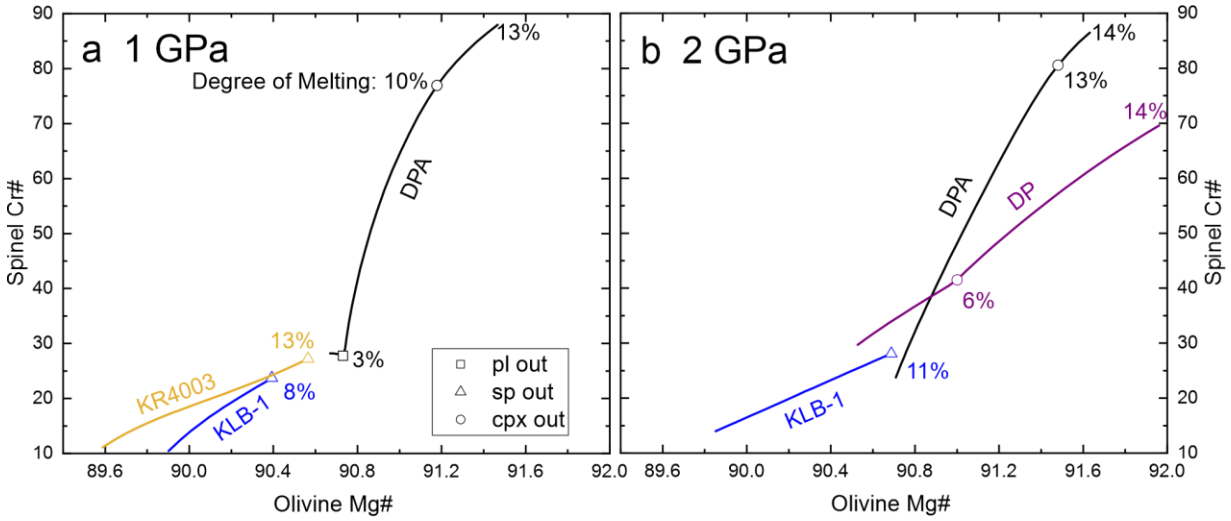

Figure 4.20 The relationship between spinel Cr# and olivine Mg# during isobaric fractional melting for a range of peridotite compositions. Degree of melting increases from left to right, with the numbers on each curve specifying the amount of melting in percent. The disappearance of phases from the residue are shown by the different symbols as specified in the legend. Compositions of KLB-1, KR4003, DP, and DPA are given in Table 3.2.

4.5 Decompression Melting

4.5.1 The Adiabat and P-T Path

To model decompression melting, I calculated polybaric fractional melting of the fertile and depleted mantle peridotites following an adiabatic P-T path. The present-day mantle potential temperature (Tp) I used to constrain the adiabat is 1300°C, with a gradient of 0.3°C/km (Ziberna et al., 2013). I also calculated decompression melting of the fertile peridotites at higher mantle potential temperatures (Herzberg et al., 2010; Herzberg and Rudnick, 2012; Servali and Korenaga, 2018) to represent decompression melting in a hotter mantle, perhaps better representing the Archean mantle. The P-T paths for decompression melting start from where the adiabat intersects the solidus of the model systems (Figure 4.21, 4.22, 4.23). Melts were extracted at 0.1 GPa intervals. The starting points of melting for the P-T paths for the decompression melting of the KLB-1, KLB-1A (added 0.29 wt% Na_2O and 0.11 wt% K_2O to KLB-1 to have the same alkalis contents as DPA, bulk composition see Table 3.2), DP, DP0.5A (Table 3.2), and DPA are summarized in Table 4.1. Compared with KLB-1, DP melts at a shallower depth, KLB-1A, DP0.5A, and DPA melts at a deeper depth.

Table 4.1 The starting point of the P-T paths for the decompression melting in this study

Bulk Composition	Tp=1300°C		Tp=1400°C		Tp=1500°C	
	P (GPa)	T (°C)	P (GPa)	T (°C)	P (GPa)	T (°C)
KLB-1	1.616	1314.54	2.308	1420.77	3.231	1529.08
KLB-1A	1.953	1317.57	-	-	-	-
DP	1.372	1312.35	-	-	-	-
DP0.5A	1.816	1316.35	-	-	-	-
DPA	2.034	1318.30	-	-	-	-

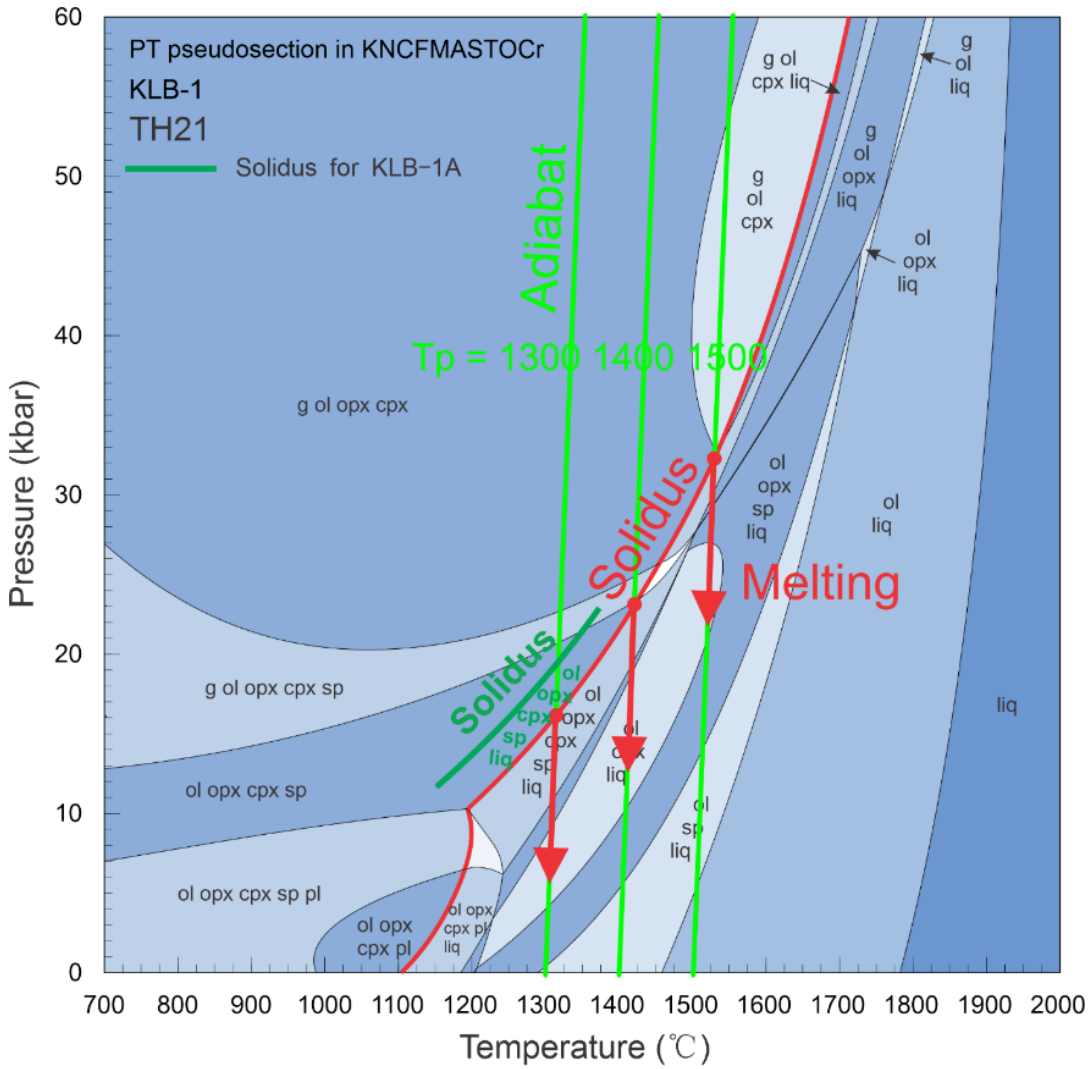

Figure 4.21 The P-T path for decompression melting of KLB-1 and KLB-1A. The solidus of KLB-1 and KLB-1A is shown by a red and dark green bold curve, respectively. The adiabat with different Tp (1300, 1400, and 1500°C) is shown by light green lines. The melting P-T paths are shown by red arrows.

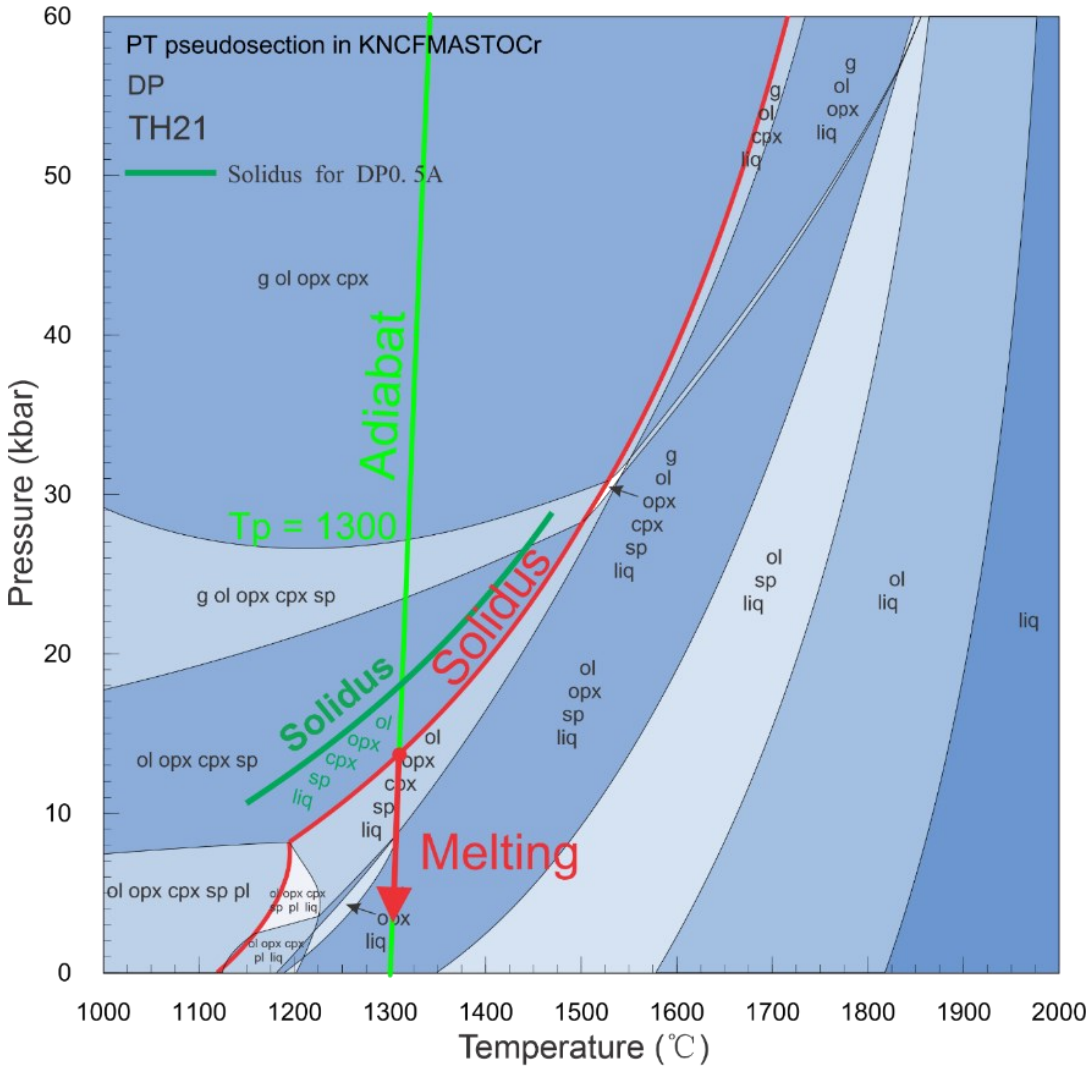

Figure 4.22 The P-T path for decompression melting of DP and DP0.5A. The solidus of DP and DP0.5A is shown by a red and dark green bold curve, respectively. The adiabat with Tp=1300°C is shown by a light green line. The melting P-T paths are shown by a red arrow.

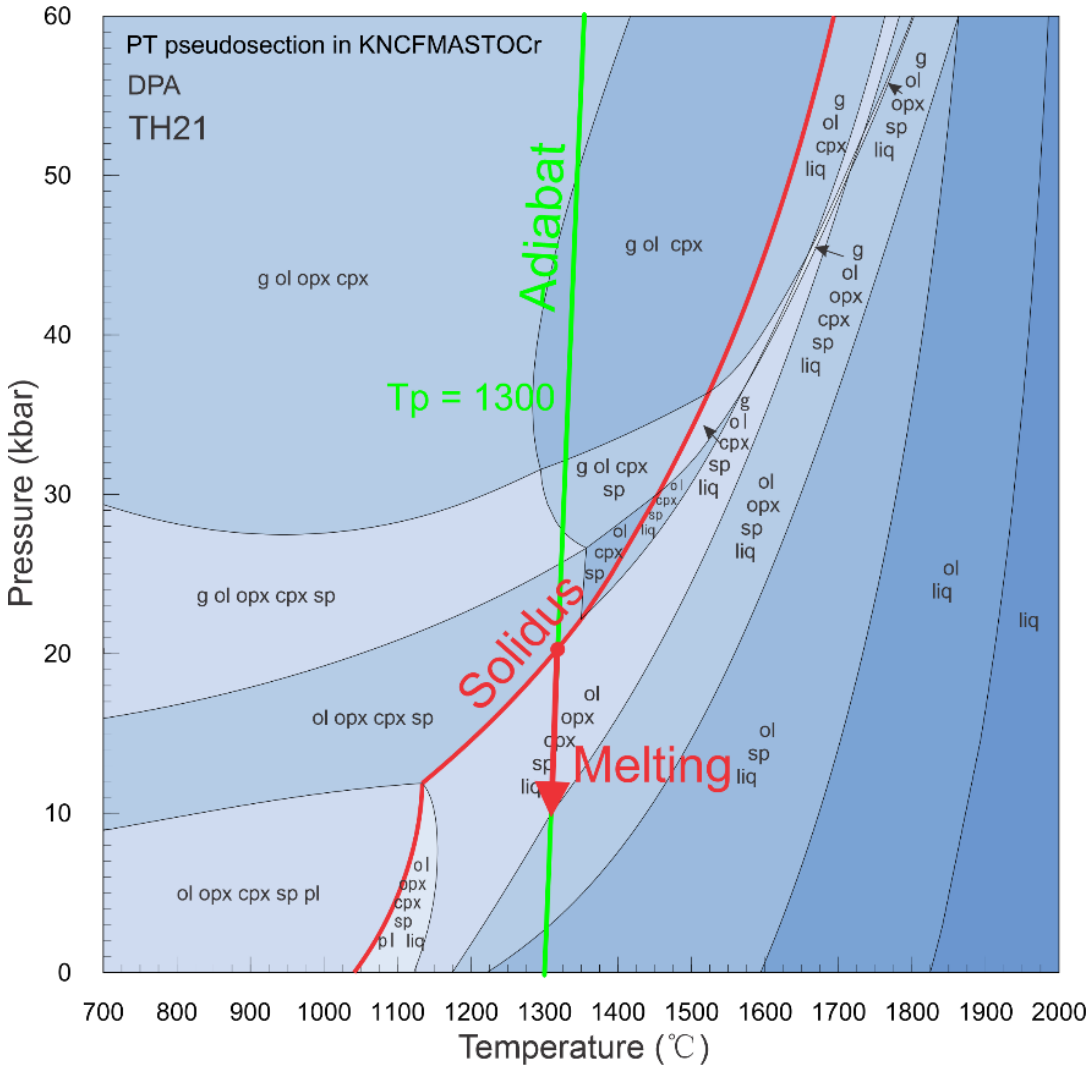

Figure 4.23 The P-T path for decompression melting of DPA.
The solidus of DPA is shown by a bold red curve. The adiabat with Tp=1300°C is shown by a light green line. The melting P-T path is shown by a red arrow.

4.5.2 Residue Mineralogy of Decompression Melting

The modal abundances of phases during decompression melting are shown in Figure 4.24. Olivine has the highest modal abundance, increasing with degree of melting. Modal orthopyroxene increases with the degree of melting before the clinopyroxene dissolves, then decreases. The amount of melt produced at each step fluctuates with the degree of melting. The modal clinopyroxene decreases with increasing degree of melting, and the clinopyroxene is the first phase to disappear during decompression melting in KLB-1 when the mantle potential temperature is 1500°C and in DP0.5A and DPA.

Modal spinel decreases with the degree of melting except for the model system of the DPA, where the modal spinel increases after the clinopyroxene dissolves. The spinel dissolves first in the model systems of the KLB-1 when the mantle potential temperature is 1300 and 1400°C and the KLB-1A and the DP when Tp=1300°C.

The amount of aggregated melt is shown in Figure 4.25. The amount of aggregated melt for the decompression melting of KLB-1 following the adiabat with Tp=1500°C is the highest, and the value for the adiabat with Tp=1400°C is the second highest. KLB-1 generates more melts before clinopyroxene out at the beginning, then generates less afterwards. The modal aggregated melt for KLB-1A is higher than KLB-1, melting following the same adiabat, and both values are higher than DP. The modal aggregated melt increases with the amount of the alkali added to the system (DPA>DP0.5A>DP) if melting following the same adiabat.

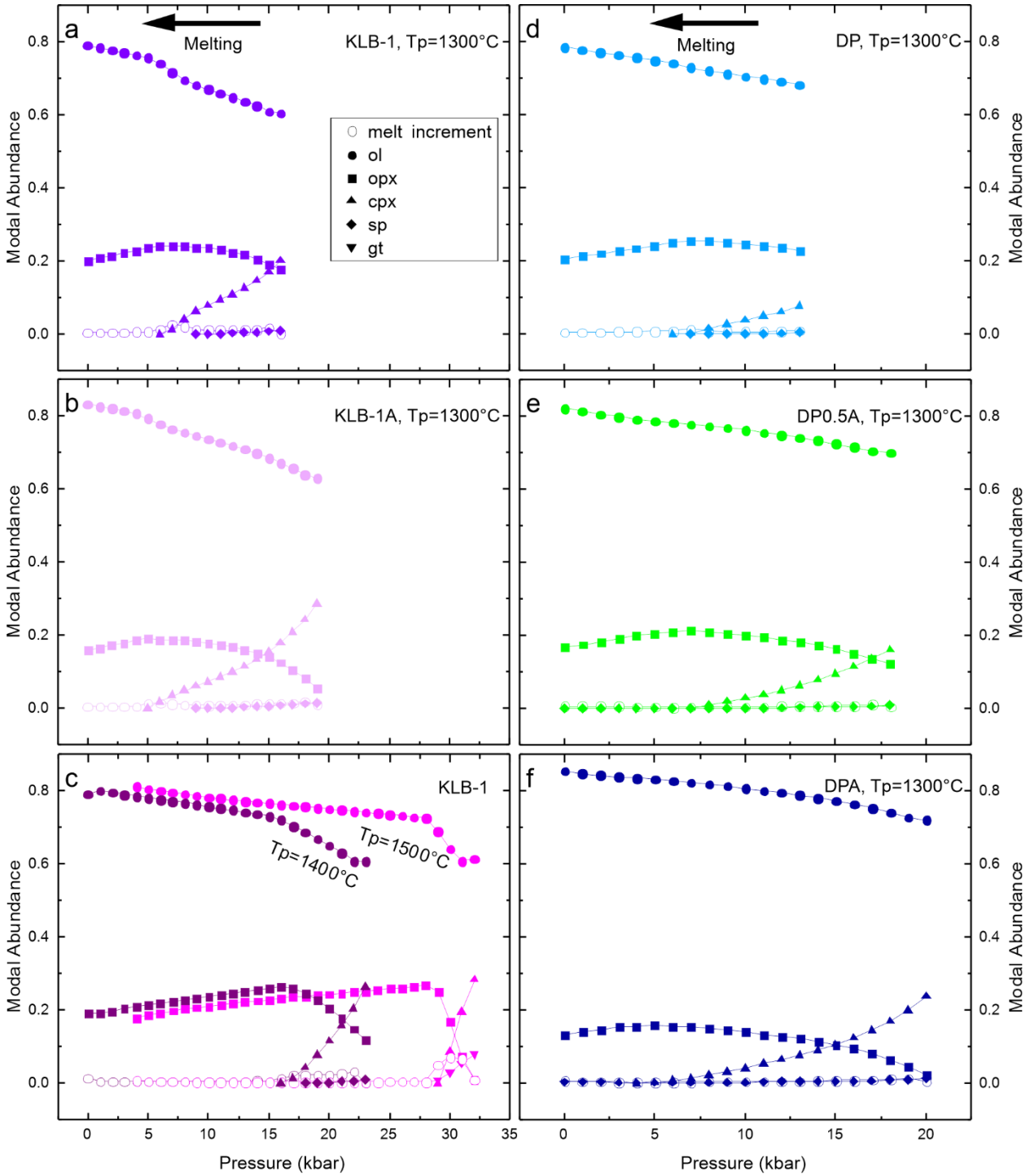

Figure 4.24 The modal abundances of phases change with the pressure during decompression melting for various peridotite compositions.
a KLB-1, Tp=1300°C; b KLB-1A, Tp=1300°C; c KLB-1, Tp=1300 and 1400°C; d DP, Tp=1300°C; e DP0.5A, Tp=1300°C; f DPA, Tp=1300°C. Different phases in residue are shown by different solid shapes, and the amount of melt is shown by hollow circles as specified in the legend.

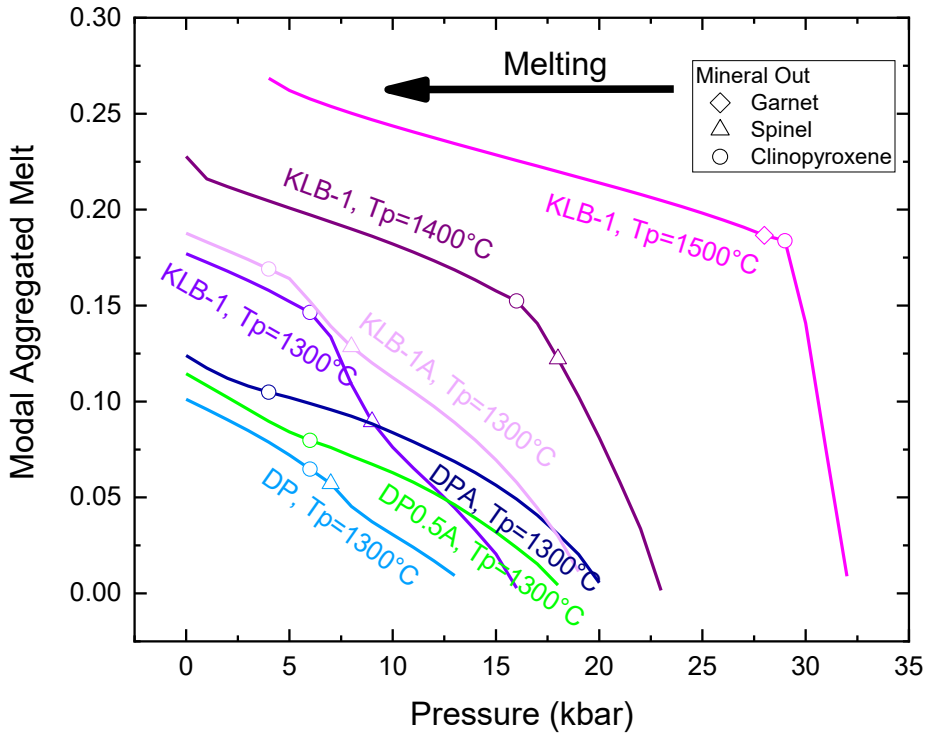

Figure 4.25 The modal aggregated melt in decompression melting for various peridotite compositions.
Degree of melting increases from left to right. The text on each curve specifies the bulk composition and mantle potential temperature. The disappearance of phases from the residue is shown by the different symbols as specified in the legend. Compositions of KLB-1, KLB-1A, DP, DP0.5A, and DPA are given in Table 3.2.

4.5.3 Evolution of Residue Chemistry during Decompression Melting

The relationship between residue Al_2O_3 and CaO changing with the degree of decompression melting of KLB-1, KLB-1A, DP, DP0.5A, and DPA is shown in Figure 4.26. Both residue Al_2O_3 and CaO decrease with the degree of melting. The Al_2O_3 content of residues of DP, DP0.5A, and DPA decreases from 2 wt% to around 0.6, 0.4, and 0.2, respectively, and residue CaO decreases from 2 wt% to around 0.5. The residue Al_2O_3 of KLB-1 decreases from 3.5 wt% to around 0.5, and the residue CaO decreases from 3 wt% to near 0 with mantle potential temperatures of 1400°C and 1500°C to around 0.5 with mantle potential temperature of 1300°C. Residue Al_2O_3 of KLB-1A decreases from around 3.5 wt% to 0.3, and residue CaO decreases from around 3 wt% to around 0.6 with a 19% degree of melting. As in batch and isobaric fractional melting, residue Al_2O_3 is lower in depleted peridotites with the same residue CaO during decompression melting. Adding alkalis decreases residue Al_2O_3 in decompression melting. Increasing mantle potential temperature increases residue Al_2O_3.

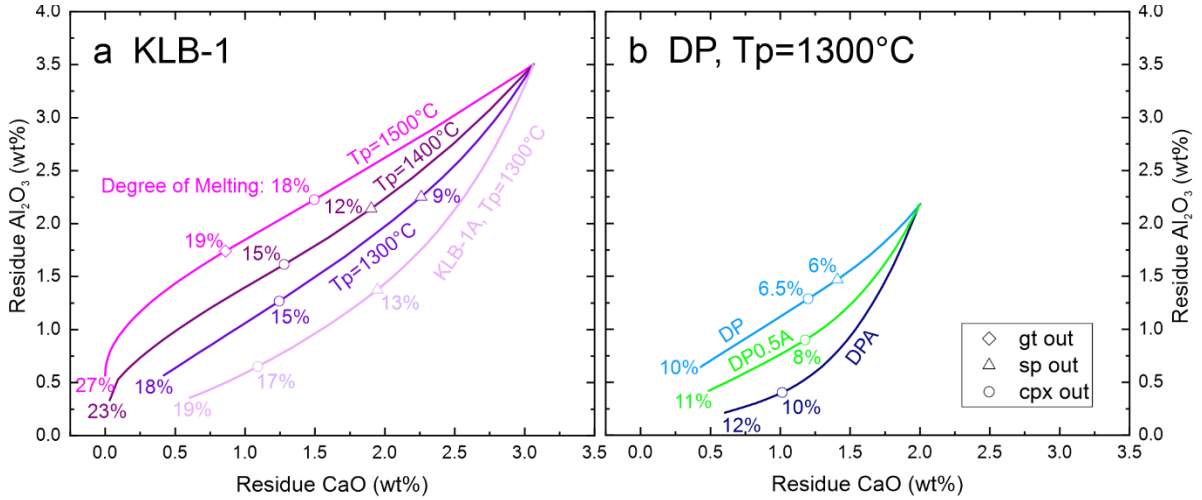

Figure 4.26 The relationship of residue Al_2O_3 and CaO during decompression melting for various peridotite compositions.
Degree of melting increases from right to left, with the numbers on each curve specifying the amount of melting in percent. The disappearance of phases from the residue is shown by the different symbols as specified in the legend. Compositions of KLB-1, KLB-1A, DP, DP0.5A, and DPA are given in Table 3.2.

The bulk residue Cr# and CaO/Al_2O_3 during decompression melting of KLB-1, KLB-1A, DP, DPA, and DP0.5A are shown in Figure 4.27. Residue Cr# increases with the degree of melting. The residue CaO/Al_2O_3 for KLB-1 and DP generally decreases with the degree of melting, while the value for the KLB-1A, DP0.5A, and DPA increases significantly with the degree of melting first and then decreases slightly in the melting of KLB-1A and DP0.5A. The decompression melting of KLB-1 with a higher potential temperature has a lower residue CaO/Al_2O_3 value. Adding alkalis increases residue CaO/Al_2O_3 in decompression melting. The maximum residue Cr# in fractional melting in lower than batch melting. The relationship of residue Cr# and CaO/Al_2O_3 in decompression melting is similar to isobaric fractional melting.

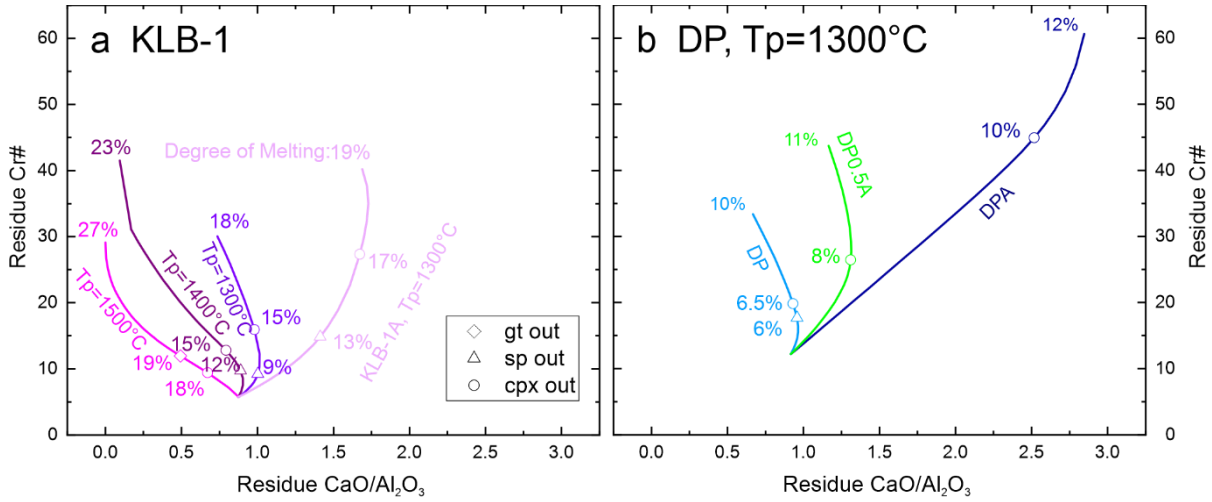

Figure 4.27 The relationship of residue Cr# and CaO/Al_2O_3 during decompression melting for various peridotite starting compositions. Degree of melting increases from bottom to top, with the numbers on each curve specifying the amount of melting in percent. The disappearance/appearance of phases from the residue is shown by the different symbols as specified in the legend. Compositions of KLB-1, KLB-1A, DP, DP0.5A, and DPA are given in Table 3.2

The relationship between bulk residue Cr/Al and FeO changing with the degree of decompression melting of KLB-1, KLB-1A, DP, DP0.5A, and DPA is shown in Figure 4.28. Residue Cr/Al increases with the degree of melting. Residue FeO of DP melting with mantle potential temperature of 1300°C and KLB-1 with mantle potential temperature of 1400°C and 1500°C decreases with the degree of melting, while the value of KLB-1, KLB-1A, DP0.5A, and DPA increases first and then decreases. Under these conditions, residue FeO in depleted peridotites is higher than in fertile peridotites. Adding alkalis increases residue FeO in decompression melting. Increasing mantle potential temperature decreases residue FeO. The maximum residue Cr/Al in fractional melting is lower than in batch melting. The trend of residue Cr/Al and FeO in decompression melting is steeper than in isobaric fractional melting.

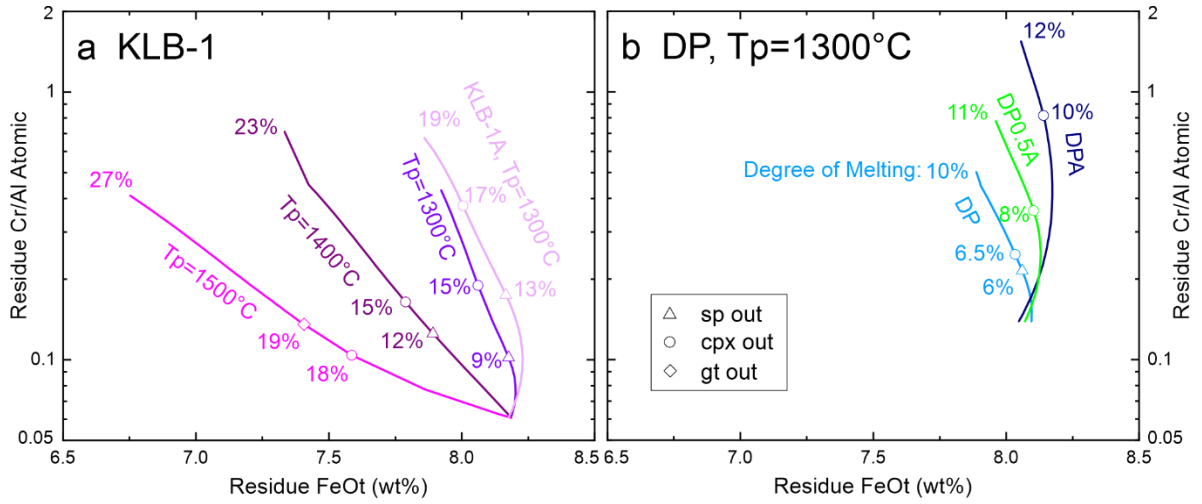

Figure 4.28 The relationship of residue Cr/Al and FeOt during decompression melting for various peridotite compositions.
Degree of melting increases from bottom to top, with the numbers on each curve specifying the amount of melting in percent. The disappearance of phases from the residue is shown by the different symbols as specified in the legend. Compositions of KLB-1, KLB-1A, DP, DP0.5A, and DPA are given in Table 3.2.

The evolution of spinel Cr# and olivine Mg# during decompression melting of KLB-1, KLB-1A, DP, and DPA is shown in Figure 4.29. Both the spinel Cr# and olivine Mg# increase with the degree of melting. The highest spinel Cr# and olivine Mg# for the DPA and DP0.5A are higher than the values for other bulk compositions. Decompression melting of KLB-1 along different mantle adiabats produces similar spinel Cr# and olivine Mg#. The spinel Cr# for KLB-1A is slightly lower than the KLB-1 with the same olivine Mg#. The spinel Cr# for the DP is slightly higher than the KLB-1 and KLB-1A.

Spinel disappears first during the decompression melting of KLB-1 and KLB-1A at ~13% melting and in DP at 6% melting. The highest spinel Cr# for KLB-1 with mantle potential temperature of 1300°C is around 20, and around 25 with the mantle potential temperature of 1400°C, whereas the olivine Mg# is around 90.4 and 90.6, respectively. The highest spinel Cr# and olivine Mg# for DP and KLB-1A is similar, around 35 and 90.9, respectively. The highest olivine Mg# for DP0.5A and DPA is around 90.4, the highest spinel Cr# for DPA is near 90, and for DP0.5A is near 80.

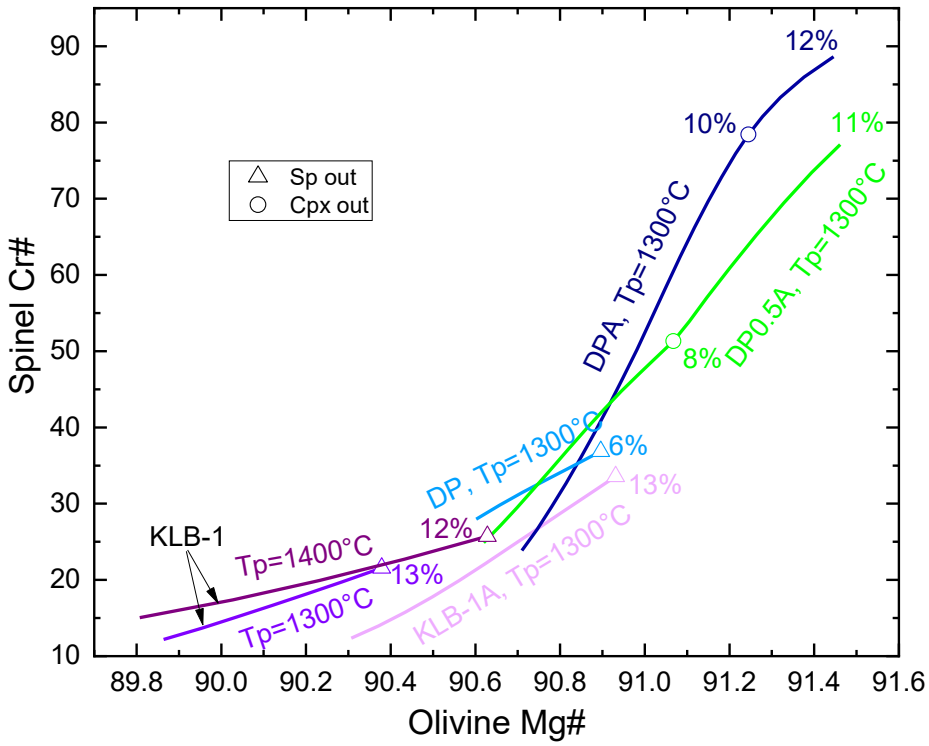

Figure 4.29 The relationship between spinel Cr# and olivine Mg# during decompression melting for various peridotite compositions.
Degree of melting increases from left to the right, with the numbers on each curve specifying the amount of melting in percent. The disappearance of phases from the residue is shown by the different symbols as specified in the legend. Compositions of KLB-1, KLB-1A, DP, DP0.5A, and DPA are given in Table 3.2.

The partitioning of Cr and Al between spinel and melt during decompression melting can help explain the trends observed (Figure 4.30), because this shows how the factors such as bulk composition and mantle potential temperature influence the preference of Cr and Al for phases. The distribution coefficient of Cr, $D_{Cr}^{Sp/Melt}$, decreases with melting, and the values for different compositions are similar, except for KLB-1 following the adiabat with the mantle potential temperature of 1400°C, the only one modelled.

The distribution coefficient of Al, $D_{Al}^{Sp/Melt}$, also decreases with melting but shows more variability with bulk composition. The model systems for the melting of KLB-1 have the highest $D_{Al}^{Sp/Melt}$. The value of $D_{Al}^{Sp/Melt}$ for the model system of the KLB-1A is lower than the KLB-1 but slightly higher than the DP. The $D_{Al}^{Sp/Melt}$ of DPA is the lowest among these bulk

compositions, and the value $D_{Al}^{Sp/Melt}$ of DP0.5A is the second-lowest. Adding alkalis thus decreases the preference of Al into spinel but has little influence on the preference of Cr.

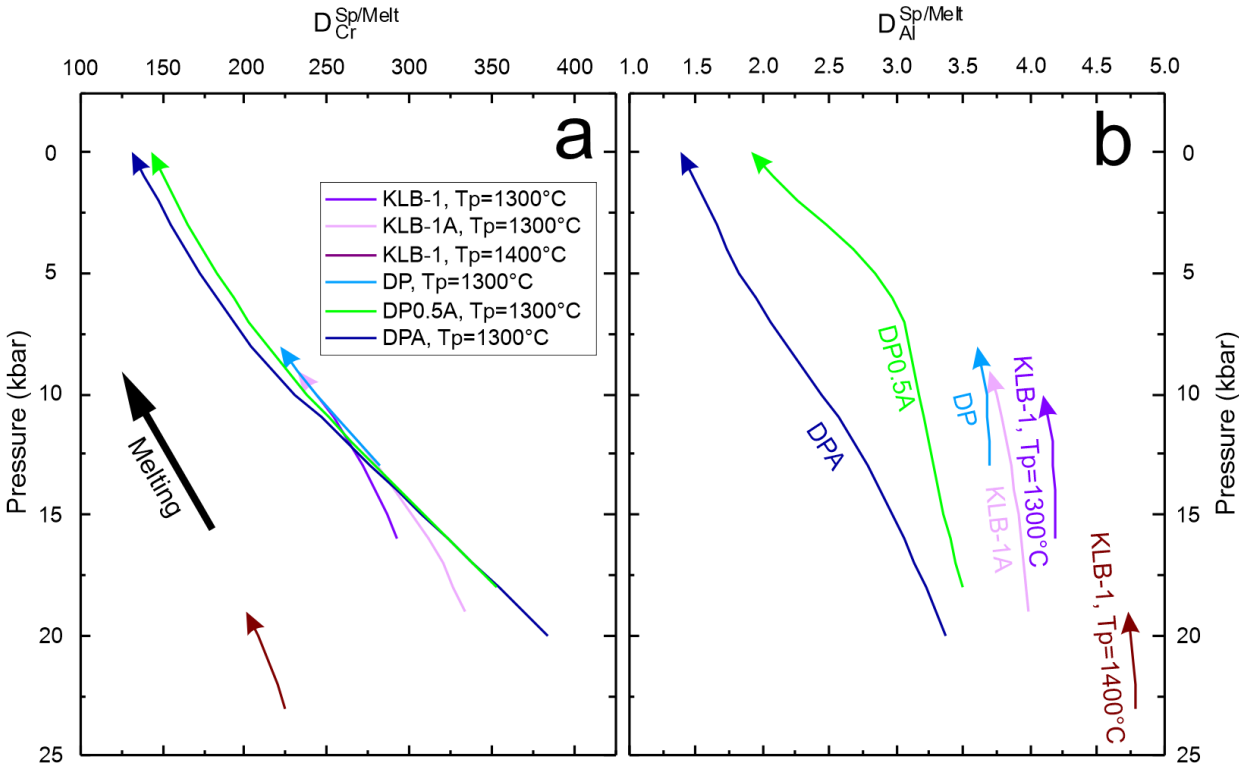

Figure 4.30 Variation of the distribution coefficient of Cr (a) and Al (b) with pressure during decompression melting of peridotite.
Degree of melting increases from bottom to top, in the direction of the arrows. The bulk composition and mantle potential temperature are specified in the legend in a.

Chapter 5 Discussion

5.1 Achieving High Degree of Melting

The Earth's mantle is below its solidus temperature in most environments, so some sort of perturbation in needed to trigger melting. The scenario most relevant to the present study is upwelling of mantle, either in deep-sourced mantle plumes or in ascending limbs of upper-mantle convection cells underneath divergent plate boundaries – plate spreading centres.

In such either mantle plume or divergent plate boundary scenarios, the extent of partial melting will be controlled by the temperature of the upwelling mantle; hotter mantle will intersect the mantle solidus deeper and hence will have a longer melting interval and will tend to melt to greater extents.

Adding volatiles is another way to trigger melting because volatiles could lower the solidus of the mantle rocks. This melting mechanism is what is envisaged to occur in subduction zones. Water liberated from the descending oceanic plate by the breakdown of hydrous minerals rises to the overlying mantle wedge and initiates melting of peridotites in the mantle wedge. Melting in the supra-subduction zone can also have a component of decompression melting due to the flow in the wedge (e.g. Kelley et al., 2010; Pearce, 2005)). As previously discussed, we cannot address this hydrous mode of melting because of the limitations of the current melt model in THERMOCALC.

To achieve a higher degree of peridotite melting, two-stage melting models that combine different types of melting can be considered. For example, mantle peridotites can partially melt in a plume and generate residues, which could further melt in the mid-ocean ridge environment (e.g. Morgan and Morgan, 1999). Or the first stage of melting happens in the mantle wedge due to fluxing from slab-derived components, and residues generated in this stage can start another stage of adiabatic decompression melting (e.g. Bénard, et al., 2018).

The above scenarios model the initial partial melting of the mantle; a full petrogenetic model needs to consider both melt generation and transport (e.g. Kelemen et al., 1995; Langmuir and Forsyth, 2007)). The interaction of the melt and surrounding mantle during ascent is another

research area where thermodynamic modelling can contribute. Our focus in this study, however, is on the compositional evolution of the residues of partial melting, not the melts.

Another factor that plays into melting is the composition of the lithology undergoing melting. The mean mantle composition is well constrained in McDonough and Sun (1995), but mantle heterogeneity, including its volatile contents, could affect these melting processes. It is well known that melting is likely to occur with the help of incompatible species (e.g. Fiquet, 2018), but only volatile species have been widely studied (e.g. Eggler, 1974; 1978; Kushiro, 1968; 1969; 1972; Millhollen et al., 1974; Presnall, 1987; Presnall et al., 1979; Wyllie and Huang, 1976). Results from this study show that adding 0.46 wt% of Na_2O and 0.12 wt% of K_2O can reduce the melting temperature by 50-100°C of a lherzolite or a depleted peridotite source.

Our calculations can provide insight as well into the melting of the hotter mantle. With a mantle potential temperature of 1500°C such as may have been present during the Archean (Herzberg et al, 2010), a lherzolitic mantle melts from 97 km depth to a melt-fraction of 27% while ascending to the surface, and the residues are harzburgite above 84 km. As the mantle potential temperature drops to 1300°C, more typical of today's mantle, lherzolites melt from 48.5 km depth to 18% melt-fraction at the surface, and the residues are harzburgite above 18 km. Depleted peridotites melt from 41.2 km depth to attain a 10% melt-fraction at the surface. Adding 0.46 wt% of Na_2O and 0.12 wt% of K_2O can trigger the melting of fertile peridotites from a depth of 58.6 km and depleted peridotites from 61 km.

5.2 Evolution of Spinel and Olivine Chemistry in Residue of Partial Melting

Melt extraction is efficient during mantle melting, so this process tends to be fractional, but not all melting is necessarily 'near-fractional' (e.g. Kelemen et al., 1997). The differences between batch and fractional melting under the same pressure are discussed in this section. Adiabatically upwelling mantle contributes most melts beneath divergent plate boundaries. Therefore, the differences between decompression melting and isobaric fractional melting are also discussed here.

The evolution of peridotite melting residues plays an essential role in forming the subcratonic lithospheric mantle (e.g., Pearson et al., 2021). Based on the thermodynamic modelling reported in Chapter 4, we can explore how spinel and olivine in the residues of partial melting evolve

under different scenarios, such as isobaric batch melting, isobaric fractional melting, and the more realistic decompression melting. This, in turn, allows an evaluation of how effective these indices might be in tracking the process of partial melting in natural peridotite samples. The mineralogy, melt inclusions, and olivine spinel mantle array of mantle peridotites are generally used to characterize the degree of melting. The evolution of the mineralogy of mantle peridotites during melting was investigated in chapter 4. The evolution of the olivine spinel mantle array during batch melting, isobaric fractional melting, and decompression melting is discussed in this section and with the effects of source compositions. The source composition also influences the chemical contents. Therefore, the differences between the melting of different fertile and depleted peridotites are also studied.

5.2.1 Isobaric Batch Melting VS Isobaric Fractional Melting

As shown in Sections 4.3.2 and 4.4.2, olivine Mg# and degree of melting from isobaric fractional melting are lower than isobaric batch melting at the same value of spinel Cr#. There are large differences in the olivine-spinel mantle array during the melting of fertile peridotites because spinel disappears first during the isobaric fractional melting of fertile peridotites. Spinel from fertile peridotites could exist to a higher degree of batch melting (over 40%) than isobaric fractional melting (less than 13%). Therefore, spinel from fertile peridotites could reach higher spinel Cr# (>60) and olivine Mg# (>93.5) in batch melting than isobaric fractional melting (spinel Cr#<30, olivine Mg#<90.8). To reach this highest spinel Cr#, the temperature in batch melting is over 170°C higher than in isobaric fractional melting (over 1550°C for batch melting, 1340°C for isobaric fractional melting at 1 GPa, over 1610°C for batch melting and 1440°C for isobaric fractional melting at 2 GPa).

At 2 GPa, spinel from DP can also exist to a higher degree of batch melting (45%) than isobaric fractional melting (14%, spinel still persists, but the calculation cannot continue because the residue becomes so refractory that it cannot be used for calculation in THERMOCALC). The highest spinel Cr# and olivine Mg# of DP during batch melting (78, 95) are also higher than isobaric fractional melting (70, 92). To reach this highest spinel Cr# for DP, the temperature in batch melting (1727°C) is higher than isobaric fractional melting (1610°C). The addition of alkalis (DPA) changes spinel stability to 1733°C with 43% batch melting and 1553°C with 14%

isobaric fractional melting at 2GPa and increases the spinel Cr# to over 85 with slightly lower olivine Mg# than DP.

As shown in Figure 3.7 and 3.12, the evolution of olivine Mg# with batch melting is near-linear, so we can analyze the slope of the spinel olivine mantle array based on spinel Cr#. The increase of spinel Cr# during melting depends on the behaviour of Cr and Al as shown in Figure 4.7. Before clinopyroxene goes out, the rapid increase of spinel Cr# mainly is a function of the sharp decrease of Al. Between cpx-out and opx-out, spinel Cr# still increases because Cr in spinel increases faster than Al. After opx-out, the shallower slope of the olivine spinel mantle array is caused by the more rapid depletion of Cr compared with Al. The evolution trend shows in the batch melting of both depleted and fertile peridotites. However, spinel-olivine relations become much different in isobaric fractional melting because spinel goes out first in fertile peridotites, and the residues from melting depleted peridotites are too refractory to continue the calculation after 14% melting.

5.2.2 Decompression Melting

The evolution of the spinel olivine mantle array for decompression melting is more like isobaric fractional melting with the same bulk composition, which suggests that pressure, at least over this range, plays a subordinate role. Spinel disappears first during decompression melting of KLB-1, KLB-1A, and DP, whereas clinopyroxene goes out first in DPA and DP0.5A. As in isobaric fractional melting, the maximum spinel Cr# of KLB-1 is <30. The highest spinel Cr# of DP is <40, much lower than isobaric fractional melting due to the more rapid disappearance of spinel in decompression melting. Adding alkalis increases spinel Cr# in decompression melting. The addition of alkalis in KLB-1 increases spinel Cr# from less than 30 to ~35, whereas the addition of alkalis in DP increases spinel Cr# from 37 to ~90. Increasing Tp for KLB-1 can also increase the maximum spinel Cr# from ~20 to ~25.

The distribution coefficient between spinel and melt shows the preference of elements for phases. As shown in Figure 4.30, the distribution coefficient of Cr and Al decreases with melting, which means both elements favour the melt as melting increases. The bulk composition does not considerably influence $D_{Cr}^{Sp/Melt}$, but depleted peridotites have lower $D_{Al}^{Sp/Melt}$ than fertile peridotites. Adding alkalis also decreases $D_{Al}^{Sp/Melt}$. The much lower $D_{Al}^{Sp/Melt}$ after adding

alkalis in DP explains the much higher spinel Cr# in DPA. Increasing Tp could decrease $D_{Cr}^{Sp/Melt}$ but increase $D_{Al}^{Sp/Melt}$, which means a hotter mantle could encourage Cr while discouraging Al from going into melts. Therefore, adding alkalis increases $D_{Cr/Al}^{Sp/Melt}$ while increasing mantle potential temperature decreases $D_{Cr/Al}^{Sp/Melt}$.

5.2.3 Modelling Results VS Natural Peridotites and Experimental Results

The spinel Cr# vs olivine Mg# results for isobaric batch melting, isobaric fractional melting, and decompression melting calculated from this study can be summarized as shown in Figure 5.5, which also shows the relationship between spinel Cr# and olivine Mg# from natural peridotites and experimental results. The OSMA area for isobaric fractional melting generally overlaps that of theoretically modelled decompression melting. The slope of OSMA from fractional melting is ~ four times steeper than batch melting and is closer to the slope defined by natural peridotites and experimental results. From this, we can conclude that single-stage, fractional melting can produce high Cr# spinels, but it requires an alkali-enriched lithology.

Erlank et al. (1987) reported three spinels with Cr#>98 and Cr_2O_3 >55 wt% from mantle xenoliths in kimberlites in South Africa. Hauri and Hart (1994) reported one spinel with Cr#>98 and Cr_2O_3 = 64.4 wt% from mantle xenolith in the island arc from Savai's, Western Samoa. The melting of DPA can generate the highest spinel Cr# in this study: the batch melting of DPA could generate spinel with Cr# near 87 and Cr_2O_3 above 61 wt%; the isobaric fractional melting of DPA can generate spinel Cr# near 88 and Cr_2O_3 over 57 wt%; the decompression melting of DPA can generate spinel Cr# ~88.6 and Cr_2O_3 over 55 wt%. Spinel Cr# in natural environment that is higher than the highest spinel Cr# in modelling results is probably generated through metamorphic equilibration with garnet after emplacement of melting residues in subcratonic lithospheric mantle (Klemme, 2004; Webb and Wood, 1986).

None of the trajectories mimic the very steep trend at high olivine Mg#, shown by cratonic mantle peridotites, and so the reason that that suite of peridotites has such a steep olivine-spinel array remains unsolved. In the cratonic trend, it's not just the high Cr# and high Mg# trends. None of the models can form the high Mg# olivine at low Cr# (~ 20).

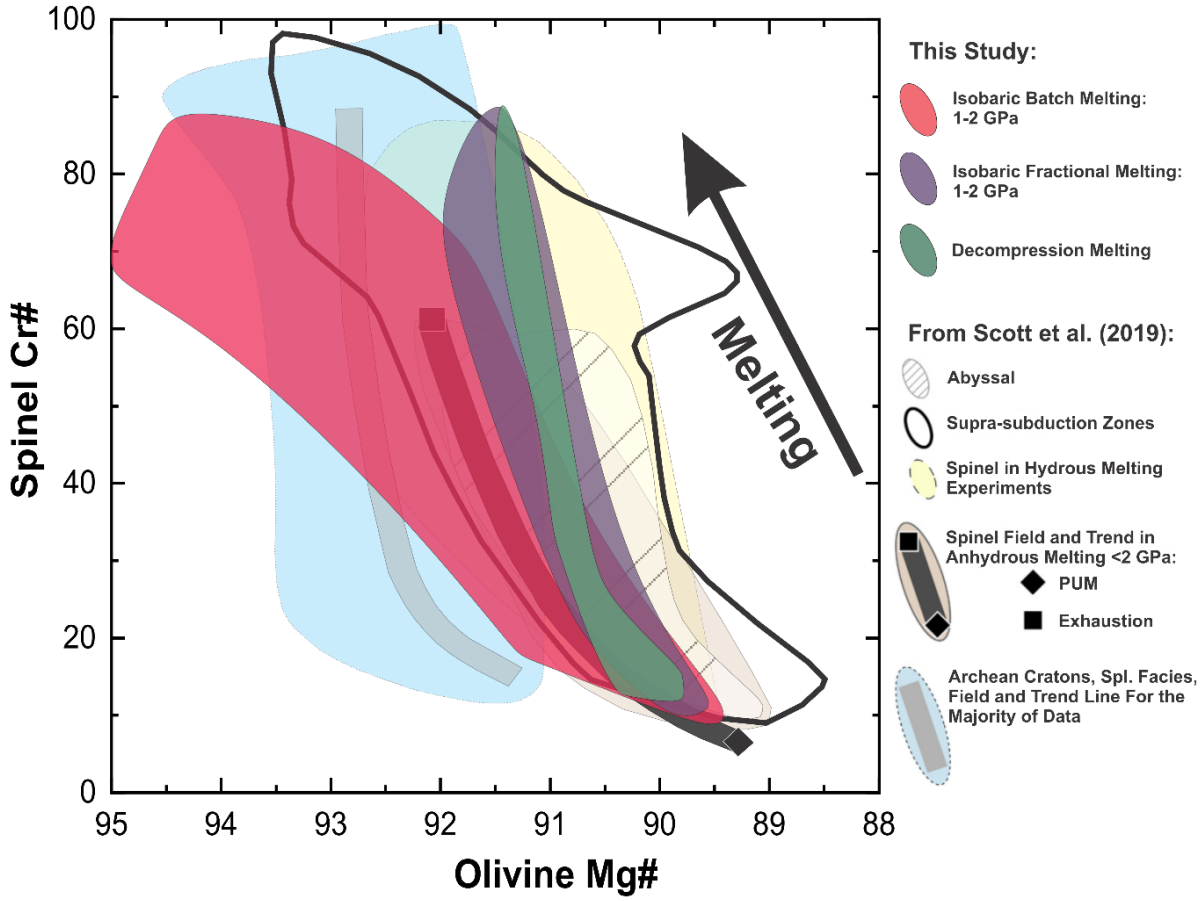

Figure 5.1 Model results of spinel Cr# versus olivine Mg# for different theoretical melting conditions compared to global fields of abyssal peridotite, supra-subduction zone peridotite, Archean peridotites and the results of peridotite anhydrous and hydrous melting experiments (additional fields after Scott et al., 2019)

Chapter 6 Conclusion

The most recent formulation of the Holland and Powell THERMOCALC model was used to model the anhydrous melting of fertile and depleted mantle peridotites based on the testing of models in chapter 3. Isobaric batch melting and isobaric fractional melting under different pressure and decompression melting are studied.

The solidus and the temperature of spinel stability for fertile peridotites are lower than for depleted peridotites. Adding 0.46 wt% of Na_2O and 0.12 wt% of K_2O can reduce the melting temperature by ~100°C of a lherzolite or a depleted peridotite source but maintains the temperature of spinel stability in batch melting. Adding alkalis can also decrease residue Al_2O_3 and increases residue CaO/Al_2O_3 and FeO in all melting scenarios.

Spinel could survive to a much higher degree of melting in batch melting (>40%) than fractional melting (<14%). For fertile peridotites, this is because spinel goes out first in fractional melting. For depleted peridotites, this is because the calculation cannot continue after 14% fractional melting, except for DP in decompression melting, where spinel goes out first. The reason why the calculation cannot continue in decompression melting is that the melting finishes when the pressure decreases to zero, but in isobaric fractional melting, the melting stops probably because the residue becomes so refractory that it does not melt anymore. Spinel in depleted peridotites could exist to a higher degree of isobaric fractional melting than fertile peridotites. In decompression melting, adding alkalis extends the spinel stability of DP to a higher degree of melting (from 6% to 12%).

The evolution of spinel Cr# and olivine Mg# on the mantle array diagram with batch melting is gentler than that with fractional melting. The slope of the OSMA trends from Archean peridotites is closer to that from decompression melting. The maximum spinel Cr# in depleted peridotites is higher than in fertile peridotites, with DPA having the highest maximum spinel Cr# in all melting models (>85). The generation of extremely high-Cr spinels requires alkali enrichment, so single-stage melting of a “normal” fertile or depleted peridotitic mantle cannot generate a high spinel Cr# (>80).

References

Abe, Y., 1997. Thermal and chemical evolution of the terrestrial magma ocean. Physics of the Earth and Planetary Interiors, 100(1-4): 27-39.

Anderson, G.M., 2005. Thermodynamics of natural systems. Cambridge University Press.

Arndt, N.T., Coltice, N., Helmstaedt, H. and Gregoire, M., 2009. Origin of Archean subcontinental lithospheric mantle: Some petrological constraints. Lithos, 109(1-2): 61-71.

Aulbach, S., 2012. Craton nucleation and formation of thick lithospheric roots. Lithos, 149: 16-30.

Baker, M.B. and Stolper, E.M., 1994. Determining the composition of high-pressure mantle melts using diamond aggregates. Geochimica et Cosmochimica Acta, 58(13): 2811-2827.

Bénard, A., Le Losq, C., Nebel, O. and Arculus, R.J., 2018. Low-Ca boninite formation by second-stage melting of spinel harzburgite residues at mature subduction zones: new evidence from veined mantle xenoliths from the West Bismarck Arc. Contributions to Mineralogy and Petrology, 173(12): 1-25.

Benn, K., Mareschal, J. and Condie, K.C., 2006. Introduction: archean geodynamics and environments. Geophysical Monograph-American Geophysical Union, 164: 1.

Berman, R.G., Engi, M., Greenwood, H.J. and Brown, T.H., 1986. Derivation of internally-consistent thermodynamic data by the technique of mathematical programming: a review with application the system MgO-SiO_2-H_2O. Journal of Petrology, 27(6): 1331-1364.

Berman, R.G., 1988. Internally-consistent thermodynamic data for minerals in the system Na2O-Na_2O-K_2O-CaO-MgO-FeO-Fe_2O_3-Al_2O_3-SiO_2-TiO_2-H_2O-CO_2. Journal of Petrology, 29(2): 445-522.

Berman, R.G., 1991. Thermobarometry using multi-equilibrium calculations; a new technique, with petrological applications. The Canadian Mineralogist, 29(4): 833-855.

Berman, R.G., Brown, T.H. and Perkins, E.H., 1987. GEOe-CALC; software for calculation and display of PTX phase diagrams. American Mineralogist, 72(7-8): 861-862.

Bodinier, J.L. and Godard, M., 2003. Orogenic, ophiolitic, and abyssal peridotites. Treatise on Geochemistry, 2: 568.

Bonatti, E., Emiliani, C., Ferrara, G., Honnorez, J. and Rydell, H., 1974. Ultramafic-carbonate breccias from the equatorial Mid Atlantic Ridge. Marine Geology, 16(2): 83-102.

Bonatti, E., Hamlyn, P. and Ottonello, G., 1981. Upper mantle beneath a young oceanic rift: peridotites from the island of Zabargad (Red Sea). Geology, 9(10): 474-479.

Boudier, F. and Coleman, R.G., 1981. Cross section through the peridotite in the Samail ophiolite, southeastern Oman Mountains. Journal of Geophysical Research: Solid Earth, 86(B4): 2573-2592.

Boyd, F.R., 1989. Compositional distinction between oceanic and cratonic lithosphere. Earth and Planetary Science Letters, 96(1-2): 15-26.

Boyd, F.R. and England, J.L., 1960. Apparatus for phase-equilibrium measurements at pressures up to 50 kilobars and temperatures up to 1750°C. Journal of Geophysical Research, 65(2): 741-748.

Boyd, F.R. and England, J.L., 1962. Effect of pressure on the melting of pyrope. Carnegie Institute of Washington Yearbook, 61: 109-112.

Boyd, F.R., England, J.L. and Davis, B.T., 1964. Effects of pressure on the melting and polymorphism of enstatite, $MgSiO_3$. Journal of Geophysical Research, 69(10): 2101-2109.

Boyd, F.R. and England, J.L., 1963. Effect of pressure on the melting of diopside, $CaMgSi_2O_6$, and albite, $NaAlSi_3O_8$, in the range up to 50 kilobars. Journal of Geophysical Research, 68(1): 311-323.

Boyd, F.R. and Meyer, H.O., 1979. The mantle sample: inclusions in kimberlites and other volcanics, 2. American Geophysical Union.

Brey, G.P. and Köhler, T., 1990. Geothermobarometry in four-phase lherzolites II. New thermobarometers, and practical assessment of existing thermobarometers. Journal of Petrology, 31(6): 1353-1378.

Brey, G.P. and Shu, Q., 2018. The birth, growth and ageing of the Kaapvaal subcratonic mantle. Mineralogy and Petrology, 112(S1): 23-41.

Canil, D., O'Neill, H.S.C., Pearson, D., Rudnick, R.L., McDonough, W.F. and Carswell, D., 1994. Ferric iron in peridotites and mantle oxidation states. Earth and Planetary Science Letters, 123(1-3): 205-220.

Canil, D. and Scarfe, C.M., 1990. Phase relations in peridotite+ CO_2 systems to 12 GPa: implications for the origin of kimberlite and carbonate stability in the Earth's upper mantle. Journal of Geophysical Research: Solid Earth, 95(B10): 15805-15816.

Carlson, R.W., Pearson, D.G. and James, D.E., 2005. Physical, chemical, and chronological characteristics of continental mantle. Reviews of Geophysics, 43(1).

Carmichael, D.M., 1969. On the mechanism of prograde metamorphic reactions in quartz-bearing pelitic rocks. Contributions to Mineralogy and Petrology, 20(3): 244-267.

Chantel, J., Manthilake, G., Andrault, D., Novella, D., Yu, T. and Wang, Y., 2016. Experimental evidence supports mantle partial melting in the asthenosphere. Science advances, 2(5): e1600246.

Charlu, T., Newton, R. and Kleppa, O., 1975. Enthalpies of formation at 970 K of compounds in the system MgO-Al_2O_3-SiO_2 from high temperature solution calorimetry. Geochimica et Cosmochimica Acta, 39(11): 1487-1497.

Chatterjee, N.D., Krüger, R., Haller, G. and Olbricht, W., 1998. The Bayesian approach to an internally consistent thermodynamic database: theory, database, and generation of phase diagrams. Contributions to Mineralogy and Petrology, 133(1): 149-168.

Connolly, J., 1990. Multivariable phase diagrams: an algorithm based on generalized thermodynamics. American Journal of Science, 290(6): 666-718.

Connolly, J. and Petrini, K., 2002. An automated strategy for calculation of phase diagram sections and retrieval of rock properties as a function of physical conditions. Journal of Metamorphic Geology, 20(7): 697-708.

Dachs, E., Geiger, C.A., Benisek, A. and Grevel, K.-D., 2012. Grossular: A crystal-chemical, calorimetric, and thermodynamic study. American Mineralogist, 97(8-9): 1299-1313.

Dalton, J.A. and Presnall, D.C., 1998a. Carbonatitic melts along the solidus of model lherzolite in the system CaO-MgO-Al_2O_3-SiO_2-CO_2 from 3 to 7 GPa. Contributions to Mineralogy and Petrology, 131(2): 123-135.

Dalton, J.A. and Presnall, D.C., 1998b. The continuum of primary carbonatitic–kimberlitic melt compositions in equilibrium with lherzolite: data from the system CaO–MgO–Al_2O_3–SiO_2–CO_2 at 6 GPa. Journal of Petrology, 39(11-12): 1953-1964.

Dasgupta, R. and Hirschmann, M.M., 2007. A modified iterative sandwich method for determination of near-solidus partial melt compositions. II. Application to determination of near-solidus melt compositions of carbonated peridotite. Contributions to Mineralogy and Petrology, 154(6): 647-661.
Davis, B., 1964. The system diopside-forsterite-pyrope at 40 kilobars. Carnegie Institute of Washington Yearbook, 63: 165-171.
Davis, B. and England, J., 1964. The melting of forsterite up to 50 kilobars. Journal of Geophysical Research, 69(6): 1113-1116.
de Capitani, C. and Brown, T.H., 1987. The computation of chemical equilibrium in complex systems containing non-ideal solutions. Geochimica et Cosmochimica Acta, 51(10): 2639-2652.
de Capitani, C. and Petrakakis, K., 2010. The computation of equilibrium assemblage diagrams with Theriak/Domino software. American Mineralogist, 95(7): 1006-1016.
De Roever, W.v., 1957. Sind die alpinotypen Peridotitmassen vielleicht tektonisch verfrachtete Bruchstücke der Peridotitschale? Geologische Rundschau, 46(1): 137-146.
Den Tex, E., 1969. Origin of ultramafic rocks, their tectonic setting and history: a contribution to the discussion of the paper “The origin of ultramafic and ultrabasic rocks” by PJ Wyllie. Tectonophysics, 7(5-6): 457-488.
Dijkstra, A.H. and Cawood, P.A., 2004. Base-up growth of ocean crust by multiple phases of magmatism: field evidence from Macquarie Island. Journal of the Geological Society, 161(5): 739-742.
Eggler, D.H., 1974. Effect of CO_2 on the melting of peridotite. Carnegie Institution of Washington Yearbook, 73: 215-224.
Eggler, D.H., 1978. The effect of CO_2 upon partial melting of peridotite in the system Na_2O-CaO-Al_2O_3-MgO-SiO_2-CO_2 to 35 kb, with an analysis of melting in a peridotite-H_2O-CO_2 system. American Journal of Science, 278(3): 305-343.
Engi, M., 1992. Thermodynamic data for minerals: a critical assessment, The stability of minerals. Springer, pp. 267-328.
Erlank, A., 1987. Evidence for mantle metasomatism in peridotite nodules from the Kimberley pipes, South Africa. Mantle metasomatism: 221-311.
Falloon, T.J., Green, D.H., Danyushevsky, L.V. and Faul, U.H., 1999. Peridotite melting at 1.0 and 1.5 GPa: an experimental evaluation of techniques using diamond aggregates and mineral mixes for determination of near-solidus melts. Journal of Petrology, 40(9): 1343-1375.
Ferry, J.t. and Spear, F., 1978. Experimental calibration of the partitioning of Fe and Mg between biotite and garnet. Contributions to mineralogy and petrology, 66(2): 113-117.
Fiquet, G., 2018. Melting in the Earth's Deep Interior, Magmas under pressure. Elsevier, pp. 115-134.
Foley, S., Yaxley, G., Rosenthal, A., Buhre, S., Kiseeva, E., Rapp, R. and Jacob, D., 2009. The composition of near-solidus melts of peridotite in the presence of CO_2 and H_2O between 40 and 60 kbar. Lithos, 112: 274-283.
Foley, S.F. and Pintér, Z., 2018. Primary melt compositions in the Earth's mantle, Magmas Under Pressure. Elsevier, pp. 3-42.
Fyfe, W., 1978. The evolution of the Earth's crust: modern plate tectonics to ancient hot spot tectonics? Chemical Geology, 23(1-4): 89-114.

Gasparik, T., 1996. Melting experiments on the enstatite-diopside join at 70–224 kbar, including the melting of diopside. Contributions to Mineralogy and Petrology, 124(2): 139-153.
Ghiorso, M.S., Hirschmann, M.M., Reiners, P.W. and Kress III, V.C., 2002. The pMELTS: A revision of MELTS for improved calculation of phase relations and major element partitioning related to partial melting of the mantle to 3 GPa. Geochemistry, Geophysics, Geosystems, 3(5): 1-35.
Ghiorso, M.S. and Sack, R.O., 1995. Chemical mass transfer in magmatic processes IV. A revised and internally consistent thermodynamic model for the interpolation and extrapolation of liquid-solid equilibria in magmatic systems at elevated temperatures and pressures. Contributions to Mineralogy and Petrology, 119(2): 197-212.
Gottschalk, M., 1997. Internally consistent thermodynamic data for rock-forming minerals in the system SiO_2-TiO_2-Al_2O_3-Fe_2O_3-CaO-MgO-FeO-K_2O-Na_2O-H_2O-CO_2. European Journal of Mineralogy: 175-223.
Griffin, W., O'Reilly, S.Y., Afonso, J.C. and Begg, G., 2009. The composition and evolution of lithospheric mantle: a re-evaluation and its tectonic implications. Journal of Petrology, 50(7): 1185-1204.
Grütter, H., Latti, D. and Menzies, A., 2006. Cr-Saturation Arrays in Concentrate Garnet Compositions from Kimberlite and their Use in Mantle Barometry. Journal of Petrology, 47(4): 801-820.
Hamlyn, P.R. and Bonatti, E., 1980. Petrology of mantle-derived ultramafics from the Owen Fracture Zone, northwest Indian Ocean: implications for the nature of the oceanic upper mantle. Earth and Planetary Science Letters, 48(1): 65-79.
Harley, S.L., 1984. An experimental study of the partitioning of Fe and Mg between garnet and orthopyroxene. Contributions to Mineralogy and Petrology, 86(4): 359-373.
Harte, B., 1999. Lower mantle mineral associations in diamonds from Sao Luiz, Brazil. Mantle petrology: Field observations and high-pressure experimentation: A tribute to Francis R.(Joe) Boyd, 6: 125-153.
Hauri, E.H. and Hart, S.R., 1994. Constraints on melt migration from mantle plumes: a trace element study of peridotite xenoliths from Savai'i, Western Samoa. Journal of Geophysical Research: Solid Earth, 99(B12): 24301-24321.
Hermann, J. and Spandler, C.J., 2008. Sediment melts at sub-arc depths: an experimental study. Journal of Petrology, 49(4): 717-740.
Herzberg, C., Condie, K. and Korenaga, J., 2010. Thermal history of the Earth and its petrological expression. Earth and Planetary Science Letters, 292(1-2): 79-88.
Herzberg, C. and O'Hara, M., 1998. Phase equilibrium constraints on the origin of basalts, picrites, and komatiites. Earth-Science Reviews, 44(1-2): 39-79.
Herzberg, C. and Rudnick, R., 2012. Formation of cratonic lithosphere: An integrated thermal and petrological model. Lithos, 149: 4-15.
Herzberg, C. and Zhang, J., 1996. Melting experiments on anhydrous peridotite KLB-1: Compositions of magmas in the upper mantle and transition zone. Journal of Geophysical Research: Solid Earth, 101(B4): 8271-8295.
Herzberg, C. and Zhang, J., 1998. Melting experiments in the systems CaO-MgO-Al_2O_3-SiO_2 and MgO-SiO_2 at 3 to 15 GPa. American Mineralogist, 83(5-6): 491-500.
Hirose, K., 1997. Melting experiments on lherzolite KLB-1 under hydrous conditions and generation of high-magnesian andesitic melts. Geology, 25(1): 42-44.

Hirose, K. and Kawamoto, T., 1995. Hydrous partial melting of lherzolite at 1 GPa: the effect of H_2O on the genesis of basaltic magmas. Earth and Planetary Science Letters, 133(3-4): 463-473.
Hirose, K. and Kushiro, I., 1993. Partial melting of dry peridotites at high pressures: determination of compositions of melts segregated from peridotite using aggregates of diamond. Earth and Planetary Science Letters, 114(4): 477-489.
Hirschmann, M., Baker, M. and Stolper, E., 1998. The effect of alkalis on the silica content of mantle-derived melts. Geochimica et Cosmochimica Acta, 62(5): 883-902.
Hirschmann, M.M., 2000. Mantle solidus: Experimental constraints and the effects of peridotite composition. Geochemistry, Geophysics, Geosystems, 1(10).
Holland, T. and Powell, R., 1985. An internally consistent thermodynamic dataset with uncertainties and correlations: 2. Data and results. Journal of metamorphic Geology, 3(4): 343-370.
Holland, T. and Powell, R., 1990. An enlarged and updated internally consistent thermodynamic dataset with uncertainties and correlations: the system K_2O–Na_2O–CaO–MgO–MnO–FeO–Fe_2O_3–Al_2O_3–TiO_2–SiO_2–C–H_2–O_2. Journal of Metamorphic Geology, 8(1): 89-124.
Holland, T. and Powell, R., 1998. An internally consistent thermodynamic data set for phases of petrological interest. Journal of Metamorphic Geology, 16(3): 309-343.
Holland, T. and Powell, R., 2011. An improved and extended internally consistent thermodynamic dataset for phases of petrological interest, involving a new equation of state for solids. Journal of Metamorphic Geology, 29(3): 333-383.
Holland, T.J., 1980. The reaction albite= jadeite+ quartz determined experimentally in the range 600–1200 °C. American Mineralogist, 65(1-2): 129-134.
Holland, T.J., Green, E.C. and Powell, R., 2018. Melting of peridotites through to granites: a simple thermodynamic model in the system KNCFMASHTOCr. Journal of Petrology, 59(5): 881-900.
Huang, F. and Sverjensky, D.A., 2019. Extended Deep Earth Water Model for predicting major element mantle metasomatism. Geochimica et Cosmochimica Acta, 254: 192-230.
Ito, E., Takahashi, E. and Matsui, Y., 1984. The mineralogy and chemistry of the lower mantle: an implication of the ultrahigh-pressure phase relations in the system MgOFeOSiO_2. Earth and Planetary Science Letters, 67(2): 238-248.
Ito, K. and Kennedy, G.C., 1967. Melting and phase relations in a natural peridotite to 40 kilobars. American Journal of Science, 265(6): 519-538.
Jennings, E.S. and Holland, T.J.B., 2015. A Simple Thermodynamic Model for Melting of Peridotite in the System NCFMASOCr. Journal of Petrology, 56(5): 869-892.
Kato, T. and Kumazawa, M., 1985. Incongruent melting of Mg_2SiO_4 at 20 GPa. Physics of the Earth and Planetary Interiors, 41(1): 1-5.
Kelemen, P.B., Shimizu, N. and Salters, V.J., 1995. Extraction of mid-ocean-ridge basalt from the upwelling mantle by focused flow of melt in dunite channels. Nature, 375(6534): 747-753.
Kelley, K.A., Plank, T., Newman, S., Stolper, E.M., Grove, T.L., Parman, S. and Hauri, E.H., 2010. Mantle melting as a function of water content beneath the Mariana Arc. Journal of Petrology, 51(8): 1711-1738.

Klemme, S., 2004. The influence of Cr on the garnet–spinel transition in the Earth's mantle: experiments in the system $MgO–Cr_2O_3–SiO_2$ and thermodynamic modelling. Lithos, 77(1-4): 639-646.
Kogiso, T., Hirschmann, M. and Pertermann, M., 2004. High-pressure partial melting of mafic lithologies in the mantle. Journal of Petrology, 45(12): 2407-2422.
Köhler, T. and Brey, G., 1990. Calcium exchange between olivine and clinopyroxene calibrated as a geothermobarometer for natural peridotites from 2 to 60 kb with applications. Geochimica et Cosmochimica Acta, 54(9): 2375-2388.
Koziol, A.M. and Newton, R.C., 1989. Grossular activity-composition relationships in ternary garnets determined by reversed displaced-equilibrium experiments. Contributions to Mineralogy and Petrology, 103(4): 423-433.
Krogh, E.J., 1988. The garnet-clinopyroxene Fe-Mg geothermometer—a reinterpretation of existing experimental data. Contributions to Mineralogy and Petrology, 99(1): 44-48.
Kudo, R. and Ito, E., 1996. Melting relations in the system $Mg_4Si_4O_{12}$ (En)-$Mg_3Al_2Si_3O_{12}$ (Py) at high pressures. Physics of the Earth and Planetary Interiors, 96(2-3): 159-169.
Kushiro, I., 1965. The liquidus relations in the systems forsterite-$CaAl_2SiO_6$-silica and forsterite-nepheline-silica at high pressures. Carnegie Institution of Washington Yearbook, 64: 103-108.
Kushiro, I., 1968. Compositions of magmas formed by partial zone melting of the earth's upper mantle. Journal of Geophysical Research, 73(2): 619-634.
Kushiro, I., 1969. The system forsterite-diopside-silica with and without water at high pressures. American Journal of Science, 267(A): 269-294.
Kushiro, I., 1972. Effect of water on the composition of magmas formed at high pressures. Journal of Petrology, 13(2): 311-334.
Kushiro, I., 2001. Partial melting experiments on peridotite and origin of mid-ocean ridge basalt. Annual Review of Earth and Planetary Sciences, 29(1): 71-107.
Lanari, P. and Duesterhoeft, E., 2019. Modeling metamorphic rocks using equilibrium thermodynamics and internally consistent databases: past achievements, problems and perspectives. Journal of Petrology, 60(1): 19-56.
Langmuir, C.H. and Forsyth, D.W., 2007. Mantle melting beneath mid-ocean ridges. Oceanography, 20(1): 78-89.
Lee, C.-T.A., Luffi, P. and Chin, E.J., 2011. Building and destroying continental mantle. Annual Review of Earth and Planetary Sciences, 39: 59-90.
McDonough, W.F. and Sun, S.-S., 1995. The composition of the Earth. Chemical Geology, 120(3-4): 223-253.
McKenzie, D., 1984. The generation and compaction of partially molten rock. Journal of Petrology, 25(3): 713-765.
McKenzie, D., 1985. The extraction of magma from the crust and mantle. Earth and Planetary Science Letters, 74(1): 81-91.
McKenzie, D. and Bickle, M., 1988. The volume and composition of melt generated by extension of the lithosphere. Journal of Petrology, 29(3): 625-679.
Mehl, L., Hacker, B.R., Hirth, G. and Kelemen, P.B., 2003. Arc-parallel flow within the mantle wedge: Evidence from the accreted Talkeetna arc, south central Alaska. Journal of Geophysical Research: Solid Earth, 108(B8).
Meyer, H.O., 1987. Inclusions in diamond. Mantle xenoliths.

Millhollen, G., Irving, A. and Wyllie, P., 1974. Melting interval of peridotite with 5.7 percent water to 30 kilobars. The Journal of Geology, 82(5): 575-587.
Miron, G.D., Wagner, T., Kulik, D.A. and Heinrich, C.A., 2016. Internally consistent thermodynamic data for aqueous species in the system Na–K–Al–Si–O–H–Cl. Geochimica et Cosmochimica Acta, 187: 41-78.
Miron, G.D., Wagner, T., Kulik, D.A. and Lothenbach, B., 2017. An internally consistent thermodynamic dataset for aqueous species in the system Ca-Mg-Na-K-Al-Si-OHC-Cl to 800 C and 5 kbar. American Journal of Science, 317(7): 755-806.
Mitchell, A.L. and Grove, T.L., 2015. Melting the hydrous, subarc mantle: the origin of primitive andesites. Contributions to Mineralogy and Petrology, 170(2).
Mitchell, A.L. and Grove, T.L., 2016. Experiments on melt–rock reaction in the shallow mantle wedge. Contributions to Mineralogy and Petrology, 171(12): 107.
Morgan, J.P. and Morgan, W.J., 1999. Two-stage melting and the geochemical evolution of the mantle: a recipe for mantle plum-pudding. Earth and Planetary Science Letters, 170(3): 215-239.
Mutlu, H., 1998. Chemical geothermometry and fluid–mineral equilibria for the Ömer–Gecek thermal waters, Afyon area, Turkey. Journal of Volcanology and Geothermal Research, 80(3-4): 303-321.
Mysen, B. and Boettcher, A., 1975. Melting of hydrous upper mantle. I. Phase equilibria of a natural peridotite at high pressures and high temperatures as a function of controlled activities of water, hydrogen and carbon dioxide. Journal of Petrology, 16: 520-548.
Newton, R.C., 2018. Thermodynamic analysis of phase equilibria in simple mineral systems, Thermodynamic Modeling of Geologic Materials. De Gruyter, pp. 1-34.
Nichols, G.T., Wyllie, P.J. and Stern, C.R., 1994. Subduction zone melting of pelagic sediments constrained by melting experiments. Nature, 371(6500): 785-788.
Nickel, K. and Green, D., 1985. Empirical geothermobarometry for garnet peridotites and implications for the nature of the lithosphere, kimberlites and diamonds. Earth and Planetary Science Letters, 73(1): 158-170.
Nimis, P. and Grütter, H., 2010. Internally consistent geothermometers for garnet peridotites and pyroxenites. Contributions to Mineralogy and Petrology, 159(3): 411-427.
Nimis, P. and Taylor, W.R., 2000. Single clinopyroxene thermobarometry for garnet peridotites. Part I. Calibration and testing of a Cr-in-Cpx barometer and an enstatite-in-Cpx thermometer. Contributions to Mineralogy and Petrology, 139(5): 541-554.
Niu, Y. and Batiza, R., 1991. An empirical method for calculating melt compositions produced beneath mid-ocean ridges: Application for axis and off-axis (seamounts) melting. Journal of Geophysical Research: Solid Earth, 96(B13): 21753-21777.
O'Hara, M., 1963a. The join diopside-pyrope at 30 kilobars. Carnegie Institution of Washington Yearbook., 62: 116-118.
O'Hara, M., 1963b. Melting of garnet peridotite at 30 kilobars. Carnegie Institution of Washington Yearbook., 62: 71-76.
O'Neill, H.S.C., 1981. The transition between spinel lherzolite and garnet lherzolite, and its use as a geobarometer. Contributions to Mineralogy and Petrology, 77(2): 185-194.
O'Neill, H.S.C. and Wall, V., 1987. The Olivine-Orthopyroxene-Spinel oxygen geobarometer, the nickel precipitation curve, and the oxygen fugacity of the Earth's Upper Mantle. Journal of Petrology, 28(6): 1169-1191.

O'Neill, H.S.C. and Wood, B., 1979. An experimental study of Fe-Mg partitioning between garnet and olivine and its calibration as a geothermometer. Contributions to Mineralogy and Petrology, 70(1): 59-70.
O'Neill, H.S.C., 1981. The transition between spinel lherzolite and garnet lherzolite, and its use as a geobarometer. Contributions to Mineralogy and Petrology, 77(2): 185-194.
O'Hara, M. and Yoder, H., 1967. Formation and fractionation of basic magmas at high pressures. Scottish Journal of Geology, 3(1): 67-117.
Ohtani, E. and Kumazawa, M., 1981. Melting of forsterite Mg2SiO4 up to 15 GPa. Physics of the Earth and Planetary Interiors, 27(1): 32-38.
Parman, S.W., Grove, T.L., Dann, J.C. and De Wit, M.J., 2004. A subduction origin for komatiites and cratonic lithospheric mantle. South African Journal of Geology, 107(1-2): 107-118.
Pearce, J.A., 2005. Mantle preconditioning by melt extraction during flow: Theory and petrogenetic implications. Journal of Petrology, 46(5): 973-997.
Pearson, D., Canil, D. and Shirey, S., 2003. Mantle samples included in volcanic rocks: xenoliths and diamonds. Treatise on geochemistry, 2: 568.
Pearson, D., Shirey, S., Carlson, R., Boyd, F.R., Pokhilenko, N. and Shimizu, N., 1995. Re□ Os, Sm□ Nd, and Rb□ Sr isotope evidence for thick Archaean lithospheric mantle beneath the Siberian craton modified by multistage metasomatism. Geochimica et Cosmochimica Acta, 59(5): 959-977.
Pearson, D.G., Scott, J.M., Liu, J., Schaeffer, A., Wang, L.H., van Hunen, J., Szilas, K., Chacko, T. and Kelemen, P.B., 2021. Deep continental roots and cratons. Nature, 596(7871): 199-210.
Pearson, D.G. and Wittig, N., 2008. Formation of Archaean continental lithosphere and its diamonds: the root of the problem. Journal of the Geological Society, 165(5): 895-914.
Pelullo, C., Iovine, R.S., Arienzo, I., Di Renzo, V., Pappalardo, L., Petrosino, P. and D'Antonio, M., 2022. Mineral-Melt Equilibria and Geothermobarometry of Campi Flegrei Magmas: Inferences for Magma Storage Conditions. Minerals, 12(3): 308.
Powell, R., 1978. Equilibrium thermodynamics in petrology: an introduction. Harper & Row.
Powell, R. and Holland, T., 1985. An internally consistent thermodynamic dataset with uncertainties and correlations: 1. Methods and a worked example. Journal of Metamorphic Geology, 3(4): 327-342.
Powell, R. and Holland, T., 1988. An internally consistent dataset with uncertainties and correlations: 3. Applications to geobarometry, worked examples and a computer program. Journal of Metamorphic Geology, 6(2): 173-204.
Powell, R., Holland, T. and Worley, B., 1998. Calculating phase diagrams involving solid solutions via non-linear equations, with examples using THERMOCALC. Journal of Metamorphic Geology, 16(4): 577-588.
Presnall, D., 1987. High-pressure phase equilibrium constraints on the origin of mid-ocean ridge basalts. Magmatic Processes, Geochemical Society, Special Publication. 1: 75-89.
Presnall, D., Dixon, J., O'donnell, T. and Dixons, S., 1979. Generation of mid-ocean ridge tholeiites. Journal of Petrology, 20(1): 3-35.
Presnall, D., Dixon, S.A., Dixon, J.R., O'donnell, T., Brenner, N., Schrock, R. and Dycus, D., 1978. Liquidus phase relations on the join diopside-forsterite-anorthite from 1 atm to 20 kbar: their bearing on the generation and crystallization of basaltic magma. Contributions to Mineralogy and Petrology, 66(2): 203-220.

Presnall, D. and Gasparik, T., 1990. Melting of enstatite ($MgSiO_3$) from 10 to 16.5 GPa and the forsterite (Mg_2SiO_4)-majorite ($MgSiO_3$) eutectic at 16.5 GPa: Implications for the origin of the mantle. Journal of Geophysical Research: Solid Earth, 95(B10): 15771-15777.
Presnall, D.C. and Walter, M.J., 1993. Melting of forsterite, Mg2SiO4, from 9.7 to 16.5 GPa. Journal of Geophysical Research: Solid Earth, 98(B11): 19777-19783.
Presnall, D.C., Weng, Y.-H., Milholland, C.S. and Walter, M.J., 1998. Liquidus phase relations in the system MgO-$MgSiO_3$ at pressures up to 25 GPa—constraints on crystallization of a molten Hadean mantle. Physics of the Earth and Planetary Interiors, 107(1-3): 83-95.
Ravna, K., 2000. The garnet–clinopyroxene Fe2+–Mg geothermometer: an updated calibration. Journal of Metamorphic Geology, 18(2): 211-219.
Ricard, Y., Šrámek, O. and Dubuffet, F., 2009. A multi-phase model of runaway core–mantle segregation in planetary embryos. Earth and Planetary Science Letters, 284(1-2): 144-150.
Servali, A. and Korenaga, J., 2018. Oceanic origin of continental mantle lithosphere. Geology, 46(12): 1047-1050.
Simon, N.S., Carlson, R.W., Pearson, D.G. and Davies, G.R., 2007. The origin and evolution of the Kaapvaal cratonic lithospheric mantle. Journal of Petrology, 48(3): 589-625.
Sobolev, A. and Shimizu, N., 1993. Ultra-depleted primary melt included in an olivine from the Mid-Atlantic Ridge. Nature, 363(6425): 151-154.
Spear, F.S., 1988. The Gibbs method and Duhem's theorem: The quantitative relationships among P, T, chemical potential, phase composition and reaction progress in igneous and metamorphic systems. Contributions to Mineralogy and Petrology, 99(2): 249-256.
Stixrude, L. and Lithgow-Bertelloni, C., 2011. Thermodynamics of mantle minerals-II. Phase equilibria. Geophysical Journal International, 184(3): 1180-1213.
Su, B. and Chen, Y., 2018. Making cratonic lithospheric mantle. Journal of Geophysical Research: Solid Earth, 123(9): 7688-7706.
Sverjensky, D.A., 2019. Thermodynamic modelling of fluids from surficial to mantle conditions. Journal of the Geological Society, 176(2): 348-374.
Takahashi, E., 1986. Melting of a dry peridotite KLB-1 up to 14 GPa: Implications on the origin of peridotitic upper mantle. Journal of Geophysical Research: Solid Earth, 91(B9): 9367-9382.
Takahashi, E., Shimazaki, T., Tsuzaki, Y. and Yoshida, H., 1993. Melting study of a peridotite KLB-1 to 6.5 GPa, and the origin of basaltic magmas. Philosophical Transactions of the Royal Society of London. Series A: Physical and Engineering Sciences, 342(1663): 105-120.
Taylor, S.R. and McLennan, S.M., 1985. The continental crust: its composition and evolution.
Taylor, W., 1998. An experimental test of some geothermometer and geobaro-meter formulations for upper mantle peridotites with application to the ther-mobarometry of fertile lherzolite and garnet websterite. Neues Jahrbuch für Mineralogie-Abhandlungen: 381-408.
Team, T.M.S., 1998. Imaging the deep seismic structure beneath a mid-ocean ridge: The MELT experiment. Science, 280(5367): 1215-1218.
Thompson Jr, J.B., 1970. Geochemical reaction and open systems. Geochimica et Cosmochimica Acta, 34(5): 529-551.

Thomsen, T.B. and Schmidt, M.W., 2008. Melting of carbonated pelites at 2.5–5.0 GPa, silicate–carbonatite liquid immiscibility, and potassium–carbon metasomatism of the mantle. Earth and Planetary Science Letters, 267(1-2): 17-31.

Tole, M.P., Ármannsson, H., Zhong-He, P. and Arnórsson, S., 1993. Fluid/mineral equilibrium calculations for geothermal fluids and chemical geothermometry. Geothermics, 22(1): 17-37.

Tomlinson, E.L. and Holland, T.J., 2021. A Thermodynamic model for the subsolidus evolution and melting of peridotite. Journal of Petrology, 62(1): egab012.

Walter, M.J., 1998. Melting of garnet peridotite and the origin of komatiite and depleted lithosphere. Journal of Petrology, 39(1): 29-60.

Webb, S.A.C. and Wood, B.J., 1986. Spinel-pyroxene-garnet relationships and their dependence on Cr/Al ratio. Contributions to Mineralogy and Petrology, 92(4): 471-480.

Workman, R.K. and Hart, S.R., 2005. Major and trace element composition of the depleted MORB mantle (DMM). Earth and Planetary Science Letters, 231(1-2): 53-72.

Wyllie, P.J. and Huang, W.-L., 1976. Carbonation and melting reactions in the system CaO–MgO–SiO2–CO2 at mantle pressures with geophysical and petrological applications. Contributions to Mineralogy and Petrology, 54(2): 79-107.

Xiang, H., 2020. GeoPS: an interactive visualization tool for thermodynamic modeling of phase equilibria. Earth and Space Science Open Archive. doi, 10.

Xiang, H. and Connolly, J.A., 2022. GeoPS: An interactive visual computing tool for thermodynamic modelling of phase equilibria. Journal of Metamorphic Geology, 40(2): 243-255.

Yakymchuk, C., 2017. Applying phase equilibria modelling to metamorphic and geological processes: recent developments and future potential. Geoscience Canada: Journal of the Geological Association of Canada/Geoscience Canada: journal de l'Association Géologique du Canada, 44(1): 27-45.

Yoder Jr, H.S., 1952. Change of melting point of diopside with pressure. The Journal of Geology, 60(4): 364-374.

Ziberna, L., Klemme, S. and Nimis, P., 2013. Garnet and spinel in fertile and depleted mantle: insights from thermodynamic modelling. Contributions to Mineralogy and Petrology, 166(2): 411-421.

Appendix A Comparison between Experiments and Calculations

Section 1 Anhydrous Melting Experiments

The anhydrous experimental running conditions and results for KLB-1 are from Falloon et al. (1999), for MM3 are from Baker and Stolper (1994) and Falloon et al. (1999).

Table A1.1a KLB-1 anhydrous melting experimental results and calculation results from TH21, WL22-3, and HGP18 models: melt composition

Run No.	Type	Mode	SiO2	Al2O3	CaO	MgO	FeO	K2O	Na2O	TiO2	Fe2O3	Cr2O3	MnO	NiO	Total
	Exp	0.22	49.70	14.60	13.20	12.40	7.80	0.01	1.16	0.55		0.33	0.17		99.92
	TH21	0.18	48.57	13.48	12.70	12.83	9.12	0.10	1.52	0.52	0.95	0.20			100.00
	Biase&Variance	-0.04	-1.13	-1.12	-0.50	0.43	1.32	0.09	0.36	-0.03	0.95	-0.13	-0.17	0.00	5.80
T-4082	WL22-3	0.15	46.60	14.75	13.82	12.55	8.84	0.13	1.83	0.52	0.86	0.10			100.00
	Biase&Variance	-0.07	-3.10	0.15	0.62	0.15	1.04	0.12	0.67	-0.03	0.86	-0.23	-0.17	0.00	12.41
	HGP18	0.15	46.72	14.64	13.71	12.52	8.91	0.13	1.81	0.48	0.93	0.15			100.00
	Biase&Variance	-0.07	-2.98	0.04	0.51	0.12	1.11	0.12	0.65	-0.07	0.93	-0.18	-0.17	0.00	11.76
	Exp	0.21	50.00	14.30	12.60	12.90	7.90	0.03	1.19	0.53		0.32	0.14		99.91
	TH21	0.19	48.65	13.20	12.44	13.19	9.29	0.10	1.45	0.50	0.96	0.22			100.00
	Biase&Variance	-0.02	-1.35	-1.10	-0.16	0.29	1.39	0.07	0.26	-0.03	0.96	-0.10	-0.14	0.00	6.10
T-4129	WL22-3	0.16	46.70	14.48	13.65	12.82	8.97	0.12	1.75	0.52	0.87	0.11			100.00
	Biase&Variance	-0.05	-3.30	0.18	1.05	-0.08	1.07	0.09	0.56	-0.01	0.87	-0.21	-0.14	0.00	14.32
	HGP18	0.16	46.82	14.35	13.54	12.80	9.04	0.12	1.73	0.48	0.94	0.17			100.00
	Biase&Variance	-0.05	-3.18	0.05	0.94	-0.10	1.14	0.09	0.54	-0.05	0.94	-0.15	-0.14	0.00	13.54
	Exp	0.26	50.80	12.80	11.20	14.70	8.39	0.01	0.99	0.46		0.45	0.14		99.94
	TH21	0.22	48.93	12.36	11.52	14.36	9.76	0.09	1.27	0.45	0.96	0.31			100.00
	Biase&Variance	-0.04	-1.87	-0.44	0.32	-0.34	1.37	0.08	0.28	-0.01	0.96	-0.14	-0.14	0.00	6.83
T-4061	WL22-3	0.18	47.06	13.69	13.03	13.66	9.34	0.11	1.56	0.50	0.90	0.15			100.00
	Biase&Variance	-0.08	-3.74	0.89	1.83	-1.04	0.95	0.10	0.57	0.04	0.90	-0.30	-0.14	0.00	21.37
	HGP18	0.18	47.20	13.56	12.91	13.65	9.39	0.10	1.53	0.48	0.95	0.22			100.00
	Biase&Variance	-0.08	-3.60	0.76	1.71	-1.05	1.00	0.09	0.54	0.02	0.95	-0.23	-0.14	0.00	19.84

Table A1.1b KLB-1 anhydrous melting experimental results and calculation results from TH21, WL22-3, and HGP18 models: residue composition

Run No.	Type	Mode	SiO2	Al2O3	CaO	MgO	FeO	K2O	Na2O	TiO2	Fe2O3	Cr2O3	MnO	NiO	Total
	Exp	0.78	43.27	0.39	0.41	47.04	8.68	0.00	0.00	0.00	0.00	0.21			100.00
	TH21	0.82	43.84	1.12	0.76	45.81	7.96	0.00	0.01	0.01	0.14	0.34			100.00
	Biase&Variance	0.04	0.57	0.73	0.35	-1.23	-0.72	0.00	0.01	0.01	0.14	0.13	0.00	0.00	3.05
T-4082	WL22-3	0.85	44.40	1.39	1.04	44.50	8.07	0.00	0.01	0.03	0.19	0.36			100.00
	Biase&Variance	0.07	1.13	1.00	0.63	-2.54	-0.61	0.00	0.01	0.03	0.19	0.15	0.00	0.00	9.56
	HGP18	0.85	44.37	1.39	1.04	44.57	8.05	0.00	0.01	0.04	0.18	0.35			100.00
	Biase&Variance	0.07	1.10	1.00	0.63	-2.47	-0.63	0.00	0.01	0.04	0.18	0.14	0.00	0.00	9.16
	Exp	0.79	43.17	0.62	0.66	46.39	8.74	0.00	0.01	0.01	0.00	0.39			99.91
	TH21	0.81	43.76	1.04	0.69	46.12	7.91	0.00	0.01	0.01	0.13	0.34			100.00
	Biase&Variance	0.02	0.59	0.42	0.03	-0.27	-0.83	0.00	0.00	0.00	0.13	-0.05	0.00	0.00	1.31
T-4129	WL22-3	0.84	44.36	1.33	0.97	44.73	8.03	0.00	0.01	0.03	0.19	0.36			100.00
	Biase&Variance	0.05	1.19	0.71	0.31	-1.66	-0.71	0.00	0.00	0.02	0.19	-0.03	0.00	0.00	5.31
	HGP18	0.84	44.33	1.32	0.95	44.82	8.01	0.00	0.01	0.03	0.17	0.35			100.00
	Biase&Variance	0.05	1.16	0.70	0.29	-1.57	-0.73	0.00	0.00	0.02	0.17	-0.04	0.00	0.00	4.95
	Exp	0.74	42.51	0.15	0.38	48.35	8.61	0.00	0.00	0.00	0.00	0.00			99.94
	TH21	0.78	43.48	0.81	0.49	47.08	7.71	0.00	0.00	0.01	0.10	0.32			100.00
	Biase&Variance	0.04	0.97	0.66	0.11	-1.27	-0.90	0.00	0.00	0.01	0.10	0.32	0.00	0.00	3.92
T-4061	WL22-3	0.82	44.22	1.15	0.76	45.40	7.92	0.00	0.01	0.02	0.16	0.36			100.00
	Biase&Variance	0.08	1.71	1.00	0.38	-2.95	-0.69	0.00	0.01	0.02	0.16	0.36	0.00	0.00	13.40
	HGP18	0.82	44.17	1.13	0.74	45.55	7.90	0.00	0.01	0.02	0.15	0.34			100.00
	Biase&Variance	0.08	1.66	0.98	0.36	-2.80	-0.71	0.00	0.01	0.02	0.15	0.34	0.00	0.00	12.33

Table A1.1c KLB-1 anhydrous melting experimental results and calculation results from TH21, WL22-3, and HGP18 models: spinel composition

Run No.	Type	Mode	SiO2	Al2O3	CaO	MgO	FeO	K2O	Na2O	TiO2	Fe2O3	Cr2O3	MnO	NiO	Total	Cr#
	Exp		0.15	56.30		21.39	9.30			0.11		12.70	0.05		100.00	13.14
	TH21	0.002	0.00	49.98	0.00	21.05	8.67	0.00	0.00	0.01	1.57	18.72			100.00	20.08
KLB1-10-2	Biase&Variance	0.002	-0.15	-6.32	0.00	-0.34	-0.63	0.00	0.00	-0.10	1.57	6.02	-0.05	0.00	79.20	
	WL22-3	0.002	0.00	51.31	0.00	21.20	8.65	0.00	0.00	0.01	1.55	17.27			100.00	18.42
	Biase&Variance	0.002	-0.15	-4.99	0.00	-0.19	-0.65	0.00	0.00	-0.10	1.55	4.57	-0.05	0.00	48.68	

Table A1.1d KLB-1 anhydrous melting experimental results and calculation results from TH21, WL22-3, and HGP18 models: olivine composition

Run No.	Type	Mode	SiO2	Al2O3	CaO	MgO	FeO	K2O	Na2O	TiO2	Fe2O3	Cr2O3	MnO	NiO	Total	Mg#
	Exp		40.10		0.17	49.01	10.10					0.05	0.13	0.37	99.93	89.64
	TH21	0.62	40.91	0.00	0.27	49.40	9.42	0.00	0.00	0.00	0.00	0.00			100.00	90.34
	Biase&Variance	0.62	0.81	0.00	0.10	0.39	-0.68	0.00	0.00	0.00	0.00	-0.05	-0.13	-0.37	1.44	
KLB1-10-2	WL22-3	0.61	40.88	0.00	0.27	49.28	9.57	0.00	0.00	0.00	0.00	0.00			100.00	90.18
	Biase&Variance	0.61	0.78	0.00	0.10	0.27	-0.53	0.00	0.00	0.00	0.00	-0.05	-0.13	-0.37	1.13	
	HGP18	0.62	40.87	0.00	0.27	49.26	9.60	0.00	0.00	0.00	0.00	0.00			100.00	90.14
	Biase&Variance	0.62	0.77	0.00	0.10	0.25	-0.50	0.00	0.00	0.00	0.00	-0.05	-0.13	-0.37	1.07	
	Exp		40.60		0.29	48.60	10.00					0.09	0.17	0.29	100.04	89.65
	TH21	0.63	40.96	0.00	0.30	49.60	9.14	0.00	0.00	0.00	0.00	0.00			100.00	90.63
	Biase&Variance	0.63	0.36	0.00	0.01	1.00	-0.86	0.00	0.00	0.00	0.00	-0.09	-0.17	-0.29	1.99	
T4130	WL22-3	0.62	40.91	0.00	0.29	49.41	9.39	0.00	0.00	0.00	0.00	0.00			100.00	90.37
	Biase&Variance	0.62	0.31	0.00	0.00	0.81	-0.61	0.00	0.00	0.00	0.00	-0.09	-0.17	-0.29	1.25	
	HGP18	0.62	40.90	0.00	0.29	49.38	9.43	0.00	0.00	0.00	0.00	0.00			100.00	90.32
	Biase&Variance	0.62	0.30	0.00	0.00	0.78	-0.57	0.00	0.00	0.00	0.00	-0.09	-0.17	-0.29	1.14	
	Exp		40.10		0.24	48.90	10.20					0.08	0.15	0.34	100.01	89.52
	TH21	0.63	40.97	0.00	0.30	49.67	9.06	0.00	0.00	0.00	0.00	0.00			100.00	90.72
	Biase&Variance	0.63	0.87	0.00	0.06	0.77	-1.14	0.00	0.00	0.00	0.00	-0.08	-0.15	-0.34	2.80	
KLB1-10-3	WL22-3	0.62	40.92	0.00	0.30	49.45	9.33	0.00	0.00	0.00	0.00	0.00			100.00	90.43
	Biase&Variance	0.62	0.82	0.00	0.06	0.55	-0.87	0.00	0.00	0.00	0.00	-0.08	-0.15	-0.34	1.88	
	HGP18	0.62	40.91	0.00	0.29	49.42	9.37	0.00	0.00	0.00	0.00	0.00			100.00	90.39
	Biase&Variance	0.62	0.81	0.00	0.05	0.52	-0.83	0.00	0.00	0.00	0.00	-0.08	-0.15	-0.34	1.76	
	Exp	0.65	40.96		0.15	49.60	9.33								100.04	90.45
	TH21	0.63	41.05	0.00	0.29	50.03	8.63	0.00	0.00	0.00	0.00	0.00			100.00	91.18
	Biase&Variance	-0.02	0.09	0.00	0.14	0.43	-0.70	0.00	0.00	0.00	0.00	0.00	0.00	0.00	0.70	
T-4082	WL22-3	0.61	41.00	0.00	0.33	49.76	8.91	0.00	0.00	0.00	0.00	0.00			100.00	90.87
	Biase&Variance	-0.04	0.04	0.00	0.18	0.16	-0.42	0.00	0.00	0.00	0.00	0.00	0.00	0.00	0.24	
	HGP18	0.62	40.99	0.00	0.32	49.74	8.95	0.00	0.00	0.00	0.00	0.00			100.00	90.83
	Biase&Variance	-0.03	0.03	0.00	0.17	0.14	-0.38	0.00	0.00	0.00	0.00	0.00	0.00	0.00	0.19	

	Exp	0.66	40.70		0.30	49.04	9.30					0.23	0.15	0.33	100.05	90.38
	TH21	0.63	41.07	0.00	0.28	50.12	8.53	0.00	0.00	0.00	0.00	0.00			100.00	91.28
	Biase&Variance	-0.03	0.37	0.00	-0.02	1.08	-0.77	0.00	0.00	0.00	0.00	-0.23	-0.15	-0.33	2.08	
T-4129	WL22-3	0.61	41.01	0.00	0.32	49.82	8.85	0.00	0.00	0.00	0.00	0.00			100.00	90.94
	Biase&Variance	-0.05	0.31	0.00	0.02	0.78	-0.45	0.00	0.00	0.00	0.00	-0.23	-0.15	-0.33	1.09	
	HGP18	0.62	41.00	0.00	0.32	49.79	8.89	0.00	0.00	0.00	0.00	0.00			100.00	90.90
	Biase&Variance	-0.04	0.30	0.00	0.02	0.75	-0.41	0.00	0.00	0.00	0.00	-0.23	-0.15	-0.33	1.01	
	Exp	0.67	41.20		0.28	49.60	8.90								99.98	90.85
	TH21	0.63	41.14	0.00	0.24	50.41	8.22	0.00	0.00	0.00	0.00	0.00			100.00	91.62
	Biase&Variance	-0.04	-0.06	0.00	-0.04	0.81	-0.68	0.00	0.00	0.00	0.00	0.00	0.00	0.00	1.12	
T-4061	WL22-3	0.62	41.05	0.00	0.30	50.00	8.66	0.00	0.00	0.00	0.00	0.00			100.00	91.14
	Biase&Variance	-0.05	-0.15	0.00	0.02	0.40	-0.24	0.00	0.00	0.00	0.00	0.00	0.00	0.00	0.24	
	HGP18	0.62	41.04	0.00	0.29	49.98	8.69	0.00	0.00	0.00	0.00	0.00			100.00	91.11
	Biase&Variance	-0.05	-0.16	0.00	0.01	0.38	-0.21	0.00	0.00	0.00	0.00	0.00	0.00	0.00	0.21	
	Exp		40.99		0.19	50.20	7.80					0.33	0.11	0.37	99.99	91.98
	TH21	0.62	41.46	0.00	0.11	51.85	6.58	0.00	0.00	0.00	0.00	0.00			100.00	93.35
	Biase&Variance	-0.05	0.47	0.00	-0.08	1.65	-1.22	0.00	0.00	0.00	0.00	-0.33	-0.11	-0.37	4.70	
T-4173	WL22-3	0.62	41.25	0.00	0.18	50.91	7.67	0.00	0.00	0.00	0.00	0.00			100.00	92.21
	Biase&Variance	-0.05	0.26	0.00	-0.01	0.71	-0.13	0.00	0.00	0.00	0.00	-0.33	-0.11	-0.37	0.85	
	HGP18	0.63	41.25	0.00	0.17	50.93	7.65	0.00	0.00	0.00	0.00	0.00			100.00	92.23
	Biase&Variance	-0.04	0.26	0.00	-0.02	0.73	-0.15	0.00	0.00	0.00	0.00	-0.33	-0.11	-0.37	0.88	89.64

Table A1.1e KLB-1 anhydrous melting experimental results and calculation results from TH21, WL22-3, and HGP18 models: opx composition

Run No.	Type	Mode	SiO2	Al2O3	CaO	MgO	FeO	K2O	Na2O	TiO2	Fe2O3	Cr2O3	MnO	NiO	Total
KLB1-10-2	Exp		53.80	5.10	0.96	32.60	6.80		0.08	0.10		0.43	0.16		100.03
	TH21	0.21	52.16	7.12	2.29	30.13	6.27	0.00	0.06	0.11	0.79	1.08			100.00
	Biase&Variance	0.21	-1.64	2.02	1.33	-2.47	-0.53	0.00	-0.02	0.01	0.79	0.65	-0.16	0.00	15.99
	WL22-3	0.22	52.04	7.34	2.20	30.03	6.38	0.00	0.07	0.12	0.81	1.01			100.00
	Biase&Variance	0.22	-1.76	2.24	1.24	-2.57	-0.42	0.00	-0.01	0.02	0.81	0.58	-0.16	0.00	17.45
	HGP18	0.23	51.77	7.65	2.32	29.94	6.16	0.00	0.07	0.23	0.79	1.07			100.00
	Biase&Variance	0.23	-2.03	2.55	1.36	-2.66	-0.64	0.00	-0.01	0.13	0.79	0.64	-0.16	0.00	21.03
T4130	Exp		53.08	6.88	2.60	30.35	5.78		0.07	0.15		0.95	0.14		100.00
	TH21	0.21	52.44	6.44	2.62	30.22	6.05	0.00	0.04	0.10	0.76	1.34			100.00
	Biase&Variance	0.21	-0.64	-0.44	0.02	-0.13	0.27	0.00	-0.03	-0.05	0.76	0.39	-0.14	0.00	1.45
	WL22-3	0.23	52.23	6.80	2.48	30.08	6.22	0.00	0.06	0.13	0.80	1.20			100.00
	Biase&Variance	0.23	-0.85	-0.08	-0.12	-0.27	0.44	0.00	-0.01	-0.02	0.80	0.25	-0.14	0.00	1.73
	HGP18	0.23	52.26	6.83	2.56	30.18	6.02	0.00	0.06	0.21	0.76	1.13			100.00
	Biase&Variance	0.23	-0.82	-0.05	-0.04	-0.17	0.24	0.00	-0.01	0.06	0.76	0.18	-0.14	0.00	1.40
KLB1-10-3	Exp		53.40	5.40	2.20	31.00	6.50		0.13	0.16		0.60	0.13		99.52
	TH21	0.21	52.62	6.15	2.71	30.30	5.99	0.00	0.04	0.09	0.74	1.36			100.00
	Biase&Variance	0.21	-0.78	0.75	0.51	-0.70	-0.51	0.00	-0.09	-0.07	0.74	0.76	-0.13	0.00	3.34
	WL22-3	0.23	52.36	6.58	2.55	30.14	6.18	0.00	0.06	0.13	0.79	1.21			100.00
	Biase&Variance	0.23	-1.04	1.18	0.35	-0.86	-0.32	0.00	-0.07	-0.03	0.79	0.61	-0.13	0.00	4.46
	HGP18	0.23	52.39	6.61	2.62	30.24	5.98	0.00	0.06	0.20	0.75	1.14			100.00
	Biase&Variance	0.23	-1.01	1.21	0.42	-0.76	-0.52	0.00	-0.07	0.04	0.75	0.54	-0.13	0.00	4.39
T-4082	Exp	0.12	55.90	2.50	1.84	33.30	5.18					1.33			100.05
	TH21	0.18	53.45	4.99	2.40	31.22	5.68	0.00	0.03	0.05	0.64	1.54			100.00
	Biase&Variance	0.06	-2.45	2.49	0.56	-2.08	0.50	0.00	0.03	0.05	0.64	0.21	0.00	0.00	17.55
	WL22-3	0.23	53.34	5.04	2.92	30.69	5.85	0.00	0.05	0.12	0.70	1.30			100.00
	Biase&Variance	0.11	-2.56	2.54	1.08	-2.61	0.67	0.00	0.05	0.12	0.70	-0.03	0.00	0.00	21.94
	HGP18	0.23	53.39	5.07	2.95	30.81	5.64	0.00	0.05	0.14	0.66	1.27			100.00
	Biase&Variance	0.11	-2.51	2.57	1.11	-2.49	0.46	0.00	0.05	0.14	0.66	-0.06	0.00	0.00	21.01

	Exp	0.13	54.70	3.75	2.50	31.80	5.71		0.04	0.09		1.19	0.16		99.94
	TH21	0.17	53.59	4.84	2.17	31.49	5.62	0.00	0.03	0.05	0.62	1.59			100.00
	Biase&Variance	0.04	-1.11	1.09	-0.33	-0.31	-0.09	0.00	-0.01	-0.04	0.62	0.40	-0.16	0.00	3.21
T-4129	WL22-3	0.23	53.45	4.93	2.71	30.93	5.82	0.00	0.04	0.11	0.69	1.33			100.00
	Biase&Variance	0.10	-1.25	1.18	0.21	-0.87	0.11	0.00	0.00	0.02	0.69	0.14	-0.16	0.00	4.29
	HGP18	0.22	53.52	4.95	2.71	31.10	5.60	0.00	0.04	0.13	0.65	1.30			100.00
	Biase&Variance	0.09	-1.18	1.20	0.21	-0.70	-0.11	0.00	0.00	0.04	0.65	0.11	-0.16	0.00	3.84
	Exp	0.06	56.70	1.80	1.50	33.80	5.30								99.10
	TH21	0.14	53.97	4.42	1.63	32.22	5.41	0.00	0.03	0.03	0.55	1.75			100.00
	Biase&Variance	0.08	-2.73	2.62	0.13	-1.58	0.11	0.00	0.03	0.03	0.55	1.75	0.00	0.00	20.21
T-4061	WL22-3	0.20	53.75	4.61	2.17	31.56	5.71	0.00	0.04	0.08	0.65	1.43			100.00
	Biase&Variance	0.14	-2.95	2.81	0.67	-2.24	0.41	0.00	0.04	0.08	0.65	1.43	0.00	0.00	24.71
	HGP18	0.20	53.88	4.61	2.12	31.82	5.46	0.00	0.04	0.10	0.60	1.39			100.00
	Biase&Variance	0.14	-2.82	2.81	0.62	-1.98	0.16	0.00	0.04	0.10	0.60	1.39	0.00	0.00	22.48

Table A1.1f KLB-1 anhydrous melting experimental results and calculation results from TH21, WL22-3, and HGP18 models: cpx composition

Run No.	Type	Mode	SiO2	Al2O3	CaO	MgO	FeO	K2O	Na2O	TiO2	Fe2O3	Cr2O3	MnO	NiO	Total
KLB1-10-2	Exp		51.10	6.80	17.20	18.80	4.10		0.63	0.32		0.92	0.12		99.99
	TH21	0.08	51.45	6.06	17.28	19.07	4.09	0.03	0.47	0.41	0.66	0.49			100.00
	Biase&Variance	0.08	0.35	-0.74	0.08	0.27	-0.01	0.03	-0.16	0.09	0.66	-0.43	-0.12	0.00	1.42
	WL22-3	0.10	51.46	6.28	16.23	19.41	4.31	0.02	0.62	0.57	0.66	0.45			100.00
	Biase&Variance	0.10	0.36	-0.52	-0.97	0.61	0.21	0.02	-0.01	0.25	0.66	-0.47	-0.12	0.00	2.49
	HGP18	0.09	51.52	6.15	17.21	18.77	4.12	0.02	0.58	0.23	0.65	0.74			100.00
	Biase&Variance	0.09	0.42	-0.65	0.01	-0.03	0.02	0.02	-0.05	-0.09	0.65	-0.18	-0.12	0.00	1.08
T4130	Exp		50.50	7.85	16.28	19.36	4.28		0.33	0.25		0.99	0.15		99.99
	TH21	0.04	51.70	5.45	17.73	19.29	3.92	0.02	0.35	0.32	0.62	0.62			100.00
	Biase&Variance	0.04	1.20	-2.40	1.45	-0.07	-0.36	0.02	0.02	0.07	0.62	-0.37	-0.15	0.00	9.99
	WL22-3	0.07	51.54	5.88	16.46	19.71	4.21	0.02	0.48	0.55	0.62	0.54			100.00
	Biase&Variance	0.07	1.04	-1.97	0.18	0.35	-0.07	0.02	0.15	0.30	0.62	-0.45	-0.15	0.00	5.84
	HGP18	0.06	51.86	5.49	17.26	19.27	4.06	0.02	0.46	0.20	0.60	0.76			100.00
	Biase&Variance	0.06	1.36	-2.36	0.98	-0.09	-0.22	0.02	0.13	-0.05	0.60	-0.23	-0.15	0.00	8.89
KLB1-10-3	Exp		51.30	6.40	17.00	19.10	4.30		0.50	0.30		1.00	0.13		100.03
	TH21	0.03	51.87	5.18	17.79	19.42	3.87	0.02	0.33	0.30	0.61	0.63			100.00
	Biase&Variance	0.03	0.57	-1.22	0.79	0.32	-0.43	0.02	-0.17	0.00	0.61	-0.37	-0.13	0.00	3.28
	WL22-3	0.06	51.66	5.68	16.46	19.86	4.19	0.02	0.45	0.54	0.61	0.54			100.00
	Biase&Variance	0.06	0.36	-0.72	-0.54	0.76	-0.11	0.02	-0.05	0.24	0.61	-0.46	-0.13	0.00	2.19
	HGP18	0.06	51.97	5.31	17.26	19.41	4.04	0.02	0.44	0.19	0.59	0.77			100.00
	Biase&Variance	0.06	0.67	-1.09	0.26	0.31	-0.26	0.02	-0.06	-0.11	0.59	-0.23	-0.13	0.00	2.30

Table A1.2a MM3 anhydrous melting experimental results and calculation results from TH21, WL22-3, and HGP18 models: melt composition

Run No.	Type	Mode	SiO2	Al2O3	CaO	MgO	FeO	K2O	Na2O	TiO2	Fe2O3	Cr2O3	MnO	NiO	Total
	Exp	0.08	50.20	18.10	11.40	10.50	6.10		2.80	0.67		0.11	0.12		100.00
	TH21	0.05	50.65	16.50	10.68	10.22	6.66	0.00	3.88	0.60	0.72	0.09			100.00
	Biase&Variance	-0.03	0.45	-1.60	-0.72	-0.28	0.56	0.00	1.08	-0.07	0.72	-0.02	-0.12	0.00	5.37
55T	WL22-3	0.03	49.35	18.14	10.88	9.70	6.01	0.00	4.98	0.30	0.59	0.06			100.00
	Biase&Variance	-0.06	-0.85	0.04	-0.52	-0.80	-0.09	0.00	2.18	-0.37	0.59	-0.05	-0.12	0.00	6.90
	HGP18	0.04	48.25	18.38	11.17	9.99	6.35	0.00	4.55	0.47	0.71	0.12			100.00
	Biase&Variance	-0.05	-1.95	0.28	-0.23	-0.51	0.25	0.00	1.75	-0.20	0.71	0.01	-0.12	0.00	7.85
	Exp	0.07	50.90	17.90	11.20	10.40	5.90		2.70	0.66		0.12	0.14		99.92
	TH21	0.05	50.65	16.50	10.68	10.22	6.66	0.00	3.88	0.60	0.72	0.09			100.00
	Biase&Variance	-0.02	-0.25	-1.40	-0.52	-0.18	0.76	0.00	1.18	-0.06	0.72	-0.03	-0.14	0.00	4.83
20	WL22-3	0.03	49.35	18.14	10.88	9.70	6.01	0.00	4.98	0.30	0.59	0.06			100.00
	Biase&Variance	-0.05	-1.55	0.24	-0.32	-0.70	0.11	0.00	2.28	-0.36	0.59	-0.06	-0.14	0.00	8.77
	HGP18	0.04	48.25	18.38	11.17	9.99	6.35	0.00	4.55	0.47	0.71	0.12			100.00
	Biase&Variance	-0.04	-2.65	0.48	-0.03	-0.41	0.45	0.00	1.85	-0.19	0.71	0.00	-0.14	0.00	11.58
	Exp	0.09	50.90	17.00	11.60	11.10	6.10		2.40	0.69		0.16	0.09		100.04
	TH21	0.06	50.17	16.17	11.21	10.64	6.93	0.00	3.43	0.61	0.74	0.10			100.00
	Biase&Variance	-0.03	-0.73	-0.83	-0.39	-0.46	0.83	0.00	1.03	-0.08	0.74	-0.06	-0.09	0.00	3.88
15	WL22-3	0.04	48.78	17.84	11.40	10.17	6.34	0.00	4.46	0.32	0.61	0.06			100.00
	Biase&Variance	-0.05	-2.12	0.84	-0.20	-0.93	0.24	0.00	2.06	-0.37	0.61	-0.10	-0.09	0.00	10.94
	HGP18	0.05	47.71	18.10	11.67	10.45	6.67	0.00	4.05	0.47	0.73	0.14			100.00
	Biase&Variance	-0.04	-3.19	1.10	0.07	-0.65	0.57	0.00	1.65	-0.22	0.73	-0.02	-0.09	0.00	15.42
	Exp	0.13	50.00	16.10	12.50	12.10	6.50		1.90	0.54		0.24	0.12		100.00
	TH21	0.10	49.34	15.39	12.27	11.52	7.41	0.00	2.57	0.60	0.77	0.14			100.00
	Biase&Variance	-0.04	-0.66	-0.71	-0.23	-0.58	0.91	0.00	0.67	0.06	0.77	-0.10	-0.12	0.00	3.22
16	WL22-3	0.06	47.75	17.17	12.41	11.11	6.97	0.00	3.47	0.38	0.66	0.08			100.00
	Biase&Variance	-0.07	-2.25	1.07	-0.09	-0.99	0.47	0.00	1.57	-0.16	0.66	-0.16	-0.12	0.00	10.36
	HGP18	0.07	47.02	17.34	12.54	11.28	7.21	0.00	3.21	0.48	0.77	0.17			100.00
	Biase&Variance	-0.06	-2.98	1.24	0.04	-0.82	0.71	0.00	1.31	-0.06	0.77	-0.07	-0.12	0.00	13.95
	Exp	0.18	50.30	14.70	12.80	13.10	6.70		1.50	0.47		0.34	0.13		100.04
	TH21	0.18	48.84	13.64	13.70	12.84	7.83	0.00	1.62	0.51	0.79	0.23			100.00
	Biase&Variance	0.00	-1.46	-1.06	0.90	-0.26	1.13	0.00	0.12	0.04	0.79	-0.11	-0.13	0.00	6.06
24	WL22-3	0.12	46.84	15.80	13.74	12.39	7.65	0.00	2.29	0.46	0.72	0.12			100.00
	Biase&Variance	-0.06	-3.46	1.10	0.94	-0.71	0.95	0.00	0.79	-0.01	0.72	-0.22	-0.13	0.00	16.66
	HGP18	0.12	46.61	15.84	13.65	12.40	7.78	0.00	2.23	0.46	0.80	0.22			100.00
	Biase&Variance	-0.06	-3.69	1.14	0.85	-0.70	1.08	0.00	0.73	-0.01	0.80	-0.12	-0.13	0.00	18.50

	Exp	0.22	50.40	13.40	13.10	13.90	7.10		1.28	0.42		0.44	0.14		100.18
	TH21	0.20	49.00	13.02	13.26	13.60	8.12	0.00	1.44	0.47	0.81	0.28			100.00
	Biase&Variance	-0.02	-1.40	-0.38	0.16	-0.30	1.02	0.00	0.16	0.05	0.81	-0.16	-0.14	0.00	3.98
21	WL22-3	0.16	46.81	14.61	14.41	13.11	7.88	0.00	1.80	0.48	0.73	0.16			100.00
	Biase&Variance	-0.07	-3.59	1.21	1.31	-0.79	0.78	0.00	0.52	0.06	0.73	-0.28	-0.14	0.00	18.18
	HGP18	0.16	46.77	14.62	14.24	13.09	7.98	0.00	1.79	0.43	0.80	0.27			100.00
	Biase&Variance	-0.07	-3.63	1.22	1.14	-0.81	0.88	0.00	0.51	0.01	0.80	-0.17	-0.14	0.00	18.36
	Exp	0.24	50.50	13.00	12.70	14.50	7.30		1.12	0.42		0.50	0.15		100.19
	TH21	0.21	49.10	12.73	12.98	13.99	8.25	0.00	1.37	0.46	0.81	0.31			100.00
	Biase&Variance	-0.02	-1.40	-0.27	0.28	-0.51	0.95	0.00	0.25	0.04	0.81	-0.19	-0.15	0.00	4.03
22	WL22-3	0.17	46.92	14.30	14.27	13.40	7.99	0.00	1.71	0.48	0.75	0.18			100.00
	Biase&Variance	-0.07	-3.58	1.30	1.57	-1.10	0.69	0.00	0.59	0.06	0.75	-0.32	-0.15	0.00	19.69
	HGP18	0.17	46.86	14.29	14.13	13.38	8.10	0.00	1.70	0.44	0.81	0.30			100.00
	Biase&Variance	-0.07	-3.64	1.29	1.43	-1.12	0.80	0.00	0.58	0.02	0.81	-0.20	-0.15	0.00	19.93
	Exp	0.27	51.00	12.10	11.50	15.70	7.40		1.00	0.35		0.58	0.17		99.80
	TH21	0.24	49.35	12.16	12.34	14.84	8.48	0.00	1.23	0.42	0.81	0.37			100.00
	Biase&Variance	-0.04	-1.65	0.06	0.84	-0.86	1.08	0.00	0.23	0.07	0.81	-0.21	-0.17	0.00	6.12
26	WL22-3	0.19	47.33	13.45	13.71	14.29	8.27	0.00	1.50	0.46	0.77	0.23			100.00
	Biase&Variance	-0.08	-3.67	1.35	2.21	-1.41	0.87	0.00	0.50	0.11	0.77	-0.35	-0.17	0.00	23.92
	HGP18	0.19	47.18	13.42	13.58	14.27	8.39	0.00	1.48	0.44	0.83	0.40			100.00
	Biase&Variance	-0.08	-3.82	1.32	2.08	-1.43	0.99	0.00	0.48	0.09	0.83	-0.18	-0.17	0.00	24.65
	Exp	0.31	51.40	12.04	10.59	16.23	7.23		1.05	0.49		0.81	0.16		100.00
	TH21	0.27	49.65	11.58	11.60	15.77	8.68	0.00	1.11	0.39	0.79	0.42			100.00
	Biase&Variance	-0.05	-1.75	-0.46	1.01	-0.46	1.45	0.00	0.06	-0.10	0.79	-0.39	-0.16	0.00	7.42
T-4243	WL22-3	0.20	47.49	13.19	13.47	14.60	8.35	0.00	1.44	0.45	0.77	0.25			100.00
	Biase&Variance	-0.11	-3.91	1.15	2.88	-1.63	1.12	0.00	0.39	-0.04	0.77	-0.56	-0.16	0.00	29.96
	HGP18	0.20	47.31	13.16	13.36	14.58	8.47	0.00	1.42	0.43	0.84	0.44			100.00
	Biase&Variance	-0.11	-4.09	1.12	2.77	-1.65	1.24	0.00	0.37	-0.06	0.84	-0.37	-0.16	0.00	30.88
	Exp	0.34	51.60	10.98	9.44	17.90	7.64		0.84	0.45		0.94	0.20		99.99
	TH21	0.33	50.43	10.30	9.90	17.95	8.91	0.00	0.90	0.32	0.74	0.55			100.00
	Biase&Variance	-0.01	-1.17	-0.68	0.46	0.05	1.27	0.00	0.06	-0.13	0.74	-0.39	-0.20	0.00	4.42
T-4330	WL22-3	0.24	48.20	12.18	12.39	15.90	8.60	0.00	1.23	0.41	0.76	0.32			100.00
	Biase&Variance	-0.10	-3.40	1.20	2.95	-2.00	0.96	0.00	0.39	-0.04	0.76	-0.62	-0.20	0.00	27.77
	HGP18	0.24	47.87	12.17	12.30	15.89	8.72	0.00	1.22	0.40	0.83	0.60			100.00
	Biase&Variance	-0.10	-3.73	1.19	2.86	-2.01	1.08	0.00	0.38	-0.05	0.83	-0.34	-0.20	0.00	29.73

	Exp	0.40	51.72	10.04	8.76	19.26	7.99		0.79	0.38		0.90	0.16		100.00
	TH21	0.35	50.66	9.95	9.42	18.58	8.92	0.00	0.85	0.30	0.72	0.59			100.00
	Biase&Variance	-0.04	-1.06	-0.09	0.66	-0.68	0.93	0.00	0.06	-0.08	0.72	-0.31	-0.16	0.00	3.55
T-4264	WL22-3	0.25	48.40	11.94	12.09	16.25	8.64	0.00	1.18	0.40	0.76	0.33			100.00
	Biase&Variance	-0.15	-3.32	1.90	3.33	-3.01	0.65	0.00	0.39	0.02	0.76	-0.57	-0.16	0.00	36.29
	HGP18	0.25	48.02	11.94	12.01	16.24	8.77	0.00	1.17	0.39	0.82	0.65			100.00
	Biase&Variance	-0.15	-3.70	1.90	3.25	-3.02	0.78	0.00	0.38	0.01	0.82	-0.25	-0.16	0.00	38.51
	Exp	0.22	49.10	12.80	12.40	15.49	7.86		0.99	0.61		0.59	0.19		100.03
	TH21	0.23	48.49	11.69	12.41	15.89	8.72	0.00	1.26	0.43	0.77	0.34			100.00
	Biase&Variance	0.01	-0.61	-1.11	0.01	0.40	0.86	0.00	0.27	-0.18	0.77	-0.25	-0.19	0.00	3.30
T-4335	WL22-3	0.17	45.66	13.37	14.14	15.11	8.67	0.00	1.66	0.49	0.72	0.20			100.00
	Biase&Variance	-0.05	-3.44	0.57	1.74	-0.38	0.81	0.00	0.67	-0.12	0.72	-0.39	-0.19	0.00	17.17
	HGP18	0.17	45.53	13.39	13.99	15.08	8.78	0.00	1.66	0.46	0.78	0.33			100.00
	Biase&Variance	-0.05	-3.57	0.59	1.59	-0.41	0.92	0.00	0.67	-0.15	0.78	-0.26	-0.19	0.00	17.80
	Exp	0.34	50.30	10.70	9.50	19.10	8.09		0.75	0.46		0.89	0.15		99.94
	TH21	0.36	49.79	9.55	9.22	19.98	9.07	0.00	0.83	0.30	0.69	0.58			100.00
	Biase&Variance	0.02	-0.51	-1.15	-0.28	0.88	0.98	0.00	0.08	-0.16	0.69	-0.31	-0.15	0.00	4.02
T-4309	WL22-3	0.24	46.33	11.65	12.28	17.85	9.21	0.00	1.21	0.41	0.72	0.33			100.00
	Biase&Variance	-0.10	-3.97	0.95	2.78	-1.25	1.12	0.00	0.46	-0.05	0.72	-0.56	-0.15	0.00	28.25
	HGP18	0.24	46.11	11.62	12.16	17.84	9.31	0.00	1.20	0.40	0.78	0.58			100.00
	Biase&Variance	-0.10	-4.19	0.92	2.66	-1.26	1.22	0.00	0.45	-0.06	0.78	-0.31	-0.15	0.00	29.55
	Exp	0.43	50.87	9.12	8.29	21.30	8.25		0.67	0.36		0.89			99.75
	TH21	0.43	50.46	8.63	7.97	21.76	8.91	0.00	0.71	0.25	0.63	0.67			100.00
	Biase&Variance	0.00	-0.41	-0.49	-0.32	0.46	0.66	0.00	0.04	-0.11	0.63	-0.22	0.00	0.00	1.61
T-4333	WL22-3	0.26	46.69	11.08	11.51	18.86	9.29	0.00	1.10	0.38	0.71	0.38			100.00
	Biase&Variance	-0.16	-4.18	1.96	3.22	-2.44	1.04	0.00	0.43	0.02	0.71	-0.51	0.00	0.00	39.63
	HGP18	0.27	46.42	11.06	11.39	18.85	9.39	0.00	1.09	0.37	0.76	0.68			100.00
	Biase&Variance	-0.16	-4.45	1.94	3.10	-2.45	1.14	0.00	0.42	0.01	0.76	-0.21	0.00	0.00	41.33
	Exp	0.46	50.30	8.60	7.80	22.90	8.31		0.62	0.32		1.01	0.17		100.03
	TH21	0.47	50.45	8.09	7.34	23.08	8.83	0.00	0.65	0.23	0.59	0.74			100.00
	Biase&Variance	0.01	0.15	-0.51	-0.46	0.18	0.52	0.00	0.03	-0.09	0.59	-0.27	-0.17	0.00	1.25
T-4326	WL22-3	0.29	47.12	10.49	10.69	19.92	9.32	0.00	1.00	0.35	0.69	0.43			100.00
	Biase&Variance	-0.16	-3.18	1.89	2.89	-2.98	1.01	0.00	0.38	0.03	0.69	-0.58	-0.17	0.00	32.92
	HGP18	0.30	46.78	10.47	10.58	19.91	9.41	0.00	0.99	0.34	0.74	0.78			100.00
	Biase&Variance	-0.16	-3.52	1.87	2.78	-2.99	1.10	0.00	0.37	0.02	0.74	-0.23	-0.17	0.00	34.56

Table A1.2b MM3 anhydrous melting experimental results and calculation results from TH21, WL22-3, and HGP18 models: residue composition

Run No.	Type	Mode	SiO2	Al2O3	CaO	MgO	FeO	K2O	Na2O	TiO2	Fe2O3	Cr2O3	MnO	NiO	Total
	Exp	0.92	45.26	2.51	2.87	40.99	7.42	0.00	0.08	0.05		0.81			100.00
	TH21	0.95	45.42	3.24	3.13	40.11	6.94	0.00	0.12	0.08	0.28	0.69			100.00
	Biase&Variance	0.03	0.15	0.74	0.26	-0.88	-0.48	0.00	0.04	0.03	0.28	-0.13	0.00	0.00	1.74
55T	WL22-3	0.97	45.58	3.50	3.30	39.44	6.95	0.00	0.17	0.10	0.29	0.68			100.00
	Biase&Variance	0.05	0.31	0.99	0.43	-1.56	-0.47	0.00	0.09	0.05	0.29	-0.14	0.00	0.00	4.01
	HGP18	0.96	46.50	4.07	3.89	37.48	6.60	0.00	0.17	0.12	0.34	0.83			100.00
	Biase&Variance	0.05	1.24	1.56	1.02	-3.51	-0.82	0.00	0.09	0.06	0.34	0.02	0.00	0.00	18.14
	Exp	0.93	45.14	2.84	2.92	40.73	7.41	0.00	0.09	0.06		0.80			100.00
	TH21	0.95	45.42	3.24	3.13	40.11	6.94	0.00	0.12	0.08	0.28	0.69			100.00
	Biase&Variance	0.02	0.27	0.41	0.21	-0.62	-0.48	0.00	0.03	0.02	0.28	-0.11	0.00	0.00	0.99
20	WL22-3	0.97	45.58	3.50	3.30	39.44	6.95	0.00	0.17	0.10	0.29	0.68			100.00
	Biase&Variance	0.05	0.43	0.66	0.38	-1.30	-0.46	0.00	0.08	0.04	0.29	-0.12	0.00	0.00	2.77
	HGP18	0.96	46.50	4.07	3.89	37.48	6.60	0.00	0.17	0.12	0.34	0.83			100.00
	Biase&Variance	0.04	1.36	1.23	0.97	-3.25	-0.81	0.00	0.08	0.05	0.34	0.03	0.00	0.00	15.67
	Exp	0.91	45.18	2.44	2.79	41.17	7.43	0.00	0.07	0.04		0.88			100.00
	TH21	0.94	45.37	3.08	2.99	40.51	6.92	0.00	0.09	0.07	0.27	0.70			100.00
	Biase&Variance	0.03	0.19	0.64	0.20	-0.66	-0.51	0.00	0.02	0.04	0.27	-0.18	0.00	0.00	1.29
15	WL22-3	0.96	45.56	3.37	3.21	39.71	6.95	0.00	0.14	0.10	0.29	0.68			100.00
	Biase&Variance	0.05	0.38	0.93	0.41	-1.46	-0.49	0.00	0.07	0.06	0.29	-0.19	0.00	0.00	3.67
	HGP18	0.95	46.49	3.92	3.76	37.80	6.59	0.00	0.14	0.11	0.34	0.85			100.00
	Biase&Variance	0.04	1.31	1.48	0.96	-3.37	-0.84	0.00	0.07	0.07	0.34	-0.02	0.00	0.00	17.00
	Exp	0.87	44.84	1.99	2.22	42.52	7.57	0.00	0.04	0.03		0.79			100.00
	TH21	0.90	45.26	2.64	2.54	41.62	6.86	0.00	0.05	0.05	0.25	0.72			100.00
	Biase&Variance	0.04	0.42	0.65	0.33	-0.90	-0.70	0.00	0.01	0.02	0.25	-0.07	0.00	0.00	2.08
16	WL22-3	0.94	45.54	3.03	2.92	40.43	6.92	0.00	0.09	0.09	0.27	0.70			100.00
	Biase&Variance	0.07	0.70	1.04	0.71	-2.09	-0.65	0.00	0.05	0.06	0.27	-0.09	0.00	0.00	6.93
	HGP18	0.93	46.50	3.54	3.41	38.58	6.57	0.00	0.10	0.10	0.32	0.88			100.00
	Biase&Variance	0.06	1.66	1.55	1.20	-3.94	-0.99	0.00	0.05	0.06	0.32	0.09	0.00	0.00	23.21

	Exp	0.82	44.83	1.36	1.67	43.88	7.37	0.00	0.03	0.03		0.83			100.00
	TH21	0.82	44.96	1.76	1.28	44.33	6.70	0.00	0.01	0.02	0.19	0.76			100.00
	Biase&Variance	0.00	0.13	0.41	-0.40	0.45	-0.67	0.00	-0.02	-0.01	0.19	-0.08	0.00	0.00	1.03
24	WL22-3	0.88	45.51	2.35	2.16	42.08	6.82	0.00	0.04	0.06	0.24	0.74			100.00
	Biase&Variance	0.06	0.68	0.99	0.49	-1.79	-0.56	0.00	0.01	0.03	0.24	-0.10	0.00	0.00	5.28
	HGP18	0.88	46.52	2.83	2.57	40.25	6.50	0.00	0.05	0.08	0.28	0.92			100.00
	Biase&Variance	0.06	1.69	1.48	0.90	-3.62	-0.87	0.00	0.02	0.05	0.28	0.08	0.00	0.00	19.82
	Exp	0.78	44.33	0.99	0.96	45.32	7.54	0.00	0.02	0.01		0.83			100.00
	TH21	0.80	44.80	1.55	1.00	45.11	6.59	0.00	0.01	0.01	0.16	0.75			100.00
	Biase&Variance	0.02	0.47	0.57	0.04	-0.20	-0.95	0.00	-0.01	0.00	0.16	-0.08	0.00	0.00	1.52
21	WL22-3	0.84	45.44	1.88	1.44	43.49	6.72	0.00	0.02	0.04	0.21	0.77			100.00
	Biase&Variance	0.07	1.10	0.89	0.48	-1.83	-0.82	0.00	0.00	0.03	0.21	-0.06	0.00	0.00	6.29
	HGP18	0.84	46.46	2.34	1.75	41.73	6.44	0.00	0.02	0.06	0.25	0.94			100.00
	Biase&Variance	0.07	2.13	1.35	0.79	-3.59	-1.09	0.00	0.00	0.05	0.25	0.11	0.00	0.00	21.09
	Exp	0.76	44.18	0.98	0.85	45.70	7.48	0.00	0.02	0.00		0.79			100.00
	TH21	0.79	44.71	1.46	0.89	45.50	6.52	0.00	0.01	0.01	0.15	0.75			100.00
	Biase&Variance	0.02	0.53	0.48	0.04	-0.20	-0.95	0.00	-0.01	0.01	0.15	-0.04	0.00	0.00	1.49
22	WL22-3	0.83	45.40	1.80	1.33	43.76	6.68	0.00	0.02	0.03	0.21	0.77			100.00
	Biase&Variance	0.07	1.22	0.82	0.48	-1.94	-0.79	0.00	0.00	0.03	0.21	-0.02	0.00	0.00	6.81
	HGP18	0.83	46.43	2.25	1.59	42.07	6.41	0.00	0.02	0.05	0.24	0.95			100.00
	Biase&Variance	0.07	2.24	1.27	0.74	-3.63	-1.07	0.00	0.00	0.05	0.24	0.16	0.00	0.00	21.59
	Exp	0.73	43.66	0.76	0.67	46.95	7.16	0.00	0.01	0.00		0.79			100.00
	TH21	0.76	44.49	1.26	0.69	46.28	6.39	0.00	0.01	0.01	0.13	0.74			100.00
	Biase&Variance	0.04	0.83	0.50	0.03	-0.67	-0.77	0.00	0.00	0.01	0.13	-0.05	0.00	0.00	2.01
26	WL22-3	0.81	45.26	1.59	1.03	44.56	6.57	0.00	0.01	0.02	0.18	0.77			100.00
	Biase&Variance	0.08	1.60	0.83	0.37	-2.39	-0.59	0.00	0.00	0.02	0.18	-0.02	0.00	0.00	9.49
	HGP18	0.81	46.29	1.99	1.21	43.01	6.30	0.00	0.02	0.03	0.21	0.94			100.00
	Biase&Variance	0.08	2.63	1.23	0.54	-3.94	-0.86	0.00	0.00	0.03	0.21	0.16	0.00	0.00	25.05
	Exp	0.69	42.96	0.30	0.51	48.52	7.11	0.00	0.01	0.00		0.59			100.00
	TH21	0.73	44.21	1.07	0.53	47.11	6.23	0.00	0.01	0.01	0.11	0.72			100.00
	Biase&Variance	0.05	1.24	0.77	0.03	-1.40	-0.88	0.00	0.00	0.00	0.11	0.13	0.00	0.00	4.91
T-4243	WL22-3	0.80	45.20	1.53	0.95	44.82	6.52	0.00	0.01	0.02	0.18	0.77			100.00
	Biase&Variance	0.11	2.24	1.22	0.44	-3.69	-0.59	0.00	0.01	0.02	0.18	0.18	0.00	0.00	20.75
	HGP18	0.80	46.24	1.91	1.11	43.31	6.26	0.00	0.02	0.03	0.20	0.94			100.00
	Biase&Variance	0.11	3.27	1.61	0.60	-5.21	-0.85	0.00	0.01	0.03	0.20	0.35	0.00	0.00	41.62

	Exp	0.65	42.37	0.18	0.38	49.09	7.35	0.00	0.00	0.00		0.63			100.00
	TH21	0.67	43.27	0.66	0.29	49.20	5.85	0.00	0.00	0.00	0.07	0.65			100.00
	Biase&Variance	0.02	0.90	0.48	-0.09	0.11	-1.49	0.00	0.00	0.00	0.07	0.02	0.00	0.00	3.30
T-4330	WL22-3	0.76	44.87	1.27	0.68	45.92	6.35	0.00	0.01	0.01	0.15	0.76			100.00
	Biase&Variance	0.11	2.50	1.08	0.30	-3.17	-1.00	0.00	0.01	0.01	0.15	0.13	0.00	0.00	18.58
	HGP18	0.76	45.91	1.60	0.78	44.53	6.09	0.00	0.01	0.02	0.16	0.90			100.00
	Biase&Variance	0.11	3.55	1.42	0.40	-4.56	-1.26	0.00	0.01	0.01	0.16	0.27	0.00	0.00	37.23
	Exp	0.78	44.36	1.39	0.95	44.72	7.35	0.00	0.02	0.02		1.20			100.00
	TH21	0.77	44.82	1.54	0.81	45.56	6.34	0.00	0.01	0.01	0.15	0.74			100.00
	Biase&Variance	-0.01	0.47	0.15	-0.13	0.84	-1.01	0.00	-0.01	-0.01	0.15	-0.45	0.00	0.00	2.22
T-4335	WL22-3	0.83	45.68	1.98	1.34	43.43	6.54	0.00	0.02	0.03	0.21	0.77			100.00
	Biase&Variance	0.05	1.32	0.59	0.40	-1.29	-0.81	0.00	0.00	0.01	0.21	-0.43	0.00	0.00	4.79
	HGP18	0.83	46.73	2.45	1.60	41.72	6.25	0.00	0.03	0.05	0.24	0.93			100.00
	Biase&Variance	0.05	2.38	1.06	0.65	-3.00	-1.10	0.00	0.01	0.02	0.24	-0.27	0.00	0.00	17.55
	Exp	0.66	43.23	0.33	0.40	48.23	7.11	0.00	0.01	0.01		0.69			100.00
	TH21	0.64	43.32	0.68	0.26	49.38	5.63	0.00	0.00	0.00	0.07	0.65			100.00
	Biase&Variance	-0.02	0.10	0.36	-0.14	1.15	-1.49	0.00	0.00	0.00	0.07	-0.04	0.00	0.00	3.69
T-4309	WL22-3	0.76	45.48	1.46	0.73	45.23	6.15	0.00	0.01	0.01	0.16	0.76			100.00
	Biase&Variance	0.10	2.25	1.13	0.33	-3.00	-0.96	0.00	0.01	0.01	0.16	0.07	0.00	0.00	16.42
	HGP18	0.76	46.58	1.81	0.83	43.81	5.87	0.00	0.02	0.02	0.18	0.90			100.00
	Biase&Variance	0.10	3.35	1.48	0.42	-4.42	-1.24	0.00	0.01	0.01	0.18	0.21	0.00	0.00	34.78

Table A1.2c MM3 anhydrous melting experimental results and calculation results from TH21, WL22-3, and HGP18 models: spinel composition

Run No.	Type	Mode	SiO2	Al2O3	CaO	MgO	FeO	K2O	Na2O	TiO2	Fe2O3	Cr2O3	MnO	NiO	Total	Cr
	Exp	0.009	0.27	43.40	0.09	20.20	9.80			0.14		27.00	0.09		100.99	29.45
	TH21	0.012	0.00	47.96	0.00	21.26	7.94	0.00	0.00	0.01	1.40	21.44			100.00	23.07
	Biase&Variance	0.003	-0.27	4.56	-0.09	1.06	-1.86	0.00	0.00	-0.13	1.40	-5.56	-0.09	0.00	58.27	
55T	WL22-3	0.013	0.00	49.37	0.00	21.43	7.87	0.00	0.00	0.01	1.35	19.97			100.00	21.35
	Biase&Variance	0.004	-0.27	5.97	-0.09	1.23	-1.93	0.00	0.00	-0.13	1.35	-7.03	-0.09	0.00	92.21	
	HGP18	0.002	0.00	50.32	0.00	21.38	8.27	0.00	0.00	0.09	1.52	18.43			100.00	19.73
	Biase&Variance	-0.007	-0.27	6.92	-0.09	1.18	-1.53	0.00	0.00	-0.05	1.52	-8.57	-0.09	0.00	127.39	
	Exp	0.012	0.19	44.20	0.05	20.40	9.50			0.09		25.60	0.11		100.14	27.98
	TH21	0.012	0.00	47.96	0.00	21.26	7.94	0.00	0.00	0.01	1.40	21.44			100.00	23.07
	Biase&Variance	0.000	-0.19	3.76	-0.05	0.86	-1.56	0.00	0.00	-0.08	1.40	-4.16	-0.11	0.00	36.57	
20	WL22-3	0.013	0.00	49.37	0.00	21.43	7.87	0.00	0.00	0.01	1.35	19.97			100.00	21.35
	Biase&Variance	0.001	-0.19	5.17	-0.05	1.03	-1.63	0.00	0.00	-0.08	1.35	-5.63	-0.11	0.00	64.01	
	HGP18	0.002	0.00	50.32	0.00	21.38	8.27	0.00	0.00	0.09	1.52	18.43			100.00	19.73
	Biase&Variance	-0.010	-0.19	6.12	-0.05	0.98	-1.23	0.00	0.00	0.00	1.52	-7.17	-0.11	0.00	93.63	
	Exp	0.013	0.18	44.20	0.08	20.00	9.30			0.17		25.00	0.11		99.04	27.51
	TH21	0.010	0.00	46.72	0.00	21.10	8.01	0.00	0.00	0.01	1.44	22.72			100.00	24.60
	Biase&Variance	-0.003	-0.18	2.52	-0.08	1.10	-1.29	0.00	0.00	-0.16	1.44	-2.28	-0.11	0.00	16.60	
15	WL22-3	0.011	0.00	48.32	0.00	21.29	7.94	0.00	0.00	0.01	1.39	21.05			100.00	22.61
	Biase&Variance	-0.002	-0.18	4.12	-0.08	1.29	-1.36	0.00	0.00	-0.16	1.39	-3.95	-0.11	0.00	38.16	
	HGP18	0.000	0.00	47.93	0.00	20.99	8.53	0.00	0.00	0.08	1.60	20.87			100.00	22.61
	Biase&Variance	-0.013	-0.18	3.73	-0.08	0.99	-0.77	0.00	0.00	-0.09	1.60	-4.13	-0.11	0.00	35.11	
	Exp	0.007	0.05	37.60	0.09	19.78	10.00			0.09		32.90	0.12		100.63	36.99
	TH21	0.007	0.00	43.34	0.00	20.68	8.19	0.00	0.00	0.01	1.56	26.22			100.00	28.87
16	Biase&Variance	0.001	-0.05	5.74	-0.09	0.90	-1.81	0.00	0.00	-0.08	1.56	-6.68	-0.12	0.00	84.07	
	WL22-3	0.008	0.00	45.61	0.00	20.93	8.12	0.00	0.00	0.01	1.49	23.83			100.00	25.95
	Biase&Variance	0.002	-0.05	8.01	-0.09	1.15	-1.88	0.00	0.00	-0.08	1.49	-9.07	-0.12	0.00	153.48	
	Exp	0.005	0.32	28.50	0.07	18.16	9.90			0.17		42.10	0.17		99.39	49.77
	TH21	0.003	0.00	35.08	0.00	19.63	8.70	0.00	0.00	0.00	1.91	34.68			100.00	39.88
24	Biase&Variance	-0.001	-0.32	6.58	-0.07	1.47	-1.20	0.00	0.00	-0.17	1.91	-7.42	-0.17	0.00	105.72	
	WL22-3	0.004	0.00	39.40	0.00	20.11	8.55	0.00	0.00	0.01	1.75	30.17			100.00	33.94
	Biase&Variance	-0.001	-0.32	10.90	-0.07	1.95	-1.35	0.00	0.00	-0.16	1.75	-11.93	-0.17	0.00	270.02	29.45

	Exp	0.003	0.24	24.00	0.11	18.00	10.22			0.10		47.60	0.19		100.46	56.17
	TH21	0.004	0.00	30.22	0.00	19.03	9.04	0.00	0.00	0.00	2.22	39.49			100.00	44.58
22	Biase&Variance	0.000	-0.24	6.22	-0.11	1.03	-1.18	0.00	0.00	-0.10	2.22	-8.11	-0.19	0.00	112.05	
	WL22-3	0.002	0.00	32.84	0.00	19.25	9.06	0.00	0.00	0.01	2.11	36.73			100.00	40.91
	Biase&Variance	-0.001	-0.24	8.84	-0.11	1.25	-1.16	0.00	0.00	-0.09	2.11	-10.87	-0.19	0.00	203.86	
	Exp	0.003	0.42	23.30	0.07	18.20	10.20			0.15		49.10	0.18		101.62	57.09
	TH21	0.004	0.00	27.53	0.00	18.74	9.16	0.00	0.00	0.00	2.39	42.18			100.00	46.71
26	Biase&Variance	0.001	-0.42	4.23	-0.07	0.54	-1.04	0.00	0.00	-0.15	2.39	-6.92	-0.18	0.00	73.01	
	WL22-3	0.002	0.00	29.19	0.00	18.79	9.35	0.00	0.00	0.01	2.40	40.26			100.00	42.86
	Biase&Variance	0.000	-0.42	5.89	-0.07	0.59	-0.85	0.00	0.00	-0.14	2.40	-8.84	-0.18	0.00	119.91	
	Exp	0.010	0.21	30.70	0.06	18.00	9.65			0.22		41.20	0.05		100.09	58.57
	TH21	0.004	0.00	30.58	0.00	19.30	8.65	0.00	0.00	0.00	2.17	39.30			100.00	50.69
T-4335	Biase&Variance	-0.006	-0.21	-0.12	-0.06	1.30	-1.00	0.00	0.00	-0.22	2.17	-1.90	-0.05	0.00	11.08	
	WL22-3	0.002	0.00	33.51	0.00	19.49	8.74	0.00	0.00	0.01	2.02	36.23			100.00	48.06
	Biase&Variance	-0.008	-0.21	2.81	-0.06	1.49	-0.91	0.00	0.00	-0.21	2.02	-4.97	-0.05	0.00	39.83	

Table A1.2d MM3 anhydrous melting experimental results and calculation results from TH21, WL22-3, and HGP18 models: olivine composition

Run No.	Type	Mode	SiO2	Al2O3	CaO	MgO	FeO	K2O	Na2O	TiO2	Fe2O3	Cr2O3	MnO	NiO	Total	Mg#
	Exp	0.53	40.70	0.00	0.22	50.50	9.14					0.13	0.11		100.80	90.78
	TH21	0.54	41.10	0.00	0.25	50.24	8.40	0.00	0.00	0.00	0.00	0.00			100.00	91.42
	Biase&Variance	0.01	0.40	0.00	0.03	-0.26	-0.74	0.00	0.00	0.00	0.00	-0.13	-0.11	0.00	0.80	
55T	WL22-3	0.53	41.08	0.00	0.25	50.15	8.52	0.00	0.00	0.00	0.00	0.00			100.00	91.30
	Biase&Variance	0.00	0.38	0.00	0.03	-0.35	-0.62	0.00	0.00	0.00	0.00	-0.13	-0.11	0.00	0.68	
	HGP18	0.54	41.07	0.00	0.25	50.12	8.56	0.00	0.00	0.00	0.00	0.00			100.00	91.25
	Biase&Variance	0.01	0.37	0.00	0.03	-0.38	-0.58	0.00	0.00	0.00	0.00	-0.13	-0.11	0.00	0.65	
	Exp	0.52	40.20	0.04	0.25	50.40	9.20					0.12	0.16		100.37	90.71
	TH21	0.54	41.10	0.00	0.25	50.24	8.40	0.00	0.00	0.00	0.00	0.00			100.00	91.42
	Biase&Variance	0.02	0.90	-0.04	0.00	-0.16	-0.80	0.00	0.00	0.00	0.00	-0.12	-0.16	0.00	1.51	
20	WL22-3	0.53	41.08	0.00	0.25	50.15	8.52	0.00	0.00	0.00	0.00	0.00			100.00	91.30
	Biase&Variance	0.01	0.88	-0.04	0.00	-0.25	-0.68	0.00	0.00	0.00	0.00	-0.12	-0.16	0.00	1.34	
	HGP18	0.54	41.07	0.00	0.25	50.12	8.56	0.00	0.00	0.00	0.00	0.00			100.00	91.25
	Biase&Variance	0.02	0.87	-0.04	0.00	-0.28	-0.64	0.00	0.00	0.00	0.00	-0.12	-0.16	0.00	1.28	
	Exp	0.55	40.80	0.03	0.22	49.80	8.98					0.13	0.13		100.09	90.81
	TH21	0.54	41.11	0.00	0.27	50.30	8.32	0.00	0.00	0.00	0.00	0.00			100.00	91.51
	Biase&Variance	-0.01	0.31	-0.03	0.05	0.50	-0.66	0.00	0.00	0.00	0.00	-0.13	-0.13	0.00	0.81	
15	WL22-3	0.53	41.09	0.00	0.26	50.18	8.47	0.00	0.00	0.00	0.00	0.00			100.00	91.35
	Biase&Variance	-0.02	0.29	-0.03	0.04	0.38	-0.51	0.00	0.00	0.00	0.00	-0.13	-0.13	0.00	0.52	
	HGP18	0.54	41.08	0.00	0.26	50.15	8.50	0.00	0.00	0.00	0.00	0.00			100.00	91.31
	Biase&Variance	-0.01	0.28	-0.03	0.04	0.35	-0.48	0.00	0.00	0.00	0.00	-0.13	-0.13	0.00	0.47	
	Exp	0.54	40.80	0.06	0.28	51.00	9.10					0.14	0.14		101.52	90.90
	TH21	0.55	41.15	0.00	0.29	50.46	8.09	0.00	0.00	0.00	0.00	0.00			100.00	91.75
	Biase&Variance	0.00	0.35	-0.06	0.01	-0.54	-1.01	0.00	0.00	0.00	0.00	-0.14	-0.14	0.00	1.47	
16	WL22-3	0.53	41.11	0.00	0.29	50.28	8.33	0.00	0.00	0.00	0.00	0.00			100.00	91.50
	Biase&Variance	-0.01	0.31	-0.06	0.01	-0.72	-0.77	0.00	0.00	0.00	0.00	-0.14	-0.14	0.00	1.26	
	HGP18	0.54	41.10	0.00	0.28	50.25	8.36	0.00	0.00	0.00	0.00	0.00			100.00	91.47
	Biase&Variance	0.00	0.30	-0.06	0.00	-0.75	-0.74	0.00	0.00	0.00	0.00	-0.14	-0.14	0.00	1.24	

	Exp	0.55	40.50	0.07	0.34	50.50	8.60					0.24	0.10		100.35	91.28
	TH21	0.55	41.25	0.00	0.33	50.88	7.54	0.00	0.00	0.00	0.00	0.00			100.00	92.33
	Biase&Variance	0.01	0.75	-0.07	-0.01	0.38	-1.06	0.00	0.00	0.00	0.00	-0.24	-0.10	0.00	1.92	
24	WL22-3	0.54	41.17	0.00	0.32	50.53	7.98	0.00	0.00	0.00	0.00	0.00			100.00	91.86
	Biase&Variance	-0.01	0.67	-0.07	-0.02	0.03	-0.62	0.00	0.00	0.00	0.00	-0.24	-0.10	0.00	0.91	
	HGP18	0.54	41.16	0.00	0.32	50.49	8.02	0.00	0.00	0.00	0.00	0.00			100.00	91.82
	Biase&Variance	0.00	0.66	-0.07	-0.02	-0.01	-0.58	0.00	0.00	0.00	0.00	-0.24	-0.10	0.00	0.84	
	Exp	0.55	40.40	0.05	0.32	50.80	8.50					0.25	0.11		100.43	91.42
	TH21	0.56	41.29	0.00	0.30	51.07	7.33	0.00	0.00	0.00	0.00	0.00			100.00	92.54
	Biase&Variance	0.01	0.89	-0.05	-0.02	0.27	-1.17	0.00	0.00	0.00	0.00	-0.25	-0.11	0.00	2.31	
21	WL22-3	0.54	41.22	0.00	0.35	50.75	7.68	0.00	0.00	0.00	0.00	0.00			100.00	92.17
	Biase&Variance	-0.01	0.82	-0.05	0.03	-0.05	-0.82	0.00	0.00	0.00	0.00	-0.25	-0.11	0.00	1.43	
	HGP18	0.54	41.21	0.00	0.34	50.70	7.74	0.00	0.00	0.00	0.00	0.00			100.00	92.11
	Biase&Variance	-0.01	0.81	-0.05	0.02	-0.10	-0.76	0.00	0.00	0.00	0.00	-0.25	-0.11	0.00	1.32	
	Exp	0.55	40.70	0.06	0.30	51.10	8.44					0.29	0.09		100.98	91.52
	TH21	0.56	41.32	0.00	0.29	51.17	7.23	0.00	0.00	0.00	0.00	0.00			100.00	92.66
	Biase&Variance	0.01	0.62	-0.06	-0.01	0.07	-1.21	0.00	0.00	0.00	0.00	-0.29	-0.09	0.00	1.95	
22	WL22-3	0.54	41.24	0.00	0.34	50.81	7.61	0.00	0.00	0.00	0.00	0.00			100.00	92.25
	Biase&Variance	-0.01	0.54	-0.06	0.04	-0.29	-0.83	0.00	0.00	0.00	0.00	-0.29	-0.09	0.00	1.16	
	HGP18	0.54	41.23	0.00	0.33	50.77	7.67	0.00	0.00	0.00	0.00	0.00			100.00	92.18
	Biase&Variance	-0.01	0.53	-0.06	0.03	-0.33	-0.77	0.00	0.00	0.00	0.00	-0.29	-0.09	0.00	1.08	
	Exp	0.55	40.70	0.06	0.28	51.60	7.90					0.37	0.14		101.05	92.09
	TH21	0.56	41.36	0.00	0.26	51.38	7.00	0.00	0.00	0.00	0.00	0.00			100.00	92.90
	Biase&Variance	0.01	0.66	-0.06	-0.02	-0.22	-0.90	0.00	0.00	0.00	0.00	-0.37	-0.14	0.00	1.45	
26	WL22-3	0.54	41.28	0.00	0.32	51.00	7.40	0.00	0.00	0.00	0.00	0.00			100.00	92.47
	Biase&Variance	-0.01	0.58	-0.06	0.04	-0.60	-0.50	0.00	0.00	0.00	0.00	-0.37	-0.14	0.00	1.10	
	HGP18	0.54	41.27	0.00	0.31	50.96	7.46	0.00	0.00	0.00	0.00	0.00			100.00	92.41
	Biase&Variance	-0.01	0.57	-0.06	0.03	-0.64	-0.44	0.00	0.00	0.00	0.00	-0.37	-0.14	0.00	1.09	
	Exp	0.59	40.83		0.27	50.80	7.50					0.49	0.10		99.99	92.35
	TH21	0.56	41.41	0.00	0.23	51.61	6.75	0.00	0.00	0.00	0.00	0.00			100.00	93.16
	Biase&Variance	-0.03	0.58	0.00	-0.04	0.81	-0.75	0.00	0.00	0.00	0.00	-0.49	-0.10	0.00	1.80	
T-4243	WL22-3	0.54	41.29	0.00	0.31	51.07	7.33	0.00	0.00	0.00	0.00	0.00			100.00	92.55
	Biase&Variance	-0.05	0.46	0.00	0.04	0.27	-0.17	0.00	0.00	0.00	0.00	-0.49	-0.10	0.00	0.57	
	HGP18	0.54	41.28	0.00	0.30	51.03	7.39	0.00	0.00	0.00	0.00	0.00			100.00	92.49
	Biase&Variance	-0.05	0.45	0.00	0.03	0.23	-0.11	0.00	0.00	0.00	0.00	-0.49	-0.10	0.00	0.52	

	Exp	0.59	40.90		0.25	50.60	7.60					0.57	0.13		100.05	92.23
	TH21	0.56	41.53	0.00	0.17	52.15	6.15	0.00	0.00	0.00	0.00	0.00			100.00	93.80
	Biase&Variance	-0.03	0.63	0.00	-0.08	1.55	-1.45	0.00	0.00	0.00	0.00	-0.57	-0.13	0.00	5.25	
T-4330	WL22-3	0.54	41.36	0.00	0.27	51.35	7.02	0.00	0.00	0.00	0.00	0.00			100.00	92.87
	Biase&Variance	-0.05	0.46	0.00	0.02	0.75	-0.58	0.00	0.00	0.00	0.00	-0.57	-0.13	0.00	1.45	
	HGP18	0.54	41.35	0.00	0.26	51.32	7.07	0.00	0.00	0.00	0.00	0.00			100.00	92.82
	Biase&Variance	-0.05	0.45	0.00	0.01	0.72	-0.53	0.00	0.00	0.00	0.00	-0.57	-0.13	0.00	1.33	
	Exp	0.60	41.50		0.22	51.00	6.70					0.54	0.11		100.07	93.14
	TH21	0.56	41.57	0.00	0.15	52.31	5.97	0.00	0.00	0.00	0.00	0.00			100.00	93.98
	Biase&Variance	-0.04	0.07	0.00	-0.07	1.31	-0.73	0.00	0.00	0.00	0.00	-0.54	-0.11	0.00	2.56	
T-4264	WL22-3	0.54	41.37	0.00	0.26	51.43	6.94	0.00	0.00	0.00	0.00	0.00			100.00	92.96
	Biase&Variance	-0.06	-0.13	0.00	0.04	0.43	0.24	0.00	0.00	0.00	0.00	-0.54	-0.11	0.00	0.56	
	HGP18	0.54	41.36	0.00	0.25	51.39	6.99	0.00	0.00	0.00	0.00	0.00			100.00	92.91
	Biase&Variance	-0.06	-0.14	0.00	0.03	0.39	0.29	0.00	0.00	0.00	0.00	-0.54	-0.11	0.00	0.56	
	Exp	0.56	41.00		0.34	50.00	8.22					0.35	0.14		100.05	91.56
	TH21	0.54	41.35	0.00	0.28	51.30	7.08	0.00	0.00	0.00	0.00	0.00			100.00	92.82
	Biase&Variance	-0.02	0.35	0.00	-0.06	1.30	-1.14	0.00	0.00	0.00	0.00	-0.35	-0.14	0.00	3.26	
T-4335	WL22-3	0.52	41.24	0.00	0.35	50.84	7.57	0.00	0.00	0.00	0.00	0.00			100.00	92.29
	Biase&Variance	-0.04	0.24	0.00	0.01	0.84	-0.65	0.00	0.00	0.00	0.00	-0.35	-0.14	0.00	1.33	
	HGP18	0.52	41.23	0.00	0.34	50.79	7.63	0.00	0.00	0.00	0.00	0.00			100.00	92.23
	Biase&Variance	-0.04	0.23	0.00	0.00	0.79	-0.59	0.00	0.00	0.00	0.00	-0.35	-0.14	0.00	1.17	
	Exp	0.57	41.10		0.24	50.48	7.50					0.56	0.10		99.98	92.31
	TH21	0.54	41.57	0.00	0.16	52.34	5.93	0.00	0.00	0.00	0.00	0.00			100.00	94.02
	Biase&Variance	-0.03	0.47	0.00	-0.08	1.86	-1.57	0.00	0.00	0.00	0.00	-0.56	-0.10	0.00	6.47	
T-4309	WL22-3	0.51	41.37	0.00	0.27	51.39	6.97	0.00	0.00	0.00	0.00	0.00			100.00	92.93
	Biase&Variance	-0.06	0.27	0.00	0.03	0.91	-0.53	0.00	0.00	0.00	0.00	-0.56	-0.10	0.00	1.51	
	HGP18	0.51	41.36	0.00	0.27	51.36	7.01	0.00	0.00	0.00	0.00	0.00			100.00	92.88
	Biase&Variance	-0.06	0.26	0.00	0.03	0.88	-0.49	0.00	0.00	0.00	0.00	-0.56	-0.10	0.00	1.41	
	Exp	0.57	41.40		0.22	50.90	6.85					0.51	0.13		100.01	92.98
	TH21	0.54	41.68	0.00	0.12	52.80	5.40	0.00	0.00	0.00	0.00	0.00			100.00	94.57
	Biase&Variance	-0.04	0.28	0.00	-0.10	1.90	-1.45	0.00	0.00	0.00	0.00	-0.51	-0.13	0.00	6.07	
T-4333	WL22-3	0.51	41.41	0.00	0.24	51.60	6.75	0.00	0.00	0.00	0.00	0.00			100.00	93.17
	Biase&Variance	-0.07	0.01	0.00	0.02	0.70	-0.10	0.00	0.00	0.00	0.00	-0.51	-0.13	0.00	0.78	
	HGP18	0.51	41.41	0.00	0.24	51.57	6.78	0.00	0.00	0.00	0.00	0.00			100.00	93.13
	Biase&Variance	-0.07	0.01	0.00	0.02	0.67	-0.07	0.00	0.00	0.00	0.00	-0.51	-0.13	0.00	0.74	

	Exp	0.54	41.20		0.20	51.20	6.69					0.53	0.20		100.02	93.17
	TH21	0.53	41.74	0.00	0.11	53.06	5.10	0.00	0.00	0.00	0.00	0.00			100.00	94.89
	Biase&Variance	-0.02	0.54	0.00	-0.09	1.86	-1.59	0.00	0.00	0.00	0.00	-0.53	-0.20	0.00	6.62	
T-4326	WL22-3	0.50	41.46	0.00	0.22	51.82	6.50	0.00	0.00	0.00	0.00	0.00			100.00	93.42
	Biase&Variance	-0.04	0.26	0.00	0.02	0.62	-0.19	0.00	0.00	0.00	0.00	-0.53	-0.20	0.00	0.81	
	HGP18	0.50	41.46	0.00	0.21	51.80	6.53	0.00	0.00	0.00	0.00	0.00			100.00	93.39
	Biase&Variance	-0.04	0.26	0.00	0.01	0.60	-0.16	0.00	0.00	0.00	0.00	-0.53	-0.20	0.00	0.77	

Table A1.2e MM3 anhydrous melting experimental results and calculation results from TH21, WL22-3, and HGP18 models: opx composition

Run No.	Type	Mode	SiO2	Al2O3	CaO	MgO	FeO	K2O	Na2O	TiO2	Fe2O3	Cr2O3	MnO	NiO	Total
	Exp	0.26	54.00	4.80	2.11	32.30	5.60		0.07	0.10		1.10	0.16		100.24
	TH21	0.27	52.68	6.71	2.25	30.75	5.58	0.00	0.08	0.10	0.64	1.22			100.00
	Biase&Variance	0.01	-1.32	1.91	0.14	-1.55	-0.02	0.00	0.01	0.00	0.64	0.12	-0.16	0.00	8.26
55T	WL22-3	0.28	52.60	6.92	2.14	30.69	5.65	0.00	0.10	0.09	0.65	1.15			100.00
	Biase&Variance	0.01	-1.40	2.12	0.03	-1.61	0.05	0.00	0.03	-0.01	0.65	0.05	-0.16	0.00	9.50
	HGP18	0.29	51.49	8.09	2.30	30.02	5.44	0.00	0.10	0.22	0.67	1.67			100.00
	Biase&Variance	0.03	-2.51	3.29	0.19	-2.28	-0.16	0.00	0.03	0.12	0.67	0.57	-0.16	0.00	23.20
	Exp	0.27	53.40	5.10	1.50	32.70	5.74		0.07	0.11		0.80	0.14		99.56
	TH21	0.27	52.68	6.71	2.25	30.75	5.58	0.00	0.08	0.10	0.64	1.22			100.00
	Biase&Variance	0.00	-0.72	1.61	0.75	-1.95	-0.16	0.00	0.01	-0.01	0.64	0.42	-0.14	0.00	8.11
20	WL22-3	0.28	52.60	6.92	2.14	30.69	5.65	0.00	0.10	0.09	0.65	1.15			100.00
	Biase&Variance	0.00	-0.80	1.82	0.64	-2.01	-0.09	0.00	0.03	-0.02	0.65	0.35	-0.14	0.00	8.98
	HGP18	0.29	51.49	8.09	2.30	30.02	5.44	0.00	0.10	0.22	0.67	1.67			100.00
	Biase&Variance	0.02	-1.91	2.99	0.80	-2.68	-0.30	0.00	0.03	0.11	0.67	0.87	-0.14	0.00	21.73
	Exp	0.24	54.40	4.50	2.06	32.20	5.50		0.05	0.07		1.00	0.14		99.92
	TH21	0.27	52.70	6.58	2.37	30.74	5.52	0.00	0.07	0.10	0.64	1.29			100.00
	Biase&Variance	0.04	-1.70	2.08	0.31	-1.46	0.02	0.00	0.02	0.03	0.64	0.29	-0.14	0.00	9.96
15	WL22-3	0.28	52.60	6.83	2.24	30.66	5.62	0.00	0.09	0.10	0.65	1.21			100.00
	Biase&Variance	0.04	-1.80	2.33	0.18	-1.54	0.12	0.00	0.04	0.03	0.65	0.21	-0.14	0.00	11.59
	HGP18	0.29	51.49	7.96	2.43	29.98	5.40	0.00	0.09	0.22	0.67	1.77			100.00
	Biase&Variance	0.06	-2.91	3.46	0.37	-2.22	-0.10	0.00	0.04	0.15	0.67	0.77	-0.14	0.00	26.61
	Exp	0.24	54.70	4.40	2.36	32.60	5.56		0.05	0.08		1.16	0.12		101.03
	TH21	0.27	52.83	6.17	2.65	30.75	5.35	0.00	0.05	0.09	0.63	1.48			100.00
	Biase&Variance	0.02	-1.87	1.77	0.29	-1.85	-0.21	0.00	0.00	0.01	0.63	0.32	-0.12	0.00	10.68
16	WL22-3	0.28	52.64	6.54	2.49	30.62	5.51	0.00	0.08	0.11	0.65	1.36			100.00
	Biase&Variance	0.04	-2.06	2.14	0.13	-1.98	-0.05	0.00	0.03	0.03	0.65	0.20	-0.12	0.00	13.25
	HGP18	0.29	51.80	7.33	2.69	30.09	5.29	0.00	0.07	0.20	0.66	1.86			100.00
	Biase&Variance	0.05	-2.90	2.93	0.33	-2.51	-0.27	0.00	0.02	0.12	0.66	0.70	-0.12	0.00	24.47

Run No.	Type	Mode	SiO2	Al2O3	CaO	MgO	FeO	K2O	Na2O	TiO2	Fe2O3	Cr2O3	MnO	NiO	Total
	Exp	0.23	54.40	3.30	2.40	32.70	5.10		0.05	0.09		1.22	0.11		99.37
	TH21	0.26	53.34	5.03	3.28	30.87	4.92	0.00	0.04	0.06	0.56	1.90			100.00
	Biase&Variance	0.03	-1.06	1.73	0.88	-1.83	-0.18	0.00	-0.01	-0.03	0.56	0.68	-0.11	0.00	9.06
24	WL22-3	0.29	52.90	5.74	3.00	30.62	5.23	0.00	0.06	0.12	0.63	1.69			100.00
	Biase&Variance	0.06	-1.50	2.44	0.60	-2.08	0.13	0.00	0.00	0.03	0.63	0.47	-0.11	0.00	13.53
	HGP18	0.30	52.49	6.12	3.16	30.35	5.04	0.00	0.06	0.16	0.61	2.01			100.00
	Biase&Variance	0.06	-1.91	2.82	0.76	-2.35	-0.06	0.00	0.01	0.07	0.61	0.79	-0.11	0.00	18.71
	Exp	0.22	55.40	2.80	2.55	33.04	5.20		0.07	0.04		1.30	0.11		100.51
	TH21	0.24	53.68	4.72	2.64	31.60	4.80	0.00	0.04	0.05	0.52	1.94			100.00
	Biase&Variance	0.01	-1.72	1.92	0.09	-1.44	-0.40	0.00	-0.03	0.01	0.52	0.64	-0.11	0.00	9.59
21	WL22-3	0.30	53.22	5.04	3.40	30.67	4.99	0.00	0.05	0.11	0.59	1.94			100.00
	Biase&Variance	0.08	-2.18	2.24	0.85	-2.37	-0.21	0.00	-0.02	0.07	0.59	0.64	-0.11	0.00	16.94
	HGP18	0.30	53.00	5.26	3.50	30.55	4.83	0.00	0.05	0.13	0.56	2.12			100.00
	Biase&Variance	0.08	-2.40	2.46	0.95	-2.49	-0.37	0.00	-0.02	0.09	0.56	0.82	-0.11	0.00	20.10
	Exp	0.21	54.70	3.00	2.30	33.10	5.10		0.06	0.01		1.37	0.11		99.75
	TH21	0.23	53.84	4.58	2.38	31.94	4.74	0.00	0.03	0.04	0.50	1.96			100.00
	Biase&Variance	0.01	-0.86	1.58	0.08	-1.16	-0.36	0.00	-0.03	0.03	0.50	0.59	-0.11	0.00	5.32
22	WL22-3	0.29	53.35	4.92	3.15	30.95	4.96	0.00	0.05	0.10	0.57	1.96			100.00
	Biase&Variance	0.08	-1.35	1.92	0.85	-2.15	-0.14	0.00	-0.01	0.09	0.57	0.59	-0.11	0.00	11.56
	HGP18	0.29	53.13	5.14	3.21	30.86	4.78	0.00	0.05	0.12	0.55	2.17			100.00
	Biase&Variance	0.08	-1.57	2.14	0.91	-2.24	-0.32	0.00	-0.01	0.11	0.55	0.80	-0.11	0.00	13.92
	Exp	0.17	55.20	2.69	1.94	33.99	4.96		0.05	0.01		1.42	0.12		100.38
	TH21	0.20	54.16	4.29	1.92	32.54	4.60	0.00	0.03	0.03	0.45	1.98			100.00
	Biase&Variance	0.03	-1.04	1.60	-0.02	-1.45	-0.36	0.00	-0.02	0.02	0.45	0.56	-0.12	0.00	6.39
26	WL22-3	0.27	53.71	4.58	2.49	31.72	4.84	0.00	0.04	0.07	0.53	2.00			100.00
	Biase&Variance	0.09	-1.49	1.89	0.55	-2.27	-0.12	0.00	-0.01	0.06	0.53	0.58	-0.12	0.00	11.89
	HGP18	0.26	53.47	4.82	2.49	31.67	4.63	0.00	0.04	0.08	0.50	2.29			100.00
	Biase&Variance	0.09	-1.73	2.13	0.55	-2.32	-0.33	0.00	-0.01	0.07	0.50	0.87	-0.12	0.00	14.39
	Exp	0.09	56.10	2.20	2.00	33.79	4.60		0.05	0.03		1.20	0.09		100.06
	TH21	0.17	54.48	4.00	1.55	33.09	4.44	0.00	0.03	0.02	0.41	1.98			100.00
	Biase&Variance	0.08	-1.62	1.80	-0.45	-0.70	-0.16	0.00	-0.02	-0.01	0.41	0.78	-0.09	0.00	7.39
T-4243	WL22-3	0.26	53.83	4.48	2.31	31.95	4.80	0.00	0.04	0.06	0.52	2.00			100.00
	Biase&Variance	0.16	-2.27	2.28	0.31	-1.84	0.20	0.00	-0.01	0.03	0.52	0.80	-0.09	0.00	14.79
	HGP18	0.25	53.56	4.73	2.30	31.89	4.58	0.00	0.04	0.08	0.49	2.33			100.00
	Biase&Variance	0.16	-2.54	2.53	0.30	-1.90	-0.02	0.00	-0.01	0.05	0.49	1.13	-0.09	0.00	18.05

Run No.	Type	Mode	SiO2	Al2O3	CaO	MgO	FeO	K2O	Na2O	TiO2	Fe2O3	Cr2O3	MnO	NiO	Total
	Exp	0.06	56.50	2.00	1.63	33.70	4.80		0.04	0.05		1.20	0.13		100.05
	TH21	0.10	55.12	3.41	0.98	34.12	4.04	0.00	0.02	0.01	0.33	1.96			100.00
	Biase&Variance	0.04	-1.38	1.41	-0.65	0.42	-0.76	0.00	-0.02	-0.04	0.33	0.76	-0.13	0.00	5.79
T-4330	WL22-3	0.22	54.27	4.09	1.71	32.77	4.62	0.00	0.03	0.04	0.47	2.01			100.00
	Biase&Variance	0.16	-2.23	2.09	0.08	-0.93	-0.18	0.00	-0.01	-0.01	0.47	0.81	-0.13	0.00	11.15
	HGP18	0.22	53.89	4.40	1.68	32.66	4.37	0.00	0.03	0.05	0.44	2.48			100.00
	Biase&Variance	0.16	-2.61	2.40	0.05	-1.04	-0.43	0.00	-0.01	0.00	0.44	1.28	-0.13	0.00	15.70
	Exp	0.21	55.30	3.70	2.60	31.80	4.89		0.08	0.07		1.55	0.13		100.12
	TH21	0.08	55.29	3.26	0.87	34.37	3.92	0.00	0.02	0.01	0.31	1.95			100.00
	Biase&Variance	-0.13	-0.01	-0.44	-1.73	2.57	-0.97	0.00	-0.06	-0.06	0.31	0.40	-0.13	0.00	11.04
T-4335	WL22-3	0.31	53.44	5.10	3.02	31.14	4.79	0.00	0.07	0.08	0.56	1.81			100.00
	Biase&Variance	0.10	-1.86	1.40	0.42	-0.66	-0.10	0.00	-0.01	0.01	0.56	0.26	-0.13	0.00	6.45
	HGP18	0.31	53.21	5.33	3.08	31.04	4.62	0.00	0.07	0.10	0.53	2.03			100.00
	Biase&Variance	0.10	-2.09	1.63	0.48	-0.76	-0.27	0.00	-0.01	0.03	0.53	0.48	-0.13	0.00	8.47
	Exp	0.09	56.40	2.40	1.42	33.60	4.61		0.05	0.04		1.50	0.08		100.10
	TH21	0.10	55.25	3.47	0.88	34.39	3.79	0.00	0.03	0.01	0.32	1.85			100.00
	Biase&Variance	0.01	-1.15	1.07	-0.54	0.79	-0.82	0.00	-0.02	-0.03	0.32	0.35	-0.08	0.00	4.28
T-4309	WL22-3	0.25	54.34	4.21	1.67	32.89	4.45	0.00	0.05	0.04	0.46	1.89			100.00
	Biase&Variance	0.16	-2.06	1.81	0.25	-0.71	-0.16	0.00	0.00	0.00	0.46	0.39	-0.08	0.00	8.46
	HGP18	0.25	54.13	4.42	1.64	32.89	4.22	0.00	0.04	0.04	0.43	2.19			100.00
	Biase&Variance	0.16	-2.27	2.02	0.22	-0.71	-0.39	0.00	-0.01	0.00	0.43	0.69	-0.08	0.00	10.62

Table A1.2f MM3 anhydrous melting experimental results and calculation results from TH21, WL22-3, and HGP18 models: cpx composition

Run No.	Type	Mode	SiO2	Al2O3	CaO	MgO	FeO	K2O	Na2O	TiO2	Fe2O3	Cr2O3	MnO	NiO	Total
	Exp	0.11	51.30	5.80	17.30	19.40	3.60		0.47	0.18		1.30	0.09		99.44
	TH21	0.13	52.20	5.44	17.18	19.36	3.61	0.00	0.68	0.40	0.55	0.57			100.00
	Biase&Variance	0.02	0.90	-0.36	-0.12	-0.04	0.01	0.00	0.21	0.22	0.55	-0.73	-0.09	0.00	1.90
55T	WL22-3	0.15	52.37	5.59	16.24	19.57	3.77	0.00	0.88	0.48	0.56	0.54			100.00
	Biase&Variance	0.04	1.07	-0.21	-1.06	0.17	0.17	0.00	0.41	0.30	0.56	-0.76	-0.09	0.00	3.52
	HGP18	0.13	51.48	6.37	17.43	18.35	3.58	0.00	0.79	0.22	0.58	1.20			100.00
	Biase&Variance	0.02	0.18	0.57	0.13	-1.05	-0.02	0.00	0.32	0.04	0.58	-0.10	-0.09	0.00	1.95
	Exp	0.12	51.60	5.60	17.70	19.00	3.24		0.52	0.22		1.25	0.12		99.25
	TH21	0.13	52.20	5.44	17.18	19.36	3.61	0.00	0.68	0.40	0.55	0.57			100.00
	Biase&Variance	0.01	0.60	-0.16	-0.52	0.36	0.37	0.00	0.16	0.18	0.55	-0.68	-0.12	0.00	1.77
20	WL22-3	0.15	52.37	5.59	16.24	19.57	3.77	0.00	0.88	0.48	0.56	0.54			100.00
	Biase&Variance	0.03	0.77	-0.01	-1.46	0.57	0.53	0.00	0.36	0.26	0.56	-0.71	-0.12	0.00	4.35
	HGP18	0.13	51.48	6.37	17.43	18.35	3.58	0.00	0.79	0.22	0.58	1.20			100.00
	Biase&Variance	0.01	-0.12	0.77	-0.27	-0.65	0.34	0.00	0.27	0.00	0.58	-0.05	-0.12	0.00	1.66
	Exp	0.11	51.80	5.00	17.20	19.60	3.60		0.44	0.14		1.46	0.07		99.31
	TH21	0.12	52.13	5.38	17.40	19.42	3.57	0.00	0.58	0.38	0.55	0.60			100.00
	Biase&Variance	0.00	0.33	0.38	0.20	-0.18	-0.03	0.00	0.14	0.24	0.55	-0.86	-0.07	0.00	1.45
15	WL22-3	0.14	52.24	5.58	16.40	19.66	3.75	0.00	0.78	0.48	0.55	0.56			100.00
	Biase&Variance	0.03	0.44	0.58	-0.80	0.06	0.15	0.00	0.34	0.34	0.55	-0.90	-0.07	0.00	2.54
	HGP18	0.12	51.38	6.34	17.59	18.42	3.55	0.00	0.69	0.20	0.57	1.26			100.00
	Biase&Variance	0.01	-0.42	1.34	0.39	-1.18	-0.05	0.00	0.25	0.06	0.57	-0.20	-0.07	0.00	3.95
	Exp	0.07	52.10	5.30	16.60	20.60	3.70		0.36	0.13		1.50	0.11		100.40
	TH21	0.08	52.14	5.09	17.82	19.58	3.44	0.00	0.42	0.31	0.52	0.69			100.00
	Biase&Variance	0.01	0.04	-0.21	1.22	-1.02	-0.26	0.00	0.06	0.18	0.52	-0.81	-0.11	0.00	3.62
16	WL22-3	0.11	52.10	5.45	16.70	19.85	3.68	0.00	0.59	0.47	0.53	0.63			100.00
	Biase&Variance	0.04	0.00	0.15	0.10	-0.75	-0.02	0.00	0.23	0.34	0.53	-0.87	-0.11	0.00	1.81
	HGP18	0.09	51.52	5.89	17.74	18.79	3.49	0.00	0.54	0.17	0.54	1.31			100.00
	Biase&Variance	0.02	-0.58	0.59	1.14	-1.81	-0.21	0.00	0.18	0.04	0.54	-0.19	-0.11	0.00	5.67

Section 2 Hydrous Melting Experiments

The anhydrous experimental running conditions and results for KLB-1 are from Hirose (1997) and Hirose and Kawamoto (1995).

Table A2.1a KLB-1 hydrous melting experimental results and calculation results from WL22-3 model: melt composition

No.	Methods	H2O	SiO2	Al2O3	CaO	MgO	FeO	K2O	Na2O	TiO2	Fe3O3	Cr2O3	MnO	Total
	Exp	0.60	49.20	15.55	12.69	12.56	7.46	0.06	1.62	0.57		0.11	0.18	99.82
40	THERMOCALC	0.71	46.54	15.42	13.39	12.66	8.37	0.14	2.01	0.54	0.84	0.09		100.00
	Biase&Variance	0.11	-2.66	-0.13	0.70	0.10	0.91	0.08	0.39	-0.03	0.84	-0.02	-0.18	9.33
	Exp	0.30	50.78	12.08	10.45	15.79	9.00	0.04	1.01	0.38		0.30	0.16	99.83
43	THERMOCALC	0.54	47.11	13.82	13.09	13.82	8.94	0.11	1.58	0.51	0.88	0.14		100.00
	Biase&Variance	0.24	-3.67	1.74	2.64	-1.97	-0.06	0.07	0.57	0.13	0.88	-0.16	-0.16	28.58
	Exp	1.60	49.50	18.70	11.74	10.46	6.56	0.04	2.18	0.67		0.04	0.12	99.89
38	THERMOCALC	2.60	46.97	17.80	11.01	11.99	7.26	0.25	3.35	0.64	0.68	0.04		100.00
	Biase&Variance	1.00	-2.53	-0.90	-0.73	1.53	0.70	0.21	1.17	-0.03	0.68	0.00	-0.12	13.46
	Exp	0.90	50.81	13.60	11.55	13.91	7.91	0.03	1.38	0.53		0.15	0.14	99.87
41	THERMOCALC	1.16	46.78	14.44	13.43	13.46	8.56	0.12	1.72	0.53	0.85	0.11		100.00
	Biase&Variance	0.26	-4.03	0.84	1.88	-0.45	0.65	0.09	0.34	0.00	0.85	-0.04	-0.14	22.03
	Exp	0.50	52.58	10.73	9.03	16.97	8.93	0.04	0.79	0.41		0.35	0.17	99.83
44	THERMOCALC	0.98	47.41	13.27	12.54	14.60	9.08	0.10	1.46	0.49	0.89	0.16		100.00
	Biase&Variance	0.48	-5.17	2.54	3.51	-2.37	0.15	0.06	0.67	0.08	0.89	-0.19	-0.17	52.65
	Exp	7.10	52.89	21.73	9.06	6.58	5.11	0.07	3.49	0.85		0.03	0.19	99.81
36	THERMOCALC	6.91	46.91	18.50	9.24	13.08	6.74	0.28	3.82	0.91	0.51	0.03		100.00
	Biase&Variance	-0.19	-5.98	-3.23	0.18	6.50	1.63	0.21	0.33	0.06	0.51	0.00	-0.19	91.67
	Exp	2.50	51.41	15.32	12.03	12.22	6.64	0.07	1.49	0.54		0.13	0.15	99.85
39	THERMOCALC	3.69	46.23	16.09	11.91	13.96	8.03	0.15	2.16	0.63	0.76	0.07		100.00
	Biase&Variance	1.19	-5.18	0.77	-0.12	1.74	1.39	0.08	0.67	0.09	0.76	-0.06	-0.15	34.85
	Exp	6.90	51.84	18.36	10.98	9.13	6.68	0.04	2.01	0.74		0.04	0.17	99.82
37	THERMOCALC	7.99	45.92	17.38	9.99	14.92	7.49	0.19	2.68	0.80	0.58	0.04		100.00
	Biase&Variance	1.09	-5.92	-0.98	-0.99	5.79	0.81	0.15	0.67	0.06	0.58	0.00	-0.17	73.27
	Exp	6.30	54.35	21.70	9.99	6.00	4.30	0.46	1.87	0.70	0.40		0.23	99.77
50	THERMOCALC	10.53	45.92	18.27	9.00	14.89	7.01	0.23	3.22	0.96	0.48	0.03		100.00
	Biase&Variance	4.23	-8.43	-3.43	-0.99	8.89	2.71	-0.23	1.35	0.26	0.08	0.03	-0.23	189.95

	Exp	Saturated	56.13	19.60	9.89	6.81	4.65	0.31	1.10	0.55	0.79	0.07	0.10	99.90
51	THERMOCALC	13.67	46.08	14.22	10.01	18.52	8.19	0.10	1.55	0.56	0.69	0.07		100.00
	Biase&Variance		-10.05	-5.38	0.12	11.71	3.54	-0.21	0.45	0.01	-0.10	0.00	-0.10	279.81
	Exp	Saturated	60.26	17.24	8.53	5.77	4.04	0.30	3.09	0.59		0.10	0.08	99.92
49	THERMOCALC	18.06	46.03	13.83	9.48	19.83	8.11	0.08	1.43	0.52	0.62	0.07		100.00
	Biase&Variance		-14.23	-3.41	0.95	14.06	4.07	-0.22	-1.66	-0.07	0.62	-0.03	-0.08	432.50

Table A2.1b KLB-1 hydrous melting experimental results and calculation results from WL22-3 model: spinel composition

No.	Methods	SiO2	Al2O3	CaO	MgO	FeO	K2O	Na2O	TiO2	Fe3O3	Cr2O3	MnO	Total	Cr#
	Exp		47.83		19.82	15.42					15.17		98.24	17.54
38	THERMOCALC	0.00	50.22	0.00	21.12	8.69	0.00	0.00	0.02	1.70	18.25		100.00	19.59
	Biase&Variance	0.00	2.39	0.00	1.30	-6.73	0.00	0.00	0.02	1.70	3.08	0.00	65.06	
	Exp		54.57		19.69	14.49					10.53		99.28	11.46
36	THERMOCALC	0.00	52.06	0.00	21.31	8.74	0.00	0.00	0.01	1.78	16.10		100.00	17.18
	Biase&Variance	0.00	-2.51	0.00	1.62	-5.75	0.00	0.00	0.01	1.78	5.57	0.00	76.12	
	Exp		34.98		16.84	18.89					27.42		98.13	34.46
37	THERMOCALC	0.00	46.49	0.00	20.42	9.46	0.00	0.00	0.01	2.18	21.45		100.00	23.63
	Biase&Variance	0.00	11.51	0.00	3.58	-9.43	0.00	0.00	0.01	2.18	-5.97	0.00	274.73	
	Exp		36.84		15.88	12.34			0.32	5.88	25.19	0.22	96.45	31.45
50	THERMOCALC	0.00	49.80	0.00	20.89	9.18	0.00	0.00	0.01	2.04	18.09		100.00	19.59
	Biase&Variance	0.00	12.96	0.00	5.01	-3.16	0.00	0.00	-0.31	-3.84	-7.10	-0.22	268.40	
	Exp		13.90		12.06	15.35			0.27	16.92	37.03	0.30	95.53	64.12
51	THERMOCALC	0.00	31.69	0.00	17.87	12.19	0.00	0.00	0.00	4.16	34.09		100.00	41.91
	Biase&Variance	0.00	17.79	0.00	5.81	-3.16	0.00	0.00	-0.27	-12.76	-2.94	-0.30	531.99	
	Exp		13.00		12.22	15.42			0.97	15.26	38.72	0.39	95.59	66.65
49	THERMOCALC	0.00	29.73	0.00	17.37	12.85	0.00	0.00	0.00	4.49	35.55		100.00	44.52
	Biase&Variance	0.00	16.73	0.00	5.15	-2.57	0.00	0.00	-0.97	-10.77	-3.17	-0.39	439.99	

Table A2.1c KLB-1 hydrous melting experimental results and calculation results from WL22-3 model: olivine composition

No.	Methods	SiO2	Al2O3	CaO	MgO	FeO	K2O	Na2O	TiO2	Fe3O3	Cr2O3	MnO	Total	Mg#
	Exp	41.39		0.26	48.75	7.86						0.16	98.26	91.71
40	THERMOCALC	41.02	0.00	0.29	49.90	8.79	0.00	0.00	0.00	0.00	0.00		100.00	91.01
	Biase&Variance	-0.37	0.00	0.03	1.15	0.93	0.00	0.00	0.00	0.00	0.00	-0.16	2.33	
	Exp	41.77		0.22	49.47	7.78						0.15	99.24	91.89
43	THERMOCALC	41.09	0.00	0.28	50.18	8.44	0.00	0.00	0.00	0.00	0.00		100.00	91.38
	Biase&Variance	-0.68	0.00	0.06	0.71	0.66	0.00	0.00	0.00	0.00	0.00	-0.15	1.44	
	Exp	41.91		0.13	49.01	9.19						0.21	100.24	90.48
38	THERMOCALC	40.95	0.00	0.20	49.59	9.26	0.00	0.00	0.00	0.00	0.00		100.00	90.52
	Biase&Variance	-0.96	0.00	0.07	0.58	0.07	0.00	0.00	0.00	0.00	0.00	-0.21	1.33	
	Exp	41.19		0.21	48.30	7.77						0.32	97.47	91.72
41	THERMOCALC	41.06	0.00	0.28	50.06	8.60	0.00	0.00	0.00	0.00	0.00		100.00	91.21
	Biase&Variance	-0.13	0.00	0.07	1.76	0.83	0.00	0.00	0.00	0.00	0.00	-0.32	3.90	
	Exp	41.98		0.22	49.96	6.85						0.13	99.01	92.86
44	THERMOCALC	41.12	0.00	0.26	50.31	8.32	0.00	0.00	0.00	0.00	0.00		100.00	91.51
	Biase&Variance	-0.86	0.00	0.04	0.35	1.47	0.00	0.00	0.00	0.00	0.00	-0.13	3.05	
	Exp	41.65		0.22	46.54	9.67						0.19	98.08	89.56
36	THERMOCALC	40.94	0.00	0.13	49.58	9.35	0.00	0.00	0.00	0.00	0.00		100.00	90.43
	Biase&Variance	-0.71	0.00	-0.09	3.04	-0.32	0.00	0.00	0.00	0.00	0.00	-0.19	9.91	
	Exp	42.00		0.24	49.82	7.59						0.13	99.65	92.13
39	THERMOCALC	41.01	0.00	0.20	49.86	8.93	0.00	0.00	0.00	0.00	0.00		100.00	90.86
	Biase&Variance	-0.99	0.00	-0.04	0.04	1.34	0.00	0.00	0.00	0.00	0.00	-0.13	2.82	
	Exp	41.14		0.23	47.25	9.20						0.16	97.82	90.15
37	THERMOCALC	40.97	0.00	0.13	49.74	9.16	0.00	0.00	0.00	0.00	0.00		100.00	90.64
	Biase&Variance	-0.17	0.00	-0.10	2.49	-0.04	0.00	0.00	0.00	0.00	0.00	-0.16	6.25	

Table A2.1d KLB-1 hydrous melting experimental results and calculation results from WL22-3 model: opx composition

No.	Methods	SiO2	Al2O3	CaO	MgO	FeO	K2O	Na2O	TiO2	Fe3O3	Cr2O3	MnO	Total
	Exp	55.22	4.29	1.90	31.40	5.78					0.59	0.11	99.18
40	THERMOCALC	53.18	5.35	2.78	30.71	5.83	0.00	0.04	0.11	0.73	1.27		100.00
	Biase&Variance	-2.04	1.06	0.88	-0.69	0.05	0.00	0.04	0.11	0.73	0.68	-0.11	7.57
	Exp	56.06	3.06	2.11	31.60	5.46					0.87	0.18	99.16
43	THERMOCALC	53.81	4.55	2.28	31.60	5.60	0.00	0.03	0.08	0.65	1.40		100.00
	Biase&Variance	-2.25	1.49	0.17	0.00	0.14	0.00	0.03	0.08	0.65	0.53	-0.18	8.08
	Exp	55.47	4.36	1.87	31.56	5.47					0.60	0.22	99.33
38	THERMOCALC	52.48	6.73	1.99	30.59	6.28	0.00	0.04	0.12	0.78	0.98		100.00
	Biase&Variance	-2.99	2.37	0.12	-0.97	0.81	0.00	0.04	0.12	0.78	0.38	-0.22	17.01
	Exp	56.06	2.78	2.13	32.07	5.31					0.84	0.17	99.19
41	THERMOCALC	53.62	4.69	2.74	31.09	5.71	0.00	0.04	0.09	0.69	1.33		100.00
	Biase&Variance	-2.44	1.91	0.61	-0.98	0.40	0.00	0.04	0.09	0.69	0.49	-0.17	11.86
	Exp	57.22	2.55	1.14	33.45	4.48					0.98	0.20	99.82
44	THERMOCALC	54.01	4.30	1.98	31.98	5.53	0.00	0.03	0.06	0.63	1.49		100.00
	Biase&Variance	-3.21	1.75	0.84	-1.47	1.05	0.00	0.03	0.06	0.63	0.51	-0.20	18.05
	Exp	55.12	5.27	0.86	31.06	6.58					0.30	0.09	99.19
36	THERMOCALC	52.86	6.35	1.57	31.06	6.48	0.00	0.03	0.10	0.77	0.80		100.00
	Biase&Variance	-2.26	1.08	0.71	0.00	-0.10	0.00	0.03	0.10	0.77	0.50	-0.09	7.67
	Exp	56.71	2.58	2.27	32.17	5.45					0.77	0.16	99.95
39	THERMOCALC	53.08	5.49	2.28	30.92	6.07	0.00	0.03	0.08	0.76	1.29		100.00
	Biase&Variance	-3.63	2.91	0.01	-1.25	0.62	0.00	0.03	0.08	0.76	0.52	-0.16	24.44
	Exp	55.39	3.99	1.45	31.36	6.23					0.61	0.13	99.03
37	THERMOCALC	53.13	5.70	1.70	31.22	6.37	0.00	0.02	0.06	0.79	1.01		100.00
	Biase&Variance	-2.26	1.71	0.25	-0.14	0.14	0.00	0.02	0.06	0.79	0.40	-0.13	8.95
	Exp	55.38	5.92	0.99	31.53	6.52			0.22		0.34		100.90
50	THERMOCALC	53.20	5.78	1.44	31.38	6.52	0.00	0.02	0.06	0.78	0.83		100.00
	Biase&Variance	-2.18	-0.14	0.45	-0.15	0.00	0.00	0.02	-0.16	0.78	0.49	0.00	5.84
	Exp	56.45	2.81	0.99	32.64	5.82			0.09		0.41	0.18	99.21
51	THERMOCALC	54.20	3.75	1.76	32.01	6.14	0.00	0.01	0.02	0.74	1.38		100.00
	Biase&Variance	-2.25	0.94	0.77	-0.63	0.32	0.00	0.01	-0.07	0.74	0.97	-0.18	8.55

Table A2.1e KLB-1 hydrous melting experimental results and calculation results from WL22-3 model: cpx composition

No.	Methods	SiO2	Al2O3	CaO	MgO	FeO	K2O	Na2O	TiO2	Fe3O3	Cr2O3	MnO	Total
	Exp	51.45	5.75	16.23	18.99	4.57		0.40	0.20		1.09	0.14	98.68
40	THERMOCALC	52.36	4.44	17.61	19.93	3.79	0.01	0.33	0.38	0.57	0.56		100.00
	Biase&Variance	0.91	-1.31	1.38	0.94	-0.78	0.01	-0.07	0.18	0.57	-0.53	-0.14	6.61
	Exp	51.90	6.48	18.91	17.55	4.06		0.39	0.18		0.90	0.10	100.37
38	THERMOCALC	51.62	5.43	18.82	18.37	3.77	0.02	0.44	0.39	0.72	0.42		100.00
	Biase&Variance	-0.28	-1.05	-0.09	0.82	-0.29	0.02	0.05	0.21	0.72	-0.48	-0.10	2.75
	Exp	51.46	6.29	20.45	15.97	3.79		0.42	0.39		0.52	0.16	99.29
36	THERMOCALC	51.87	4.74	20.49	17.66	3.49	0.01	0.37	0.27	0.79	0.30		100.00
	Biase&Variance	0.41	-1.55	0.04	1.69	-0.30	0.01	-0.05	-0.12	0.79	-0.22	-0.16	6.22
	Exp	52.39	4.75	20.29	17.13	3.99		0.26	0.21		0.98	0.10	100.00
37	THERMOCALC	52.07	4.18	21.01	17.79	3.37	0.01	0.24	0.17	0.79	0.38		100.00
	Biase&Variance	-0.32	-0.57	0.72	0.66	-0.62	0.01	-0.02	-0.04	0.79	-0.60	-0.10	2.76
	Exp	52.87	4.47	21.31	16.93	3.50		0.19	0.28		0.85	0.11	100.40
50	THERMOCALC	52.11	4.11	21.43	17.51	3.31	0.01	0.25	0.16	0.82	0.29		100.00
	Biase&Variance	-0.76	-0.36	0.12	0.58	-0.19	0.01	0.06	-0.12	0.82	-0.56	-0.11	2.12
	Exp	53.08	4.46	21.95	16.89	4.55		0.22	0.31		0.21	0.16	101.67
51	THERMOCALC	53.03	2.42	22.02	18.11	3.03	0.01	0.13	0.03	0.76	0.46		100.00
	Biase&Variance	-0.05	-2.04	0.07	1.22	-1.52	0.01	-0.09	-0.28	0.76	0.25	-0.16	8.74
	Exp	53.66	2.11	21.37	16.83	3.56		0.26	0.26		0.60	0.13	98.65
49	THERMOCALC	53.32	2.01	22.50	18.07	2.86	0.00	0.11	0.02	0.70	0.41		100.00
	Biase&Variance	-0.34	-0.10	1.13	1.24	-0.70	0.00	-0.15	-0.24	0.70	-0.19	-0.13	4.06

Experiments from Mitchell and Grove (2015) were modelled using THERMOCALC and PMELTS.

Table A2.2a Mitchell and Grove (2015) melting experimental results and calculation results from THERMOCALC and PMELTS: melt composition

No.	Methods	Mode	SiO2	Al2O3	CaO	MgO	FeO	K2O	Na2O	TiO2	Fe2O3	Cr2O3	MnO	NiO	H2O	Total
	Exp	0.207	53.00	17.00	10.28	7.84	5.10	0.32	2.00	0.73		0.13	0.14	0.02	3.80	100.36
	THERMOCALC	0.560	46.43	7.71	5.93	19.31	7.08	0.24	1.01	0.34	0.51	0.31			11.13	100.00
C507	Biase&Variance	0.354	-6.57	-9.29	-4.35	11.47	1.98	-0.08	-0.99	-0.39	0.51	0.18	-0.14	-0.02	7.33	339.05
	PMELTS	0.444	46.69	8.87	6.58	15.59	6.10	0.28	1.15	0.38	0.64	0.85	0.11	0.14	12.63	100.00
	Biase&Variance	0.238	-6.31	-8.13	-3.70	7.75	1.00	-0.04	-0.85	-0.35	0.64	0.72	-0.03	0.12	8.83	260.42
	Exp	0.244	52.10	14.90	11.00	11.10	5.90	0.32	1.80	0.65		0.21	0.14	0.02	2.60	100.74
	THERMOCALC	0.571	46.24	7.54	5.79	19.93	7.23	0.24	0.99	0.33	0.51	0.35			10.86	100.00
C508	Biase&Variance	0.327	-5.86	-7.36	-5.21	8.83	1.33	-0.08	-0.81	-0.32	0.51	0.14	-0.14	-0.02	8.26	264.68
	PMELTS	0.466	46.39	8.47	6.28	17.03	6.39	0.26	1.09	0.37	0.61	0.81	0.11	0.14	12.05	100.00
	Biase&Variance	0.222	-5.71	-6.43	-4.72	5.93	0.49	-0.06	-0.71	-0.28	0.61	0.60	-0.03	0.12	9.45	222.27
	Exp	0.205	51.20	17.00	10.50	9.00	5.50	0.32	2.10	0.80		0.08	0.07		4.00	100.57
	THERMOCALC	0.498	47.55	8.60	6.63	18.31	7.21	0.32	1.25	0.38	0.56	0.29			8.90	100.00
C494	Biase&Variance	0.293	-3.65	-8.40	-3.87	9.31	1.71	0.00	-0.85	-0.42	0.56	0.21	-0.07	0.00	4.90	213.73
	PMELTS	0.414	48.97	9.74	7.13	14.60	5.87	0.35	1.37	0.42	0.70	0.93	0.09	0.10	9.74	100.00
	Biase&Variance	0.210	-2.23	-7.26	-3.37	5.60	0.37	0.03	-0.73	-0.38	0.70	0.85	0.02	0.10	5.74	135.38
	Exp	0.269	52.20	14.50	10.30	11.70	5.20	0.25	1.90	0.70		0.23	0.10		3.40	100.48
	THERMOCALC	0.498	47.55	8.60	6.63	18.31	7.21	0.32	1.25	0.38	0.56	0.29			8.90	100.00
C490	Biase&Variance	0.229	-4.65	-5.90	-3.67	6.61	2.01	0.07	-0.65	-0.32	0.56	0.06	-0.10	0.00	5.50	148.74
	PMELTS	0.414	48.97	9.74	7.13	14.60	5.87	0.35	1.37	0.42	0.70	0.93	0.09	0.10	9.74	100.00
	Biase&Variance	0.145	-3.23	-4.76	-3.17	2.90	0.67	0.10	-0.53	-0.28	0.70	0.70	-0.01	0.10	6.34	93.55
	Exp	0.280	52.80	14.20	10.40	12.00	5.80	0.30	1.70	0.70		0.29	0.12		2.20	100.51
	THERMOCALC	0.328	47.49	11.61	9.11	15.28	7.34	0.57	2.05	0.56	0.66	0.21			5.10	100.00
C498	Biase&Variance	0.049	-5.31	-2.59	-1.29	3.28	1.54	0.27	0.35	-0.14	0.66	-0.08	-0.12	0.00	2.90	58.78
	PMELTS	0.338	55.28	12.04	8.79	10.78	4.45	0.52	1.89	0.51	0.72	0.30	0.03	0.03	4.65	100.00
	Biase&Variance	0.059	2.48	-2.16	-1.61	-1.22	-1.35	0.22	0.19	-0.19	0.72	0.01	-0.09	0.03	2.45	23.37
	Exp	0.244	51.90	14.00	10.00	9.60	5.80	0.29	1.50	0.50		0.10	0.11	0.01	6.40	100.21
	THERMOCALC	0.478	42.26	8.70	6.97	18.64	7.10	0.30	1.23	0.41	0.53	0.19			13.65	100.00
C561	Biase&Variance	0.234	-9.64	-5.30	-3.03	9.04	1.30	0.01	-0.27	-0.09	0.53	0.09	-0.11	-0.01	7.25	266.56
	PMELTS	0.378	47.89	10.42	7.76	10.38	4.66	0.33	1.35	0.45	0.74	0.97	0.10	0.11	14.84	100.00
	Biase&Variance	0.134	-4.01	-3.58	-2.24	0.78	-1.14	0.04	-0.15	-0.05	0.74	0.87	-0.01	0.10	8.44	108.40

	Exp	0.293	53.10	13.10	10.00	9.60	5.70	0.29	1.50	0.52		0.10	0.10	0.01	5.40	99.42
	THERMOCALC	0.506	43.37	8.28	6.58	19.30	7.23	0.28	1.15	0.38	0.53	0.24			12.67	100.00
C555	Biase&Variance	0.213	-9.73	-4.82	-3.42	9.70	1.53	-0.01	-0.35	-0.14	0.53	0.14	-0.10	-0.01	7.27	279.34
	PMELTS	0.400	47.42	9.85	7.32	12.25	5.25	0.31	1.27	0.42	0.71	0.94	0.11	0.12	14.02	100.00
	Biase&Variance	0.107	-5.68	-3.25	-2.68	2.65	-0.45	0.02	-0.23	-0.10	0.71	0.84	0.01	0.11	8.62	132.82
	Exp	0.354	53.40	11.20	8.30	13.80	6.40	0.25	1.17	0.48		0.20	0.11	0.00	4.70	100.01
	THERMOCALC	0.519	43.84	8.10	6.41	19.59	7.27	0.27	1.11	0.37	0.52	0.26			12.25	100.00
C554	Biase&Variance	0.165	-9.56	-3.10	-1.89	5.79	0.87	0.02	-0.06	-0.11	0.52	0.06	-0.11	0.00	7.55	196.16
	PMELTS	0.411	47.22	9.59	7.13	13.13	5.49	0.30	1.24	0.41	0.69	0.92	0.11	0.13	13.65	100.00
	Biase&Variance	0.057	-6.18	-1.61	-1.17	-0.67	-0.91	0.05	0.07	-0.07	0.69	0.72	0.00	0.13	8.95	124.56
	Exp	0.377	53.90	10.10	7.50	14.50	6.40	0.20	1.10	0.41		0.21	0.11	0.00	6.00	100.43
	THERMOCALC	0.547	44.80	7.74	6.05	20.19	7.32	0.25	1.04	0.35	0.51	0.30			11.45	100.00
C553	Biase&Variance	0.170	-9.10	-2.36	-1.45	5.69	0.92	0.05	-0.06	-0.06	0.51	0.09	-0.11	0.00	5.45	153.70
	PMELTS	0.437	46.80	9.03	6.71	15.05	5.96	0.28	1.17	0.39	0.65	0.86	0.11	0.14	12.85	100.00
	Biase&Variance	0.059	-7.10	-1.07	-0.79	0.55	-0.44	0.08	0.07	-0.02	0.65	0.65	0.00	0.14	6.85	100.47
	Exp	0.423	52.00	9.30	7.00	17.30	7.70	0.20	0.93	0.36		0.24	0.12	0.01	3.70	98.86
	THERMOCALC	0.584	45.93	7.32	5.63	20.90	7.32	0.23	0.96	0.32	0.49	0.36			10.55	100.00
C559	Biase&Variance	0.162	-6.07	-1.98	-1.37	3.60	-0.38	0.03	0.03	-0.04	0.49	0.12	-0.12	-0.01	6.85	102.94
	PMELTS	0.474	46.30	8.32	6.19	17.54	6.45	0.26	1.07	0.36	0.60	0.80	0.11	0.15	11.85	100.00
	Biase&Variance	0.051	-5.70	-0.98	-0.81	0.24	-1.25	0.06	0.14	0.00	0.60	0.56	-0.01	0.14	8.15	102.87
	Exp	0.303	52.40	12.90	10.00	13.00	6.70	0.11	1.60	0.60		0.40	0.09	0.04	1.90	99.74
	THERMOCALC	0.466	46.86	8.89	6.93	19.36	7.79	0.36	1.36	0.40	0.58	0.34			7.14	100.00
C470	Biase&Variance	0.164	-5.54	-4.01	-3.07	6.36	1.09	0.25	-0.24	-0.20	0.58	-0.06	-0.09	-0.04	5.24	125.80
	PMELTS	0.429	49.89	9.47	6.92	16.57	6.27	0.36	1.38	0.40	0.66	0.73	0.08	0.08	7.20	100.00
	Biase&Variance	0.127	-2.51	-3.43	-3.08	3.57	-0.43	0.25	-0.22	-0.20	0.66	0.33	-0.01	0.04	5.30	69.27
	Exp	0.184	50.70	16.10	10.30	12.00	6.00	0.40	3.10	0.80		0.13	0.13	0.02		99.68
	THERMOCALC	0.168	48.81	15.77	11.58	10.99	6.95	1.13	3.59	0.38	0.70	0.10			0.00	100.00
C481	Biase&Variance	-0.016	-1.89	-0.33	1.28	-1.01	0.95	0.73	0.49	-0.42	0.70	-0.03	-0.13	-0.02	0.00	8.70
	PMELTS	0.109	52.93	17.12	6.92	9.83	4.46	1.84	5.49	0.81	0.50	0.08	0.01	0.01	0.00	100.00
	Biase&Variance	-0.075	2.23	1.02	-3.38	-2.17	-1.54	1.44	2.39	0.01	0.50	-0.05	-0.12	-0.01	0.00	32.57
	Exp	0.271	51.80	12.40	10.40	15.00	7.40	0.13	2.10	0.50		0.30	0.14	0.03	0.30	100.50
	THERMOCALC	0.193	48.79	14.88	11.57	11.85	7.34	0.99	3.24	0.51	0.70	0.13			0.00	100.00
C471	Biase&Variance	-0.077	-3.01	2.48	1.17	-3.15	-0.06	0.86	1.14	0.01	0.70	-0.17	-0.14	-0.03	-0.30	29.17
	PMELTS	0.166	51.42	15.66	8.83	11.97	5.44	1.20	3.89	0.76	0.69	0.10	0.01	0.01	0.00	100.00
	Biase&Variance	-0.105	-0.38	3.26	-1.57	-3.03	-1.96	1.07	1.79	0.26	0.69	-0.20	-0.13	-0.02	-0.30	31.30

	Exp	0.287	48.90	12.30	10.00	14.00	7.30	0.31	1.80	0.60		0.34	0.14	0.04	3.10	98.83
	THERMOCALC	0.474	44.71	8.53	6.75	21.66	8.36	0.35	1.32	0.39	0.56	0.37			7.00	100.00
C473	Biase&Variance	0.187	-4.19	-3.77	-3.25	7.66	1.06	0.04	-0.48	-0.21	0.56	0.03	-0.14	-0.04	3.90	117.95
	PMELTS	0.465	49.17	8.74	6.43	18.90	6.69	0.33	1.27	0.37	0.61	0.67	0.08	0.09	6.65	100.00
	Biase&Variance	0.178	0.27	-3.56	-3.57	4.90	-0.61	0.02	-0.53	-0.23	0.61	0.33	-0.06	0.05	3.55	63.30
	Exp	0.318	48.90	11.40	9.80	16.00	7.60	0.40	2.00	0.47		0.39	0.08	0.07	2.80	99.91
	THERMOCALC	0.378	45.76	10.12	8.09	19.48	8.57	0.49	1.74	0.48	0.61	0.30			4.35	100.00
C463	Biase&Variance	0.060	-3.14	-1.28	-1.71	3.48	0.97	0.09	-0.26	0.01	0.61	-0.09	-0.08	-0.07	1.55	30.34
	PMELTS	0.429	51.58	9.52	7.00	18.24	6.54	0.41	1.49	0.41	0.63	0.40	0.05	0.05	3.67	100.00
	Biase&Variance	0.111	2.68	-1.88	-2.80	2.24	-1.06	0.01	-0.51	-0.06	0.63	0.01	-0.03	-0.02	0.87	26.12
	Exp	0.259	50.00	12.80	10.10	15.00	7.80	0.43	2.00	0.60		0.30	0.14	0.06	0.10	99.33
	THERMOCALC	0.199	47.74	14.19	11.43	13.26	7.94	0.97	3.10	0.56	0.68	0.14			0.00	100.00
C474	Biase&Variance	-0.060	-2.26	1.39	1.33	-1.74	0.14	0.54	1.10	-0.04	0.68	-0.16	-0.14	-0.06	-0.10	13.88
	PMELTS	0.158	48.19	14.46	8.71	14.77	6.99	1.26	3.99	0.77	0.70	0.11	0.02	0.02	0.00	100.00
	Biase&Variance	-0.101	-1.81	1.66	-1.39	-0.23	-0.81	0.83	1.99	0.17	0.70	-0.19	-0.12	-0.04	-0.10	13.90
	Exp	0.306	49.00	10.70	9.20	17.90	8.30	0.46	2.10	0.60		0.40	0.11	0.05	0.90	99.72
	THERMOCALC	0.206	46.94	13.50	11.21	14.64	8.45	0.93	2.93	0.59	0.66	0.15			0.00	100.00
C465	Biase&Variance	-0.100	-2.06	2.80	2.01	-3.26	0.15	0.47	0.83	-0.01	0.66	-0.25	-0.11	-0.05	-0.90	29.01
	PMELTS	0.167	45.35	12.92	8.65	17.88	8.61	1.20	3.76	0.73	0.71	0.12	0.04	0.03	0.00	100.00
	Biase&Variance	-0.138	-3.65	2.22	-0.55	-0.02	0.31	0.74	1.66	0.13	0.71	-0.28	-0.07	-0.02	-0.90	23.37

Table A2.2b Mitchell and Grove (2015) melting experimental results and calculation results from THERMOCALC: residue composition

No.	Methods	Mode	SiO2	Al2O3	CaO	MgO	FeO	K2O	Na2O	TiO2	Fe2O3	Cr2O3	MnO	NiO	Total
	Exp	0.793	44.32	0.74	1.31	44.91	8.19	0.00	0.02	0.03		0.35	0.12	0.20	100.18
C507	THERMOCALC	0.440	41.13	0.12	0.06	51.68	6.52	0.00	0.00	0.00	0.05	0.45			100.00
	Biase&Variance	-0.354	-3.19	-0.62	-1.26	6.77	-1.66	0.00	-0.02	-0.03	0.05	0.10	-0.12	-0.20	60.80
	Exp	0.756	43.96	0.51	0.69	45.61	8.05	0.00	0.01	0.03		0.35	0.10	0.26	99.57
C508	THERMOCALC	0.429	41.19	0.10	0.05	51.84	6.35	0.00	0.00	0.00	0.04	0.41			100.00
	Biase&Variance	-0.327	-2.77	-0.41	-0.63	6.23	-1.70	0.00	-0.01	-0.03	0.04	0.06	-0.10	-0.26	50.01
	Exp	0.795	44.50	0.71	1.21	44.32	8.02	0.00	0.02	0.05		0.34	0.12	0.09	99.38
C494	THERMOCALC	0.502	42.44	0.31	0.12	49.97	6.60	0.00	0.00	0.00	0.07	0.49			100.00
	Biase&Variance	-0.293	-2.06	-0.40	-1.09	5.65	-1.42	0.00	-0.02	-0.05	0.07	0.15	-0.12	-0.09	39.58
	Exp	0.731	43.43	0.56	0.54	46.61	7.00	0.00	0.01	0.02		0.56	0.11	0.05	98.87
C490	THERMOCALC	0.502	42.44	0.31	0.12	49.97	6.60	0.00	0.00	0.00	0.07	0.49			100.00
	Biase&Variance	-0.229	-0.99	-0.25	-0.42	3.36	-0.39	0.00	-0.01	-0.02	0.07	-0.06	-0.11	-0.05	12.66
	Exp	0.720	43.33	0.40	0.45	46.74	7.41	0.00	0.01	0.01		0.50	0.05	0.07	98.97
C498	THERMOCALC	0.672	46.00	1.11	0.57	44.76	6.76	0.00	0.01	0.01	0.17	0.61			100.00
	Biase&Variance	-0.049	2.67	0.71	0.11	-1.98	-0.65	0.00	0.00	-0.01	0.17	0.11	-0.05	-0.07	12.04
	Exp	0.756	44.07	0.31	0.37	45.66	8.45	0.00	0.01	0.02		0.17	0.09	0.23	99.37
C561	THERMOCALC	0.522	45.97	0.79	0.32	45.76	6.43	0.00	0.00	0.00	0.13	0.60			100.00
	Biase&Variance	-0.234	1.90	0.47	-0.05	0.10	-2.02	0.00	0.00	-0.02	0.13	0.43	-0.09	-0.23	8.19
	Exp	0.707	42.21	0.09	0.20	48.54	8.14	0.00	0.00	0.01		0.05	0.08	0.00	99.33
C555	THERMOCALC	0.494	45.10	0.63	0.22	47.05	6.32	0.00	0.00	0.00	0.11	0.57			100.00
	Biase&Variance	-0.213	2.90	0.54	0.02	-1.49	-1.82	0.00	0.00	-0.01	0.11	0.52	-0.08	0.00	14.50
	Exp	0.646	40.93	0.05	0.16	49.80	7.96	0.00	0.00	0.00		0.00	0.11	0.19	99.19
C554	THERMOCALC	0.481	44.63	0.55	0.19	47.70	6.28	0.00	0.00	0.00	0.10	0.55			100.00
	Biase&Variance	-0.165	3.71	0.50	0.03	-2.10	-1.68	0.00	0.00	0.00	0.10	0.55	-0.11	-0.19	21.59
	Exp	0.623	40.40	0.08	0.08	51.44	7.79	0.00	0.00	0.01		0.62	0.11	0.17	100.69
C553	THERMOCALC	0.453	43.45	0.37	0.12	49.26	6.22	0.00	0.00	0.00	0.07	0.50			100.00
	Biase&Variance	-0.170	3.05	0.29	0.04	-2.17	-1.57	0.00	0.00	-0.01	0.07	-0.12	-0.11	-0.17	16.63
	Exp	0.577	40.46	0.07	0.05	51.18	7.84	0.00	0.00	0.02		0.37	0.11	0.12	100.22
C559	THERMOCALC	0.416	41.45	0.12	0.05	51.72	6.20	0.00	0.00	0.00	0.04	0.41			100.00
	Biase&Variance	-0.162	0.99	0.05	0.00	0.54	-1.64	0.00	0.00	-0.02	0.04	0.04	-0.11	-0.12	3.99
	Exp	0.697	43.78	0.38	0.38	48.17	7.38	0.00	0.01	0.02		0.19	0.11	0.00	100.41
C470	THERMOCALC	0.534	44.41	0.55	0.20	48.02	6.22	0.00	0.01	0.00	0.09	0.50			100.00
	Biase&Variance	-0.164	0.64	0.17	-0.19	-0.15	-1.16	0.00	0.00	-0.02	0.09	0.32	-0.11	0.00	1.95

	Exp	0.816	45.64	1.66	1.60	42.81	7.75	0.00	0.07	0.04		0.42	0.11	0.01	100.11
C481	THERMOCALC	0.832	47.13	2.29	1.70	40.81	6.96	0.01	0.10	0.17	0.27	0.57			100.00
	Biase&Variance	0.016	1.49	0.63	0.10	-2.00	-0.80	0.01	0.03	0.13	0.27	0.15	-0.11	-0.01	7.38
	Exp	0.729	44.98	0.93	0.73	45.67	7.80	0.00	0.03	0.03		0.26	0.10	0.00	100.52
C471	THERMOCALC	0.807	47.05	2.01	1.30	41.73	6.88	0.00	0.07	0.12	0.25	0.58			100.00
	Biase&Variance	0.077	2.07	1.09	0.57	-3.94	-0.92	0.00	0.04	0.09	0.25	0.32	-0.10	0.00	22.34
	Exp	0.713	44.56	0.73	0.54	46.18	7.26	0.00	0.02	0.03		0.30	0.08	0.00	99.70
C473	THERMOCALC	0.526	46.37	0.74	0.23	46.33	5.70	0.00	0.01	0.00	0.10	0.51			100.00
	Biase&Variance	-0.187	1.81	0.01	-0.30	0.15	-1.56	0.00	0.00	-0.03	0.10	0.21	-0.08	0.00	5.89
	Exp	0.682	44.77	0.55	0.40	46.96	7.06	0.00	0.02	0.01		0.32	0.09	0.00	100.18
C463	THERMOCALC	0.622	46.89	1.04	0.39	44.93	6.01	0.00	0.02	0.00	0.14	0.57			100.00
	Biase&Variance	-0.060	2.12	0.49	-0.01	-2.03	-1.04	0.00	0.00	-0.01	0.14	0.25	-0.09	0.00	10.02
	Exp	0.741	45.16	1.26	0.79	44.68	7.41	0.00	0.04	0.04		0.28	0.09	0.00	99.75
C474	THERMOCALC	0.801	47.33	2.10	1.24	41.61	6.71	0.00	0.08	0.10	0.25	0.58			100.00
	Biase&Variance	0.060	2.17	0.84	0.46	-3.07	-0.70	0.00	0.04	0.06	0.25	0.29	-0.09	0.00	15.71
	Exp	0.694	45.17	1.16	0.62	45.34	7.21	0.00	0.03	0.01		0.16	0.08	0.01	99.80
C465	THERMOCALC	0.794	47.55	2.17	1.19	41.52	6.56	0.00	0.10	0.08	0.25	0.57			100.00
	Biase&Variance	0.100	2.37	1.01	0.57	-3.81	-0.65	0.00	0.07	0.07	0.25	0.41	-0.08	-0.01	22.20

Table A2.2c Mitchell and Grove (2015) melting experimental results and calculation results from THERMOCALC and PMELTS: spinel composition

No.	Methods	Mode	SiO2	Al2O3	CaO	MgO	FeO	K2O	Na2O	TiO2	Fe2O3	Cr2O3	MnO	NiO	Total	Cr#
	Exp	0.003	0.20	20.00	0.07	16.60	11.80		0.00	0.27		51.30	0.17	0.02	100.43	63.24
C490	THERMOCALC	0.003	0.00	15.07	0.00	16.48	12.45	0.00	0.00	0.00	5.42	50.58			100.00	69.25
	Biase&Variance	0.000	-0.20	-4.93	-0.07	-0.12	0.65	0.00	0.00	-0.27	5.42	-0.72	-0.17	-0.02	54.80	
	Exp	0.002	0.20	19.40	0.15	16.90	11.50		0.00	0.30		50.60	0.20	0.04	99.29	63.63
C498	PMELTS	0.006	0.00	17.22	0.00	16.88	9.72	0.00	0.00	0.99	8.24	46.96			100.01	64.66
	Biase&Variance	0.004	-0.20	-2.18	-0.15	-0.02	-1.78	0.00	0.00	0.69	8.24	-3.64	-0.20	-0.04	89.65	
	Exp	0.006	0.50	8.30	0.10	15.30	14.30			0.29		62.00	0.22	0.04	101.05	83.36
C553	THERMOCALC	0.002	0.00	13.88	0.00	16.41	12.44	0.00	0.00	0.00	5.52	51.74			100.00	71.43
	Biase&Variance	-0.004	-0.50	5.58	-0.10	1.11	-1.86	0.00	0.00	-0.29	5.52	-10.26	-0.22	-0.04	172.01	
	Exp	0.003	0.40	8.10	0.12	15.00	14.40			0.25		61.50	0.21	0.03	100.01	83.59
C559	THERMOCALC	0.002	0.00	12.50	0.00	16.47	12.12	0.00	0.00	0.00	5.51	53.39			100.00	74.13
	Biase&Variance	-0.001	-0.40	4.40	-0.12	1.47	-2.28	0.00	0.00	-0.25	5.51	-8.11	-0.21	-0.03	123.10	

Table A2.2d Mitchell and Grove (2015) melting experimental results and calculation results from THERMOCALC and PMELTS: olivine composition

No.	Methods	Mode	SiO2	Al2O3	CaO	MgO	FeO	K2O	Na2O	TiO2	Fe2O3	Cr2O3	MnO	NiO	Total	Mg#
	Exp	0.60	40.70	0.10	0.21	49.70	9.30			0.01		0.11	0.12	0.26	100.51	90.50
	THERMOCALC	0.44	41.49	0.00	0.06	51.99	6.47	0.00	0.00	0.00	0.00	0.00			100.00	93.47
C507	Biase&Variance	-0.16	0.79	-0.10	-0.15	2.29	-2.83	0.00	0.00	-0.01	0.00	-0.11	-0.12	-0.26	13.98	
	PMELTS	0.56	41.23	0.00	0.17	50.84	7.33	0.00	0.00	0.00	0.00	0.00	0.08	0.37	100.00	92.52
	Biase&Variance	-0.04	0.53	-0.10	-0.04	1.14	-1.97	0.00	0.00	-0.01	0.00	-0.11	-0.04	0.11	5.50	
	Exp	0.57	40.80	0.05	0.22	50.00	8.90			0.00		0.18	0.10	0.35	100.60	90.92
	THERMOCALC	0.43	41.52	0.00	0.05	52.12	6.31	0.00	0.00	0.00	0.00	0.00			100.00	93.64
C508	Biase&Variance	-0.15	0.72	-0.05	-0.17	2.12	-2.59	0.00	0.00	0.00	0.00	-0.18	-0.10	-0.35	11.93	
	PMELTS	0.53	41.26	0.00	0.17	50.99	7.13	0.00	0.00	0.00	0.00	0.00	0.08	0.37	100.00	92.73
	Biase&Variance	-0.04	0.46	-0.05	-0.05	0.99	-1.77	0.00	0.00	0.00	0.00	-0.18	-0.02	0.02	4.38	
	Exp	0.58	40.80	0.06	0.19	49.40	9.10			0.02		0.11	0.13	0.12	99.93	90.63
	THERMOCALC	0.47	41.43	0.00	0.07	51.74	6.76	0.00	0.00	0.00	0.00	0.00			100.00	93.17
C494	Biase&Variance	-0.12	0.63	-0.06	-0.12	2.34	-2.34	0.00	0.00	-0.02	0.00	-0.11	-0.13	-0.12	11.41	
	PMELTS	0.59	41.16	0.00	0.19	50.55	7.60	0.00	0.00	0.00	0.00	0.00	0.10	0.39	100.00	92.22
	Biase&Variance	0.00	0.36	-0.06	0.00	1.15	-1.50	0.00	0.00	-0.02	0.00	-0.11	-0.03	0.27	3.79	
	Exp	0.56	40.79	0.04	0.21	51.10	7.60			0.00		0.15	0.12	0.06	100.07	92.30
	THERMOCALC	0.47	41.43	0.00	0.07	51.74	6.76	0.00	0.00	0.00	0.00	0.00			100.00	93.17
C490	Biase&Variance	-0.10	0.64	-0.04	-0.14	0.64	-0.84	0.00	0.00	0.00	0.00	-0.15	-0.12	-0.06	1.59	
	PMELTS	0.59	41.16	0.00	0.19	50.55	7.60	0.00	0.00	0.00	0.00	0.00	0.10	0.39	100.00	92.22
	Biase&Variance	0.02	0.37	-0.04	-0.02	-0.55	0.00	0.00	0.00	0.00	0.00	-0.15	-0.02	0.33	0.57	
	Exp	0.57	41.10	0.03	0.20	50.80	8.00			0.00		0.19	0.04	0.09	100.45	91.88
	THERMOCALC	0.49	41.26	0.00	0.14	50.97	7.63	0.00	0.00	0.00	0.00	0.00			100.00	92.25
C498	Biase&Variance	-0.08	0.16	-0.03	-0.06	0.17	-0.37	0.00	0.00	0.00	0.00	-0.19	-0.04	-0.09	0.24	
	PMELTS	0.66	41.00	0.00	0.25	49.85	8.36	0.00	0.00	0.00	0.00	0.00	0.13	0.41	100.00	91.40
	Biase&Variance	0.08	-0.10	-0.03	0.05	-0.95	0.36	0.00	0.00	0.00	0.00	-0.19	0.09	0.32	1.19	
	Exp	0.57	40.60	0.01	0.07	49.90	9.30			0.00		0.00	0.09	0.30	100.27	90.53
	THERMOCALC	0.39	41.35	0.00	0.07	51.40	7.18	0.00	0.00	0.00	0.00	0.00			100.00	92.74
C561	Biase&Variance	-0.18	0.75	-0.01	0.00	1.50	-2.12	0.00	0.00	0.00	0.00	0.00	-0.09	-0.30	7.44	
	PMELTS	0.62	41.09	0.00	0.14	50.26	8.07	0.00	0.00	0.00	0.00	0.00	0.09	0.36	100.00	91.74
	Biase&Variance	0.05	0.49	-0.01	0.07	0.36	-1.23	0.00	0.00	0.00	0.00	0.00	0.00	0.06	1.89	

	Exp	0.64	41.20		0.12	50.40	8.47			0.01			0.08		100.28	91.38
	THERMOCALC	0.39	41.41	0.00	0.06	51.64	6.89	0.00	0.00	0.00	0.00	0.00			100.00	93.03
C555	Biase&Variance	-0.25	0.21	0.00	-0.06	1.24	-1.58	0.00	0.00	-0.01	0.00	0.00	-0.08	0.00	4.07	
	PMELTS	0.60	41.14	0.00	0.15	50.47	7.81	0.00	0.00	0.00	0.00	0.00	0.08	0.36	100.00	92.01
	Biase&Variance	-0.04	-0.06	0.00	0.03	0.07	-0.66	0.00	0.00	-0.01	0.00	0.00	0.00	0.36	0.58	
	Exp	0.60	40.80		0.12	51.60	8.26						0.11	0.20	101.09	91.76
	THERMOCALC	0.40	41.43	0.00	0.06	51.74	6.77	0.00	0.00	0.00	0.00	0.00			100.00	93.16
C554	Biase&Variance	-0.20	0.63	0.00	-0.06	0.14	-1.49	0.00	0.00	0.00	0.00	0.00	-0.11	-0.20	2.70	
	PMELTS	0.59	41.16	0.00	0.15	50.56	7.68	0.00	0.00	0.00	0.00	0.00	0.08	0.36	100.00	92.14
	Biase&Variance	-0.01	0.36	0.00	0.03	-1.04	-0.58	0.00	0.00	0.00	0.00	0.00	-0.03	0.16	1.57	
	Exp	0.61	40.80		0.08	51.80	7.72			0.01			0.11	0.17	100.69	92.28
	THERMOCALC	0.40	41.48	0.00	0.05	51.96	6.51	0.00	0.00	0.00	0.00	0.00			100.00	93.43
C553	Biase&Variance	-0.20	0.68	0.00	-0.02	0.16	-1.21	0.00	0.00	-0.01	0.00	0.00	-0.11	-0.17	2.00	
	PMELTS	0.56	41.21	0.00	0.15	50.77	7.42	0.00	0.00	0.00	0.00	0.00	0.08	0.36	100.00	92.42
	Biase&Variance	-0.04	0.41	0.00	0.08	-1.03	-0.30	0.00	0.00	-0.01	0.00	0.00	-0.03	0.19	1.36	
	Exp	0.58	40.70	0.02	0.05	51.40	7.80			0.02			0.11	0.12	100.22	92.15
	THERMOCALC	0.41	41.54	0.00	0.05	52.22	6.19	0.00	0.00	0.00	0.00	0.00			100.00	93.77
C559	Biase&Variance	-0.17	0.84	-0.02	0.00	0.82	-1.61	0.00	0.00	-0.02	0.00	0.00	-0.11	-0.12	4.00	
	PMELTS	0.53	41.27	0.00	0.16	51.04	7.08	0.00	0.00	0.00	0.00	0.00	0.08	0.37	100.00	92.78
	Biase&Variance	-0.05	0.57	-0.02	0.11	-0.36	-0.72	0.00	0.00	-0.02	0.00	0.00	-0.03	0.25	1.05	
	Exp	0.56	40.80	0.04	0.17	51.60	7.90			0.01			0.12		100.64	92.09
	THERMOCALC	0.45	41.44	0.00	0.08	51.79	6.69	0.00	0.00	0.00	0.00	0.00			100.00	93.24
C470	Biase&Variance	-0.11	0.64	-0.04	-0.09	0.19	-1.21	0.00	0.00	-0.01	0.00	0.00	-0.12	0.00	1.94	
	PMELTS	0.57	41.18	0.00	0.21	50.63	7.45	0.00	0.00	0.00	0.00	0.00	0.11	0.41	100.00	92.37
	Biase&Variance	0.01	0.38	-0.04	0.04	-0.97	-0.45	0.00	0.00	-0.01	0.00	0.00	-0.01	0.41	1.46	
	Exp	0.48	39.50	0.08	0.27	50.90	9.28						0.11	0.01	100.15	90.72
	THERMOCALC	0.51	41.09	0.00	0.29	50.20	8.42	0.00	0.00	0.00	0.00	0.00			100.00	91.40
C481	Biase&Variance	0.03	1.59	-0.08	0.02	-0.70	-0.86	0.00	0.00	0.00	0.00	0.00	-0.11	-0.01	3.79	
	PMELTS	0.51	40.80	0.00	0.33	48.92	9.22	0.00	0.00	0.00	0.00	0.00	0.19	0.54	100.00	90.44
	Biase&Variance	0.04	1.30	-0.08	0.06	-1.98	-0.06	0.00	0.00	0.00	0.00	0.00	0.08	0.53	5.89	
	Exp	0.53	41.20	0.07	0.24	50.20	8.60			0.01			0.10		100.42	91.23
	THERMOCALC	0.51	41.13	0.00	0.28	50.37	8.22	0.00	0.00	0.00	0.00	0.00			100.00	91.61
C471	Biase&Variance	-0.03	-0.07	-0.07	0.04	0.17	-0.38	0.00	0.00	-0.01	0.00	0.00	-0.10	0.00	0.19	
	PMELTS	0.52	40.85	0.00	0.37	49.15	8.91	0.00	0.00	0.00	0.00	0.00	0.19	0.53	100.00	90.77
	Biase&Variance	-0.01	-0.35	-0.07	0.13	-1.05	0.31	0.00	0.00	-0.01	0.00	0.00	0.09	0.53	1.63	

	Exp	0.50	39.60	0.05	0.16	51.60	8.20			0.02			0.07		99.70	91.81
	THERMOCALC	0.39	41.49	0.00	0.07	51.98	6.46	0.00	0.00	0.00	0.00	0.00			100.00	93.48
C473	Biase&Variance	-0.11	1.89	-0.05	-0.09	0.38	-1.74	0.00	0.00	-0.02	0.00	0.00	-0.07	0.00	6.73	
	PMELTS	0.53	41.24	0.00	0.19	50.87	7.17	0.00	0.00	0.00	0.00	0.00	0.11	0.43	100.00	92.68
	Biase&Variance	0.04	1.64	-0.05	0.03	-0.73	-1.03	0.00	0.00	-0.02	0.00	0.00	0.04	0.43	4.46	
	Exp	0.52	41.00	0.06	0.16	51.00	7.70			0.01		0.20	0.09		100.22	92.19
	THERMOCALC	0.43	41.39	0.00	0.11	51.53	6.97	0.00	0.00	0.00	0.00	0.00			100.00	92.95
C463	Biase&Variance	-0.08	0.39	-0.06	-0.05	0.53	-0.73	0.00	0.00	-0.01	0.00	-0.20	-0.09	0.00	1.02	
	PMELTS	0.56	41.17	0.00	0.23	50.56	7.46	0.00	0.00	0.00	0.00	0.00	0.14	0.45	100.00	92.35
	Biase&Variance	0.04	0.17	-0.06	0.07	-0.44	-0.24	0.00	0.00	-0.01	0.00	-0.20	0.05	0.45	0.54	
	Exp	0.49	40.00	0.09	0.24	50.90	8.51			0.03			0.09		99.86	91.42
	THERMOCALC	0.49	41.15	0.00	0.28	50.44	8.14	0.00	0.00	0.00	0.00	0.00			100.00	91.70
C474	Biase&Variance	0.01	1.15	-0.09	0.04	-0.46	-0.37	0.00	0.00	-0.03	0.00	0.00	-0.09	0.00	1.68	
	PMELTS	0.48	40.86	0.00	0.36	49.21	8.79	0.00	0.00	0.00	0.00	0.00	0.20	0.57	100.00	90.89
	Biase&Variance	0.00	0.86	-0.09	0.12	-1.69	0.28	0.00	0.00	-0.03	0.00	0.00	0.11	0.57	4.05	
	Exp	0.48	40.80	0.12	0.24	50.70	8.12			0.01			0.09	0.01	100.09	91.76
	THERMOCALC	0.48	41.16	0.00	0.27	50.51	8.06	0.00	0.00	0.00	0.00	0.00			100.00	91.79
C465	Biase&Variance	0.00	0.36	-0.12	0.03	-0.19	-0.06	0.00	0.00	-0.01	0.00	0.00	-0.09	-0.01	0.20	
	PMELTS	0.45	40.90	0.00	0.35	49.35	8.59	0.00	0.00	0.00	0.00	0.00	0.21	0.61	100.00	91.11
	Biase&Variance	-0.04	0.10	-0.12	0.11	-1.35	0.47	0.00	0.00	-0.01	0.00	0.00	0.12	0.60	2.45	

Table A2.2e Mitchell and Grove (2015) melting experimental results and calculation results from THERMOCALC and PMELTS: opx composition

No.	Methods	Mode	SiO2	Al2O3	CaO	MgO	FeO	K2O	Na2O	TiO2	Fe2O3	Cr2O3	MnO	NiO	Total
	Exp	0.182	56.50	2.50	2.10	32.70	5.50		0.04	0.13		0.94	0.10		100.51
C494	THERMOCALC	0.032	55.93	2.29	0.64	34.64	4.56	0.00	0.02	0.01	0.35	1.57			100.00
	Biase&Variance	-0.150	-0.57	-0.21	-1.46	1.94	-0.94	0.00	-0.02	-0.12	0.35	0.63	-0.10	0.00	7.68
	Exp	0.155	56.30	2.10	1.79	33.50	5.10		0.04	0.07		1.07	0.06		100.03
C490	THERMOCALC	0.032	55.93	2.29	0.64	34.64	4.56	0.00	0.02	0.01	0.35	1.57			100.00
	Biase&Variance	-0.123	-0.37	0.19	-1.15	1.14	-0.54	0.00	-0.02	-0.06	0.35	0.50	-0.06	0.00	3.46
	Exp	0.134	57.10	1.70	1.58	33.60	5.40		0.05	0.07		1.00	0.10		100.60
C498	THERMOCALC	0.183	54.88	3.20	1.36	33.14	5.13	0.00	0.03	0.02	0.49	1.75			100.00
	Biase&Variance	0.049	-2.22	1.50	-0.22	-0.46	-0.27	0.00	-0.02	-0.05	0.49	0.75	-0.10	0.00	8.33
	Exp	0.178	56.60	1.30	1.34	33.50	6.00	0.00	0.03	0.08		0.71	0.11		99.67
C561	THERMOCALC	0.132	55.88	2.28	0.84	34.32	4.84	0.00	0.01	0.00	0.36	1.46			100.00
	Biase&Variance	-0.047	-0.72	0.98	-0.50	0.82	-1.16	0.00	-0.02	-0.08	0.36	0.75	-0.11	0.00	4.46
	Exp	0.060	57.40	1.04	1.09	34.00	5.54	0.00	0.01	0.06		0.62	0.09		99.85
C555	THERMOCALC	0.099	56.07	2.16	0.67	34.66	4.63	0.00	0.01	0.00	0.33	1.46			100.00
	Biase&Variance	0.038	-1.33	1.12	-0.42	0.66	-0.91	0.00	0.00	-0.05	0.33	0.84	-0.09	0.00	5.29
	Exp	0.034	57.10	0.86	0.84	35.30	5.37	0.02	0.04	0.03		0.06	0.10		99.72
C554	THERMOCALC	0.083	56.15	2.11	0.61	34.80	4.53	0.00	0.01	0.00	0.32	1.46			100.00
	Biase&Variance	0.049	-0.95	1.25	-0.23	-0.50	-0.84	-0.02	-0.03	-0.03	0.32	1.40	-0.10	0.00	5.53
	Exp	0.132	56.30	1.80	1.28	33.70	5.18		0.05	0.05		0.98	0.08		100.36
C470	THERMOCALC	0.086	55.95	2.34	0.63	34.70	4.43	0.00	0.02	0.01	0.34	1.58			100.00
	Biase&Variance	-0.047	-0.35	0.54	-0.65	1.00	-0.75	0.00	-0.03	-0.04	0.34	0.60	-0.08	0.00	2.88
	Exp	0.306	54.50	3.80	2.40	32.20	5.72		0.14	0.09		1.00	0.11		100.36
	THERMOCALC	0.264	53.61	4.98	2.66	31.05	5.48	0.00	0.11	0.08	0.64	1.39			100.00
C481	Biase&Variance	-0.042	-0.89	1.18	0.26	-1.15	-0.24	0.00	-0.03	-0.01	0.64	0.39	-0.11	0.00	4.21
	PMELTS	0.251	55.56	3.69	1.97	32.60	5.49	0.00	0.10	0.18	0.41	0.00	0.00	0.00	100.00
	Biase&Variance	-0.054	1.06	-0.11	-0.43	0.40	-0.23	0.00	-0.04	0.09	0.41	-1.00	-0.11	0.00	2.71
	Exp	0.185	55.90	3.40	2.13	32.60	5.49		0.10	0.09		1.00	0.10		100.36
	THERMOCALC	0.268	54.04	4.48	2.34	31.64	5.34	0.00	0.10	0.08	0.59	1.38			100.00
C471	Biase&Variance	0.084	-1.86	1.08	0.21	-0.96	-0.15	0.00	0.00	-0.01	0.59	0.38	-0.10	0.00	6.13
	PMELTS	0.236	55.86	3.26	2.22	32.76	5.33	0.00	0.07	0.13	0.38	0.00	0.00	0.00	100.00
	Biase&Variance	0.052	-0.04	-0.14	0.09	0.16	-0.16	0.00	-0.03	0.04	0.38	-1.00	-0.10	0.00	1.24
	Exp	0.216	56.00	2.30	1.40	33.70	5.10		0.06	0.05		1.00	0.11		100.36
C473	THERMOCALC	0.136	56.21	2.21	0.56	35.02	4.16	0.00	0.04	0.01	0.30	1.50			100.00
	Biase&Variance	-0.080	0.21	-0.09	-0.84	1.32	-0.94	0.00	-0.02	-0.04	0.30	0.50	-0.11	0.00	3.73

	Exp	0.162	56.80	2.10	1.15	34.10	5.00		0.08	0.03		0.70	0.07		100.36
	THERMOCALC	0.189	55.74	2.70	0.83	34.33	4.48	0.00	0.06	0.01	0.38	1.48			100.00
C463	Biase&Variance	0.027	-1.06	0.60	-0.32	0.23	-0.52	0.00	-0.02	-0.02	0.38	0.78	-0.07	0.00	2.67
	PMELTS	0.008	57.24	1.70	1.53	34.82	4.40	0.00	0.02	0.06	0.24	0.00	0.00	0.00	100.00
	Biase&Variance	-0.154	0.44	-0.40	0.38	0.71	-0.60	0.00	-0.06	0.03	0.24	-0.70	-0.07	0.00	1.92
	Exp	0.252	55.10	3.50	1.84	32.70	5.30	0.01	0.12	0.05		0.83	0.09		100.36
	THERMOCALC	0.282	54.20	4.51	2.18	31.88	5.16	0.00	0.13	0.08	0.56	1.31			100.00
C474	Biase&Variance	0.029	-0.90	1.01	0.34	-0.82	-0.14	-0.01	0.01	0.03	0.56	0.48	-0.09	0.00	3.20
	PMELTS	0.274	55.77	3.52	2.31	32.72	5.09	0.00	0.09	0.13	0.36	0.00	0.00	0.00	100.00
	Biase&Variance	0.022	0.67	0.02	0.47	0.02	-0.21	-0.01	-0.03	0.08	0.36	-0.83	-0.09	0.00	1.55
	Exp	0.207	55.40	3.60	1.52	32.80	5.07		0.10	0.02		0.53	0.07		100.36
	THERMOCALC	0.291	54.33	4.55	2.04	32.05	4.99	0.00	0.17	0.07	0.55	1.25			100.00
C465	Biase&Variance	0.084	-1.07	0.95	0.52	-0.75	-0.08	0.00	0.07	0.05	0.55	0.72	-0.07	0.00	3.70
	PMELTS	0.306	55.77	3.65	2.40	32.76	4.84	0.00	0.10	0.13	0.34	0.00	0.00	0.00	100.00
	Biase&Variance	0.098	0.37	0.05	0.88	-0.04	-0.23	0.00	0.00	0.11	0.34	-0.53	-0.07	0.00	1.39

Table A2.2f Mitchell and Grove (2015) melting experimental results and calculation results from THERMOCALC and PMELTS: cpx composition

No.	Methods	Mode	SiO2	Al2O3	CaO	MgO	FeO	K2O	Na2O	TiO2	Fe2O3	Cr2O3	MnO	NiO	Total
	Exp	0.029	53.00	5.20	15.10	21.40	4.10		0.57	0.23		1.20	0.06		100.86
	THERMOCALC	0.061	54.14	4.01	5.78	28.45	4.85	0.09	0.66	1.55	0.18	0.29			100.00
C481	Biase&Variance	0.032	1.14	-1.19	-9.32	7.05	0.75	0.09	0.09	1.32	0.18	-0.91	-0.06	0.00	142.30
	PMELTS	0.108	52.61	5.62	16.42	19.90	3.84	0.00	0.62	0.33	0.66	0.00	0.00	0.00	100.00
	Biase&Variance	0.079	-0.39	0.42	1.32	-1.50	-0.26	0.00	0.05	0.10	0.66	-1.20	-0.06	0.00	6.30

Experiments from Mitchell and Grove (2016) were modelled using WL22-3 model.

Table A2.3a Mitchell and Grove (2016) melting experimental results and calculation results from WL22-3 model: melt composition

No.	Methods	Mode	SiO2	Al2O3	CaO	MgO	FeO	K2O	Na2O	TiO2	Fe2O3	Cr2O3	H2O	MnO	NiO	Total
	Exp	0.189	54.70	5.65	4.80	17.00	9.00	0.10	0.44	0.35		0.19	5.00	0.15	0.02	97.40
C608	THERMOCALC	0.369	43.48	3.12	2.81	24.33	8.36	0.06	0.35	0.16	0.94	0.63	15.76			100.00
	Biase&Variance	0.180	-11.22	-2.53	-1.99	7.33	-0.64	-0.04	-0.09	-0.19	0.94	0.44	10.76	-0.15	-0.02	307.22
	Exp	0.272	54.70	9.60	8.30	12.30	6.40	0.26	1.21	0.52		0.13	5.80	0.12	0.00	99.34
C602	THERMOCALC	0.423	43.74	7.03	6.13	20.08	7.29	0.18	1.00	0.37	0.71	0.27	13.18			100.00
	Biase&Variance	0.152	-10.96	-2.57	-2.17	7.78	0.89	-0.08	-0.21	-0.15	0.71	0.14	7.38	-0.12	0.00	247.79
	Exp	0.188	54.00	10.90	9.20	10.30	6.10	0.27	1.47	0.57		0.12	7.00	0.13		100.06
C603	THERMOCALC	0.402	43.06	7.35	6.46	19.63	7.22	0.20	1.06	0.39	0.73	0.24	13.65			100.00
	Biase&Variance	0.214	-10.94	-3.55	-2.74	9.33	1.12	-0.07	-0.41	-0.18	0.73	0.12	6.65	-0.13	0.00	273.22
	Exp	0.167	52.70	11.14	8.90	10.50	5.94	0.30	1.37	0.56		0.09	8.50	0.12	0.02	100.14
C604	THERMOCALC	0.396	42.39	7.46	6.59	19.37	7.11	0.20	1.09	0.40	0.74	0.22	14.43			100.00
	Biase&Variance	0.229	-10.31	-3.68	-2.31	8.87	1.17	-0.10	-0.28	-0.16	0.74	0.13	5.93	-0.12	-0.02	240.91
	Exp	0.153	57.50	13.60	10.40	4.70	4.40	0.21	1.89	0.84		0.06	7.50	0.10		101.20
C605	THERMOCALC	0.382	41.72	7.71	6.82	19.00	7.01	0.21	1.14	0.42	0.75	0.19	15.03			100.00
	Biase&Variance	0.230	-15.78	-5.89	-3.58	14.30	2.61	0.00	-0.75	-0.42	0.75	0.13	7.53	-0.10	0.00	565.85
	Exp	0.526	52.20	14.45	10.10	9.20	5.71	0.44	2.06	0.72		0.06	5.50	0.17	0.01	100.62
C584	THERMOCALC	0.764	42.55	10.72	9.08	16.74	6.77	0.31	1.65	0.58	0.32	0.09	11.19			100.00
	Biase&Variance	0.239	-9.65	-3.73	-1.02	7.54	1.06	-0.13	-0.41	-0.14	0.32	0.03	5.69	-0.17	-0.01	198.74
	Exp	0.499	52.50	15.00	10.30	8.40	6.10	0.37	1.78	0.72		0.06	5.70	0.13	0.01	101.07
C592	THERMOCALC	0.785	42.49	10.43	8.84	17.03	6.72	0.30	1.59	0.56	0.32	0.10	11.63			100.00
	Biase&Variance	0.286	-10.01	-4.57	-1.46	8.63	0.62	-0.07	-0.19	-0.16	0.32	0.04	5.93	-0.13	-0.01	233.48
	Exp	0.459	52.20	15.70	9.00	7.20	5.68	0.50	2.20	0.53		0.05	6.80	0.12	0.01	99.99
C587	THERMOCALC	0.742	41.95	11.01	9.08	16.42	6.77	0.32	1.71	0.60	0.31	0.07	11.76			100.00
	Biase&Variance	0.283	-10.25	-4.69	0.08	9.22	1.09	-0.18	-0.49	0.07	0.31	0.02	4.96	-0.12	-0.01	238.28
	Exp	0.449	53.30	16.30	9.30	6.60	5.00	2.58	2.20	0.47		0.03	6.00	0.14	0.01	101.93
C590	THERMOCALC	0.690	41.22	11.81	8.61	15.92	6.87	0.35	1.86	0.66	0.30	0.06	12.34			100.00
	Biase&Variance	0.241	-12.08	-4.49	-0.69	9.32	1.87	-2.23	-0.34	0.19	0.30	0.03	6.34	-0.14	-0.01	302.39
	Exp	0.410	52.90	16.90	8.70	6.20	5.50	0.41	2.20	0.51		0.02	7.30	0.12		100.76
C591	THERMOCALC	0.692	40.47	11.75	8.25	15.93	6.81	0.35	1.85	0.66	0.29	0.05	13.59			100.00
	Biase&Variance	0.282	-12.43	-5.15	-0.45	9.73	1.31	-0.06	-0.35	0.15	0.29	0.03	6.29	-0.12	0.00	317.27

Table A2.3b Mitchell and Grove (2016) melting experimental results and calculation results from WL22-3 model: residue composition

No.	Methods	Mode	SiO2	Al2O3	CaO	MgO	FeO	K2O	Na2O	TiO2	Fe2O3	Cr2O3	MnO	NiO	Total
	Exp	0.811	40.39	0.02	0.07	51.48	6.77	0.00	0.00	0.00		0.12	0.13	0.01	98.98
C608	THERMOCALC	0.631	41.60	0.00	0.01	52.48	5.91	0.00	0.00	0.00	0.00	0.00			100.00
	Biase&Variance	-0.180	1.20	-0.02	-0.06	1.01	-0.85	0.00	0.00	0.00	0.00	-0.12	-0.13	-0.01	3.22
	Exp	0.728	40.66	0.03	0.08	51.38	7.64	0.00	0.00	0.04		0.19	0.11	0.02	100.16
C602	THERMOCALC	0.577	43.29	0.23	0.12	49.81	6.27	0.00	0.00	0.00	0.06	0.22			100.00
	Biase&Variance	-0.152	2.62	0.20	0.04	-1.56	-1.37	0.00	0.00	-0.04	0.06	0.02	-0.11	-0.02	11.26
	Exp	0.812	42.91	0.17	0.27	48.13	7.49	0.00	0.00	0.02		0.37	0.11	0.03	99.50
C603	THERMOCALC	0.598	43.91	0.32	0.16	48.95	6.33	0.00	0.00	0.00	0.07	0.25			100.00
	Biase&Variance	-0.214	1.00	0.15	-0.11	0.83	-1.17	0.00	0.00	-0.02	0.07	-0.12	-0.11	-0.03	3.12
	Exp	0.833	43.66	0.29	0.34	47.39	7.38	0.00	0.01	0.02		0.45	0.11	0.01	99.67
C604	THERMOCALC	0.604	44.21	0.37	0.18	48.51	6.37	0.00	0.00	0.00	0.08	0.27			100.00
	Biase&Variance	-0.229	0.55	0.08	-0.15	1.12	-1.02	0.00	-0.01	-0.02	0.08	-0.18	-0.11	-0.01	2.67
	Exp	0.847	41.86	0.16	0.96	47.00	7.45	0.00	0.01	0.03		0.40	0.11	0.02	98.00
C605	THERMOCALC	0.618	44.60	0.43	0.23	47.93	6.42	0.00	0.00	0.00	0.10	0.29			100.00
	Biase&Variance	-0.230	2.74	0.27	-0.73	0.93	-1.02	0.00	0.00	-0.03	0.10	-0.11	-0.11	-0.02	10.05
	Exp	0.475	42.56	0.53	4.75	41.70	8.87	0.00	0.05	0.01		1.07	0.18	0.05	99.76
C584	THERMOCALC	0.236	51.82	1.92	1.29	38.04	5.82	0.00	0.01	0.01	0.21	0.87			100.00
	Biase&Variance	-0.239	9.26	1.39	-3.46	-3.66	-3.05	0.00	-0.03	0.00	0.21	-0.20	-0.18	-0.05	122.42
	Exp	0.501	43.31	0.55	4.90	41.12	8.92	0.00	0.06	0.03		0.88	0.15	0.11	100.02
C592	THERMOCALC	0.215	51.65	1.83	1.17	38.49	5.75	0.00	0.01	0.01	0.20	0.89			100.00
	Biase&Variance	-0.286	8.34	1.29	-3.73	-2.64	-3.17	0.00	-0.05	-0.02	0.20	0.01	-0.15	-0.11	102.19
	Exp	0.541	43.30	0.79	6.59	39.07	9.04	0.00	0.07	0.04		0.96	0.16	0.13	100.17
C587	THERMOCALC	0.258	52.22	2.02	2.05	36.73	5.87	0.00	0.02	0.01	0.23	0.83			100.00
	Biase&Variance	-0.283	8.92	1.23	-4.54	-2.34	-3.17	0.00	-0.05	-0.03	0.23	-0.13	-0.16	-0.13	117.33
	Exp	0.551	43.22	0.97	6.13	39.56	8.60	0.00	0.06	0.07		1.36	0.19	0.06	100.24
C590	THERMOCALC	0.310	52.30	2.24	4.29	34.24	5.86	0.00	0.05	0.02	0.27	0.73			100.00
	Biase&Variance	-0.241	9.08	1.27	-1.85	-5.32	-2.74	0.00	-0.01	-0.05	0.27	-0.63	-0.19	-0.06	123.90
	Exp	0.590	44.29	1.12	7.01	37.60	9.09	0.00	0.08	0.08		1.06	0.17	0.07	100.58
C591	THERMOCALC	0.308	52.45	2.24	4.83	33.57	5.83	0.00	0.05	0.02	0.28	0.72			100.00
	Biase&Variance	-0.282	8.16	1.12	-2.18	-4.03	-3.26	0.00	-0.02	-0.06	0.28	-0.34	-0.17	-0.07	99.77

Table A2.3c Mitchell and Grove (2016) melting experimental results and calculation results from WL22-3 model: spinel composition

No.	Methods	Mode	SiO2	Al2O3	CaO	MgO	FeO	K2O	Na2O	TiO2	Fe2O3	Cr2O3	MnO	NiO	Total	Cr#
	Exp	0.003	0.90	7.30	0.30	14.68	19.00		0.00	0.78		56.99	0.49	0.45	100.89	83.97
C602	THERMOCALC	0.000	0.00	10.93	0.00	16.00	14.46	0.00	0.00	0.00	8.64	49.97			100.00	75.42
	Biase&Variance	-0.002	-0.90	3.63	-0.30	1.32	-4.54	0.00	0.00	-0.78	8.64	-7.02	-0.49	-0.45	161.47	
	Exp	0.004	0.70	7.70	0.13	13.80	20.30			0.42		55.00	0.26	0.02	98.33	82.73
C603	THERMOCALC	0.000	0.00	11.83	0.00	16.02	14.62	0.00	0.00	0.00	8.72	48.81			100.00	73.47
	Biase&Variance	-0.004	-0.70	4.13	-0.13	2.22	-5.68	0.00	0.00	-0.42	8.72	-6.19	-0.26	-0.02	169.37	
	Exp	0.005	0.60	7.70	0.12	14.20	23.00			0.49		52.50	0.28	0.02	98.91	82.06
C604	THERMOCALC	0.000	0.00	12.29	0.00	16.01	14.79	0.00	0.00	0.00	8.86	48.06			100.00	72.40
	Biase&Variance	-0.005	-0.60	4.59	-0.12	1.81	-8.21	0.00	0.00	-0.49	8.86	-4.44	-0.28	-0.02	190.63	
	Exp	0.004	0.89	8.00	0.18	14.10	17.60			0.43		59.00	0.27	0.02	100.49	83.19
C605	THERMOCALC	0.000	0.00	13.09	0.00	16.04	14.91	0.00	0.00	0.00	8.92	47.03			100.00	70.67
	Biase&Variance	-0.004	-0.89	5.09	-0.18	1.94	-2.69	0.00	0.00	-0.43	8.92	-11.97	-0.27	-0.02	260.94	

Table A2.3d Mitchell and Grove (2016) melting experimental results and calculation results from WL22-3 model: olivine composition

No.	Methods	Mode	SiO2	Al2O3	CaO	MgO	FeO	K2O	Na2O	TiO2	Fe2O3	Cr2O3	MnO	NiO	Total	Mg#
	Exp	0.817	41.30	0.01	0.07	52.60	6.86			0.00			0.13	0.01	100.98	93.18
C608	THERMOCALC	0.631	41.60	0.00	0.01	52.48	5.91	0.00	0.00	0.00	0.00	0.00			100.00	94.06
	Biase&Variance	-0.187	0.30	-0.01	-0.06	-0.12	-0.95	0.00	0.00	0.00	0.00	0.00	-0.13	-0.01	1.02	
	Exp	0.735	40.80	0.01	0.08	51.50	7.60			0.04			0.11	0.02	100.16	92.35
C602	THERMOCALC	0.524	41.48	0.00	0.05	51.95	6.52	0.00	0.00	0.00	0.00	0.00			100.00	93.42
	Biase&Variance	-0.211	0.68	-0.01	-0.03	0.45	-1.08	0.00	0.00	-0.04	0.00	0.00	-0.11	-0.02	1.83	
	Exp	0.696	40.90	0.01	0.10	50.60	7.79			0.01			0.11	0.04	99.56	92.05
C603	THERMOCALC	0.523	41.45	0.00	0.06	51.82	6.68	0.00	0.00	0.00	0.00	0.00			100.00	93.26
	Biase&Variance	-0.173	0.55	-0.01	-0.04	1.22	-1.11	0.00	0.00	-0.01	0.00	0.00	-0.11	-0.04	3.04	
	Exp	0.635	39.90	0.01	0.08	51.60	7.91			0.01			0.10	0.01	99.62	92.08
C604	THERMOCALC	0.519	41.43	0.00	0.06	51.74	6.77	0.00	0.00	0.00	0.00	0.00			100.00	93.17
	Biase&Variance	-0.116	1.53	-0.01	-0.02	0.14	-1.14	0.00	0.00	-0.01	0.00	0.00	-0.10	-0.01	3.68	
	Exp	0.696	40.10		0.10	51.30	8.08			0.02			0.11	0.03	99.74	91.88
C605	THERMOCALC	0.517	41.41	0.00	0.06	51.64	6.89	0.00	0.00	0.00	0.00	0.00			100.00	93.04
	Biase&Variance	-0.179	1.31	0.00	-0.04	0.34	-1.19	0.00	0.00	-0.02	0.00	0.00	-0.11	-0.03	3.27	
	Exp	0.364	40.20		0.11	48.90	10.30			0.00			0.19	0.06	99.76	89.43
C584	THERMOCALC	0.081	41.23	0.00	0.12	50.87	7.78	0.00	0.00	0.00	0.00	0.00			100.00	92.10
	Biase&Variance	-0.284	1.03	0.00	0.01	1.97	-2.52	0.00	0.00	0.00	0.00	0.00	-0.19	-0.06	11.35	
	Exp	0.376	40.80		0.10	48.60	10.34			0.00			0.15	0.14	100.13	89.34
C592	THERMOCALC	0.078	41.26	0.00	0.11	51.00	7.62	0.00	0.00	0.00	0.00	0.00			100.00	92.27
	Biase&Variance	-0.298	0.46	0.00	0.01	2.40	-2.72	0.00	0.00	0.00	0.00	0.00	-0.15	-0.14	13.44	
	Exp	0.374	39.80	0.03	0.10	48.80	11.24			0.00			0.17	0.18	100.32	88.56
C587	THERMOCALC	0.078	41.18	0.00	0.12	50.62	8.08	0.00	0.00	0.00	0.00	0.00			100.00	91.78
	Biase&Variance	-0.297	1.38	-0.03	0.02	1.82	-3.16	0.00	0.00	0.00	0.00	0.00	-0.17	-0.18	15.23	
	Exp	0.384	40.40	0.02	0.09	49.00	10.40			0.01			0.22	0.09	100.23	89.36
C590	THERMOCALC	0.082	41.07	0.00	0.11	50.18	8.64	0.00	0.00	0.00	0.00	0.00			100.00	91.19
	Biase&Variance	-0.302	0.67	-0.02	0.02	1.18	-1.76	0.00	0.00	-0.01	0.00	0.00	-0.22	-0.09	4.98	
	Exp	0.389	41.00	0.01	0.11	48.00	11.21			0.01			0.19	0.11	100.64	88.42
C591	THERMOCALC	0.076	41.05	0.00	0.10	50.07	8.79	0.00	0.00	0.00	0.00	0.00			100.00	91.04
	Biase&Variance	-0.313	0.05	-0.01	-0.01	2.07	-2.42	0.00	0.00	-0.01	0.00	0.00	-0.19	-0.11	10.21	

Table A2.3e Mitchell and Grove (2016) melting experimental results and calculation results from WL22-3 model: opx composition

No.	Methods	Mode	SiO2	Al2O3	CaO	MgO	FeO	K2O	Na2O	TiO2	Fe2O3	Cr2O3	MnO	NiO	Total
	Exp	0.113	56.80	0.90	1.30	34.20	5.20		0.03	0.05		0.60	0.12	0.04	99.24
C603	THERMOCALC	0.074	56.28	1.87	0.65	34.89	4.57	0.00	0.02	0.00	0.41	1.31			100.00
	Biase&Variance	-0.039	-0.52	0.97	-0.65	0.69	-0.63	0.00	-0.01	-0.05	0.41	0.71	-0.12	-0.04	3.19
	Exp	0.191	57.40	1.00	1.20	34.30	5.20	0.01	0.06	0.06		0.51	0.12	0.01	99.87
C604	THERMOCALC	0.085	56.22	1.90	0.71	34.77	4.65	0.00	0.02	0.00	0.42	1.31			100.00
	Biase&Variance	-0.106	-1.18	0.90	-0.49	0.47	-0.55	-0.01	-0.04	-0.06	0.42	0.80	-0.12	-0.01	3.80
	Exp	0.121	57.20	0.74	1.15	34.50	5.23		0.01	0.08		0.63	0.14	0.03	99.71
C605	THERMOCALC	0.101	56.11	1.97	0.81	34.58	4.75	0.00	0.02	0.00	0.45	1.31			100.00
	Biase&Variance	-0.020	-1.09	1.23	-0.34	0.08	-0.48	0.00	0.01	-0.08	0.45	0.68	-0.14	-0.03	3.74

Table A2.3f Mitchell and Grove (2016) melting experimental results and calculation results from WL22-3 model: cpx composition

No.	Methods	Mode	SiO2	Al2O3	CaO	MgO	FeO	K2O	Na2O	TiO2	Fe2O3	Cr2O3	MnO	NiO	Total
	Exp	0.161	53.60	1.80	22.00	17.80	3.30	0.01	0.24	0.10		0.90	0.12		99.87
C587	THERMOCALC	0.007	54.31	1.57	21.34	19.11	2.60	0.03	0.25	0.04	0.31	0.43			100.00
	Biase&Variance	-0.154	0.71	-0.23	-0.66	1.31	-0.70	0.02	0.01	-0.06	0.31	-0.47	-0.12	0.00	3.53
	Exp	0.150	54.10	1.90	22.10	17.60	3.10		0.23	0.17		1.00	0.11	0.01	100.32
C590	THERMOCALC	0.040	54.08	1.84	21.46	18.82	2.75	0.03	0.25	0.05	0.35	0.39			100.00
	Biase&Variance	-0.110	-0.02	-0.06	-0.64	1.22	-0.35	0.03	0.02	-0.12	0.35	-0.61	-0.11	-0.01	2.54
	Exp	0.183	54.10	2.40	22.10	17.10	3.54		0.24	0.19		0.74	0.12		100.53
C591	THERMOCALC	0.048	54.06	1.80	21.66	18.68	2.74	0.03	0.24	0.05	0.36	0.37			100.00
	Biase&Variance	-0.135	-0.04	-0.60	-0.44	1.58	-0.80	0.03	0.00	-0.14	0.36	-0.37	-0.12	0.00	3.99

Appendix B THERMOCALC Calculation Results

Section 1 (excel sheet 1): anhydrous results from TH21 model

Section 2 (excel sheet 2): anhydrous results from WL22-3 and HGP18 model

Section 3 (excel sheet 3): hydrous results from WL22-3 model

Section 4 (excel sheet 4): Isobaric fractional melting results from TH21 model

Section 5 (excel sheet 5): Decompression melting results from TH21 model

Appendix C THERMOCALC-Running Files

Section 1 a-x File: TH21

Section 2 a-x File: HGP18

Section 3 a-x File: WL22-3

Section 4 Dataset: ds634

Section 5 Dataset: ds633

Section 6 Other Running Files

Link to Appendix B and C in University of Alberta Dataverse:

https://doi.org/10.5683/SP3/13TIXK

Supplementary Data for Thermodynamic Models for the Melting of Mantle Peridotites _ Daoheng Wang MSc Thesis Supplementary Online Dataset